

**Novel oxidative treatment processes for unselective removal of organic  
contaminants in groundwater remediation**

**Emil Ferdinand Bein**

Vollständiger Abdruck der von der TUM School of Engineering and Design der  
Technischen Universität München zur Erlangung des akademischen Grades eines

**Doktors der Ingenieurwissenschaften (Dr.-Ing.)**

genehmigten Dissertation.

*Vorsitz:* apl. Prof. Dr. Brigitte Helmreich

*Prüfer der Dissertation:*

1. Priv.-Doz. Dr. Uwe Hübner
2. Prof. Dr. Jörg E. Drewes
3. Prof. Dr. Yunho Lee

Die Dissertation wurde am 29.01.2024 bei der Technischen Universität München  
eingereicht und durch die TUM School of Engineering and Design am 06.06.2024  
angenommen.



## ABSTRACT

Widespread organic groundwater contamination originating from anthropogenic activities requires improved future protection of water bodies and effective remedial efforts. Besides known problems such as BTEX (benzene, toluene, ethylbenzene, xylene isomers) contamination from oil- and gas-related operations or release of chlorinated solvents from industrial activities, other emerging contaminants are continuously added to the list of concerning substances. Even though contamination has occurred over decades and treatment technologies have been developed to cope with it, progress is still required concerning the choice of efficient treatment with a focus on achieving complete removal of hazardous organic matter. In this dissertation, oxidative treatment technologies intended for in-situ use, commonly known as in-situ chemical oxidation (ISCO) processes, were investigated with a focus on oxidant delivery techniques and reaction mechanisms among monocyclic aromatic and aliphatic organic contaminants.

In particular, gas-liquid membrane contactors for in-situ ozone delivery were tested as a novel method for oxidant injection into contaminated groundwater. Therefore, an extensive literature review was conducted first with the aim of identifying critical operational parameters and selecting suitable membrane materials. The review revealed that mass transfer coefficients and material stability were the highest for fluorinated, highly hydrophobic (PVDF/PTFE) membrane materials, and that mass transfer could be accurately predicted by dimensionless correlations. This was the case for ex situ membrane contacting module geometries with parallel or counter-current operation, the only contacting geometry with well-described performance. The high hydrophobicity of these materials prevents pores from being wetted in a gas-liquid membrane contacting operation, enhancing mass transfer in small operational volumes. In comparison, silicone-based polydimethylsiloxane membranes (PDMS) had much higher membrane resistances and lower mass transfer, however, could be a cost-effective alternative with limited resistance towards ozone.

In a second step, laboratory scale steady-state flow-through experiments were conducted to investigate the performance of PTFE and PDMS membrane materials for ozone dissolution as permeable reactive barrier (PRB) in a natural water matrix with spiked aromatic and aliphatic model contaminants and added subsequent soil layers. The investigation could reveal adverse and positive aspects of using gas-liquid membrane contactors. Most notably, mass transfer can be roughly estimated using dimensionless design correlations derived for other gases, and the amount of ozone to be released can therefore be controlled well. However, monocyclic aromatic contaminants cause limited ozone distribution due to the high ozone-consumption of their hydroxylated

transformation products (TPs), making the ISCO application of this technology, for example in the case of BTEX contamination, more challenging. Soil layers proved to be of minor relevance for both aromatic and aliphatic contamination, as most oxidation (i.e., compound removal) was not affected by addition of different ozone-consuming layers.

Next, TP formation in the oxidative treatment of BTEX was studied to systematically shed light on the unknown, however, often claimed synergies of chemical oxidation and subsequent biological degradation. Circulation experiments with  $O_3/H_2O_2$  and  $UV/H_2O_2$  treatment processes were done with additionally spiked probe compounds to measure hydroxyl radical exposures. Results with benzene, toluene, ethylbenzene (BTE), and benzoic acid (BA) confirmed the previously established hypothesis of synergistic effects of ozone and hydroxyl radicals ( $O_3/H_2O_2$  treatment) in breaking down TPs of monocyclic aromatics further. This was done in direct comparison with  $UV/H_2O_2$  as control treatment. These synergies did not lead to improved biodegradability of remaining DOC compared to  $UV/H_2O_2$  treatment and also not compared to biodegradation of the parent compound in case of BA.

In the last experimental part of the dissertation, catalytic peroxydisulfate (PMS) activation was tested as an alternative approach for unselective degradation of organic contamination in water by generating sulfate radicals. In the chosen technology approach, catalytically active  $MnO_2$  material was immobilized on natural sand by modifying the synthesis conditions. The generated material could serve as PRB with in-situ PMS activation, as well as for other water purification purposes. Removal performances were tested in a catalytic filtration column (CFC), where solutions containing PMS and spiked contaminants were pumped through. Overall, the CFC removed a large variety of organic contaminants both in natural groundwater but also wastewater treatment plant effluent. Furthermore, no apparent performance changes were observed in the time of operation. Thus, it was promising for water decontamination applications, where unselective oxidation of a mixture of contaminants is needed. Further optimization and testing strategies were suggested as part of this chapter.

Lastly, experimental results were discussed with respect to technological and economic feasibility, identified roadblocks, and requirements for a successful groundwater remediation operation. Briefly, the performance of in-situ ozone release by gas-liquid membrane contactor operation is severely suppressed in presence of, for example, monocyclic aromatic compounds, due to their ozone-consuming transformation products after initial attack of  $\cdot OH$  radicals on parent compounds. Therefore, it cannot be recommended for use in BTEX clean-up operations. For removal of 1,4-dioxane or other aliphatic groundwater contaminants, results were more promising, however, require a study design that focuses on different injection geometries in porous media (i.e.,

borewells, cross-section excavation, etc.) to identify practically feasible and effective treatment options. The established mass transfer estimation tools can be used for further dimensioning of membrane material. The coupling of chemical oxidation and biodegradation may have synergies under certain conditions, however, possible disadvantages may not be analytically tracked, if the mineralization of remaining organic matter after treatment is not quantified. Biological degradation experiments should motivate future research projects to look more in depth into transformation mechanisms and biodegradability after chemical oxidation. Moreover, catalytic PMS activation results were discussed in light of recent advances of catalytic oxidation. The path ahead of such technology requires more experimental standardization and common understanding of appropriate tools to assess the process effectivity, once a new material is introduced.

## ZUSAMMENFASSUNG

Weitverbreitete Kontamination von Grundwasser durch organische Schadstoffe, zurückzuführen auf anthropogene Aktivitäten, erfordert sowohl verbesserten Schutz der Gewässer als auch wirksame Sanierungsmaßnahmen. Neben bekannten Problemen wie Kontamination durch BTEX-Stoffe (Benzol, Toluol, Ethylbenzol, Xylol-Isomere), welche durch Aktivitäten im Rahmen der Gas- und Öl-Lagerung sowie -Produktion in Grundwasser eingetragen werden, sowie chlorierte Lösungsmittel aus der Industrie, kommen ständig neue Schadstoffe hinzu, die beobachtet werden müssen. Obwohl Kontamination von Grundwasser bereits über Jahrzehnte hinweg stattgefunden hat und zum Teil effektive Behandlungstechnologien entwickelt wurden um sie zu beseitigen, gibt es weiterhin Entwicklungen bei der Wahl einer effizienten Behandlung mit dem Fokus auf der vollständigen Entfernung gefährlicher organischer Stoffe. In dieser Dissertation wurden oxidative Behandlungstechnologien für den In-situ-Einsatz, gemeinhin als „in-situ chemical oxidation“ (ISCO) bekannt, untersucht, wobei der Schwerpunkt auf neuartigen Eintragstechniken von Oxidationsmitteln und deren Reaktionsmechanismen mit monozyklischen aromatischen und aliphatischen organischen Schadstoffen lag.

Insbesondere wurden Gas-Flüssig-Membrankontaktoren für den In-situ-Ozoneintrag als neuartige Behandlungsmethode für kontaminiertes Grundwasser getestet. Zunächst wurde eine umfangreiche Literaturrecherche durchgeführt, um die wichtigsten Prozessparameter zu ermitteln und geeignete Membranmaterialien auszuwählen. Die Analyse ergab, dass die Massentransferkoeffizienten und die Materialstabilität von fluorierten, stark hydrophoben Membranmaterialien (PVDF/PTFE) am höchsten waren und der Massentransfer durch dimensionslose Korrelationen gut vorhergesagt werden konnte. Dies war der Fall für Membranmodule mit Parallel- oder Gegenstrombetrieb, der einzigen Modulgeometrie mit gut dokumentierten Betriebsdaten. Die hohe Hydrophobie der getesteten fluorierten Materialien verhindert, dass Flüssigkeit in die Poren beim Betrieb der Kontaktoren eindringen kann, wodurch der Massentransfer in kleinen Volumen verbessert wird. Im Vergleich dazu wiesen Membranen aus Polydimethylsiloxan (PDMS) auf Silikonbasis wesentlich höhere Membranwiderstände und einen niedrigeren Massentransfer auf, könnten jedoch eine kostengünstige Alternative mit zeitlich begrenzter Stabilität gegenüber Ozon darstellen.

In einem zweiten Schritt wurden Durchflusseexperimente im stationären Betrieb im Labormaßstab durchgeführt, um die Leistung von PTFE- und PDMS-Membranmaterialien für den Ozoneintrag als „permeable reactive barrier“ (PRB) in einer natürlichen Wassermatrix mit zugegebenen aromatischen und aliphatischen

Modellschadstoffen und installierten Bodenschichten zu untersuchen. Die Untersuchung konnte negative und positive Aspekte des Einsatzes von Gas-Flüssig-Membrankontaktoren aufzeigen. Der Massentransfer kann mit Hilfe von dimensionslosen Designkorrelationen, die für andere Gase abgeleitet wurden, grob abgeschätzt werden, sodass die einzutragende Ozonmenge kontrolliert werden kann. Monozyklische aromatische Schadstoffe verursachen jedoch aufgrund des hohen Ozonkonsums ihrer hydroxylierten Transformationsprodukte (TPs) eine begrenzte Ozonausbreitung, was die ISCO-Anwendung dieser Technologie z. B. bei BTEX-Kontaminationen erschwert. Die Bodenschichten erwiesen sich sowohl für die aromatische als auch für die aliphatische Kontamination als wenig relevant, da die Oxidation (d. h. die Entfernung der Stoffe) durch die Zugabe verschiedener ozonkonsumierender Schichten nicht beeinflusst wurde.

Als Nächstes wurde die TP-Bildung bei der oxidativen Behandlung von BTEX untersucht, um die unbekannt, aber oft postulierten Synergie zwischen chemischer Oxidation und anschließendem biologischen Abbau systematisch zu untersuchen. Dafür wurden Zirkulationsexperimente mit  $O_3/H_2O_2$ - und  $UV/H_2O_2$ -Behandlungsverfahren durchgeführt, bei denen zur Messung der Exposition gegenüber Hydroxylradikalen zusätzlich Indikatorsubstanzen zugegeben wurden. Die Ergebnisse mit Benzol, Toluol, Ethylbenzol (BTE) und Benzoesäure (BA) bestätigten die zuvor aufgestellte Hypothese einer synergistischen Wirkung von Ozon und Hydroxylradikalen ( $O_3/H_2O_2$ -Behandlung) beim weitergehenden Abbau von Transformationsprodukten monozyklischer Aromaten. Dies war im direkten Vergleich mit Behandlung durch  $UV/H_2O_2$  als Kontrolle ersichtlich. Diese Synergieeffekte führten nicht zu einer verbesserten biologischen Abbaubarkeit des verbleibenden DOC im Vergleich zur  $UV/H_2O_2$ -Behandlung, und auch nicht im Vergleich zum biologischen Abbau der Ausgangsverbindung im Falle von BA.

Im letzten experimentellen Teil der Dissertation wurde die katalytische Aktivierung von Peroxymonosulfat (PMS) als alternativer Ansatz für den nichtselektiven Abbau von organischen Verunreinigungen in Wasser durch die Erzeugung von Sulfat-Radikalen getestet. Bei dem gewählten technologischen Ansatz wurde katalytisch aktives  $MnO_2$  durch Anpassung der Synthesebedingungen auf natürlichem Sand immobilisiert. Das erzeugte Material könnte sowohl als PRB in Kombination mit in-situ PMS-Aktivierung als auch für andere Wasserreinigungszwecke dienen. Die Entfernungsleistung wurde in einer katalytischen Filtrationssäule (CFC) getestet, durch die Lösungen mit PMS und aufkonzentrierten Schadstoffen gepumpt wurden. Insgesamt entfernte die CFC eine Vielzahl von organischen Schadstoffen sowohl aus natürlichem Grundwasser als auch aus dem Kläranlagenablauf. Außerdem wurden keine offensichtlichen Leistungsänderungen während der Betriebszeit festgestellt. Somit war die Säule vielversprechend für Anwendungen im Bereich der Wasserdekontamination, bei denen

eine nichtselektive Oxidation einer Vielzahl von Verunreinigungen erforderlich ist. Im Rahmen dieses Kapitels wurden weitere Optimierungs- und Teststrategien vorgeschlagen.

Zuletzt wurden die Ergebnisse im Hinblick auf die technologische und wirtschaftliche Machbarkeit, die identifizierten Hindernisse und die Voraussetzungen für eine erfolgreiche Grundwassersanierung diskutiert. Zusammenfassend lässt sich sagen, dass die Leistung des In-situ-Ozoneintrages mit Gas-Flüssig-Membrankontaktoren in Gegenwart von monozyklischen aromatischen Verbindungen aufgrund von deren ozonkonsumierenden Transformationsprodukten nach der initialen Reaktion der Ausgangsstoffe mit  $\cdot\text{OH}$ -Radikalen stark reduziert wird. Daher kann die Technologie nicht für den Einsatz bei der BTEX-Dekontamination empfohlen werden. Für die Entfernung von 1,4-Dioxan oder anderen aliphatischen Grundwasserverunreinigungen waren die Ergebnisse vielversprechender, erfordern jedoch für weitergehende Untersuchungen ein Studiendesign, das sich auf verschiedene Injektions-Geometrien in porösen Medien konzentriert (d. h. Bohrlöcher, Querschnittsgrabungen usw.), um praktisch durchführbare und wirksame Behandlungsoptionen zu ermitteln. Die etablierten Tools zur Abschätzung des Massentransfers können für die weitere Dimensionierung der Membranmodule verwendet werden. Die Kombination von chemischer Oxidation und biologischem Abbau kann unter bestimmten Bedingungen zu Synergien führen, jedoch können mögliche Nachteile nicht analytisch erfasst werden, wenn die Mineralisierung der verbleibenden organischen Substanz nach der Behandlung nicht quantifiziert wird. Die durchgeführten biologischen Abbauxperimente sollten künftige Forschungsprojekte dazu motivieren, die Umwandlungsmechanismen und die biologische Abbaubarkeit nach der chemischen Oxidation eingehender zu untersuchen. Darüber hinaus wurden die Ergebnisse der katalytischen PMS-Aktivierung im Lichte der jüngsten Fortschritte bei der katalytischen Oxidation diskutiert. Der weitere Fortschritt einer solchen Technologie erfordert eine stärkere experimentelle Standardisierung und ein geteiltes Verständnis für geeignete Werkzeuge zur Bewertung der Prozesseffektivität, sobald ein neues Material eingeführt wird.



## DANKSAGUNG

An dieser Stelle möchte ich von ganzem Herzen meinen Dank an wichtige Wegbegleiter:innen der letzten fünf Jahre aussprechen.

Zuallererst danke ich PD Dr. Uwe Hübner für das Privileg, dass ich am Lehrstuhl für Siedlungswasserwirtschaft über mehrere Jahre unter seine Betreuung forschen durfte. Ich habe mich in dieser Zeit immer gefördert und im besten Sinne gefordert gefühlt. Du hast bei mir echte Leidenschaft für Oxidationschemie wecken können. Auch Prof. Dr. Jörg E. Drewes gilt mein großer Dank für die hervorragenden Arbeitsbedingungen am Lehrstuhl und das offene Ohr für alle Belange.

Bei Prof. Dr. Yunho Lee bedanke ich mich für die Begutachtung und Bewertung dieser wissenschaftlichen Arbeit und die wertvollen Hinweise und Fragen. Daran anknüpfend möchte ich mich auch herzlich bei Prof. Dr. Brigitte Helmreich bedanken, die nicht nur den Vorsitz dieser Prüfungskommission übernommen hat, sondern am Lehrstuhl mit viel Geduld Probleme löst, sollten sie denn auftauchen. Prof. Dr. Konrad Koch und Dr. Christian Wurzbacher waren am Lehrstuhl ebenfalls Konstanten, die ich nicht hätte missen wollen.

Dr. Johann Müller, Dr. Oliver Knoop und Dr. Ignacio Sottorff danke ich für die analytischen Lehrstunden und Hilfestellungen, ohne die die Suche nach den Nadeln im Heuhaufen sicherlich nicht geklappt hätte. Hubert Moosrainer und Maximilian Damberger bin ich sehr dankbar für die wichtige Unterstützung bei der Herstellung von experimentellen Aufbauten. Das Gleiche gilt für Myriam Reif, die mir immer im Labor geholfen hat, wo es ging. Auf der administrativen Seite danke ich insbesondere Susanne Wießler, die mit immer guter Miene das größte Chaos, das wir angerichtet haben, in Ordnung gebracht hat.

Was wäre diese Zeit ohne die besten Kolleg:innen und manchmal auch Leidensgenoss:innen gewesen? Für alle Diskussionen, jeden Spaß und Unfug, und Unterstützung in Rat und Tat möchte ich neben vielen anderen danken: Carolina Feickert Fenske, Jonas Aniol, Edwin Chingate Barbosa, Millaray Sierra Olea, Nebojša Ilić, Philipp Sperle, Philipp Stinshoff, Felix Müller, Natalie Pérez Curtidor, Lea Rosenberger, Daniel Nieß, Alexander Mitranescu, Javad Ahmadi, Sonia Kau, Mariana Kluge, Sema Karakurt-Fischer, Veronika Zhiteneva, Thomas Lippert und Christoph Schwaller. Ich werde die Atmosphäre vermissen.

In meiner Zeit als wissenschaftlicher Mitarbeiter haben mich zahlreiche Personen über ihre studentischen Arbeiten unterstützt und wesentlich zum Gelingen dieser Arbeit

beigetragen. Mein Dank hierfür geht an Erin Kim, Giulia Pasquazzo, Kristina Mraz, Carl Witthöft, Mario Contreras Vomend, Erzen Duraku, Afrina Andalib und Sophie Petersen.

Zuletzt danke ich auch den vielen Menschen, die mir privat eine riesige Stütze in dieser ganzen Zeit waren, die durch die Corona-Pandemie nicht nur positive Überraschungen bereithielt. Liebe „Nasen“, ihr seid die Besten. Danke, liebe Danika und liebe Familie, für die unendliche Unterstützung und Loyalität.

# CONTENTS

<b>ABSTRACT</b>	<b>I</b>
<b>ZUSAMMENFASSUNG</b>	<b>IV</b>
<b>DANKSAGUNG</b>	<b>VII</b>
<b>LIST OF FIGURES</b>	<b>XIII</b>
<b>LIST OF TABLES</b>	<b>XIX</b>
<b>ABBREVIATIONS AND ACRONYMS</b>	<b>XXI</b>
<b>1 INTRODUCTION</b>	<b>1</b>
<b>2 STATE-OF-THE-ART</b>	<b>4</b>
2.1 In-situ chemical oxidation.....	4
2.1.1 Oxidant selection for ISCO treatment.....	4
2.1.2 Oxidant and porous media interactions.....	8
2.1.3 Conventional injection technologies.....	9
2.1.4 Gas-permeable membranes for passive ozone gas release – An effective new treatment technology?.....	10
2.2 Immobilized catalysts for PMS activation.....	11
2.2.1 Activation mechanisms.....	11
2.2.2 The challenge of immobilizing catalysts.....	14
2.2.3 Potential fields of application.....	15
2.3 Fate of organic transformation products after oxidative groundwater remediation.....	16
2.4 Bioremediation as alternative to ISCO approaches?.....	17
<b>3 RESEARCH OBJECTIVES, HYPOTHESES, AND DISSERTATION STRUCTURE</b>	<b>20</b>
3.1 Research objective 1.....	20
3.2 Research objective 2.....	20
3.3 Research objective 3.....	21
3.4 Research objective 4.....	23
3.5 Dissertation structure.....	23
<b>4 OZONE MEMBRANE CONTACTORS FOR WATER AND WASTEWATER TREATMENT: A CRITICAL REVIEW ON MATERIALS SELECTION, MASS TRANSFER AND PROCESS DESIGN</b>	<b>26</b>
4.1 Abstract.....	26
4.2 Introduction.....	27
4.3 Methods and literature data.....	29
4.4 Membrane materials and their stability.....	31
4.4.1 Polymeric membranes.....	32
4.4.2 Inorganic membranes.....	36

4.5	Mass transfer in ozone membrane contacting systems .....	37
4.5.1	Estimation of mass transfer coefficients .....	37
4.5.2	Agreement of calculated mass transfer coefficients with experimental data from literature .....	39
4.6	Impact of liquid velocity and fiber geometry on mass transfer coefficients .....	43
4.7	Mass transfer enhancement .....	45
4.8	Implications for designing large-scale applications.....	50
4.8.1	Efficient design and operation of modules.....	50
4.8.2	Comparison to standard injection methods .....	53
4.9	Conclusions .....	55
4.10	Acknowledgement.....	56
<b>5</b>	<b>GROUNDWATER REMEDIATION BY IN-SITU MEMBRANE OZONATION: REMOVAL OF ALIPHATIC 1,4-DIOXANE AND MONOCYCLIC AROMATIC HYDROCARBONS</b>	<b>57</b>
5.1	Abstract .....	57
5.2	Introduction .....	58
5.3	Materials and methods.....	60
5.3.1	Chemicals and reagents.....	60
5.3.2	Ozone batch experiments .....	61
5.3.3	Membrane-based ozone delivery .....	61
5.3.4	In-situ oxidation of BA and DIOX.....	63
5.3.5	Experimental mass transfer estimations .....	63
5.3.6	Modeling of mass transfer rates .....	65
5.3.7	Analytical methods .....	65
5.4	Results .....	66
5.4.1	Ozone decomposition in presence of BA and DIOX .....	66
5.4.2	In-situ ozonation of BA and DIOX .....	67
5.4.3	Mass transfer estimations .....	71
5.5	Conclusions .....	75
5.6	Acknowledgement.....	76
<b>6</b>	<b>ADVANCED OXIDATION PROCESSES FOR REMOVAL OF MONOCYCLIC AROMATIC HYDROCARBON FROM WATER: EFFECTS OF O<sub>3</sub>/H<sub>2</sub>O<sub>2</sub> AND UV/H<sub>2</sub>O<sub>2</sub> TREATMENT ON PRODUCT FORMATION AND BIOLOGICAL POST-TREATMENT</b>	<b>77</b>
6.1	Abstract .....	77
6.2	Introduction .....	78
6.3	Materials and methods.....	80
6.3.1	Chemicals and reagents.....	80
6.3.2	Oxidation experiments .....	80
6.3.3	Aerobic biodegradation experiments .....	83
6.3.4	Analytical methods .....	83

6.4	Results.....	85
6.4.1	Removal kinetics during O <sub>3</sub> /H <sub>2</sub> O <sub>2</sub> and UV/H <sub>2</sub> O <sub>2</sub> treatment.....	85
6.4.2	Product formation during BTE oxidation .....	86
6.4.3	Coupling chemical oxidation and biodegradation.....	89
6.5	Conclusions .....	93
6.6	Acknowledgement.....	94
<b>7</b>	<b>A NOVEL CATALYTIC FILTRATION PROCESS USING MnO<sub>2</sub>@SAND AND PEROXYMONOSULFATE FOR UNSELECTIVE REMOVAL OF ORGANIC CONTAMINANTS FROM WATER</b>	<b>95</b>
7.1	Abstract .....	95
7.2	Introduction .....	96
7.3	Materials and methods .....	98
7.3.1	Synthesis of MnO <sub>2</sub> @sand .....	98
7.3.2	Material characterization .....	99
7.3.3	Catalytic oxidation experiments .....	99
7.3.4	Analytical methods .....	101
7.4	Results.....	101
7.4.1	Characteristics of MnO <sub>2</sub> @sand.....	101
7.4.2	PMS decomposition and process stability.....	103
7.4.3	Rhodamine B decomposition.....	104
7.4.4	Reactivity with a wide range of contaminants in TW and WW.....	106
7.4.5	Benchmarking the CFC process as potential drinking water or advanced wastewater treatment step.....	109
7.5	Conclusions .....	111
7.6	Acknowledgement.....	111
<b>8</b>	<b>DISCUSSION AND FUTURE RESEARCH NEEDS</b>	<b>113</b>
8.1	The applicability of gas-liquid membrane contactors for in-situ ozonation of contaminated groundwater .....	113
8.1.1	The challenge of material stability and mass transfer .....	113
8.1.2	Transfer to ISCO applications .....	115
8.2	Coupling chemical and biological transformation of monocyclic aromatic hydrocarbon—Tackling the unknowns .....	119
8.3	Catalytic oxidation for water decontamination .....	122
8.3.1	PMS-activation—A feasible treatment alternative?.....	122
8.3.2	Future research needs in the field of catalytic oxidation.....	124
<b>9</b>	<b>OVERALL CONCLUSION AND OUTLOOK</b>	<b>127</b>
<b>10</b>	<b>APPENDIX</b>	<b>129</b>
10.1	List of publications.....	129
10.2	List of supervised student theses .....	131
10.3	Supplementary information for Chapter 5.....	132

10.3.1	Chemicals and reagents .....	132
10.3.2	Analytical methods .....	132
10.3.3	Text S1: Batch experiments to compare DIOX and BA removal with ozone membrane contacting experiments .....	133
10.3.4	Text S2: Detailed procedure to obtain experimental mass transfer coefficients .....	134
10.3.5	Text S3: Determination of ozone decay $k_d$ from membrane to sampling port .....	136
10.3.6	Text S4: Ozone decomposition in presence of toluene .....	137
10.3.7	Text S5: Dissolved ozone measurements during BA in-situ ozonation experiments .....	138
10.3.8	Text S6: Ozone exposure data and its handling .....	139
10.3.9	Text S7: Estimation of ozone mass transfer with dimensionless correlations and numerical modeling.....	142
10.4	Supplementary information for Chapter 6 .....	144
10.4.1	Text S1: Selection of hydroxyl radical probe compounds .....	144
10.4.2	Text S2: Further notes on biodegradation experiments with biological sand.....	146
10.4.3	Reaction rate constants.....	147
10.4.4	Chemicals and reagents.....	148
10.4.5	Analytical methods .....	148
10.4.6	Experimental data tables .....	150
10.4.7	Additional result figures.....	153
10.5	Supplementary information for Chapter 7 .....	158
10.5.1	Text S1: Detailed explanation of sand pre-treatment and properties .....	158
10.5.2	Text S2: Characterization of different synthesized catalyst batches and their use in the experiments .....	158
10.5.3	Text S3: Additional material characterization results .....	159
10.5.4	Text S4: Additional data on used tap water and catalyst longevity experiments .....	162
10.5.5	Text S5: Sand control experiments .....	163
10.5.6	Text S6: Additional data on Rh-B oxidation experiments .....	164
10.5.7	Text S7: Detailed results of TOrCs removal and CFC adsorption behavior .....	166
10.5.8	Text S8: Statistical analysis of six TOrCs – correlation of second order rate constants and removal values .....	169
10.6	Ozonation of gabapentin in water—Investigating reaction kinetics and transformation mechanisms of a primary amine using isotopically labeled ozone (Article V) .....	172
10.6.1	Abstract .....	172
10.6.2	Introduction .....	173
10.6.3	Materials and methods .....	175
10.6.4	Results.....	178
10.6.5	Supporting information .....	187
10.6.6	Acknowledgement .....	188

## LIST OF FIGURES

Figure 1: Simplified scheme of an ISCO treatment site using ozone through sparging wells, based on Reddy et al. (1995). .....	9
Figure 2: Scheme of a PRB consisting of membrane walls that are diffusing ozone to groundwater.....	11
Figure 3: Schematic of two different upscaling approaches, a) catalyst separation, b) catalyst immobilization on support structure. ....	15
Figure 4: Dissertation structure summarizing research objectives, hypotheses, and corresponding publications. ....	25
Figure 5: Comparison of experimental ( $K_{exp}$ ) and calculated ( $K_{cal}$ , Lévêque) mass transfer coefficients of the overall data set with the diagonal showing whether $K_{exp}$ is larger or smaller than calculated values (n=108). ....	40
Figure 6: Impact of liquid velocities on (a) experimental and (b) calculated mass transfer coefficients. ....	44
Figure 7: Illustration of the concentration profile in the resistance-in-series model with (red) and without (blue) a fast chemical reaction of ozone on the liquid side. The gas is diffusing through a porous membrane to the liquid phase (adopted and modified from Phattaranawik et al. (2005)). ....	48
Figure 8: Hypothesized dissolved ozone and peroxide concentration at the fiber entrance and exit with water of low reactivity and hydrogen peroxide as feed during peroxone treatment (concentration profiles adopted from Jansen (2005) and modified). .....	49
Figure 9: Typical ozone membrane contacting configuration in a circular module with the liquid flowing on the lumen side and gas on the shell side.....	52
Figure 10: Experimental $K_a$ values for all membranes (n=108) and for hydrophobic PVDF and PTFE membranes only (n=55, as well included in the dataset on the left side). ....	53
Figure 11: Experimental set-up for ozone membrane contacting experiments in cross flow mode. Single components: (1) Oxygen gas cylinder; (2) Ozone generator with integrated pressure and flow control; (3) Stainless steel reactor filled with glass beads; (4) Gear pump; (5) Flow meter; (6) Sampling port (and needle valve); (7) Catalytic ozone gas destruction; (8) Optional soil layer; (9) Flange for opening the reactor. ....	62
Figure 12: Ozone consumption in presence of different BA and DIOX concentrations in TW (pH 7.6-7.7). “Control“ refers to the same experiment without spiked contaminant. Ozone decomposition with 8.2 $\mu\text{M}$ BA and 11.3 $\mu\text{M}$ DIOX (1 $\text{mg L}^{-1}$ ) has been obtained as triplicates (n=3), the remaining data from single experiments (n=1). Actual initial dissolved ozone concentrations were $75.2 \pm 4.0 \mu\text{M}$ in BA and $111.0 \pm 5.8 \mu\text{M}$ in DIOX experiments. ....	67

- Figure 13: Removal of DIOX (a) and BA (b) as measured in the effluent of the membrane ozonation reactor as function of the empty bed volumes treated (EBVT) with different porous media layers installed ( $n=1$ ). Actual concentrations in the feed were  $5.34 \pm 0.17 \text{ mg L}^{-1}$  (DIOX) and  $5.16 \pm 0.19 \text{ mg L}^{-1}$  (BA). Ozone gas concentration was  $200 \text{ g Nm}^{-3}$  and the liquid flow velocity was  $150 \text{ cm d}^{-1}$  in all experiments. c) Dissolved ozone concentration in the reactor effluent in all DIOX experiments.....69
- Figure 14: a) Removal of DIOX and BA ( $5 \text{ mg L}^{-1}$ ) in batch experiments conducted with tap water and ozone stock solution. The reaction time corresponds to 1 EBVT (DIOX) and 0.75 EBVT (BA). b) Illustration of fast reactions in the liquid-side boundary layer of the PDMS membrane, based on the film theory (Sirkar, 1992) and ozone decomposition and reaction with BA (von Gunten, 2003; Wang et al., 2022c).....71
- Figure 15: Ozone exposure in pH 7 phosphate buffer as function of liquid velocity, calculated with different probe compounds. a) PTFE, b) PDMS, c) Experimental mass transfer coefficients according to the novel procedure compared to the empirical correlation  $Sh = 0.824 Re^{0.39} Sc^{0.33}$ , developed by Fang et al. (2002) for  $0.0004 < Re < 0.6$ . The legend in a) also applies to b).....73
- Figure 16: Modeling results for the case study with a  $5 \times 1 \text{ m}$  contaminated cross-section. a) Change of ozone gas concentration in the PDMS tube, depending on the gas flow rate  $Q_g$  in  $\text{L min}^{-1}$ . b) Resulting mass transfer efficiency (% of ozone gas used, blue squares) and the ozone flux averaged over the membrane tube length (red crosses). .....75
- Figure 17: Experimental set-ups for recirculation experiments: a) ozone membrane contacting, b) UV-C irradiation. 1: gear pump, 2: flow meter, 3: PTFE membrane, 4: sampling port, 5: needle valve, 6: stirred feed solution.....81
- Figure 18: Removal of (a) benzene during BTE oxidation experiments and (b) BA during separate experiments as function of  $\cdot\text{OH}$  exposure. Displayed linear fits were calculated with  $\text{O}_3/\text{H}_2\text{O}_2$  data points. The shown UV/ $\text{H}_2\text{O}_2$  experiment with BA was performed in diluted TW instead of PBS. ....86
- Figure 19: Concentration of hydroxylated TPs over the course of UV/ $\text{H}_2\text{O}_2$  treatment. Parent compounds: benzene (phenol), toluene (o-cresol), ethylbenzene (o-ethylphenol). .....87
- Figure 20: Absorbance change over the whole spectrum during oxidative treatment (a), and for selected wavelengths as a function of  $\cdot\text{OH}$  exposure (b,c). Initial BTE concentrations were  $0.43/0.28/0.18 \text{ mM}$  (UV/ $\text{H}_2\text{O}_2$ ) and  $0.25/0.25/0.12 \text{ mM}$  ( $\text{O}_3/\text{H}_2\text{O}_2$ ) (see also SI, Table 20-Table 23).....88
- Figure 21: Chemical oxidation of BA and subsequent biodegradation. a) Changes of BA concentrations and TOC vs.  $\cdot\text{OH}$  radical exposure. b) Degradation of DOC in shaken batches of selected samples withdrawn in oxidation experiments. Standard deviations originate from DOC data of three individual batches containing the same water matrix



- (n=3). TOC from a) was taken as initial value. The shaker was temporarily interrupted on day 5-6 (samples 0a and 1a) with dissolved oxygen levels staying well above 7 mg L<sup>-1</sup> during that time. Data of more batches is visualized in Figure 39 (SI)..... 90
- Figure 22: EEMs (a) before UV/H<sub>2</sub>O<sub>2</sub> oxidation (0a), (b) after oxidation (1a), and (c) after biodegradation (1a). ..... 91
- Figure 23: Integrated peak areas of identified TPs, grouped by retention time, before and after biological degradation for samples treated with a) UV/H<sub>2</sub>O<sub>2</sub> (sample 1a), and b) O<sub>3</sub>/H<sub>2</sub>O<sub>2</sub> (sample 1b), and the respective control samples without chemical oxidation (0a and 0b)..... 93
- Figure 24: a) MnO<sub>2</sub>@sand synthesis procedure, and b) experimental set-up used for longevity and contaminant removal experiments..... 100
- Figure 25: (a) SEM micrographs of suspended α-MnO<sub>2</sub>, and (b-d) different morphologies observed for MnO<sub>2</sub> deposited onto sand (MnO<sub>2</sub>@sand). All shown morphologies were found on one sand grain. (e) XRD pattern of suspended α-MnO<sub>2</sub>, red rectangles indicate a match with JCPDS 044-0141. (f) XPS spectrum of suspended α-MnO<sub>2</sub>, (g) XPS spectrum of MnO<sub>2</sub>@sand..... 102
- Figure 26: a) PMS decomposition and Mn leaching test of a newly synthesized catalytic column (CFC3) with 0.6 mM PMS in TW. Asterisks indicate if Mn was below the LOQ of 5 µg L<sup>-1</sup>. The vertical line at 360 min indicates the replacement of the feed solution. 0.61 mM PMS was in the feed solution before the experiment and 0.6 mM by the time of replacement (360 min). The replacement solution had a PMS concentration of 0.6 mM with no noteworthy changes over 230 min. b) Change of Mn coating after different hours of total operation (here including the pre-exposure). ..... 104
- Figure 27: a) Dependence of Rh-B removal on PMS feed solution concentrations. "CFC" is the removal in the catalyst column, calculated based on the initial PMS/Rh-B feed concentration. "Feed" is the Rh-B removal in the feed bottle after ca. 75 min due to direct PMS reactions. Each data point represents one steady-state column experiment. b) PMS decomposition for different feed solution concentrations and the control (c) with 35 g washed sand. Asterisks indicate that removal was estimated using LOQ/4 as effluent concentration as PMS was below LOQ..... 105
- Figure 28: Removal of TORCs without observed direct PMS reactivity in TW (a) and WW (b) based on three independent experiments for each water matrix (n=3). "CFC" refers to the removal observed in the column and "Feed" to the removal observed in the feed bottle from start to end of the experiment (ca. 75 min). c) PMS (0.6 mM) decomposition in the same experiments..... 108
- Figure 29: Correlation of experimentally observed removal of six TORCs and the removal based on (multivariate) linear regression with their reported second order reaction

rate constants. Regression was performed a) with $\cdot\text{OH}$ and $\text{SO}_4^-$ , b) only $\text{SO}_4^-$ , and c) only $\cdot\text{OH}$ .....	109
Figure 30: Structural formulas of a) benzoic acid (BA) and b) 1,4-dioxane (DIOX)...	115
Figure 31: a) Removal of DIOX and BA in batch experiments as function of consumed ozone (assuming 100% consumption in BA batches). b) Residual dissolved ozone concentration after the experiment vs. the initial dissolved ozone concentrations for DIOX experiments.....	133
Figure 32: Removal of DIOX as function of ozone dose in batch experiments with two different solution volumes. ....	134
Figure 33: a) Comparison of measured ( $c_{\text{meas}}$ ) and calculated ( $c_{\text{cal}}$ ) concentrations at the effluent sampling port of the cross flow experimental set-up for different flow rates (1 - 7.2 L h <sup>-1</sup> ). $c_{\text{cal}}$ was determined using $k_d$ with the highest Pearson correlation coefficient $r$ ( $1.36 \cdot 10^{-4} \text{ s}^{-1}$ ). b) $r$ of $c_{\text{cal}}$ and $c_{\text{meas}}$ between $1 \cdot 10^{-9} \text{ s}^{-1} < k_d < 1 \cdot 10^{-3} \text{ s}^{-1}$ . ....	136
Figure 34: Absorbance change (258 nm) over time as directly measured in the measurement cell for a control without toluene (a) and two repetitions with 0.0082 mM toluene (b, c). ....	138
Figure 35: Schematic of the finite membrane piece and its dimensions. Water is flowing perpendicular to the membrane, as shown in the top view display. ....	143
Figure 36: Photolytic decay of 0.1 $\mu\text{M}$ pCBA in a UV-C control experiment with 10 mg/L BA and no $\text{H}_2\text{O}_2$ added. ....	144
Figure 37: Comparison of linearized BA removal vs. $\text{OH}$ exposure in UV/ $\text{H}_2\text{O}_2$ treatment, if calculated either using PRI ( $6.7 \cdot 10^9 \text{ M}^{-1} \text{ s}^{-1}$ Real et al. (2009)), GBP ( $9.1 \cdot 10^9 \text{ M}^{-1} \text{ s}^{-1}$ Lee et al. (2014)), or CBZ ( $5.85 \cdot 10^9 \text{ M}^{-1} \text{ s}^{-1}$ Pereira et al. (2007)) in case of UV/ $\text{H}_2\text{O}_2$ . The slopes of the different exposure data sets indicate that CBZ agrees best, both with ozonation experiments but also with the reported rate constants of benzoic acid and BTE.....	145
Figure 38: Control experiment with 0.1 $\mu\text{M}$ GBP, PRI and CBZ (0.05 $\mu\text{M}$ ) with 10 mg/L BA and no $\text{H}_2\text{O}_2$ added, exposed to UV-C light as in the oxidation experiments to demonstrate photo-resistance.....	145
Figure 39: a) Changes of BA concentrations and TOC vs. $\cdot\text{OH}$ radical exposure. b) additional biological degradation batch tests (b). ....	146
Figure 40: a) Proposed transformation pathway of benzene with first attack of $\cdot\text{OH}$ and subsequent ozone attack, resulting in short-chained aliphatic compounds (phenol ozonation adapted from Ramseier and von Gunten (2009)). Other intermediate products such as catechol or benzoquinone may form, and quantities may change depending on the ozone:benzene stoichiometry. b) Demonstration of increased reactivity of intermediates with ozone. Sources of reported reaction rate constants can be found in Table 15. ....	147

Figure 41: Removal of BTE as function of recirculated volumes in both oxidative treatment processes. Initial concentrations of BTE were 0.42/0.28/0.18 mM in the displayed UV/H <sub>2</sub> O <sub>2</sub> experiment (a), and 0.25/0.25/0.12 mM in the O <sub>3</sub> /H <sub>2</sub> O <sub>2</sub> experiment. Variations of initial BTE concentrations are observed due to losses during solution preparation. ....	153
Figure 42: Removal of (a) toluene in BTE oxidation experiments and (b) ethylbenzene (same experiments) as function of ·OH exposure. Second order reaction rate constants based on this data were 8.6·10 <sup>9</sup> M <sup>-1</sup> s <sup>-1</sup> or 8.3·10 <sup>9</sup> M <sup>-1</sup> s <sup>-1</sup> for toluene and 8.2·10 <sup>9</sup> M <sup>-1</sup> s <sup>-1</sup> or 8.5·10 <sup>9</sup> M <sup>-1</sup> s <sup>-1</sup> for ethylbenzene, if either UV/H <sub>2</sub> O <sub>2</sub> or O <sub>3</sub> /H <sub>2</sub> O <sub>2</sub> data is used. This agrees closely with 8.1·10 <sup>9</sup> M <sup>-1</sup> s <sup>-1</sup> (Schuler and Albarran, 2002), and 7.5·10 <sup>9</sup> M <sup>-1</sup> s <sup>-1</sup> (Buxton et al., 1988) as reported in the literature. ....	153
Figure 43: UV spectra of BTE oxidation experiments, O <sub>3</sub> /H <sub>2</sub> O <sub>2</sub> (a), and UV/H <sub>2</sub> O <sub>2</sub> (b). Numbers indicate the steps of oxidation (0 is no oxidation, the highest number is the highest dose).....	154
Figure 44: UV spectra of BA oxidation experiments for biological treatment, UV/H <sub>2</sub> O <sub>2</sub> (a), and O <sub>3</sub> /H <sub>2</sub> O <sub>2</sub> (b), Numbers indicate the steps of oxidation (0 is no oxidation, the highest number is the highest dose). ....	154
Figure 45: EEMs (a) before O <sub>3</sub> /H <sub>2</sub> O <sub>2</sub> oxidation (0b), (b) after oxidation (1b), after biological degradation (1b). ....	154
Figure 46. EEM after biological degradation of BA (sample (0a), not chemically oxidated).....	155
Figure 47: Transformation of BTE to phenol, o-cresol, and o-ethylphenol. ....	155
Figure 48: Exemplary products from phenol ozonation, as observed by Ye and Schuler (1989). ....	155
Figure 49: Fluorescence (320/450 nm) in the first 6 min of the HRMS run of (1a) before (purple line) and after biological degradation (green line). ....	156
Figure 50: Fluorescence (320/450 nm) in the first 6 min of the HRMS run of (0a) before (purple line) and after biological degradation (green line). ....	156
Figure 51: Fluorescence (320/450 nm) in the first 6 min of the HRMS run of (1b) before (purple line) and after biological degradation (green line). ....	156
Figure 52: Fluorescence (320/450 nm) in the first 6 min of the HRMS run of (0b) before (purple line) and after biological degradation (green line). ....	157
Figure 53: Fluorescence (290/410 nm) in the first 6 min of the HRMS run of (1a) before biological degradation (green line). ....	157
Figure 54: Test of long-term PMS decomposition of CFC2 that was used for Rh-B and TOrcs experiments after the shown exposure. ....	159
Figure 55: Additional SEM images of the coating of used CFC2 (a,b and c) and new CFC2 (d).....	160

Figure 56: Mn2p and C1 XPS scans of new MnO <sub>2</sub> @sand (a, b), used MnO <sub>2</sub> @sand (c, d), and unattached $\alpha$ -MnO <sub>2</sub> powder (e, f). .....	161
Figure 57: EDS analysis results of coated material (MnO <sub>2</sub> @sand), a) coating area, b) blank area on the same sand grain with no coating based on SEM micrographs... 162	162
Figure 58: Comparison of sand placed in the column used for experiments before and after the hydrothermal synthesis coating. ....	162
Figure 59: Control experiment with 35 g sand, as used for synthesis of coated sand material. Removal of 0.58 mM PMS was well below 10% over 120 min. ....	164
Figure 60: Adsorption test results (TW, no PMS) of compounds that are not directly reacting with PMS. ....	166
Figure 61: Correlation of experimentally observed removal of six TOrCs and the removal based on (multivariate) linear regression with their reported second order reaction rate constants. ....	170
Figure 62: Combined plot of the model fit to determine the species-specific reaction rate constant of deprotonated reactive species 3 (black line), the dissociation of GBP (blue color, y-axis on the right), assuming pKa1 = 3.68 and pKa2=10.7, and observed reaction rate constants at different pH values (red squares). ....	180
Figure 63: Investigated transformation pathways for the reaction of gabapentin with ozone, adapted from Lim et al. (Lim et al., 2019; Lim et al., 2022). All GBP-related compounds are displayed deprotonated. Compounds marked by an asterisk were detected and quantified, masses and fragmentation for suspected TP170 could be detected, but not confirmed by a standard. ....	181
Figure 64: Formation of NO <sub>3</sub> <sup>-</sup> and TP186 during ozonation of GBP (compound concentrations on the left y-axis, dissolved ozone concentration on the right y-axis, n=3). ....	182
Figure 65: a) Formation of both, labeled and unlabeled NOV and GBP TP186 as function of ozone dose in 18O experiments. The concentration of GBP TP186-18O for the lowest ozone dose was below the LOQ. b) Average share of labeled and not labeled NOV and GBP TP186 of the respective total concentration (n=7 for NOV, n=6 for TP186). ....	184

## LIST OF TABLES

Table 1: Selected oxidants and their characteristics in ISCO treatment processes. Adapted from Siegrist et al. (2011) and Huling and Pivetz (2006), and completed with PMS data. ....	5
Table 2: Selected water constituents and contaminants and their reactivity with sulfate radicals, ozone, and hydroxyl radicals. ....	7
Table 3: Membrane materials proposed for ozone delivery. ....	35
Table 4: Root mean square error and normalized root mean square error (RMSE and NRMSE) of $K_{exp}$ compared to $K_{cal}$ , calculated with the L�ev�eque solution and the Kreulen modification for all membrane materials, and the Gz range for every dataset. ....	41
Table 5: Mass transfer of different membrane modules for approximately the same liquid velocity. ....	45
Table 6: Second-order reaction rate constants of probe compounds used in this study.	64
Table 7: Direct comparison of in section 5.4.3.1 calculated and experimentally determined K and the difference based on $K_{cal}/K_{exp}$ for PTFE and PDMS membranes. ....	117
Table 8: List of compounds used throughout this study. ....	132
Table 9: Standard soil (A2.1) characteristics. ....	132
Table 10: Details of HSGC-FID method for 1,4-dioxane quantification. ....	132
Table 11: Additional data on removal of DIOX in control experiments. ....	134
Table 12: Indigo measurements in the effluent of experiments with BA and different porous media layers. ....	138
Table 13: Ozone exposure calculated with probe compound removal. ....	140
Table 14: Experimental conditions and calculated parameters for probe compound removal experiments. ....	141
Table 15: Second order reaction rate constants of benzene, phenol and reported TPs in ozonation of phenol with ozone and $\cdot OH$ radicals. ....	147
Table 16: List of all chemical substances used in experiments. ....	148
Table 17: Instrument settings of Agilent 7980 GC and Agilent 7697A HS module. ...	148
Table 18: HPLC-UV methods for detection of phenol, o-cresol, and o-ethylphenol and benzoic acid. ....	148
Table 19: UPLC-TOF methods for detection of TPs of benzoic acid. ....	149
Table 20: Results of $O_3/H_2O_2$ membrane ozonation experiment. ....	150
Table 21: Results of UV/ $H_2O_2$ experiment (1). ....	150
Table 22: Results of UV/ $H_2O_2$ experiment (2). ....	150
Table 23: Results of UV/ $H_2O_2$ experiment (3). ....	150

Table 24: Results of BA biological degradation experiments (DOC). .....	151
Table 25: Summary of identified compounds in HRMS analysis with proposed structure (if possible), time, and integrated peak area. ....	152
Table 26: Particle size distribution of washed sand used for synthesis. The sum of shown percentages is not exactly 100% as this is the mean value of two analyses. ....	158
Table 27: Overview on different synthesized batches and their use in experiments. ...	158
Table 28: Water quality parameters of a representative tap water (TW) sample withdrawn during the time of experiments. ....	163
Table 29: pH measurement of inflow and outflow in the longevity test. ....	163
Table 30: Removal of Rh-B in a control experiment with 0.6 mM PMS and 10 mg L <sup>-1</sup> Rh-B. ....	164
Table 31: Removal of Rh-B in a control experiment with 0.12 mM PMS, 10 mg L <sup>-1</sup> Rh-B and 50 mM TBA. ....	165
Table 32: Measured Mn concentrations in the inflow and effluent of various different experiments. ....	165
Table 33: Comparison of different PMS:Rh-B ratios used in selected studies to achieve a Rh-B removal of >90%. ....	165
Table 34: Adsorption test results (TW, no PMS) of all analyzed compounds. Adsorption >10% is highlighted in red color. ....	167
Table 35: Removal of TOrCs (WW, 0.6 mM PMS, n=3). The removal is related to the feed concentration before the start of the experiment. Removal higher than 20 % via direct PMS reaction is highlighted in red. ....	167
Table 36: Removal of TOrCs (TW, 0.6 mM PMS, n=3). The removal calculation is related to the feed concentration before the start of the experiment. Removal higher than 20 % via direct PMS reaction is highlighted in red. ....	168
Table 37: PMS concentrations as measured in TW and WW experiments (n=3). ....	169
Table 38: Representative pH values in the inflow and outflow for TOrCs oxidation experiments. ....	169
Table 39: Reported second order reaction rate constants of statistically evaluated compounds for reactions with sulfate and hydroxyl radicals. ....	169
Table 40: Computed sulfate and hydroxyl radical exposures for TW and WW (n=3 each) for all investigated scenarios. ....	171
Table 41: Observed second order reaction rate constants for gabapentin with ozone. The species-specific rate constant ( $k_{s3}$ ) was calculated by fitting rate constants and pK <sub>a2</sub> (10.7). ....	179
Table 42: Results of quantum chemical calculations for GBP, ethylamine, and glycine, grouped by reactions of the discussed primary amine / amino acid pathways. ....	186
Table 43: Removal of TOrCs in wastewater ozonation experiments. ....	187

## ABBREVIATIONS AND ACRONYMS

a	Specific surface area, $m^{-1}$
A	Average membrane surface area, $m^2$
AAS	Atomic absorption spectroscopy
ACN	Acetonitrile
AOP/AOPs	Advanced oxidation process(es)
$a_s$	Specific internal membrane surface area, $m^{-1}$
BA	Benzoic acid
BOD <sub>5</sub>	Biochemical oxygen demand in five days
BS	Baked sand
BTE	Benzene, toluene, and ethylbenzene
BTEX	Benzene, toluene, ethylbenzene, and xylene isomers
$c^*_{O_3,l}$	Saturation concentration in the liquid phase in equilibrium with the partial pressure in the gas phase, $mg\ L^{-1}$
$c_{A,l}$	Concentration of compound A in the liquid phase, $mg\ L^{-1}$
CBZ	Carbamazepine
CEC	Chemicals of emerging concern
CFC	Catalytic filtration column
$c_{g,in}$	Ozone gas concentration at the entrance of the membrane tube, $mg\ L^{-1}$
$c_{g,out}$	Ozone gas concentration at the exit of the membrane tube, $mg\ L^{-1}$
$c_{l,out}$	Dissolved gas concentration in the outflow
$c_{O_3,g}$	Gas-side ozone concentration, $mg\ L^{-1}$
$c_{O_3,int}$	Ozone concentration at the gas-liquid interface, $mg\ L^{-1}$
COD	Chemical oxygen demand
$c^r_{O_3,int}$	Ozone concentration at the gas-liquid interface in presence of a chemical reaction on the liquid side, $mg\ L^{-1}$
$c_{sat,in}$	Saturation concentration in the liquid phase in equilibrium with the partial pressure in the gas phase at the entrance of the membrane tube, $mg\ L^{-1}$
$c_{sat,out}$	Saturation concentration in the liquid phase in equilibrium with the partial pressure in the gas phase at the exit of the membrane tube, $mg\ L^{-1}$
$D_{A,l}$	Diffusion coefficient of reaction partner with an injected gas A in water, $m^2\ s^{-1}$
$\Delta c$	Characteristic concentration difference, $mg\ L^{-1}$
$\Delta c_{cr}$	Characteristic gas concentration difference between gas and liquid phase in a cross flow gas-liquid membrane contactor, $mg\ L^{-1}$
$D_{B,l}$	Diffusion coefficient of reactive gas B in water, $m^2\ s^{-1}$
$d_e$	Effective fiber diameter, m
$D_F$	Fick diffusion coefficient, $m^2\ s^{-1}$
$d_i$	Inner diameter of a hollow fiber, m
DI	Deionized
DIOX	1,4-dioxane
$D_k$	Knudsen diffusion coefficient, $m^2\ s^{-1}$
$D_{O_3,l}$	Diffusion coefficient of ozone in water, $m^2\ s^{-1}$
$D_{O_3,m}$	Effective diffusion coefficient of ozone in membrane pores, $m^2\ s^{-1}$
DOC	Dissolved organic carbon
E	Overall enhancement factor
$E_\infty$	Instantaneous enhancement factor
EBVT	Empty bed volumes treated
EEM	Excitation emission matrix
$E_l$	Enhancement factor on the liquid side
EPR	Electron paramagnetic resonance
ESI	Electrospray ionization
GBP	Gabapentin
Gz	Graetz number
Ha	Hatta number

$H_i$	Dimensionless Henry's law constant
$H_{O_3}$	Henry's law constant for ozone in water, $\text{mol m}^{-3} \text{Pa}^{-1}$
HPLC-DAD/HPLC-UV	High pressure liquid chromatography coupled with DAD detection
HPLC-MS	High pressure liquid chromatography coupled with mass spectrometry
HS-GC/FID	Headspace gas chromatography coupled with flame ionization detection
ISCO	In-situ chemical oxidation
J	Membrane flux, $\text{g m}^{-2} \text{s}^{-1}$ or $\text{mol m}^{-2} \text{s}^{-1}$
$J^r$	Membrane flux in presence of a chemical reaction on the liquid side, $\text{g m}^{-2} \text{s}^{-1}$ or $\text{mol m}^{-2} \text{s}^{-1}$
K	Overall mass transfer coefficient, $\text{m s}^{-1}$
$K_{a_s}$	Volumetric mass transfer coefficient in gas-liquid membrane contactors, $\text{s}^{-1}$
$k_{A,O_3}$	Second-order reaction rate constant of compound A with ozone, $\text{M}^{-1} \text{s}^{-1}$
$K_{cal}$	Calculated mass transfer coefficient, $\text{m s}^{-1}$
$k_d$	Pseudo first order ozone decay rate in water, $\text{s}^{-1}$
$K_{exp}$	Experimentally determined mass transfer coefficient, $\text{m s}^{-1}$
$k_g$	Mass transfer coefficient in the gas-side boundary layer, $\text{m s}^{-1}$
$k_l$	Mass transfer coefficient in the liquid-side boundary layer, $\text{m s}^{-1}$
$k_l a$	Volumetric mass transfer coefficient in a bubble forming unit, $\text{s}^{-1}$
$k_m$	Mass transfer coefficient in the membrane, $\text{m s}^{-1}$
$k_{OH}$	Second-order reaction rate constant of a compound with hydroxyl radicals, $\text{M}^{-1} \text{s}^{-1}$
$K^r$	Overall mass transfer coefficient in presence of a chemical reaction on the liquid side, $\text{m s}^{-1}$
$k_l^r$	Mass transfer coefficient in the liquid-side boundary layer in presence of a chemical reaction, $\text{m s}^{-1}$
L	Fiber length, m
LC-HRMS	Liquid chromatography coupled with high resolution mass spectrometry
MeOH	Methanol
N	Mass transfer rate, $\text{mg s}^{-1}$
NOM	Natural organic matter
PAH	Polycyclic aromatic hydrocarbon
PBS	Phosphate buffer solution
pCBA	Para-chlorobenzoic acid
$p_d$	Penetration depth of gas diffusion into the liquid phase, m
PDMS	Polydimethylsiloxane
PDS	Peroxydisulfate
PFAS	Per- and polyfluoroalkyl substances
$P_m$	Permeability, $\text{mol m}^{-1} \text{s}^{-1} \text{Pa}^{-1}$
PMS	Peroxymonosulfate
PP	Polypropylene
PRB	Permeable reactive barrier
PRI	Primidone
PTFE	Polytetrafluoroethylen
PVDF	Polyvinylidene fluoride
R	Universal gas constant, $\text{J mol}^{-1} \text{K}^{-1}$
Re	Reynolds number
Rh-B	Rhodamine B
RT	Retention time
Sc	Schmidt number
SEM	Scanning electron microscopy
SOM	Soil organic matter
SVOC	Semi-volatile organic carbon
t-BuOH/TBA	Tertiary butanol
$T_l$	Liquid-side temperature, K
TOC	Total organic carbon
TOrCs	Trace organic chemicals



TP	Transformation product
TW	Tap water
UPW	Ultrapure water
$v_g$	Gas velocity, $m\ s^{-1}$
$v_l$	Liquid velocity, $m\ s^{-1}$
VOC	Volatile organic carbon
WW	Wastewater
XPS	X-ray photoelectron spectroscopy
XRD	X-ray diffraction
$z$	Stoichiometric constant
$\epsilon_m$	Membrane porosity
$\theta$	Membrane pore tortuosity
$\nu$	Kinematic viscosity of water, $m^2\ s^{-1}$
$\nu_g$	Kinematic viscosity of oxygen, $m^2\ s^{-1}$
$\tau_m$	Membrane wall thickness, m
$\phi$	Hollow fiber module packing density

## 1 INTRODUCTION

Contaminated groundwater poses a great challenge to the protection of human health and the overall aquatic environment, as microbial contaminants and chemical substances of chronic or acute toxicity may on the one hand pollute water sources for human societies, and on the other hand cause long lasting damage on ecosystems and their services. Even though the microbial hazards in drinking water are considered most important due to their acute effects such as diarrheal diseases, exposure to chemicals can also be significant (WHO, 2022). For instance, it has been estimated that approximately 94 to 220 million people, most of them living in Asia, may currently be exposed to carcinogenic arsenic through drinking water from groundwater abstraction (Podgorski and Berg, 2020). Other very abundant inorganic chemicals in groundwater are, for example, nitrate ions that are released through various activities such as agriculture and waste disposal (Power and Schepers, 1989; Wakida and Lerner, 2005). Especially groundwater contamination by nitrate infiltration from excessive life stock farming practices has been recognized as severe problem in European countries such as Germany and Denmark (Ortmeyer et al., 2022) but also worldwide. Nitrate is also known for its adverse impact on health if exposed to chronically, and both substances are therefore regulated for drinking water supply in many countries (e.g., EU Drinking Water Directive).

In addition to inorganic chemicals, organic groundwater contaminants are especially concerning due to their large variety, new synthesis protocols and products, and often unknown transformation mechanisms that make analytical tracking of their occurrence and fate much more challenging. In the US, “Superfund Remedy Reports” are regularly published and provide information on frequently encountered groundwater contaminant groups. From 1981 to 2020, volatile organic carbon (VOC) was found in the groundwater of 86% of the contaminated sites, followed by metals (68%), and semi-volatile organic carbon (SVOC, 57%) (United States Environmental Protection Agency, 2023). VOC can, for example, consist of halogenated solvents (e.g., trichloroethene) or the commonly found benzene, toluene, ethylbenzene, and xylene isomers (BTEX) that can originate from gas stations, oil and gas drilling sites, or spills during industrial activities. (Gelman and Binstock, 2008; Gross et al., 2013; López et al., 2008). SVOC can be polycyclic aromatic hydrocarbon or phenols and may also originate from petroleum derived products and industrial discharges (Mohammadi et al., 2021; Peters et al., 1999).

Besides these largely known and studied types of organic contamination, new challenges have been identified from the early 2000s. To differentiate substances found in natural water bodies that were not analyzed or present before, the term “chemicals of emerging concern” (CEC) or “emerging (groundwater) contaminants” has become common (Luo et al., 2014; Stuart et al., 2012). For many of these CEC, such as traces of personal care products or pharmaceuticals, monitoring and risk assessment is being undertaken (Sharma et al., 2019), while other CEC may be subject to immediate remedial action. One prominent example is the global presence of poly- and perfluoroalkyl substances (PFAS) in groundwater, which are extraordinarily resistant to biological degradation and multiple other established treatment processes (Rahman et al., 2014; Xu et al., 2021a). Similarly, the ether 1,4-dioxane (DIOX) is known for its low biodegradability, high solubility in water and long persistence in the environment (Adamson et al., 2014; Adamson et al., 2015). It often co-occurs along with chlorinated solvents such as 1,1,1-trichloroethene (Adamson et al., 2014), which indicates it also may be present at some of the sites covered by the Superfund Remedy Reports. In general, the amount of CEC found in groundwater is not necessarily increasing because of elevated release, but foremost due to analytical advancements that allow product identification with extensive data base support and limits of detection in the very low  $\text{ng L}^{-1}$  range (Gaston et al., 2019; Richardson and Kimura, 2020). While CEC may require further attention and monitoring, substance prioritization needs to be addressed to identify relevant substances among thousands of chemicals that may partially be present only in low  $\text{ng L}^{-1}$  concentrations (Gaston et al., 2019).

The versatility of water qualities, contaminant types and concentrations, and hydrogeological conditions make the design of a remediation strategy largely a site-specific effort. Depending on the location and contaminant, the actual remediation goal and monitoring technique may vary greatly. Various technologies have been developed in the past decades to cope with the clean-up challenges. Among these, in-situ chemical oxidation (ISCO) is in particular an attractive group of processes, where reactive species are either injected or generated in the subsurface to react with dissolved target contaminants in a reactive zone (Siegrist et al., 2011). This allows the improvement of chemical water quality without expensive and energy-intensive extraction and purification of groundwater. The technology is based on chemical reactions and, therefore, allows a high degree of process control by choosing the right oxidant for the respective contaminant.

In this dissertation, innovative chemical oxidation treatment technologies based on ozone ( $\text{O}_3$ ), hydrogen peroxide ( $\text{H}_2\text{O}_2$ ), and peroxydisulfate (PDS) are explored as novel decontamination strategies with a focus on injection technology, activation mechanisms (i.e., generation of powerful radical species), and transformation product

(TP) formation and its implications for subsequent biodegradation. The dissertation is divided in two parts, where the first part introduces the concept of gas-liquid membrane contactors for in-situ ozone delivery and discusses the applicability for groundwater remediation using experimental and modeling tools. Briefly, membranes are proposed to be installed as permeable reactive barrier (PRB) in the saturated subsurface in order to cover an entire contaminated cross-section with constant ozone release. Additionally, TP formation in ozone-based treatment and biodegradability of TPs originating from monocyclic aromatic hydrocarbon is studied. The second part of the dissertation introduces another alternative treatment technology, namely heterogeneous catalytic activation of PMS on fixed bed catalytic media that can also serve as PRB, or is generally also applicable for unselective oxidative treatment as part of advanced water treatment, e.g., for removal of CEC that are present in trace concentrations below  $1 \mu\text{g L}^{-1}$  in many water sources (trace organic chemicals, TOrcs). Overall, this dissertation aims to both advance fundamental knowledge on transformation mechanisms in ISCO applications and explore the potential application of novel engineered treatment technologies.

## 2 STATE-OF-THE-ART

### 2.1 In-situ chemical oxidation

#### 2.1.1 Oxidant selection for ISCO treatment

In ISCO field applications, commonly applied oxidants are permanganate ( $\text{MnO}_4^-$ ), ozone ( $\text{O}_3$ ), peroxydisulfate (PDS,  $\text{S}_2\text{O}_8^{2-}$ ), and hydrogen peroxide ( $\text{H}_2\text{O}_2$ ) (Huling and Pivetz, 2006; Siegrist et al., 2011). Among these, ISCO treatment involving permanganate and hydrogen peroxide seem to be the widest applied based on field data in the US, however, also ozone- and persulfate-based treatment got more relevant in the early 2000s (Huling and Pivetz, 2006; Krembs et al., 2010). An overview of different oxidants and their characteristics is provided in Table 1. Less common but documented cases also exist, where sodium percarbonate ( $\text{Na}_2\text{CO}_3 \cdot 1.5\text{H}_2\text{O}$ ) and calcium peroxide ( $\text{CaO}_2$ ) have been tested or used for ISCO treatment. These are not further discussed here due to limited data and relevance for this dissertation (Siegrist et al., 2011). However, the persulfate salt peroxymonosulfate (PMS,  $\text{KHSO}_5$ ) is included in this section due to similar properties as peroxydisulfate and its potential to be activated by natural groundwater or soil constituents in ISCO treatment (Yu et al., 2016). The large amount of studies dealing with PMS and its activation using heterogeneous catalysts is discussed in section 2.2.

Activation in the context of ISCO means that the initially added oxidant is transformed into more powerful reactants, as direct reactions of the oxidant with the contaminant are often slow. In case of  $\text{H}_2\text{O}_2$ , activation would lead to the production of hydroxyl radicals ( $\cdot\text{OH}$ ) that have an oxidation potential of +2.8 V and react unselectively with a large variety of functional groups. In the ISCO context, this is typically achieved by reactions of  $\text{H}_2\text{O}_2$  with dissolved metal constituents in water that either occur naturally or are added to stimulate the process (Siegrist et al., 2011; Yang et al., 2020). Permanganate, conversely, only reacts directly with target compounds without activation to another species. Its advantage is the long lifetime, thus significant  $\text{MnO}_4^-$  concentrations can be delivered and distributed by diffusion, where it slowly reacts with selected contaminants (Siegrist et al., 2011; Struse et al., 2002). A special case is ozone, where not only aromatic parts of DOC or metal constituents but also ozone-self decay in water at neutral or alkaline pH lead to production of  $\cdot\text{OH}$  (Nöthe et al., 2009; von Gunten, 2003). In groundwater remediation, the aspect of activation of ozone through the organic

contaminant itself is rarely discussed in the scientific literature and one of the focuses of this dissertation (chapter 5).

Besides single oxidant approaches, there are also combinations of oxidants or novel activation methods that have been suggested or adapted from other applications such as the “peroxone” process ( $O_3/H_2O_2$ ), which is well known from the removal of trace organic chemicals (TOrcs) in municipal wastewater or surface water (Acero and von Gunten, 2001; Katsoyiannis et al., 2011). This has even been expanded to a combination of  $O_3$ ,  $H_2O_2$  and PDS in some groundwater remediation studies (Cashman et al., 2019; Cashman et al., 2022). Additionally, heterogeneous catalytic processes have gained great attention, where, for instance, PMS is activated by heterogeneous catalytic materials via surface reactions and this has also been suggested as alternative treatment approach for in-situ groundwater remediation recently (Wang et al., 2022b; Wang et al., 2022a).

Table 1: Selected oxidants and their characteristics in ISCO treatment processes. Adapted from Siegrist et al. (2011) and Huling and Pivetz (2006), and completed with PMS data.

Oxidant or combination of oxidants	Oxidant chemical	Primary reactive species	Activation	Form <sup>d</sup>
Permanganate	$KMnO_4$	$MnO_4^-$	None	Solid
Ozone	$O_3$ produced from air/oxygen	$O_3$ , $\cdot OH$	None, soil constituents <sup>a</sup>	Gaseous
Hydrogen peroxide	$H_2O_2$	$\cdot OH$	Iron ( $Fe^{2+}/Fe^{3+}$ ) or other metals in soil initiate Fenton reaction	Liquid
Peroxone	$O_3$ and $H_2O_2$	$\cdot OH$ , $O_3$	Reactions of $O_3$ and $H_2O_2$	Gaseous/liquid
Peroxydisulfate (PDS)	$Na_2S_2O_8$	$S_2O_8^{2-}$ , $SO_4^{\cdot -}$ , $(\cdot OH)^b$	Heat	Solid
Peroxymonosulfate (PMS)	$KHSO_5 \cdot 0.5KHSO_4 \cdot 0.5K_2SO_4$ (“Oxone”)	$HSO_5^-$ , $SO_4^{\cdot -}$ , $(\cdot OH)^{b,c}$	Heat, metals, catalytic materials	Solid

<sup>a</sup> Both organic and metal constituents of soil can potentially help activating ozone to hydroxyl radicals or other species (Lim et al., 2002; Ying et al., 2021). <sup>b</sup> Hydroxyl radicals can be produced by reactions of sulfate radicals with other parts of the water matrix, for instance chloride ions (Lutze et al., 2015). <sup>c</sup> Other activation mechanisms, for example mediated electron transfer or singlet oxygen generation have been reported (Shahzad et al., 2020; Shen et al., 2022; Zhang et al., 2022). <sup>d</sup> at 20°C and 1 atm.

The oxidant selection for treatment depends on various factors, however, most importantly on the reactivity of the generated or injected reactive species with the target contaminant and the potential scavengers or promoters being present either in soil or groundwater. As chemistry of individual oxidants is complicated and this dissertation is about ozone- and persulfate-based processes, the following discussion will focus on

mechanisms only relevant for these oxidants. Removal of an exemplary compound A is described as

$$\ln\left(\frac{c_A}{c_{A,0}}\right) = -k_{A,B} \int [B] dt \quad \text{Eq. 1}$$

where  $c_A$  is the contaminant concentration after oxidant exposure,  $c_{A,0}$  the initial contaminant concentration,  $k_{A,B}$  the second order reaction rate constant of A and oxidant B in  $M^{-1} s^{-1}$  and  $\int [B] dt$  the exposure of A to oxidant B in  $M \cdot s$ . Second order reaction rate constants of reactive species (see Table 2 for examples) with contaminants and scavengers can be used to (roughly) assess feasibility of treatment, since they provide a strong indication, first, if treatment generally is possible (not considering any competition), and, second, what scavenger(s) might become critical for operation. The exposure to the oxidant  $\int [B] dt$  is highly-scenario specific and depends on multiple primary and secondary reactions with all reactants present, and is extremely difficult to forecast.

Exemplary relevant scavengers for processes involving  $SO_4^{\cdot-}$ ,  $\cdot OH$ , and  $O_3$  are nitrite ( $NO_2^-$ ), carbonate/bicarbonate ( $CO_3^{2-}$ ,  $HCO_3^-$ ), metal ions ( $Fe^{2+}/Fe^{3+}$ ) or generally background dissolved organic carbon (DOC) that competes with the target contaminant (Table 2). In case of ozone, background DOC can also promote removal of target contaminants due to secondary  $\cdot OH$  production (Nöthe et al., 2009). Scavengers for the aforementioned processes are reactive with the oxidant or its activated form, but do not result in reactive species that could also contribute to contaminant removal. For instance, elevated water alkalinity (e.g., high bicarbonate/carbonate concentration) will severely reduce the  $\cdot OH$  or also  $SO_4^{\cdot-}$  available for any contamination in  $\cdot OH/SO_4^{\cdot-}$ -based processes. Reactions of  $\cdot OH$  with  $HCO_3^-$  and  $CO_3^{2-}$  result in carbonate radicals ( $CO_3^{\cdot-}$ ) that are not as unselective as  $\cdot OH$ , and especially in ozonation processes not important, as ozone already reacts fast with most compounds that would react with  $CO_3^{\cdot-}$  (von Gunten, 2003). Similar suppression of contaminant oxidation has been observed in presence of  $SO_4^{\cdot-}$  (Criquet and Leitner, 2009). Reactivity of  $HCO_3^-$  with  $\cdot OH$  is  $8.5 \cdot 10^6 M^{-1} s^{-1}$ , thus three orders of magnitude smaller than with most organic contaminants. However, it is typically present in concentrations up to several hundreds of  $mg L^{-1}$ , which is in most cases much higher than the organic contamination and important in second order reactivity considerations. The non-selective behavior of  $\cdot OH$  is reflected in its extremely short lifetime in water, where exposure typically amounts in values below  $10^{-9} M \cdot s$  during ozonation and UV/ $H_2O_2$  treatment of surface water (Rosenfeldt et al., 2006). Exposure of  $O_3$  and  $SO_4^{\cdot-}$  is typically higher as they react more selectively and are therefore more stable than  $\cdot OH$  (Lee et al., 2020).

The way second order reaction rate constants can be effectively used in order to select a treatment technology is demonstrated in some exemplary cases in natural water. For example, 1,4-dioxane (DIOX) is a compound where treatment with  $\text{SO}_4^{\cdot-}$  may be less successful compared with  $\cdot\text{OH}$ -based treatment in high alkalinity water without other major constituents. This is due to a second order reaction rate constant that is two orders of magnitude lower, whereas reactions of  $\text{SO}_4^{\cdot-}$  with alkalinity ( $\text{HCO}_3^-$ ) are even higher than in the case of  $\cdot\text{OH}$  (Table 2). A second example are benzene and toluene, where similar reactivities are reported for both radical species (Table 2). Similar as for the previous case, other scavengers in the water matrix are crucial. For example,  $\text{SO}_4^{\cdot-}$  generally reacts slower with natural organic matter as  $\cdot\text{OH}$  (Lei et al., 2022; Westerhoff et al., 1999) and, therefore, if water contains benzene and toluene and NOM,  $\text{SO}_4^{\cdot-}$  could be a good choice. It must be noted here that no general statement on background NOM reactivity with radical species can be made due to its highly variable composition. Reactivity of NOM isolates of different rivers, groundwater bodies, and lakes with  $\cdot\text{OH}$  has been found to vary considerably ( $k_{\text{OH}} = 2.6\text{-}8.1 \cdot 10^8 \text{ M}^{-1} \text{ s}^{-1}$ ) in ozonation experiments. NOM tends to be more reactive with  $\cdot\text{OH}$  and  $\text{O}_3$  with increasing specific ultraviolet absorbance, i.e., content of aromatic carbon (SUVA, absorbance at 254 nm divided by DOC in  $\text{mgC L}^{-1}$ ) (Westerhoff et al., 1999). A similar correlation could be established for  $\text{SO}_4^{\cdot-}$  (Lei et al., 2022). A third example is naphthalene as representative of PAHs, where the reactivity with ozone is 5 or 6 orders of magnitude lower as with  $\text{SO}_4^{\cdot-}$  and  $\cdot\text{OH}$  (Table 2). However, assuming that naphthalene is the only organic compound in the exemplary water, ozone exposures will be much larger, as scavenging of ozone by direct reactions with most inorganic constituents other than nitrite is very limited (e.g.,  $k_{\text{O}_3}$  of ozone and nitrate and bicarbonate is  $\ll 0.1 \text{ M}^{-1} \text{ s}^{-1}$ ). Therefore, this could – depending on the water matrix – potentially achieve better removal performance of naphthalene as with a process, where only  $\cdot\text{OH}$  is formed due to multiple scavenging reactions. In any case, a detailed water analysis and lab-scale experiments are needed to understand the oxidant dose–removal relationship.

Table 2: Selected water constituents and contaminants and their reactivity with sulfate radicals, ozone, and hydroxyl radicals.

	$k_{\text{SO}_4} (\text{M}^{-1} \text{ s}^{-1})$	$k_{\text{O}_3} (\text{M}^{-1} \text{ s}^{-1})$	$k_{\text{OH}} (\text{M}^{-1} \text{ s}^{-1})$	References
<b>Scavengers/promoters</b>				
$\text{HCO}_3^-$	$9.1 \cdot 10^6$	$<0.01$	$8.5 \cdot 10^6$	Neta et al. (1988), Buxton et al. (1988), Hoigné et al. (1985)
$\text{NO}_2^-$	$8.8 \cdot 10^8$	$3.7 \cdot 10^5$	$1 \cdot 10^{10}$	Neta et al. (1988), Hoigné et al. (1985)
$\text{NO}_3^-$	2.1	$<0.0001$	$<1 \cdot 10^5$	Neta et al. (1988), Hoigné et al. (1985), Keen et al. (2012)



Fe <sup>2+</sup>	9.9·10 <sup>8</sup>	8.2·10 <sup>5</sup>	3.2·10 <sup>8</sup>	Neta et al. (1988), Lögager et al. (1992)
Cl <sup>-</sup>	3.1·10 <sup>8</sup>	<0.001	4.3·10 <sup>9</sup>	Neta et al. (1988), Hoigné et al. (1985)
NOM	0.7-3.7·10 <sup>7</sup> <sup>a</sup>	n.a. <sup>a</sup>	2.6-8.1·10 <sup>8</sup> (mean = 3.6·10 <sup>8</sup> )	Lei et al. (2022), Westerhoff et al. (1999)
<b>Target contaminants</b>				
Benzene	3·10 <sup>9</sup>	2	7.8·10 <sup>9</sup>	Neta et al. (1988), Hoigné and Bader (1983a), Buxton et al. (1988)
Toluene	3.1·10 <sup>9</sup>	14	8.1·10 <sup>9</sup>	Merga et al. (1994), Hoigné and Bader (1983a), Schuler and Albarran (2002)
1,4-dioxane	1.6·10 <sup>7</sup>	0.32	2.8·10 <sup>9</sup>	Neta et al. (1988), Hoigné and Bader (1983a), Buxton et al. (1988)
Naphthalene	n.a.	3·10 <sup>3</sup>	1.2·10 <sup>10</sup>	Hoigné and Bader (1983a), Buxton et al. (1988)

<sup>a</sup> As sulfate radicals and ozone are more selective oxidants, the reactivity will highly depend on the DOC composition and should be evaluated for each case separately.

### 2.1.2 Oxidant and porous media interactions

Besides oxidant reactions with dissolved substances in water, the involvement of particulate matter is important to consider in case of ISCO operations. In fact, it can have a severe impact on the radius of influence of the oxidant that is in any case delivered from a limited number of points. Both O<sub>3</sub> and PDS are known to interact with natural porous media such as organic-rich clay and solid metal components (Siegrist et al., 2011; Tsitonaki et al., 2010). For O<sub>3</sub>, especially reactions with soil organic matter (SOM) and solid metal particles are of relevance. For instance, batch experiments with 20 g L<sup>-1</sup> soil (0.32 % TOC, 8,870 mg kg<sup>-1</sup> Iron) demonstrated accelerated ozone decay with a more than six times higher first order decay rate compared to the control without soil, and even after one hour of pre-ozonation substantially elevated decay rates were observed (Ying et al., 2021). Results from several studies indicate that both components (SOM and metal oxides) can be responsible for lasting ozone consumption and also in some cases for ·OH production, which would be a desired side-effect (Jung et al., 2004; Lim et al., 2002; Ying et al., 2021). Indeed, natural soil components have already been suggested for engineered catalytic ozonation systems (Kohantorabi et al., 2022).

Unfortunately, many reaction mechanisms in natural soil systems are still poorly understood and there is a limited amount of studies dealing with it. Therefore, the

estimation of the ozone or other oxidants radius of influence after injection in subsurface media is hard to undertake without any experimental data.

### 2.1.3 Conventional injection technologies

A large variety of oxidant delivery methods has been developed. Extensive field data analyses have previously been undertaken to identify the most common ones and assess their applicability for ISCO processes (Krembs et al., 2010). Most frequently, the oxidant was either directly pushed into the subsurface by a push probe technique or wells were drilled and injection took place via these wells. Unlike persulfate salts (dissolved) or  $\text{H}_2\text{O}_2$ , this is not applicable for gaseous ozone. Therefore, sparging wells are common and recommended for operation (Nimmer et al., 2000; Siegrist et al., 2011). A simplified scheme is shown in Figure 1, where ozone is generated on-site and the mixture of ozone/air is then pushed into the saturated porous media below the contaminant plume, where VOC is present in both, the saturated and unsaturated zone because of its volatility and lower density than water. Vapor extraction wells are also required as the sparging operation causes gas flows that may result in VOC release. In comparison, persulfate salts or  $\text{H}_2\text{O}_2$  can be injected in dissolved form and, therefore, some of the requirements for ozone injection do not apply.

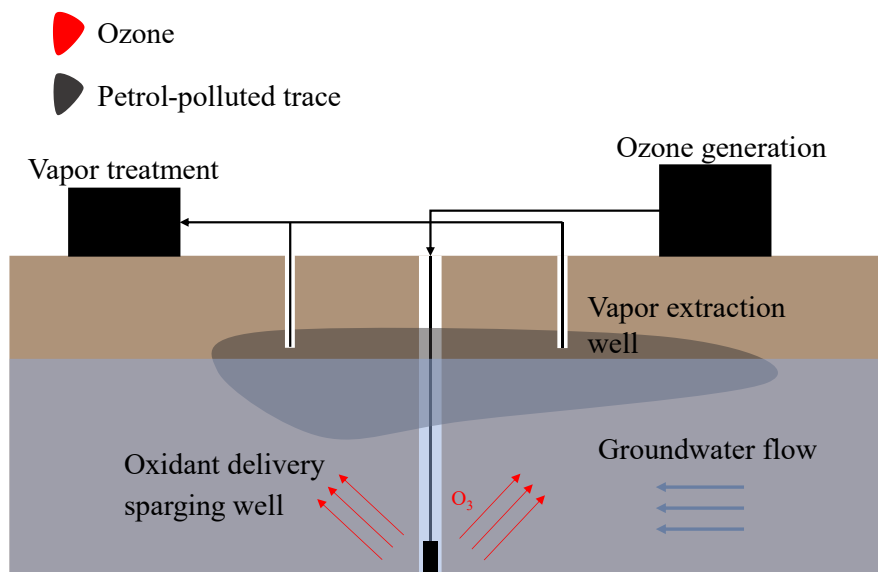


Figure 1: Simplified scheme of an ISCO treatment site using ozone through sparging wells, based on Reddy et al. (1995).

Sparging as injection technology, although common for ISCO treatment with ozone, has some disadvantages. Especially the phenomenon of air channeling, predominantly in fine porous media, can inhibit effective distribution of the oxidant (Clayton, 1998). Additionally, the aforementioned requirement to treat gas streams containing VOC as result of pushing gas into the ground makes operation complicated.

### 2.1.4 Gas-permeable membranes for passive ozone gas release – An effective new treatment technology?

The first part of this dissertation (chapters 4 and 5) investigates the potential to use gas-diffusing membranes for ozone distribution as novel and potentially advantageous ISCO process. An extensive review on the physical and chemical fundamentals of gas-liquid membrane contactors for ozone delivery is provided in chapter 4. Thus, this section intends to provide an overview on existing in-situ gas delivery approaches for groundwater remediation (oxidation, reduction, stimulation of biodegradation) and expected differences and potential advantages over conventional injection methods.

The key feature of gas-liquid membrane contacting is that gas is directly dissolved at the gas-liquid interface, therefore, no or very limited bubble formation is supposed to occur in the liquid phase (Gabelman and Hwang, 1999). In the proposed set-up, ozone is generated and then delivered to membrane tubing that is placed in the subsurface. This can either be a full excavation of a contaminated cross-section (Figure 2), where membrane tubing is placed as permeable reactive barrier (PRB), or vertical wells, where membrane modules with a high surface area are installed and distribute ozone. The membrane tubes can be designed with closed or open end. However, the unstable nature of ozone makes storage complicated and immediate usage desirable. Thus, operation with open gas exit and subsequent destruction of residual ozone seems easier because of the unnecessary temporary storages solution that would be needed in a closed end operation, where ozone is only removed from the membrane tubes via diffusion.

Both geometries have been tested at lab- and field-scale for other gases such as  $H_2$  and  $O_2$  but not for  $O_3$  (Chaplin et al., 2009; Edstrom et al., 2005; Gibson et al., 1998; Haugen et al., 2002; Patterson et al., 2004). Several lab-scale studies focused on modeling and performance analysis of passive  $H_2$  dissolution to stimulate biological nitrate reduction using hollow fiber membrane modules (Fang et al., 2002; Fang et al., 2004; Haugen et al., 2002; Schnobrich et al., 2007). This was later applied in two field-scale studies, where several hollow fiber membrane modules were installed in a contaminated aquifer to deliver hydrogen (Chaplin et al., 2009; Edstrom et al., 2005). In these studies, remedial goals, i.e., the effective reduction of contaminants was not achieved and the authors argued that  $H_2$  delivery was too small with the chosen membrane wells and the ongoing biological activity. Alternatively, Patterson et al. (2004) installed five polymer mat panels consisting each of  $24 \times 12$  m of PDMS tubing in a "flow-through box" (i.e., PRB) for in-situ oxidation of ammonium by oxygen delivery. After the start of operation, ammonium concentration within the PRB substantially decreased, coupled with increasing nitrate concentrations, which indicates successful nitrification. However,

downstream data was inconclusive and it was suggested that different water sources may have mixed.

The field studies highlight difficulties in designing the membrane system to fully cover the relevant contaminant plume and achieve spatially satisfying treatment. However, especially for ozonation the diffusion mechanism of gas-liquid membrane contactors could be highly advantageous, as all ozone will be directly dissolved and, therefore, immediately delivered to the contaminants, potentially resulting in better oxidant-contaminant-mixing as in active sparging operation. This is also important due to the short lifetime of ozone compared to other oxidants such as PDS/PMS or  $\text{H}_2\text{O}_2$ . Compared to aeration, there is a high interest in using  $\text{O}_3$  as efficiently as possible due to the high additional energy input. This could be achieved via passive dissolution by keeping a higher share of the gas dissolved in the liquid phase, whereas a large portion could directly leave the liquid phase in sparging operation. Furthermore, mass transfer can be controlled by the membrane surface and the ozone gas concentration, i.e., the partial gas pressure. However, it is largely unknown how the technology could be applied due to a lack of experimental data for ISCO. Thus, existing knowledge on  $\text{H}_2$  and  $\text{O}_2$  delivery cannot be directly transferred and experimental studies and modeling are required to assess the potential.

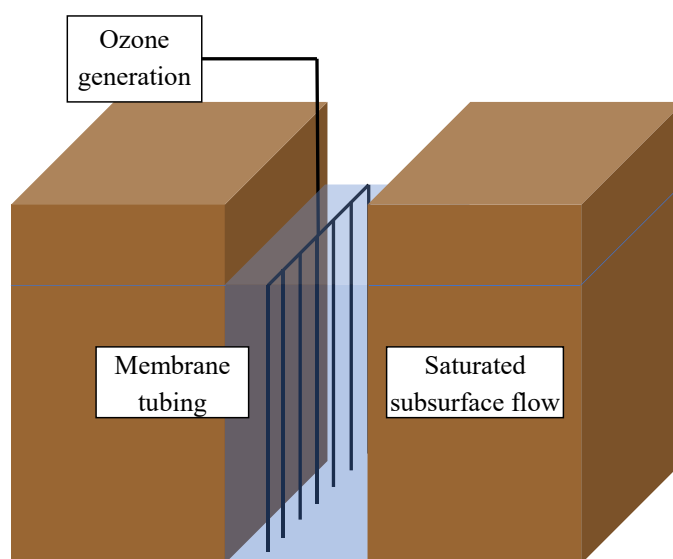


Figure 2: Scheme of a PRB consisting of membrane walls that are diffusing ozone to groundwater.

## 2.2 Immobilized catalysts for PMS activation

### 2.2.1 Activation mechanisms

Catalytic oxidation processes for water treatment, such as catalytic ozonation, Fenton and Fenton-like reactions or PMS/PDS activation by heterogeneous catalysts, are an

increasingly popular research topic (Hodges et al., 2018; Kohantorabi et al., 2021; Xiang et al., 2022; Yu et al., 2020). PMS activation has become one of the most popular research fields, as PMS is considered very reactive with heterogeneous (i.e., solid) catalysts due to its chemical properties (Lee et al., 2020). PMS salt (most commonly  $\text{KHSO}_5$ ) originates from “Caro’s acid” ( $\text{H}_2\text{SO}_5$ ) and has an asymmetrical structure with its peroxide group attached to a sulfate group, as compared to PDS, which is symmetrical (Wacławek et al., 2017). PMS has been found to be more reactive with various dissolved transition metals than for example PDS (Anipsitakis and Dionysiou, 2004). Consequently, numerous novel catalysts containing transition metals such as Co, Mn, and Cu were synthesized in the recent past and proposed as highly efficient treatment technology combined with PMS, and removal mechanisms have been investigated (Ahn et al., 2019; Amirache et al., 2021; Lin et al., 2017a; Marinescu et al., 2018; Park et al., 2018; Shahzad et al., 2020; Shen et al., 2022). There exists an exhaustive list of new composite materials with bases such as graphene oxide with other materials mixed in. This section does not aim to provide a comprehensive overview of all synthesis protocols and material advancements (the reader is referred to Kohantorabi et al. (2021) for an extensive list of studies) but aims to highlight controversies in the studies of activation mechanisms. In fact, different and partially contradictory results have been reported on radical species and activation mechanisms. Furthermore, to the author’s knowledge there is no systematic guidance available on how to choose a synthesis protocol for certain activation mechanisms and water treatment challenges, which emphasizes that the field is still in an explorative phase.

Various activation mechanisms have been reported in the past that are summarized in this section. It must be emphasized that from the author’s perspective, with few exceptions, the aim of catalytic water treatment processes involving persulfate salts should be the production of  $\text{SO}_4^{\cdot-}$  and/or  $\cdot\text{OH}$  radicals, as they are some of the most potent radical species that are capable of decomposing a large variety of organic contaminants (Lee et al., 2020; Wacławek et al., 2017). This is especially important for emerging challenges in water and wastewater treatment, such as the removal of CECs that have multiple structures with more or less reactive functional groups. State-of-the-art processes, e.g., ozonation, already prove capable of producing  $\cdot\text{OH}$  in an energy-efficient way (Miklos et al., 2018b). In case of PMS, formation of both powerful radicals ( $\text{SO}_4^{\cdot-}$  and  $\cdot\text{OH}$ ) is stoichiometrically possible without other external reactants than catalysts that donate electrons (see section 7.2, Eq. 23-25). This was experimentally demonstrated for example by Wang et al. (2015), where phenol was degraded by PMS and  $\text{MnO}_2$ . In this study, quenching experiments showed moderate inhibition of phenol degradation with *t*-BuOH (reacts selectively with  $\cdot\text{OH}$ ) and stronger inhibition in presence of ethanol (reacts with  $\cdot\text{OH}$  and  $\text{SO}_4^{\cdot-}$ ). Additionally, a strong TOC reduction by over 80% could be achieved, which is a strong indication of unselective radical attack.

Contrary to  $\cdot\text{OH}/\text{SO}_4^{\cdot-}$ -based processes, “selective oxidation” has by some authors been considered as major goal to prevent undesired by-product formation that can occur in unselective oxidation of organic matter (Yang et al., 2021). One group of selective oxidation mechanisms are “non-radical pathways” that have been described in different studies (Shahzad et al., 2020; Shen et al., 2022; Zhang et al., 2022). A key feature is that compound removal is observed without detection of any radical species and little PMS consumption. Also, strong TOC reduction due to accumulation of TPs on the catalyst surface (i.e., no mineralization) was reported (Zhang et al., 2022). It is believed that in this mechanism, electrons are directly transferred from an organic compound to PMS, effectively oxidizing the contaminant without other reactive species, and is therefore also called mediated electron transfer (Lee et al., 2020). However, from the author’s perspective, the practicability of “selective oxidation” outside of the laboratory has not been demonstrated yet, since all selective removal mechanisms thus far were only capable of removing highly electron-rich unsaturated compounds, and selectivity for other contaminant groups could not be achieved. Furthermore, it is unclear in which actual real-world scenario the removal of only activated compounds is desirable, while other organic compounds persist in the water.

Aside from that, several research groups reported alternative removal mechanisms, where for example singlet oxygen ( $^1\text{O}_2$ ) or superoxide radicals ( $\text{O}_2^{\cdot-}$ ) are formed from catalytic PMS activation (Guo et al., 2019; Li et al., 2019b; Ma et al., 2018; Shahzad et al., 2020). Some results have raised doubts regarding these alternative removal mechanisms. The interpretation of experimental data to claim that  $^1\text{O}_2$  can be a potent oxidant has recently been questioned by Lee et al. (2020). For example, l-histidine has been used as selective  $^1\text{O}_2$  scavenger to prove its contribution, however, it is also known to decompose PMS directly (Yang et al., 2018b).  $^1\text{O}_2$  is highly selective and can react with unsaturated organic compounds and some phenolic structures (Frimer, 1979). However, it seems doubtful that  $^1\text{O}_2$  is able to mineralize organic contamination, i.e., lead to a substantial reduction of TOC, as it has been reported for oxidation of for example 2,4-dichlorophenol, Rh-B, and methylene blue (Guo et al., 2019; Li et al., 2019b), which would include the attack of aliphatic intermediate products. Furthermore, inconsistency between quenching tests and radical signals from electron paramagnetic resonance (EPR) data were recently pointed out by Wang et al. (2021), which can lead to further confusion for the identification of the actual reactive species.

The variety of synthesis protocols and experimental results can cause confusion. For example, there are cases where mediated electron transfer and radical-driven oxidation were both reported for the same material ( $\alpha\text{-MnO}_2$ ) with PMS, which could mean that slight differences in catalyst synthesis change the entire process (Shen et al., 2022; Wang et al., 2015). This demonstrates that the interpretation of experimental data on formation

of reactive species and reproducibility is challenging and it is further challenged by the fact that multiple studies chose to work with structurally differing model contaminants such as rhodamine B (Rh-B), carbamazepine (CBZ), AO7 dye, different chlorophenols, or bisphenol A (Kohantorabi et al., 2021). Generally, there is a lack of standardization that makes different experiments comparable, e.g., pH adjustment and buffer selection, contaminants and their concentration, and catalyst concentration (and how the catalyst concentration is defined). Some of the aforementioned compounds, e.g., bisphenol A, are besides with  $\cdot\text{OH}$  and  $\text{SO}_4^{\cdot-}$  also very reactive with more selective oxidants such as singlet oxygen ( $^1\text{O}_2$ ) (Lee et al., 2020). Yang et al. (2018a) could show that bisphenol A was successfully degraded without the involvement of  $\cdot\text{OH}$  and  $\text{SO}_4^{\cdot-}$  using a  $\text{Fe}^0$ -montmorillonite/PMS system by quenching  $\cdot\text{OH}$  and  $\text{SO}_4^{\cdot-}$  with tertiary butanol (t-BuOH) and methanol, claiming that  $^1\text{O}_2$  and  $\text{O}_2^{\cdot-}$  were responsible for removal. However, it is unclear how the reaction would proceed if compounds resistant to  $^1\text{O}_2$  would be present in the same experimental set-up. The reaction with  $^1\text{O}_2$  may dominate, while  $\cdot\text{OH}$  or  $\text{SO}_4^{\cdot-}$  could still be important for reactions with other contaminant types. Overall, the field is advancing material synthesis, but some experimental standardization seems to be crucial to approach practical applications in large scale.

### 2.2.2 The challenge of immobilizing catalysts

For any large-scale application, multiple other aspects than oxidation performance must be considered, and one of the greatest challenges is the design of a process with catalyst retention. Different separation solutions have been discussed, for example design of magnetic catalysts that can be separated from the treated effluent through magnetic forces (Gómez-Pastora et al., 2017) or membrane separation to retain the powdered material (Zhang et al., 2011) (Figure 3a). Membrane separation may be a general solution for catalyst retention; however, it severely reduces the flexibility of process design, i.e., establishing a membrane-free process that requires less pumping energy. In contrast, the approach chosen in the experimental part of this dissertation aims for an immobilization of the catalytic surface on a support material, as shown in Figure 3b (Borovik et al., 2020). There exist examples of coating strategies with natural sand, zeolite, or carbon felt as support (Devi et al., 2014; Gümüş and Akbal, 2017; Xu et al., 2021b). In the listed studies, immobilization was achieved by integrating the support structure in the synthesis protocol and precipitating the catalyst on the structure. The potential advantage of immobilized catalytic structures could be that the water to be treated can be guided through the catalyst column with less turbulence compared to a stirred reactor, as no mixing is required, which could minimize physical detachment and leaching. Despite some suggested solutions how to tackle immobilization problems, most studies to date do not include this aspect in their study design and to the author's knowledge, there is very limited documented knowledge

on how immobilized catalysts perform in more application-oriented process designs. It also remains unclear if some of the studied catalysts are even suitable for catalyst immobilization. Thus, finding the right immobilization technique remains a challenge that deserves more attention in future catalytic oxidation research efforts.

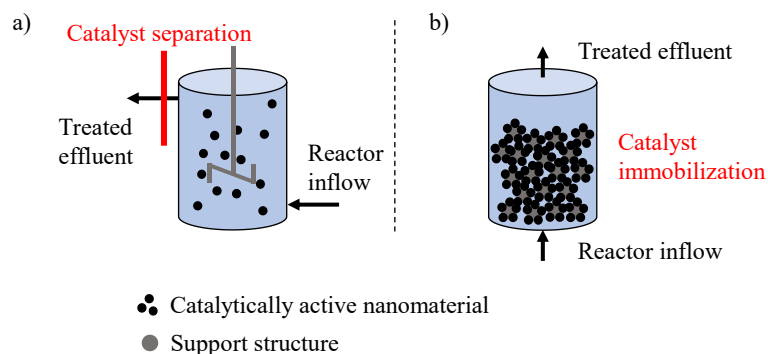


Figure 3: Schematic of two different upscaling approaches, a) catalyst separation, b) catalyst immobilization on support structure.

### 2.2.3 Potential fields of application

One of the main advantages of catalytic activation of PMS (or other oxidants), especially in an immobilized configuration, is that there is no need for additional on-site energy input, making it very promising for decentralized and small-scale water treatment systems (Mauter et al., 2018). The potential treatment objectives could be the partial mineralization of highly toxic organic contamination by radical generation for facilitated post-treatment, or disinfection of hazardous microorganisms (Hodges et al., 2018; Mauter et al., 2018). Additionally, catalytically active granular material possesses potential to be used for ISCO as part of a PRB. By choosing a material that is more permeable than the surrounding aquifer, water can be driven to the PRB and forced through the reactive material (Thiruvengkatachari et al., 2008). In a traditional PRB definition, reactive material is installed with the aim of provoking direct reactions of material and contaminant (Thiruvengkatachari et al., 2008), whereas in this approach previous injection of an oxidant is required and the PRB serves only as oxidant activation zone. This has already been suggested in some studies with PDS and copper oxide or sulfidized  $\text{Fe}^0$  (Cho et al., 2022; Rayaroth et al., 2020; Yin et al., 2022). In case of the tested  $\text{Fe}^0$ , oxidation to  $\text{Fe}^{2+}$  is observed, making it a finite reaction compared to a catalytic, i.e., continued oxidation in a full redox cycle (Rayaroth et al., 2020). Therefore, material replacement must be taken into account for long-term operation.

While PRBs are not new and have been applied in remediation (United States Environmental Protection Agency, 2023), the concept of coupling an oxidant and a subsequent catalytic barrier for planned and regionally limited oxidant activation is a



recent development and may become more feasible with the increasing progress in developing and understanding catalytic materials that have a minimum of adverse side-effects to the environment.

### **2.3 Fate of organic transformation products after oxidative groundwater remediation**

The majority of studies on ISCO focus on the removal of the target contaminant. However, chemical oxidation typically results in TPs, as substantially larger doses are required to achieve full mineralization to inorganic products (Hodges et al., 2018). It is well known that for example ozonation can increase the biodegradability of the residual organic matter (Hammes et al., 2006; Hübner et al., 2012; Hübner et al., 2014; Hübner et al., 2015a; Zucker et al., 2018). This is the case for overall wastewater DOC but also generally believed to be the case for most TOrCs that can be found in WWTP effluent. Modern analytical tools and the progress made in analyzing TPs allow a differentiated picture of that generalized assumption. Hübner et al. (2015a) conducted a review of TP formation in ozonation of TOrCs and the potential for subsequent biodegradation using experimental data on TP formation and structure-based modeling tools (BIOWIN and UM-PPS). Modeling indicates that biodegradability of TPs of olefinic and some aromatic compounds (if ring cleavage takes place) is improved compared to their parent compounds. Contrarily, tertiary amines are oxidized to an N-oxide, which is typically biologically transformed back to a tertiary amine, therefore, no advantage seems to be gained. Complete mass balances of ozonation reactions could not be successfully established in most studies aiming to analyze the TPs (Hübner et al., 2015a). This is implying that most TPs may not even be tracked analytically and their fate remains unknown. In a more recent experimental study, Gulde et al. (2021) spiked 51 micropollutants into lake water which was then ozonated at different doses and filtered through a pre-conditioned sand column for biological post-treatment. Samples were analyzed for TPs using high-resolution MS coupled with HPLC, providing a more thorough picture of transformation. In fact, only a small fraction of detected TPs (35 out of 187) were abated in the biological post-treatment and of those, only 24 were abated better than their parent compounds. It was also concluded that many TPs were probably not identified by the analytical methods and, therefore, the synergistic effects of ozonation and biodegradation could be better than quantified. Nevertheless, a substantial amount of persistent TPs remained after ozonation. Thus, it cannot be generalized that chemical oxidation under all circumstances increases biodegradability.

While transformation of organic contaminants in oxidative treatment of wastewater is a heavily investigated subject matter, surprisingly few studies have incorporated the extent of organic matter removal, respectively the formation of persistent transformation

products in their proposed ISCO treatment. Individual studies looked into oxidation of single compounds and transformation mechanisms with more or less established processes. For example, Cui et al. (2017) studied oxidation of ethylbenzene in a modified sodium percarbonate-Fe(III) system and found several hydroxylated intermediate products by high-resolution MS. Similarly, Hatipoglu et al. (2010) investigated transformation of toluene in a photo-Fenton process. Concerning persulfate-based processes, van Buren et al. (2021) could recently show that organosulfates were formed in case of 25 out of 28 mostly aromatic groundwater contaminants. Furthermore, the presence of nitrite during persulfate-based ISCO treatment of phenolic substances can lead to nitro-compounds by formation of nitrite radicals, which may even lead to more toxic TPs (Ji et al., 2017). Most of the reaction chemistry of a large portion of groundwater contaminants, e.g., reactivity with the oxidant and possible reaction mechanisms, may be understood by general progress in reaction chemistry (e.g., Lim et al. (2022), von Sonntag and von Gunten (2012)). A link, however, between transformation product formation, their microbial abatement and the parent compounds fate in a biological system in direct comparison is generally missing in the ISCO context. In an extensive review, Sutton et al. (2011) discuss the general potential to successfully couple ISCO and bioremediation. Most studies listed and analyzed nevertheless focused on improved removal of parent compounds and not a more successful overall remediation in terms of mineralization (Cassidy et al., 2009; Nam et al., 2001). It would be insightful to conduct studies that include the monitoring of transformation products and the overall fate of organic matter.

A pressing question is the fate of microbial life after the injection of harsh oxidants such as PDS/PMS or O<sub>3</sub>, where a substantial inactivation is to be expected due to the known disinfection performances. However, some studies could show that microbial activity could regenerate after chemical oxidation events using PDS or O<sub>3</sub> (Liang et al., 2009; Sutton et al., 2014). Additionally, inactivation may only be relevant at close distance to the injection points, whereas downstream microbial life may be unaffected by the oxidant injection and activation in the subsurface. This is especially the case for ozonation which has a short lifetime compared to H<sub>2</sub>O<sub>2</sub> or permanganate and also the PRB approach discussed in 2.2.3, where PMS is immediately activated within the catalytic granular layer.

## **2.4 Bioremediation as alternative to ISCO approaches?**

As pointed out in 2.1, ISCO processes are established and versatile in their application. One clear advantage is that the oxidant can be chosen with respect to the contaminant type and the dose controlled in order to achieve a satisfying breakdown of the targeted substance. It comes along with substantial investments in chemicals and equipment and, therefore, alternative remediation may exist or be subject to future

development that require less energy. This section focuses on bioremediation as a potentially resource-saving alternative. According to the Superfund remediation program, bioremediation was the most frequently chosen in-situ treatment approach for groundwater 2018-2020 (United States Environmental Protection Agency, 2023).

Contaminants that show potential for bioremediation and very recalcitrant compounds must be differentiated. For instance, bioremediation of the so called “forever chemicals” PFAS seems to be extremely challenging due to the limited abilities of microorganisms to perform defluorination as compared to dechlorination (Wackett, 2021). However, conventional chemical oxidation can also be largely excluded for these chemicals. In contrast, multiple contaminants found in the environment such as BTEX or chlorinated solvents (trichloroethene, TCE) show potential for biodegradation, especially if stimulating measures are taken. Strategies for bioremediation can largely be grouped in augmentation, where isolated species known to be capable of degradation are added to the site, and modification of the physical/chemical condition at the site (Ritter and Scarborough, 1995). While the first approach shows great potential with further developments in analyzing and isolating microbial communities, the latter one can be straightforward. For instance, BTEX are biodegraded well up to concentrations of several hundred mg L<sup>-1</sup> in the right chemical/physical conditions, i.e., aerobic environments (El-Naas et al., 2014; Farhadian et al., 2008; Kao et al., 2006). Aerobic environments are typically better for BTEX degradation because of the thermodynamically less favored hydroxylation of the aromatic ring in an anaerobic pathway, while (di-)hydroxylated intermediates as a result are crucial for further breakdown of the aromatic ring by cleavage between two hydroxy-groups (Cao et al., 2009). Such an establishment of oxic conditions can also be achieved by oxygen release via gas-permeable membranes, as demonstrated in the past (Gibson et al., 1998). The advantage of sole bioremediation by stimulating the redox conditions is the potential establishment of a bacterial system capable of cleaving the aromatic ring, while chemical oxidation may result in intermediates that are not biodegradable at all. As discussed in 2.3, this aspect is hardly discussed in the literature. TCE can also be degraded by stimulating aerobic or anaerobic biodegradation, for example by providing oxygen or using the presence of other suitable organic nutrients, respectively (DeWeerd et al., 1998; Pant and Pant, 2010). The stimulating conditions, for example oxygen introduction, are often less chemically intense than ISCO processes, where large amounts of aggressive chemicals have to be supplied. Unfortunately, it is very difficult to elaborate clear advantages of different approaches over another due to the site specifics and the uniqueness of each remediation case. Overall, the data available indicates a preference of bioremediation over ISCO. However, it cannot be derived that biodegradation is generally preferred, as the contaminant type is

not included in this statistic and may have heavily impacted the decision-making in the individual contamination scenarios.

## **3 RESEARCH OBJECTIVES, HYPOTHESES, AND DISSERTATION STRUCTURE**

### **3.1 Research objective 1**

#### **Review membrane material and mass transfer analysis to determine critical process requirements of gas-liquid membrane contactors for ozone dissolution in water**

Several experimental studies exist on testing of gas-liquid membrane contactors for ozonation of water, however, information on scale-up and long-term operation is scarce. To cope with this gap, a literature review was conducted for the identification of ozone-resistant materials with the aim to minimize membrane resistance, while allowing high ozone mass transfer from the gas to the liquid phase. Therefore, existing studies on ozone mass transfer were collected and mass transfer data was compared in parallel flow contactors, which was the most abundant module design and thus allowed a wide comparison. By using dimensionless correlations of mass transfer, membrane geometry, and hydraulics, it was possible to identify materials performing better or worse, completing existing knowledge on ozone mass transfer for water and wastewater treatment. Furthermore, used materials were assessed with respect to their chemical stability and availability. The literature review enabled selection of membrane materials and gas-liquid membrane contacting designs for a follow-up lab-scale investigation for ISCO treatment of organic contaminants.

### **3.2 Research objective 2**

#### **Evaluate the operation of ozone-releasing gas-liquid membrane contactors for ISCO applications with different contaminant types and porous media effects**

The aim of this research objective was to validate that ozone-diffusing membranes installed in-situ for ISCO treatment are capable of removing different contamination types under simulated realistic conditions. This also helps in understanding largely unknown roadblocks for the application of the technology. Realistic conditions here mean a groundwater matrix, contaminant concentrations of 5 mg L<sup>-1</sup>, and creeping groundwater-like flow conditions (< 200 cm d<sup>-1</sup>). Two groups of contaminants were investigated whose treatment with ozone is distinctly differing from each other, namely deactivated monocyclic aromatic and saturated aliphatic compounds. The intermediates formed during oxidation of monocyclic aromatic compounds are highly reactive with

ozone and, therefore, consume a lot of ozone, which is in stark contrast to saturated aliphatic compounds. Representatives of those groups were benzoic acid (aromatic) and 1,4-dioxane (aliphatic).

An additional part of this objective was to investigate the ozone mass transfer into creeping flow conditions with varying flow velocity and different generally suitable membrane materials. Herein a novel indicator compound method was used to measure ozone exposure and later converted into ozone mass transfer from membrane to the liquid phase.

Two hypotheses were formulated to evaluate the questions raised in *research objective 2*:

*Hypothesis 2.1: Removal of benzoic acid (concentrations  $\geq 5 \text{ mg L}^{-1}$ ) as monocyclic aromatic compound is not affected by ozone-reactions with different subsequent porous media layers in membrane-based ISCO treatment with ozone due to fast reactions of aromatic intermediate products in proximity of the point of ozone release, whereas removal of aliphatic 1,4-dioxane changes by soil properties due to the promoting or inhibiting effects of ozone-soil reactions.*

*Hypothesis 2.2: Ozone membrane mass transfer in simulated groundwater flow conditions can be accurately predicted ( $\leq 20\%$  difference) using empirical dimensionless correlations set up for different gases and membrane materials.*

A bench-scale experimental set-up was used to test hypothesis 2.1, investigating removal of the model contaminants in steady-state conditions with different subsequent porous media layers that are either reactive or inert in presence of dissolved ozone. Furthermore, the same experimental set-up was also used to determine experimental mass transfer coefficients to test hypothesis 2.2.

### **3.3 Research objective 3**

**Investigate the potential synergies of different reactive oxygen species in ozone-based advanced oxidation processes ( $\text{O}_3/\text{H}_2\text{O}_2$ ) on the transformation of monocyclic aromatic hydrocarbon**

Although ozone-based AOPs (standalone  $\text{O}_3$  and  $\text{O}_3/\text{H}_2\text{O}_2$ ) have been employed for large-scale remediation of groundwater contaminated with monocyclic BTEX compounds, the exact transformation mechanisms are not well understood. Potential synergies of ozone and hydroxyl radicals formed at the same time may be a distinguishing feature of ozone-based AOPs compared to other AOPs that do not involve ozone. These synergistic advantages could be follow-up reactions of ozone-reactive intermediates that

are known to be formed in AOPs involving monocyclic aromatic compounds. Two hypotheses were formulated to investigate potential advantages of ozone-based AOPs (here  $O_3/H_2O_2$ ) over processes only involving hydroxyl radicals as main reactant (here UV/ $H_2O_2$ ).

The first difference and potential advantage of  $O_3/H_2O_2$  is the suspected formation of smaller and less aromatic TPs in ozone-based treatment compared with UV/ $H_2O_2$  based on known reactions chemistry in both AOP types. An additional question is whether such differences in the transformation product profile also result in different biodegradability of the residual DOC. Although biodegradation of oxidized monocyclic aromatic hydrocarbon has been studied before, mineralization is far less known. This is especially complicated due to the analytical challenges around measuring volatile DOC. Therefore, non-volatile benzoic acid is chosen as model compound here for further biodegradation experiments.

***Hypothesis 3.1:*** Oxidation of monocyclic aromatic hydrocarbon using  $O_3/H_2O_2$  treatment leads to less formation of hydroxylated aromatic transformation products compared to UV/ $H_2O_2$  treatment if compounds are exposed similarly to hydroxyl radicals.

***Hypothesis 3.2:*** If benzoic acid as monocyclic aromatic model compound is similarly removed by  $O_3/H_2O_2$  and UV/ $H_2O_2$  treatment, remaining DOC is mineralized better after the ozone-based treatment in subsequent aerobic biodegradation tests.

To test hypothesis 3.1, benzene, toluene, and ethylbenzene (BTE) were treated in a closed loop configuration, where buffered solutions were constantly recirculated and treated either with  $O_3/H_2O_2$  or UV/ $H_2O_2$ . Samples were analyzed for formation of hydroxylated intermediates and absorbance changes to distinguish the degree of breakdown of the parent compounds in both processes.

Hypothesis 3.2 was tested by employing the experimental set-ups used for hypothesis 3.1 as a first step to oxidize benzoic acid. Experimental conditions were chosen in order to achieve similar hydroxyl radical exposure in both AOPs ( $O_3/H_2O_2$  and UV/ $H_2O_2$ ). Subsequently, biological degradation was studied in shake batch experiments, where mineralization of oxidized benzoic acid was measured by analyzing DOC concentrations over time.

### 3.4 Research objective 4

#### Explore PMS-based catalytic oxidation processes for unselective removal of organic contaminants

Catalytic oxidation processes are a set of emerging technologies that are researched as they potentially enable highly efficient on-site treatment of recalcitrant contaminants without external energy input. As extension of the ozone-based treatment technologies, a catalytic process for activation of peroxydisulfate (PDS) is discussed with the focus on establishing an immobilized process solution with lasting activity. Besides process stability, the question is whether the process is capable of removing a wide range of contaminants, which is mainly determined by the functional groups present and the radical species produced by reactions of catalyst and oxidant (PDS).

*Hypothesis 4.1: A newly synthesized immobilized MnO<sub>2</sub> catalyst activates pre-dosed PDS to form sulfate radicals for unselective oxidation*

To test hypothesis 4.1, a synthesis protocol was developed to stably attach MnO<sub>2</sub> of desired morphology and crystallinity onto technical sand, which is then used as a “catalytic filtration column”. Subsequently, this column was integrated to an experimental set-up to investigate compound removal by PDS-activation. Various settings were tested to prove on the one hand lasting catalytic performance, and on the other hand limited unwanted side effects such as catalyst leaching. Furthermore, sulfate radical formation was tested with a statistical analysis of second-order reaction rate constants of chemicals containing various functional groups and observed compound removal.

### 3.5 Dissertation structure

The results of this dissertation are based on one critical review article and three original research articles (**Articles I-IV**) that underwent a peer-review process and are already published. Each results chapter of this dissertation comprises one of the articles. Additionally, another article (**Article V**) that is not part of the main body of this dissertation contains the determined second-order reaction rate constant of gabapentin, which is important input for the methodology of chapter 5, and is, therefore, appended as author’s version.

Chapter 4 comprises **Article I**, which is a critical review article, and addresses research objective 1. It contains a thorough overview on engineering design of gas-liquid membrane contactors for ozonation and analyzes mass transfer data. Chapter 5 comprises **Article II** and includes testing of hypotheses 2.1 and 2.2, where the effect of contaminant



and soil properties on removal performance of in-situ treatment with ozone permeable membranes as well as ozone mass transfer were investigated. This is coupled with a modeling approach applying validated mass transfer equations, that can be used for scale-up considerations of ISCO with this type of gas-liquid membrane contacting technology. Chapter 6 consists of **Article III**, which is centered around transformation mechanisms of monocyclic aromatic carbon treated with ozone-based AOPs in the context of ISCO. Hypotheses 3.1 and 3.2 are tested as part of this chapter.

Finally, chapter 7, which is based on **Article IV**, explores alternative oxidative treatment by activating PMS through granular catalytic media, where the focus lies on achieving unselective oxidation of a wide range of different contaminants with the formed radical species (Hypothesis 4.1).

In summary, chapters 4 and 5 deal with gas-liquid membrane contactors for in-situ groundwater remediation with ozone, whereas chapter 6 takes an in-depth look at ozone transformation mechanisms of an important contaminant class, also employing gas-liquid membrane contacting as part of the experimental design. Lastly, chapter 7 introduces an ozone-free process alternative for treating contaminated groundwater or wastewater. The structure of the dissertation is summarized in Figure 4.

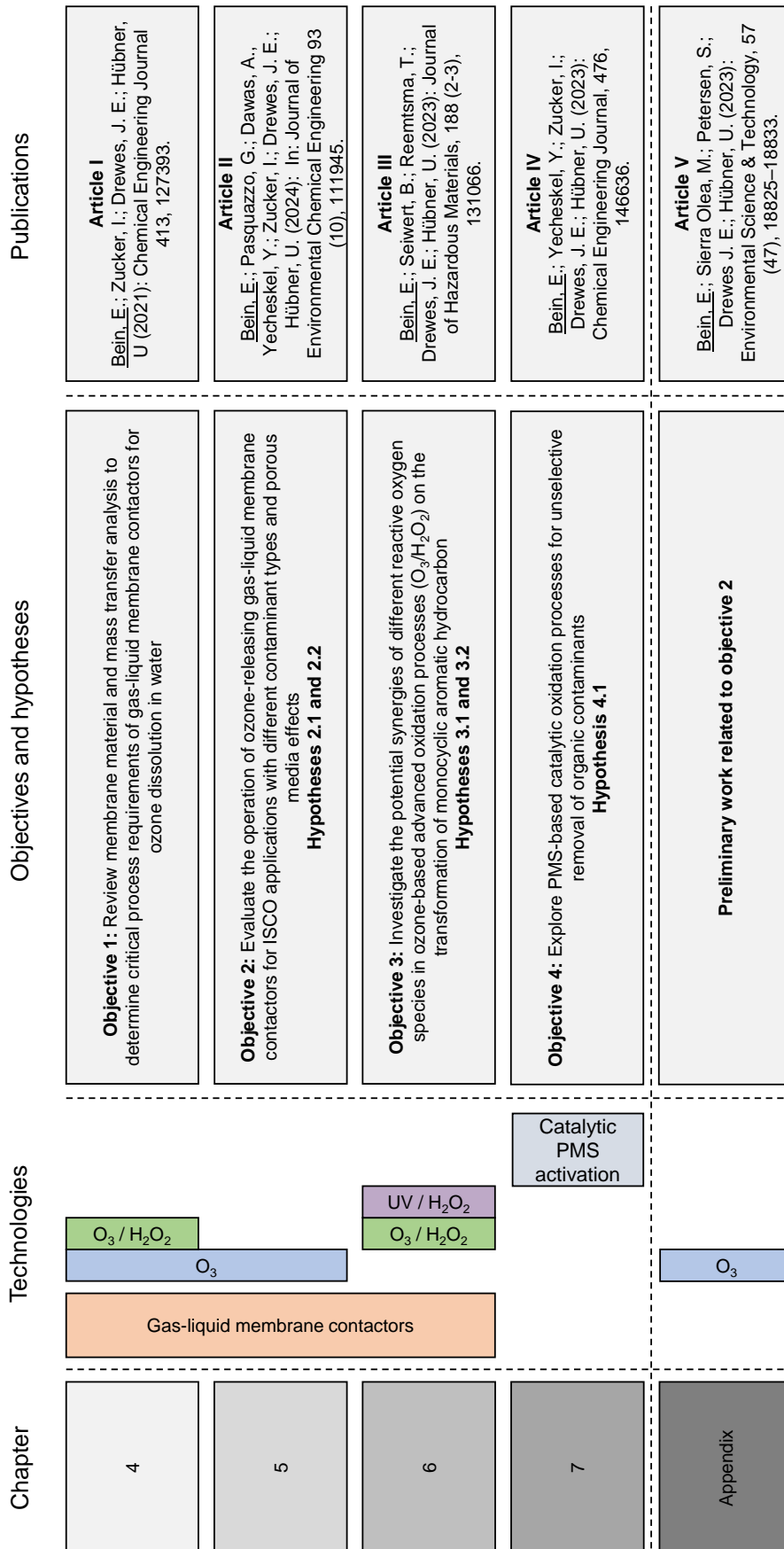


Figure 4: Dissertation structure summarizing research objectives, hypotheses, and corresponding publications.

## 4 OZONE MEMBRANE CONTACTORS FOR WATER AND WASTEWATER TREATMENT: A CRITICAL REVIEW ON MATERIALS SELECTION, MASS TRANSFER AND PROCESS DESIGN

The following chapter presents investigations related to *research objective 1: Review membrane material and mass transfer analysis of gas-liquid membrane contactors for ozone dissolution in water.*

This chapter has been published with some editorial changes as follows:

*Bein, Emil; Zucker, Ines; Drewes, Jörg E.; Hübner, Uwe (2021): Ozone membrane contactors for water and wastewater treatment: A critical review on materials selection, mass transfer and process design. In: Chemical Engineering Journal 413 (18), 127393. DOI: 10.1016/j.cej.2020.127393.*

Author contributions: Emil Bein: Conceptualization, Methodology, Formal analysis, Investigation, Writing – Original Draft, Writing – Review & Editing, Ines Zucker: Funding acquisition, Writing - Review & Editing, Jörg E. Drewes: Funding acquisition, Writing - Review & Editing, Uwe Hübner: Conceptualization, Methodology, Supervision, Funding acquisition, Writing – Review & Editing

### 4.1 Abstract

Gas-liquid membrane contactors are frequently proposed as promising alternative for traditional ozone injection methods in water treatment. However, information on successfully implemented large-scale applications is scarce. This review discusses the state of research of ozone membrane contactors for water and wastewater applications with a focus on material stability, mass transfer performance, and process design. It aims to identify favorable operating conditions, the benefits compared to traditional injection methods and critical aspects for upscaling. Reported experimental ozone mass transfer coefficients (K) in hollow fiber and single tube contactors were analyzed for relevant influential parameters and compared to calculations using the Lévêque solution and the Kreulen modification. Volumetric mass transfer coefficients ( $K_{as}$ ) were used for comparison with other ozone delivery methods. Differences between experimental and calculated mass transfer coefficients increased towards lower mass transfer and liquid

velocity, potentially due to enhanced membrane resistances and ozone decay. The highest mass transfer coefficients were found for hydrophobic polyvinylidene fluoride (PVDF) and polytetrafluoroethylene (PTFE) membranes, while polydimethylsiloxane (PDMS), hydrophilic PVDF, and inorganic membranes showed lower transfer efficiencies. Although mass transfer enhancement by fast ozone depletion in the liquid bulk and in the boundary layer can be significant during water treatment, this design-factor is mostly neglected for ozone membrane contactors examined in the peer-reviewed literature. PVDF and PTFE hollow fiber modules exhibit higher volumetric mass transfer coefficients compared to traditional injection methods including bubble columns and venturi injectors, but full-scale and economic studies are missing to assess potential benefits of this new ozone injection method. In addition, long-term material stability is uncertain for most materials. Overall, this study provides a comprehensive comparison of gas-liquid contactors, suggesting future areas of research.

**Keywords:** gas-liquid membrane contactor; ozonation; mass transfer; water treatment; advanced oxidation processes.

## 4.2 Introduction

Various trace organic chemicals originating from anthropogenic sources present in the aquatic environment are posing a potential threat to ecosystems and drinking water sources (Luo et al., 2014; Schwarzenbach et al., 2006). Due to its strong oxidative potential, ozone is suggested as a promising oxidant for the removal of recalcitrant organic contaminants from water and wastewater (Broséus et al., 2009; Hollender et al., 2009). Ozone is generated onsite from pure oxygen or air, injected to water, and reacts directly as an electrophilic chemical with many inorganic and organic substances. In addition, ozone reactions with water constitutes, or additives like  $H_2O_2$ , can result in the formation of highly reactive secondary oxidants, most importantly hydroxyl radicals. Both, the direct reaction with ozone and indirect oxidation are important for an efficient oxidation of target contaminants and recent findings suggest that energy efficiency of radical formation during ozonation is superior to most other advanced oxidation processes (AOPs) in specific water matrices such as groundwater or tertiary effluent (Miklos et al., 2018b).

Ozone gas is typically dissolved in the liquid by sparging gas bubbles into a column or by injection into side streams via venturi injectors (Langlais et al., 1991; Rakness et al., 2018). An emerging approach to introduce gaseous ozone to aqueous solutions is the use of membranes, facilitating a bubble-free gas-liquid contact (so called ozone membrane contactors). Gas-liquid membrane contactors separate the gas and liquid phase by a porous or non-porous hydrophobic membrane, while diffusion-driven gas exchange

takes place on the liquid side without bubble formation (Baker, 2012). Compared to conventional gas injection methods, these contactors offer a high level of process control as the internal surface area remains constant with varying flow rates. They are considered to have a smaller footprint due to high specific surface areas and mass transfer efficiencies (Gabelman and Hwang, 1999; Nagy, 2019). For ozonation of water, some specific advantages have been discussed in the past. It was suggested that gas-liquid membrane contactors inhibit foaming due to the bubble-free diffusion mechanism (Janknecht et al., 2000b; Janknecht et al., 2001). Additionally, multiple injection points may be used to keep local ozone concentrations low, thus reduce by-product formation during treatment (Merle et al., 2017). It was also hypothesized that the large number of dosing points can increase the transformation efficiency of organic micropollutants (Stylianou et al., 2018b). From an economic point of view, higher ozone transfer efficiencies and a lower energy demand as compared to conventional processes are listed as potential advantages of ozone contactors by Pines et al. (2005), contrary to Gottschalk et al. (2010) who assume a comparably high energy demand.

With research about ozone membrane contactors starting in the 1990s (Gottschalk et al., 1998; Guha et al., 1995; Shanbhag et al., 1995; Shanbhag et al., 1998; Shanbhag and Sirkar, 1998), there are still ongoing experimental activities at lab-scale, promoting this technology for water and wastewater treatment with ozone only, or as a peroxone process ( $O_3/H_2O_2$ ) (Li et al., 2019a; Merle et al., 2017; Sabelfeld and Geißen, 2019; Stylianou et al., 2015a; Stylianou et al., 2015b; Stylianou et al., 2016; Stylianou et al., 2018b; Zhang et al., 2017; Zhang and Wang, 2011; Zoumpouli et al., 2018). According to Gabelman and Hwang (1999), ozone membrane contacting has become widely used in Japanese semiconductor industries to clean wafers, a field of application also suggested by Gottschalk et al. (1998), Bush et al. (1998) and Noda et al. (2002). However, design and operation of ozone membrane contactors at a larger scale with several  $m^3 h^{-1}$  was not reported to date. The lack of documented large-scale projects for water and wastewater treatment, although frequently discussed in research, raises questions regarding the significance of reported advantages and potential limitations in scalability which were less documented and might inhibit a wider use.

Several studies investigated the effectivity of ozone membrane contactors for treating drinking water sources such as surface water and groundwater with ozone only (Jansen et al., 2005; Jansen, 2005; Jansen et al., 2006; Leiknes et al., 2005) or by the peroxone process through hydrogen peroxide injection prior to ozonation (Merle et al., 2017; Stylianou et al., 2018b; Stylianou et al., 2018a). Major treatment goal for ozonation was to oxidize natural organic matter to meet color and odor requirements, while studies applying the peroxone process mostly aimed to remove recalcitrant trace organic chemicals. More process- or material-related studies address membrane flux or mass

transfer of the investigated membrane modules and single tube contactors in clean conditions. Different operating parameters such as ozone gas concentration, temperature, liquid velocity or gas velocity were varied to characterize mass transfer (Kukuzaki et al., 2010; Pines et al., 2005; Stylianou et al., 2016). Some studies investigated the enhancement of ozone mass transfer, caused by ozone consumption by reactive constituents in feed water thus facilitating further ozone diffusion through the contactor (Phattaranawik et al., 2005; Zhang et al., 2017). Although the evaluation of mass transfer experiments could provide valuable information on desirable conditions, there is neither a quantitative or qualitative comparison of a wide range of materials and modules, nor a full comparison to other injection methods.

Recently, results from previous studies on ozone membrane contacting were reviewed and summarized (Schmitt et al., 2020), but a critical assessment of this technology for water and wastewater treatment using data analysis methods has not been undertaken yet. This study aims to provide a comprehensive overview of the state of research about ozone membrane contacting for water and wastewater treatment applications with a focus on membrane material stability, mass transfer efficiency and module design approaches for large-scale installations. Mass transfer coefficients were collected from literature, correlated to evaluate effects of relevant parameters including flow velocity and membrane material, and compared with calculated coefficients from theoretical considerations to check plausibility of existing design methods. In addition, mass transfer enhancement, an important factor for designing ozone membrane systems, is discussed with a focus on the peroxone process. Ultimately, our data analysis allows comparison of gas-liquid membrane contactors to conventional injection methods and the identification of beneficial process settings as well as potential uncertainties which might hinder their scale up for water or wastewater treatment.

### **4.3 Methods and literature data**

Overall, 38 experimental or modeling studies investigating the ozone injection through porous and non-porous membranes were identified from peer-reviewed sources. Some additional studies employed inorganic membranes without any surface modification (Heng et al., 2007; Heng et al., 2008; Ho et al., 2012; Kit Chan et al., 2012; Wenten et al., 2012) or polymeric hollow fibers (Li and Yeung, 2019; Wang et al., 2019) without liquid-side overpressure to create fine ozone bubbles. As these configurations represent micro-bubble sparging, we did not include them in this review. The term ozone membrane contactor is used in this study for describing a gas-liquid membrane contacting technology with gas-filled pores and a liquid-side overpressure, where no bubble formation takes place.

(Volumetric) mass transfer coefficients were collected from peer-reviewed literature data to facilitate a quantitative comparison of different membrane materials and reactor geometries and to evaluate the calculation of mass transfer based on resistance-in-series theory (Sirkar, 1992). Through the comparison of mass transfer coefficients, effects of ozone gas concentration and temperature can be ruled out. In addition, volumetric mass transfer coefficients, named  $K_{as}$ , were determined as the product of mass transfer coefficient and specific internal surface area and used to compare ozone membrane contacting with other ozone injection methods.

Studies were accepted for this data set if the experimental set-up met the following criteria:

- Straight hollow fiber membrane modules or single tubes tested
- Water flow on the lumen side and ozone gas flow on the shell side of the fibers/tube
- Countercurrent operation
- Demineralized or ultrapure water was used as feed water, either acidic or at neutral pH
- Controlled temperature, ozone gas flow rate and concentration, and gas pressure
- Specific information on membranes properties and used geometry was provided

Where available, mass transfer coefficients were extracted from text, tables or figures. When mass transfer coefficients were not reported, we derived them from flux values [ $J$  in  $\text{g m}^{-2} \text{s}^{-1}$  or  $\text{mol m}^{-2} \text{s}^{-1}$ ], liquid-side ozone concentration  $c_{O_3,l}$  in  $\text{mg L}^{-1}$ , temperature in K, and gas-side ozone concentration  $c_{O_3,g}$  in  $\text{mg L}^{-1}$  as

$$K = \frac{J}{c_{O_3,l}^* - c_{O_3,l}} \quad \text{Eq. 2}$$

where saturation concentration of ozone in water  $c_{O_3,l}^*$  in  $\text{mg L}^{-1}$  depends on the reported ozone gas concentration  $c_{O_3,g}$  in  $\text{mg L}^{-1}$ , and Henry's law constant ( $H_{O_3} = 10^{-4} \text{ mol m}^{-3} \text{ Pa}^{-1}$ ), which was temperature-corrected for every data point (Sander, 2015). This simplified concentration difference neglects a pressure drop in the system, which is approximately valid in small lab-scale systems with a comparably high gas flow rate. In one case (Zhang et al., 2017), mass transfer and liquid-side velocity were provided in dimensionless numbers (Sherwood and Graetz number), which were converted according to common definitions (see also section 4.5.1).

A total of 108 mass transfer coefficients from eight studies representing 11 different membrane modules and largely differing operational conditions could be extracted by this procedure. Other important parameters such as membrane material, manufacturer, module length, fiber diameters, gas-side ozone concentration, temperature, dissolved ozone concentration, liquid-side velocity and pH are included whenever available (see supplemental information, <https://doi.org/10.17632/v47hfh4dz2.2>). Liquid-side velocities in some cases have been reported as flow rate. The flow rate was converted to a liquid-side velocity considering the geometry of the cross-sectional area.

Mass transfer coefficients were usually determined on the liquid side by measuring dissolved ozone concentrations in pure water. For this, the indigo method (Bader and Hoigné, 1981) was used in all studies except in case of Zhang et al. (Zhang et al., 2017), who directly determined ozone concentrations in water photometrically at 260 nm. The exact measurement procedure and the reagents used may affect accuracy of resulting values, but the degree of impact cannot be discussed here as this was not reported in detail.

#### **4.4 Membrane materials and their stability**

Due to the high oxidation potential of ozone, only a rather low number of materials meets the requirements of ozone membrane contactors (i.e., ozone resisting materials). Typical contactor materials can be roughly grouped in porous and non-porous polymers, and inorganic materials. Porous membranes always require a liquid-side overpressure for bubble free operation and a transmembrane pressure lower than the breakthrough pressure (Luis, 2018). Otherwise, gas bubbles would form and the subsequent gas exchange results in sparging. No liquid-side overpressure is needed for non-porous membranes. As compared to porous membranes, gas is not diffusing through pores in non-porous membranes, but directly partitions through the material through solution-diffusion mechanism (Dingemans et al., 2008).

Authors reported advantages and drawbacks of their tested materials with respect to performance characteristics, i.e., mass transfer and chemical stability. As stability towards ozone and hydroxyl ( $\cdot\text{OH}$ ) radicals can only be guaranteed to a certain degree, it is an important criterion to consider. Gottschalk et al. (2010) estimate the lifetime of polymeric membranes to be between one and five years for application in semiconductor industries with high ozone concentrations. Chemical stability can be theoretically assessed by analyzing the potential locations in the structure of the compound for ozone or OH-radicals attack (von Gunten, 2003). Practical experience discussed in the literature can enrich the basic chemical assessment and experimentally indicate ozone resistivity. This section seeks to identify, group and discuss relevant tested materials with respect to



their stability and material-related mass transfer limitations. A brief overview of tested membrane materials is provided in Table 3.

#### 4.4.1 Polymeric membranes

Polymeric membranes employed for gas-liquid membrane contacting offer the advantage of hydrophobicity to differing degrees by nature due to their non-polar structure. Hollow fiber configurations can be produced with small diameters of a few  $\mu\text{m}$  and thus can be bundled to achieve a very high specific internal membrane surface area.

Commonly used porous membrane materials are polyvinylidene fluoride (PVDF) and polytetrafluoroethylene (PTFE), both fluoropolymers, which show the strongest chemical stability among the polymer group, as the electronegativity of the fluorine atoms and the absence of carbon double bonds in the structure prevent an ozone or OH-radical attack. However, data on long-term performance of such polymeric ozone membrane contacting units are scarce. Santos et al. (2015) exposed various membrane materials to  $5.25 \text{ g h}^{-1}$  ozone gas for two and four hours and could not observe major changes in morphology, chemical bonds, and composition of PVDF and PTFE membranes based on scanning electron microscopy (SEM), Fourier-transform infrared spectroscopy (FTIR), and thermogravimetric analyses. Nevertheless, previous studies indicate that PVDF is susceptible for material alterations which may take place over time. Bamperng et al. (2010) treated dye solutions with ozone membrane contactors and observed an ozone flux decline by 30% for PVDF membranes compared to PTFE over 16 hours and  $40 \text{ mg L}^{-1}$  ozone gas concentration. They hypothesized that changes of material properties by oxidation could result in membrane wetting, which corresponds to an increased resistance for ozone transfer through the wetted membrane walls. Previous studies testing microfiltration of water with residual ozone concentrations indicate the strong impact of PVDF crystallinity on reactivity towards ozone. The higher the crystallinity, the stronger the resistance of PVDF towards ozone (Hashino et al., 2000; Mori et al., 1998).

With the exception of the study conducted by Bamperng et al. (2010), potential performance drops were not investigated or reported for PVDF membranes. Summarized PVDF flux data is comparable with each other as further discussed in section 4.6. However, crystallinity is not addressed in ozone membrane contacting studies and it is unclear how the tested modules have been produced and how they would perform on the long run. For PTFE membranes, no property changes over time have been reported, thus this membrane type seems to be the best choice from a material stability perspective. Nevertheless, it should be noted that unlimited ozone and radical stability cannot be guaranteed for any polymer in long-term exposure scenarios. For example, defluorination and leaching of fluoropolymers or impurities from such membranes were reported before

in harsh conditions (such as thermolysis (Ellis et al., 2001) and chemical cleaning (Rabuni et al., 2015)) and may also occur during long-lasting water treatment using ozone (Tu et al., 2005).

Another polymer frequently tested in the context of ozone contactors is polydimethylsiloxane (PDMS), which is a non-porous material. Since PDMS is non-porous, the maximum transport depends on the permeability of the gas in the material (Shanbhag et al., 1995; Shanbhag et al., 1998; Shanbhag and Sirkar, 1998; Zoumpouli et al., 2018). The non-porous structure of PDMS eliminates the need for overpressure to achieve bubble-free (passive) dissolution of ozone, as gas bubbles do not penetrate through membrane pores. This may allow reduction of energy costs related to the built-up of a liquid-side pressure. The permeability of a silicone membrane for ozone is about  $1.05 \cdot 10^{-12} \text{ mol m}^{-1} \text{ s}^{-1} \text{ Pa}^{-1}$  as compared to oxygen permeability of  $2.24 \cdot 10^{-13} \text{ mol m}^{-1} \text{ s}^{-1} \text{ Pa}^{-1}$ . As ozone is over four times more permeable than oxygen in PDMS membranes (Shanbhag and Sirkar, 1998), selectivity may be inherently achieved. The membrane resistance of a non-porous membrane can be estimated from membrane wall thickness  $\tau_m$ , Henry's law constant of ozone in water  $H_{O_3,l}$ , and permeability of ozone in the membrane  $P_m$  as

$$\frac{1}{k_{m,np}} = \frac{\tau_m}{H_{O_3,l} P_m} \quad \text{Eq. 3}$$

Therefore, a PDMS tube with wall thickness of 0.6 mm will have a large membrane resistance of  $4.71 \cdot 10^4 \text{ s m}^{-1}$  (Côté et al., 1989). For comparison, the membrane resistance for a PTFE tube of the same geometry with a porosity of 50% and a tortuosity factor of 1.5 (see section 4.5.1, Eq. 7) would result in a resistance of  $22.25 \text{ s m}^{-1}$ , assuming an ozone diffusion coefficient in the pores of  $1.62 \cdot 10^{-5} \text{ m}^2 \text{ s}^{-1}$  (Sabelfeld and Geißen, 2019). This difference of membrane resistance becomes relevant for applications where the liquid-side resistance is low due to a high applied liquid velocity. In case of a high liquid velocity (e.g.,  $> 0.01 \text{ m s}^{-1}$ ), the membrane resistance would severely limit mass transfer in PDMS membranes compared to porous PTFE membranes.

Another drawback of PDMS (other than high membrane resistance) is the material deterioration over time, as PDMS changes its properties with long-term exposure to ozone. It is hypothesized from UV/ozone applications that substitution of methyl groups by oxygen result in the formation of  $\text{SiO}_x$  networks, reportedly reaching from the surface into the membrane structure 6 to 10  $\mu\text{m}$  after exposure (Berdichevsky et al., 2004; Fu et al., 2010). For some coating applications, PDMS is actively treated with UV, ozone or both combined to increase surface roughness and hydrophilicity by reducing the water contact angle (Graubner et al., 2004; Matienzo and Egitto, 2006). In an ozone membrane

contacting application, however, the gas continuously permeates through the material, thus the material must withstand long-term exposure to ozone. Zoumpouli et al. (2018) tested PDMS membranes over several months in repetitive experiments of more than 12 hours every single run and could not find a decline in performance. Due to the lack of a systematic, comparative perspective on PDMS membrane longevity it is not possible to assess the lifetime reduction by ozonation and how this relates to material costs, environmental sustainability aspects and performance characteristics.

Polypropylene (PP) was tested as potential candidate for ozone membrane contacting, most likely due to its hydrophobicity and the successful operation in other gas-liquid contacting processes (Ciardelli et al., 2001; Ciardelli et al., 2003; Guha et al., 1995). However, PP is not ozone-resistant and material failures occur after few hours of exposure (Santos et al., 2015). The hydrogen atoms in the methyl groups and in the carbon chain are suspected to be removed and replaced by peroxy radicals (POO<sup>·</sup>), finally forming either carbonyls, carboxylic acids or hydroperoxides, which results in a slow but steady material breakdown (Walzak et al., 1995).

Table 3: Membrane materials proposed for ozone delivery.

Name	Group / Subgroup	Structure	Chemical stability in presence of ozone	References
Polytetrafluoro-ethylen (PTFE)	Fluoro-polymers	$\left[ \begin{array}{cc} \text{F} & \text{F} \\   &   \\ -\text{C} & -\text{C}- \\   &   \\ \text{F} & \text{F} \end{array} \right]_n$	Very high	Merle et al., 2017, Pines et al., 2005, Gottschalk et al., 1998, (Guha et al., 1995), (Zhang et al., 2017), Noda et al., 2002, Bamperng et al., 2010, Janknecht et al., 2004
Polyvinylidene fluoride (PVDF)	Fluoro-polymers	$\left[ \begin{array}{cc} \text{H} & \text{F} \\   &   \\ -\text{C} & -\text{C}- \\   &   \\ \text{H} & \text{F} \end{array} \right]_n$	High	Pines et al., 2005, Li et al., 2019a, Zoumpouli et al., 2018, Zhang and Wang, 2011, Jansen et al., 2006, Leiknes et al., 2005, Jansen et al., 2005, Phattaranawik et al., 2005, Atchariyawut et al., 2009, Steiner et al., 2010, Zhang et al., 2009
Polydimethyl-siloxane (PDMS)	Siloxanes	$\left[ \begin{array}{c} \text{CH}_3 \\   \\ -\text{Si}-\text{O}- \\   \\ \text{CH}_3 \end{array} \right]_n$	Medium	Guha et al., 1995, Shanbhag et al., 1995, Shanbhag et al., 1998, Shanbhag and Sirkar, 1998
Polypropylene (PP)	Polyolefin	$\left[ \begin{array}{c} \text{CH}_3 \\   \\ -\text{CH}-\text{CH}_2- \\   \end{array} \right]_n$	Low	Guha et al., 1995, Ciardelli et al., 2001, Ciardelli et al., 2003
Aluminum oxide ( $\alpha$ -Al <sub>2</sub> O <sub>3</sub> )	Inorganic	n.a.	Very high <sup>a</sup>	Janknecht et al., 2000b, Janknecht et al., 2001, Stylianou et al., 2018b, Zhang et al., 2017, Stylianou et al., 2016, Stylianou et al., 2015a, Stylianou et al., 2015b, Stylianou et al., 2018a, Janknecht et al., 2000a
Zirconia (ZrO <sub>2</sub> ), Potassium titanyl phosphate (KTiOPO <sub>4</sub> ), Coerdiete (2MgO-2Al <sub>2</sub> O <sub>3</sub> -5SiO <sub>2</sub> )	Inorganic	n.a.	Very high <sup>a</sup>	Janknecht et al., 2000b, Janknecht et al., 2004, Janknecht et al., 2000a
Porous <i>Shirasu</i> glass (high share of SiO <sub>2</sub> and Al <sub>2</sub> O <sub>3</sub> )	Inorganic	n.a.	Very high <sup>a</sup>	Kukuzaki et al., 2010

<sup>a</sup>Chemical stability is only assessed for the inorganic material base, not for any layer added to create a hydrophobic surface.

#### 4.4.2 Inorganic membranes

Another alternative for ozone membrane contactors are inorganic membranes made out of pure  $\alpha$ -aluminum oxide,  $\alpha$ -Al<sub>2</sub>O<sub>3</sub> (Stylianou et al., 2015a), porous glass with a high silicon dioxide content (Kukuzaki et al., 2010) or a multilayer construction of inorganic compounds to control porosity (Picard et al., 2001). Due to their high physical and chemical stability, their hydrophilicity, and the ongoing reduction of production costs inorganic membranes are receiving increasing attention for membrane filtration processes (Lee et al., 2015a).

A hydrophobic surface on the liquid side of organic and inorganic ozone membrane contactors can be obtained by surface modification of conventional membrane materials. This is especially relevant for inorganic membranes due to their hydrophilicity compared to other discussed polymeric materials. For example, surface fluorination via well-established silane chemistry will lower the membrane surface energy, forming hydrophobic membrane surface (Matsumoto et al., 2002). The layer addition can be achieved by soaking or rinsing the membrane surface in a solution consisting of a surfactant and the layer compound. In the studies referring to ozone membrane contacting, trichloromethylsilane and 1H,1H,2H,2H-perfluorodecyltriethoxysilane caused a large water contact angle of 143° (Stylianou et al., 2015a) and 145° (Picard et al., 2004) on the modified membrane. Toluene (Kukuzaki et al., 2010; Stylianou et al., 2015a), ethanol (Stylianou et al., 2015a) and chloroform (Picard et al., 2001) were used as solvents for the surfactant. After soaking or rinsing with the mixture, the membranes were in some cases additionally rinsed with the solvent and dried to remove the liquid from the soaking either by heating or applying vacuum. While Picard et al. (2004) observed a large contact angle with longer fluorinated chains of the silanes, Stylianou et al. (2015a) achieved the highest value with trichloromethylsilane, a short-chained surfactant without fluorine. Kukuzaki et al. (2010) who manufactured and tested porous *Shirasu* glass membranes used 3,3,4,4,5,5,6,6,6-nonafluorohexyltrichlorosilane, a long-chained fluorinated silane in accordance with Picard et al. (2004). They measured a contact angle of approximately 104 – 108° (Kukuzaki et al., 2010). The finally established water contact angle of the resulting hydrophobic surface depends on several factors such as the surface characteristics of the membrane material (i.e., surface polarity, crystallinity, porosity and pore types), thus results of the procedures cannot be generalized.

Although the chemical stability of the inorganic base material is high and most likely not a critical factor, the hydrophobic layer might be damaged over time and the modification procedure has to be repeated. Stylianou et al. (2015a) emphasized the high stability of trichloromethylsilane in their tests with high ozone concentrations and in a second study, Stylianou et al. (2016) could not observe a change of the hydrophobic

surface character using the same surfactant over three months of experiments with ozone. The alternative long-chained fluorosilanes contain carbon-carbon bonds, thus may undergo ozone/OH-radical attack over time, similarly to PP. Besides individual observations there are no systematic studies on long-term exposure of surfactants to ozone, which would be needed for a comprehensive assessment of how stable surface-treated inorganic membranes are.

## 4.5 Mass transfer in ozone membrane contacting systems

### 4.5.1 Estimation of mass transfer coefficients

The flux of gas through a membrane is defined as

$$J = K \Delta c \quad \text{Eq. 4}$$

where  $K$  is the overall mass transfer coefficient in  $\text{m s}^{-1}$ , which depends on a series of resistances from gas- to liquid-phase (Sirkar, 1992), and  $\Delta c$  is the characteristic concentration difference in  $\text{mg L}^{-1}$ , a parameter that can take into account the module geometry and flow configuration, such as counter- or co-current operation, analogous to heat transfer (Bergman et al., 2011). If no major pressure drop on the gas-side is assumed, it describes the concentration difference between saturation concentration  $c_{\text{O}_3,\text{l}}^*$  and liquid-side concentration  $c_{\text{O}_3,\text{l}}$  (Pines et al., 2005; Sabelfeld and Geißen, 2019). If the pressure drop along the module is known,  $\Delta c$  can be described by a logarithmic mean concentration difference for counter-current flow (Phattaranawik et al., 2005). This pressure-drop consideration is especially relevant for large-scale design in case of open-ended modules, where a large pressure drop on the gas-side is needed to achieve high efficiency of ozone injection. Hence, another option for avoiding waste of ozone would be the establishment of a gas recycling scheme, which keeps the pressure drop on the gas-side low (Janknecht et al., 2001).

Assuming gas-filled pores in case of a perfectly hydrophobic porous membrane, the resistances-in-series model for ozone membrane contactors based on the liquid phase can be stated as

$$\frac{1}{K} = \frac{1}{H_i k_g} + \frac{1}{H_i k_m} + \frac{1}{k_l E_l} \quad \text{Eq. 5}$$

where  $H_i$  is the dimensionless Henry's law constant (also named solubility or partitioning coefficient),  $E_l$  is the liquid-side enhancement factor and with single resistances on the gas-side  $1/k_g$ , in the membrane  $1/k_m$  and on the liquid side  $1/k_l$  as stated by the film theory (Luis, 2018). Several notations and variations to describe resistances in series in gas-liquid membrane contacting exist, based on differing assumptions, i.e., neglecting gas-side and membrane resistance (Ahmed and Semmens, 1992; Fang et al.,

2002), neglecting gas-side resistance in case of non-porous silicone (PDMS) membranes (Côté et al., 1989; Orgill et al., 2019), or taking into account all contributions (Sabelfeld and Geißen, 2019). As membrane resistance is less affected by gas flowing through dry pores, but increases due to water entering the pores, an additional resistance for wetted pores can optionally be included in Eq. 5 (Sabelfeld and Geißen, 2019). As opposed to inert gases, reactivity of ozone with feed water significantly changes mass transfer, as ozone is being consumed on the liquid side, facilitating further transfer (Phattaranawik et al., 2005), thus an enhancement factor  $E_1$  has to be included in the resistance terms for reactive water (section 4.7). In the used definition,  $H_i$  is written as

$$H_i = \frac{H_{O_3,l}}{R T_l} \quad \text{Eq. 6}$$

where  $H_{O_3,l}$  is the Henry's law constant for ozone in water in  $\text{Pa m}^3 \text{mol}^{-1}$ ,  $R$  the universal gas constant in  $\text{J mol}^{-1} \text{K}^{-1}$ , and  $T_l$  the liquid temperature in K.  $H_{O_3,l}$  needs to be corrected for temperature changes, as gas solubility increases with decreasing temperature (Sander, 2015). If the membrane is non-porous, such as in the case of PDMS membranes, the solubility of  $k_m$  is not defined by porosity, but the material's permeability characteristics (Berry et al., 2017; Orgill et al., 2019). For porous membranes, the membrane resistance depends on the diffusion of gas through the pores, respectively its hindrance by membrane walls and can be approximated with membrane specifics as

$$k_m = \frac{D_{O_3,m} \varepsilon_m}{\theta \tau_m} \quad \text{Eq. 7}$$

where  $D_{O_3,m}$  is the effective ozone diffusion in the pores in  $\text{m}^2 \text{s}^{-1}$ ,  $\varepsilon_m$  the membrane porosity,  $\theta$  the tortuosity and  $\tau_m$  the wall thickness in m.  $D_{O_3,m}$  is characterized by Fick and Knudsen diffusion coefficients ( $D_K$  and  $D_F$ ):

$$\frac{1}{D_{O_3,m}} = \frac{1}{D_K} + \frac{1}{D_F}. \quad \text{Eq. 8}$$

This takes into account the collision of gas with the membrane structure.  $k_g$  and  $k_l$  can be approximated by specifying operational parameters and by using existing empirical or theoretical dimensionless correlations (Gabelman and Hwang, 1999; Wickramasinghe et al., 1992; Yang and Cussler, 1986). For tube side fluid flow, the L  v  que solution is well established:

$$Sh = 1.62 \left( \frac{d_i}{L} Re Sc \right)^{\frac{1}{3}} = 1.62 Gz^{\frac{1}{3}}. \quad \text{Eq. 9}$$

It includes the dimensionless Sherwood number  $Sh = \frac{k_l d_{in}}{D_{O_3,l}}$ , Reynolds number  $Re = \frac{v_l d_{in}}{\nu}$ , Schmidt number  $Sc = \frac{\nu}{D_{O_3,l}}$ , and Graetz number  $Gz = \frac{d_i^2 v_l}{L D_{O_3,l}}$ .  $L$  is the fiber length

in  $m$ ,  $d_i$  the inner fiber diameter in  $m$ ,  $D_{O_3,l}$  the diffusion coefficient of ozone in water in  $m^2 s^{-1}$ ,  $v_l$  the liquid-side velocity in  $m s^{-1}$ , and  $\nu$  the kinematic viscosity of water in  $m^2 s^{-1}$ . Kreulen et al. (1993b) modified this solution by fitting it with numerical simulation results:

$$Sh = (3.67^3 + 1.62^3 Gz)^{\frac{1}{3}}. \quad \text{Eq. 10}$$

They suggest it is valid for all Graetz-numbers, while the L ev eque-solution is valid for a flow range of  $Gz > 4$ . For shell side flow across fibers, there exist various correlations of the general form

$$Sh = A Re^b Sc^c \quad \text{Eq. 11}$$

where  $A$ ,  $b$  and  $c$  are empirical parameters. By substitution and rearrangement of Eqs. 4, 6, 8 and 10, all influencing parameters can be included in one equation for the direct determination of mass transfer coefficients in a porous, hydrophobic hollow fiber ozone membrane contacting unit, written exemplarily as

$$\frac{1}{K} = \frac{1}{H_i \frac{D_{O_3,l}}{d_i} (0.53 - 0.58 \phi) \left(\frac{v_g d_e}{v_g}\right)^{0.53} \left(\frac{D_{O_3,l}}{v_g}\right)^{\frac{1}{3}}} + \frac{\theta \tau_m H_i}{D_{O_3,m} \varepsilon_m} \quad \text{Eq. 12}$$

$$+ \frac{1}{E_l \frac{D_{O_3,l}}{d_i} \left(\frac{v_l D_{O_3,l} d_i^2}{L \nu^2}\right)^{\frac{1}{3}}}$$

where  $d_e$  is the effective diameter for the gas flow on the shell side as defined by Yang and Cussler (1986) and  $A$ ,  $b$  and  $c$  (Eq. 11) is replaced by example values determined by Costello et al. (1993) for oxygen transfer from aerated water on the shell side to the lumen side in a PP hollow fiber membrane module. The factor  $A$  as written here includes the packing density  $\phi$  of the module. Eq. 12 summarizes the main parameters influencing the mass transfer coefficient.

#### 4.5.2 Agreement of calculated mass transfer coefficients with experimental data from literature

For calculating mass transfer coefficients, the assumption was made that the liquid-side resistance dominates the resistance-in-series model as described by Eq. 5 ( $K = k_l$ ) in section 4.5.1, and no enhancement factor  $E_l$  impacts mass transfer. Exceptionally, for non-porous PDMS membranes a resistance term was included in the calculation using Eq. 3. This is due to the assumption that the membrane resistance of non-porous membranes is larger by several orders of magnitude as compared to porous membranes (section 4.4.1). Reported  $K$  values are distributed over three orders of magnitude in this data collection (Figure 5). PTFE and hydrophobic PVDF membranes exhibit the highest mass transfer



coefficients with a maximum value of  $5.62 \cdot 10^{-5} \text{ m s}^{-1}$  for PTFE, while the lowest recorded K value is  $4.45 \cdot 10^{-8} \text{ m s}^{-1}$  with a PDMS membrane. The level of agreement of theory and experimental values is expressed by (normalized) root mean square errors (RMSE and NRMSE), here calculated for K values produced by L ev eque solution and the Kreulen modification (Eqs. 8 and 9) for every material and the overall data set (Table 4).

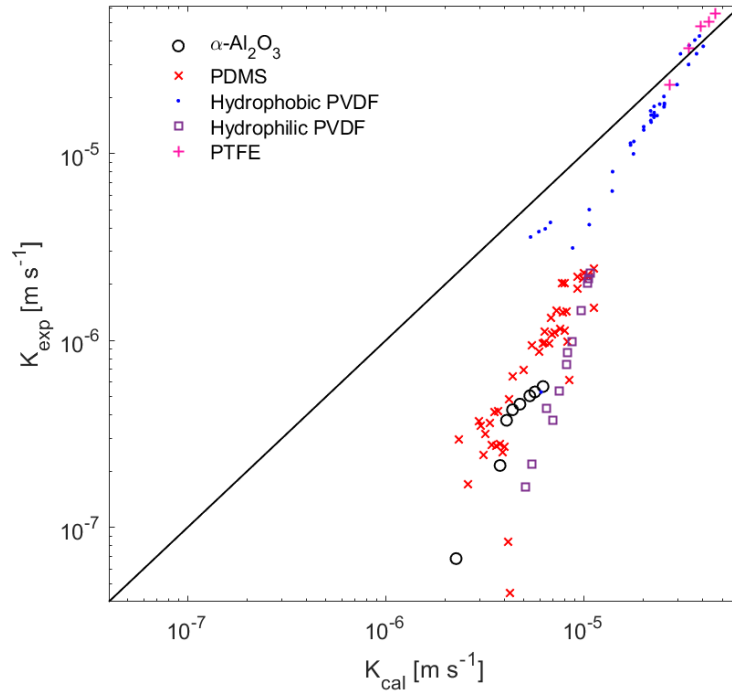


Figure 5: Comparison of experimental ( $K_{exp}$ ) and calculated ( $K_{cal}$ , L ev eque) mass transfer coefficients of the overall data set with the diagonal showing whether  $K_{exp}$  is larger or smaller than calculated values (n=108).

A direct comparison of the two calculation methods shows that the L ev eque solution produces marginally better agreement with experimental data than the modification by Kreulen et al. (1993b) and is therefore taken for further analysis. The RMSE was similar for all materials ( $4.29 \cdot 10^{-6} - 7.28 \cdot 10^{-6} \text{ m s}^{-1}$ ), while NRMSE results of 0.27 and 0.19 indicate that observed K values with hydrophobic PVDF and PTFE membranes agree satisfyingly with the calculation. Experimental K values of  $\alpha\text{-Al}_2\text{O}_3$ , PDMS and hydrophilic PVDF membranes differed on average by 94, 90 and 89% from calculated values. This is a clear difference to the included hydrophobic fluoropolymers. Based on the overall dataset, the agreement of observed K values with the L ev eque solution largely differs depending on the magnitude of the values: the higher the K values the better experimental values agree with the proposed calculation. Thus, reported K values for hydrophobic PVDF and PTFE are higher than for other materials and agree better with the L ev eque solution.

Table 4: Root mean square error and normalized root mean square error (RMSE and NRMSE) of Kexp compared to Kcal, calculated with the L ev eque solution and the Kreulen modification for all membrane materials, and the Gz range for every dataset.

Material	L�ev�eque		Kreulen		Gz range [-]
	RMSE [m s <sup>-1</sup> ]	NRMSE [-]	RMSE [m s <sup>-1</sup> ]	NRMSE [-]	
$\alpha$ -Al <sub>2</sub> O <sub>3</sub> (n=8)	4.29·10 <sup>-6</sup>	0.94	4.30·10 <sup>-6</sup>	0.94	238.93 – 4,957.48
PDMS (n=45)	5.59·10 <sup>-6</sup>	0.90	5.65·10 <sup>-6</sup>	0.90	29.74 – 1,141.89
Hydrophilic PVDF (n=12)	7.28·10 <sup>-6</sup>	0.89	7.36·10 <sup>-6</sup>	0.89	99.05 – 958.77
Hydrophobic PVDF (n=38)	5.67·10 <sup>-6</sup>	0.27	7.14·10 <sup>-6</sup>	0.32	3.66 – 1,965.04
PTFE (n=5)	7.14·10 <sup>-6</sup>	0.19	7.11·10 <sup>-6</sup>	0.19	790.41 – 3,927.85
Total (n=108)	5.82·10 <sup>-6</sup>	0.44	6.40·10 <sup>-6</sup>	0.47	3.66 – 4,957.48

Except eight data points, all experimental values are below the calculated mass transfer coefficient. One reason for this overestimation in K values potentially lies in the experimental procedure: since lower mass transfer coefficients typically correspond to low liquid velocities or longer residence times (respectively), significant ozone loss may have occurred in the systems due to its natural decay in aqueous solution. Hence, the measured dissolved ozone concentration in the effluent is lower than it is within the membrane fibers. Degassing due to transition to ambient pressure might also influence the measured dissolved ozone concentration (Sabelfeld and Gei en, 2019). However, it still seems unlikely that ozone decay in the system (e.g., in the experiments with PDMS membranes, a tubing length of 20 cm and ozone measurement at the outlet, Zoumpouli et al. (2018)) would cause differences of more than one order of magnitude.

Ozone decay in water is also affected by pH (Gardoni et al., 2012) with hydroxyl anion reactions at higher pH leading to lower dissolved ozone concentrations in ozonated effluents. Indeed, experiments with inorganic membranes and PDMS with reported low K values were performed in neutral water, while other membranes were mostly tested at acidic conditions. However, the ozone decay rate should stay below 0.001 s<sup>-1</sup> in pure water at pH 7 (Gardoni et al., 2012), thus the effect is considered to be small for the applied contact times.

Another possible explanation for the relatively low experimental K values is the inaccuracy arising from the used theoretical correlation, which is more valid for higher Gz/Re numbers (Wickramasinghe et al., 1992). However, the range of Gz numbers was comparable in the investigated data and in almost all cases Gz was larger than the critical threshold of four (Gz<sub>min</sub> = 3.66). The general suitability of Eq. 9 to predict mass transfer was demonstrated in other cases, where N<sub>2</sub>O was transferred to water or volatile organic carbon was transferred from liquid to gas phase (Kreulen et al., 1993a; Semmens et al., 1989). Additionally, the error could not be reduced by using the Kreulen modification, which aims to correct for lower Gz numbers. Indeed, the Kreulen modification produced slightly higher calculated K values than the L ev eque solution, which decreases accuracy especially in the low Gz ranges of the data set.

Instead of inaccuracies arising from the calculated liquid-side mass transfer, we hypothesize that large parts of the discrepancy of  $\alpha$ -Al<sub>2</sub>O<sub>3</sub>, hydrophilic PVDF and PDMS with the Lévêque solution can be explained by membrane resistances. The differences in mass transfer between hydrophilic (Steiner et al., 2010) and hydrophobic PVDF (Atchariyawut et al., 2009; Bamperng et al., 2010; Jansen et al., 2005; Zhang et al., 2017) support this assumption. Steiner et al. (2010) flushed the hydrophilic PVDF membrane module with dry air before each experimental run to dry the pores. Nevertheless, pore wetting most likely occurred to a larger extent and strongly reduced the diffusion in the membrane pores, thus increased the membrane resistance. The same phenomenon can be observed for inorganic membranes without surface modification (Janknecht et al., 2000b; Kukuzaki et al., 2010). Wetting is a problem for long-term operation of membranes in several applications (Mansourizadeh and Ismail, 2009; Shaulsky et al., 2019). Losses in performance are reported even for highly hydrophobic membranes in gas-liquid membrane contacting applications, caused by morphology changes, chemical oxidation and liquid-phase characteristics (Mosadegh-Sedghi et al., 2014; Wang et al., 2005). The membrane resistance in a partially wetted membrane contactor for CO<sub>2</sub> mass transfer was quantified by Rangwala (Rangwala, 1996) using the Wilson-Plot method. It confirmed that even low wetting below 2% fractional depth of liquid penetration reduced  $k_m$  to a level, where it also substantially affects overall mass transfer. The inorganic  $\alpha$ -Al<sub>2</sub>O<sub>3</sub> membrane included in this evaluation has a modified surface to increase hydrophobicity. Nevertheless, the experimental mass transfer coefficients are much lower than calculated values. The obtained data comprises only one module with a comparably high wall thickness of 3.1 mm (Stylianou et al., 2016). However, the resistance in gas-filled pores should still be much smaller than the liquid-side resistance. Therefore, besides wetting, other factors such as the additional surfactant layer stability and material structure sensitivity may contribute to mass transfer hindrance. Although membrane resistance was included for PDMS membranes, the calculation resulted in an overestimation of overall mass transfer. This is in accordance with the numerical modeling approach used by Zoumpouli et al. (2018) for their comparison.

The analyzed literature data indicate that mass transfer coefficients obtained using hydrophobic fluoropolymers are dominated by the liquid-side resistance, while for  $\alpha$ -Al<sub>2</sub>O<sub>3</sub>, PDMS, and hydrophilic PVDF, the membrane and its surface properties also significantly affects the overall mass transfer. The experimental procedure and the ozone decay in the system may also contribute to discrepancies to some extent, especially in the low Gz range. It should be noted that the data does not provide any information about trends during long-term ozone exposure. As discussed in section 4.4, estimation of flux changes over time during ozone membrane contacting requires more detailed

investigation, as the gathered data were presumably created from short-term experiments with fresh membrane materials.

#### 4.6 Impact of liquid velocity and fiber geometry on mass transfer coefficients

The liquid velocity is considered an important design parameter for membrane contactors as it strongly affects mass transfer, dissolved ozone concentration, and pressure drop in the system. Figure 6a and b demonstrate the experimental and calculated K values as a function of respective liquid velocity. The direct comparison revealed that both data sets follow the same trend of increasing mass transfer with rising velocity. Calculated K values, however, are closer together than the experimental data.

In detail, experimentally determined mass transfer through hydrophobic PVDF and PTFE membranes significantly increases with increasing velocities. In case of the other materials, K values remain below  $3 \cdot 10^{-6} \text{ m s}^{-1}$  with a lower increase of K with velocity for  $\alpha\text{-Al}_2\text{O}_3$  and PDMS. The material's limitations become more important for velocities larger than  $10^{-2} \text{ m s}^{-1}$ , as the increase of membrane resistances in relation to liquid-side resistances limits the positive effect of liquid velocity on overall mass transfer. Such a membrane resistance is integrated in the calculation of K for PDMS membranes only (Figure 6b, see also section 4.4.1) and corresponds to the reduced overall mass transfer in the experimental data, caused by membrane resistance. Nevertheless, the experimental and calculated values for PDMS deviate largely as discussed in section 4.5.2.

The comparison of experimental and calculated K values of  $\alpha\text{-Al}_2\text{O}_3$  membranes suggests that, although porous and thus with low membrane resistance in theory, a resistance of similar size as in case of PDMS membrane reduces mass transfer in reality. This may be related to the surface modification, which may allow a partial pore-wetting, or the resistance caused by the added layer itself by reducing the effective contact area between gas and liquid. Pore wetting or other membrane resistances do not seem to be a large problem for investigated hydrophobic fluoropolymers, as mass transfer coefficients continue increasing towards higher velocities in the observed range. The good agreement of hydrophobic PVDF and PTFE is somewhat remarkable since experiments were carried out with differing experimental set-ups and analytical methods, and with membranes from four different sources (see supplemental information, <https://doi.org/10.17632/v47hfh4dz2.2>).

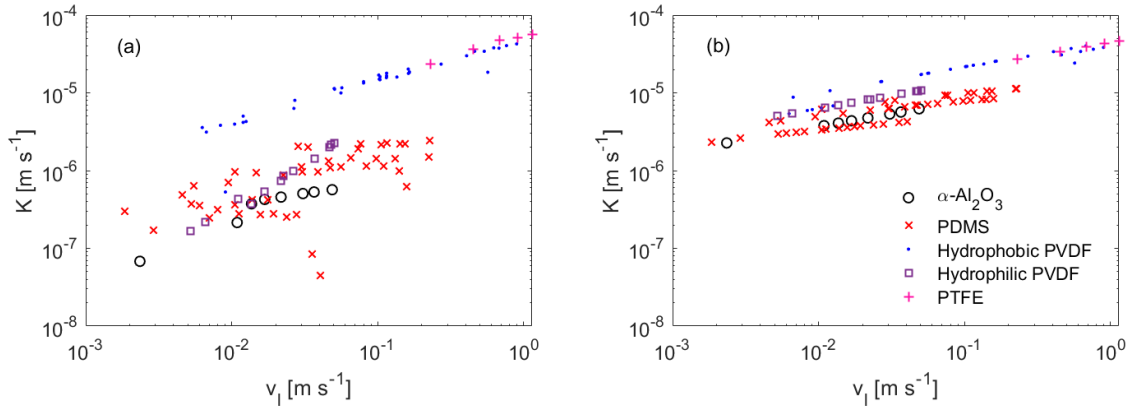


Figure 6: Impact of liquid velocities on (a) experimental and (b) calculated mass transfer coefficients.

Except one outlier, all experimental  $K$  values of hydrophobic PVDF and PTFE were higher than observed for other membrane materials, regardless of the flow velocity. In many cases, this difference exceeds one order of magnitude. The reviewed hydrophobic PVDF and PTFE membranes had porosities ranging from 50 to 75% and pore sizes between 0.17 and 1  $\mu\text{m}$ , which is not supposed to have a major impact on overall mass transfer (Pines et al., 2005). Parts of the higher mass transfer rates of the fluoropolymers can be explained by module geometry and the mass transfer theory. The calculated  $K$  values in Figure 6b visualize that a more favorable geometrical structure largely improves mass transfer at the same liquid flow velocity. Hydrophobic PVDF and PTFE hollow fibers had an inner diameter between 0.5 and 2.6 mm and a fiber/module length of 15.5 to 32 cm. All hydrophobic PVDF and PTFE data points were generated with inner diameters below 0.97 mm, except of the commercially available PVDF module (Pall UMP-153) with an inner fiber diameter of 2.6 mm used by Steiner et al. (2010) (hydrophilized), Atchariyawut et al. (2009), and Leiknes et al. (2005). The smaller diameters at similar fiber lengths result in higher calculated  $K$  values (Eq. 9) compared to larger diameters used in the other studies (Table 5). Exemplary data in Table 5 shows that this trend is less pronounced for experimental  $K$  values at the same liquid velocity of approximately  $0.01 \text{ m s}^{-1}$ . For instance, the six data points generated with the hydrophobic version of the Pall UMP-153 module with 2.6 mm inner fiber diameter seem to be very close to the hydrophobic PVDF data points generated with smaller diameters (Figure 6a).

Table 5: Mass transfer of different membrane modules for approximately the same liquid velocity.

Membrane material	$d_i$ [mm]	L [m]	$v_l$ [m s <sup>-1</sup> ]	$K_{exp}$ [m s <sup>-1</sup> ]	$K_{cal}$ [m s <sup>-1</sup> ]	Study
$\alpha$ -Al <sub>2</sub> O <sub>3</sub>	7.8	0.340	0.011	$2.15 \cdot 10^{-7}$	$3.78 \cdot 10^{-6}$	Stylianou et al., 2016
PVDF	2.6	0.203	0.010	$3.96 \cdot 10^{-6}$	$6.39 \cdot 10^{-6}$	Leiknes et al., 2005
PDMS	1.6	0.200	0.084	$1.16 \cdot 10^{-6}$	$7.64 \cdot 10^{-6}$	Zoumpouli et al., 2018
PVDF	0.5	0.260	0.012	$4.17 \cdot 10^{-6}$	$1.07 \cdot 10^{-5}$	Jansen et al., 2005

The improvement of mass transfer with smaller fiber diameters can also be observed for calculated mass transfer coefficients of PDMS membrane tubing (Figure 6b), which had inner diameters of approximately 1.0, 1.6 and 3.2 mm, respectively. Additionally, membrane resistance is different within PDMS data due to differing wall thicknesses (approximately 0.6, 0.8 and 1.6 mm). These effects are less visible in the experimental data, where the variation is high. Although generally beneficial for mass transfer, there is a hydraulic limitation of reducing fiber diameters since too small diameters substantially increase the pressure drop due to wall friction, which could lead to excessive pumping energy required in long-term operation. Given the higher accuracy of the L ev eque-solution for hydrophobic PVDF and PTFE under the investigated conditions, we assume that the impact of module geometry and material performance can be exploited for further optimization, thus designing an efficient and effective process if these materials are used.

## 4.7 Mass transfer enhancement

An important parameter of the liquid-side resistance term in Eq. 12 is the mass transfer enhancement, expressed as factor  $E_l$ , which increases complexity of ozone mass transfer compared to transfer of inert or less-reactive gases (Kuo, 1982). The ozone gas exchange procedure on the liquid side can be described by different competing concepts, including the aforementioned film theory (section 4.5.1), but as well the surface renewal and the penetration theory, which all assume a bulk liquid separated from an exchange volume (Cussler, 2011; Jansen, 2005). If one or several fast reacting compounds in the liquid phase quickly consume ozone, chemical reactions may already occur in the exchange volume. This leads to an increased concentration gradient (Figure 7) and thus to enhanced mass transfer. The enhancement  $E_l$  can be defined as the ratio of liquid-side mass transfer coefficients with a chemical reaction taking place ( $k_l^r$ ) and in pure water ( $k_l$ ):

$$E_l = \frac{k_l^r}{k_l}. \quad \text{Eq. 13}$$

Another way of describing enhancement is the total enhancement factor  $E$ , defined as ratio of flux in presence of a reaction over flux without any reaction (Gottschalk et al., 2010), or the ratio of overall mass transfer coefficients, given that liquid flow rate, gas flow rate and gas-side ozone concentration are kept the same:

$$E = \frac{J^r}{J} = \frac{K^r}{K}. \quad \text{Eq. 14}$$

It should be noted that  $E$  is different from the enhancement factor on the liquid side ( $E_l$ ) as it does include the effect of other resistances in Eq. 5 on the flux. In most studies, Eqs. 12 and 13 are not differentiated and  $E_l$  is treated as overall enhancement due to the minor impact of gas-side and porous membrane resistance (Jansen et al., 2005; Leiknes et al., 2005; Zhang et al., 2017). Most recent studies, however, emphasize that especially the gas-side resistance should not be neglected for ozone membrane contactors (Sabelfeld and Geißen, 2019; Zhang et al., 2017), and liquid-side enhancement  $E_l$  as in Eq. 13 and overall enhancement  $E$  (Eq. 14) should be distinguished. As this is not the case for most studies, specific differences between  $E_l$  and  $E$  cannot be further discussed here.

An important parameter to assess the magnitude of mass transfer enhancement is the dimensionless Hatta number ( $Ha$ ). It also indicates the location, where a reaction takes place. For a second-order reaction of ozone with reactant A,  $Ha$  can be written as

$$Ha = \frac{\sqrt{k_{A,O_3} c_{A,l} D_{O_3,l}}}{k_l} \quad \text{Eq. 15}$$

where  $k_{A,O_3}$  is the compound's second-order reaction rate constant with ozone and  $c_{A,l}$  the reactant concentration in the liquid phase. If  $Ha < 0.3$ , the enhancement is negligible, and the reaction takes place in the bulk liquid. If  $0.3 < Ha < 2$ , the reaction speed is considered to be moderate, and the reaction takes place in the exchange volume and in the bulk liquid. Values of  $2 < Ha < E_\infty$  indicate a fast reaction with complete reaction taking place in the boundary layer, such as schematically drawn in Figure 7. When  $Ha$  exceeds  $E_\infty$ , the theoretical instantaneous enhancement, an instantaneous reaction takes place with  $E_l = E_\infty$ , which is characterized by a diffusion limitation of both reactants in the boundary layer. According to the penetration theory,  $E_\infty$  is defined as

$$E_\infty = \sqrt{\frac{D_{O_3,l}}{D_{A,l}}} + \sqrt{\frac{D_{A,l}}{D_{O_3,l}}} \frac{c_{A,l}}{z c_{O_3,int}}. \quad \text{Eq. 16}$$

This includes diffusivity  $D_{A,l}$  of compound A, ozone concentration at the gas liquid interface  $c_{O_3,int}$  and the stoichiometric constant  $z$  for the reaction with ozone.  $E_\infty$  only depends on the ozone-reactive substance concentrations and diffusion characteristics and assumes that the reactant transport is the only limiting factor (Jansen, 2005).  $E_l$  can be calculated by using approximate solutions based on diffusion and reaction kinetics (van

Swaaaj and Versteeg, 1992). Calculations by DeCoursey (1974) showed satisfying accuracy compared to numerical simulations for gas-liquid hollow fiber contactors under condition of  $Gz > 120 D_{A,l} D_{B,l}^{-1}$ , with diffusion coefficient of the reactive compound  $D_{A,l}$  and of the gas in the liquid phase  $D_{B,l}$  (Kumar et al., 2003). According to DeCoursey (1974), the enhancement factor on the liquid side can be estimated as

$$E_l = -\frac{Ha^2}{2(E_\infty - 1)} + \sqrt{\frac{Ha^4}{4(E_\infty - 1)^2} + \frac{E_\infty Ha^2}{E_\infty - 1} + 1} \quad \text{Eq. 17}$$

This approach was used to predict mass transfer enhancement during ozone membrane contacting with elevated concentrations of sodium nitrite ( $k_{O_3,NaNO_2} = 3.7 \cdot 10^5 \text{ M}^{-1} \text{ s}^{-1}$  (Phattaranawik et al., 2005)) up to 2,000 mg L<sup>-1</sup> in a flat sheet PVDF contactor (2005). Enhancement was determined experimentally for different flow velocities. For comparison, the authors iteratively determined the ozone concentration at the gas-liquid interface to calculate enhancement factors using Eqs. 14 to 16. Interestingly, they found deviations lower than 5% between modeled and experimental values after modifying Eq. 13 to

$$E = \frac{k_l^r c_{O_3,int}^r}{k_l c_{O_3,int}} \quad \text{Eq. 18}$$

where  $c_{O_3,int}^r$  is the interfacial ozone concentration with reaction and  $c_{O_3,int}$  without reaction. This takes into account that the enhancement not only changes the mass transfer coefficient, but also the interfacial ozone concentration (see Figure 7), which is also part of  $\Delta c$  in Eq. 4.

However, more challenging is the use of such approximation techniques if the compounds in the feed water are heterogeneous and hard to characterize. Jansen et al. (2005) used PVDF hollow fibers to investigate reaction kinetics of ozone and humic substances and mass transfer enhancement through this reaction on a fundamental level. At very high humic substance concentrations of 40 to 400 mg L<sup>-1</sup> DOC, enhancement of ozone mass transfer up to factors of 20-30 occurred with significant enhancement of 6-7 for the lowest concentration of 40 mg L<sup>-1</sup> DOC. Specific rate constants for the reaction of humic acids with ozone were not determined in this study but a previous study observed fast pseudo first-order ozone decay of 0.04 L mg<sup>-1</sup> s<sup>-1</sup> already in presence of significantly lower concentration of isolated humic acids from Suwannee river (2 mg L<sup>-1</sup> DOC) (von Sonntag and von Gunten, 2012). In a reversed approach, they used Eq. 16 to estimate the stoichiometric ozone consumption and the averaged diffusion coefficient of humic substances. In difference to DeCoursey (1974), they defined  $E_l (\approx E) = Ha$  if  $2 < Ha \ll E_\infty$ . By varying the liquid velocity and with this the liquid-side mass transfer  $k_l$ , they could



assess whether the reaction was instantaneous ( $E_1 = E_\infty$ ) or fast ( $2 < E_1 \ll E_\infty$ ), as  $E_1$  should be independent of  $k_1$  if the reaction is only fast (Eqs. 3 and 14, with E replaced by Ha).

There are only few other studies directly addressing mass transfer enhancement using ozone membrane contactors. Bamperng et al. (2010) observed flux changes by adding different dyes to feed water. Zhang et al. (2017) measured the enhanced flux for different reactive compounds, e.g., phenol, sodium nitrite or hydrogen peroxide in the liquid feed, but did not further analyze this concerning mass transfer enhancement theory. The reports on observed enhancement indicate a substantially higher ozone mass transfer to be expected for wastewater streams with high contents of organic substances, either natural or of industrial source. The magnitude of enhancement factors at lower concentrations of reactive compounds, perhaps only a few  $\text{mg L}^{-1}$  DOC, is unclear as available studies used rather high concentrations to demonstrate the effect of enhancement. The data produced by Jansen et al. (Jansen et al., 2005) indicates enhancement factors up to 5 for humic substance concentrations below  $40 \text{ mg L}^{-1}$  DOC. Whether the enhancement during treatment of natural water or wastewater is relevant or not requires further investigation.

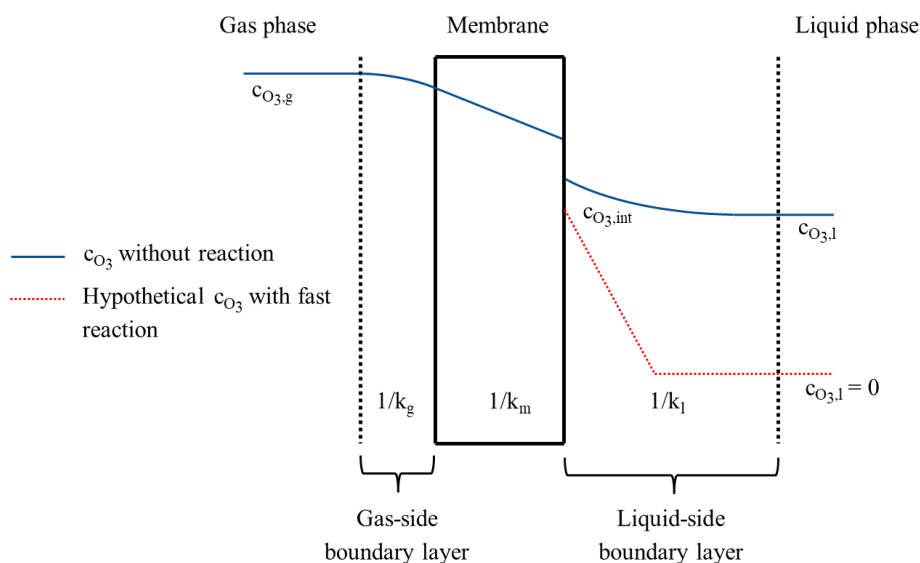


Figure 7: Illustration of the concentration profile in the resistance-in-series model with (red) and without (blue) a fast chemical reaction of ozone on the liquid side. The gas is diffusing through a porous membrane to the liquid phase (adopted and modified from Phattaranawik et al. (2005)).

Another important application with respect to mass transfer enhancement is the peroxone process ( $O_3/H_2O_2$ ) with peroxide injection prior to membrane contacting. Ozone quickly reacts with the hydrogen peroxide anion ( $k_{O_3,H_2O_2^-} = 5.5 \cdot 10^6 \text{ M}^{-1} \text{ s}^{-1}$  (von Sonntag and von Gunten, 2012)), which finally results in the formation of hydroxyl radicals. Enhancement due to peroxide injection, however, was not considered relevant in several studies on membrane-based peroxone treatment. Stylianou et al. (2018b) adjusted the peroxide dose based on ozone mass transfer in their feed reactive surface

water, assuming that reactivity of water constituents with ozone is dominant compared to peroxide. Zoumpouli et al. (2018) did not include any adjustment of their peroxide dose due to enhancement. They observed little effects of peroxide addition on radical exposure in different types of water and different peroxide doses. In their PMDS membrane material, however, effects of enhancement may be less important due to the much higher membrane resistance compared to porous membranes (section 4.6).

Systematic investigations on how to consider mass transfer enhancement in the control of ozone/peroxide ratio in combination with design of appropriate membrane surface areas are missing. The challenge to adjust  $H_2O_2/O_3$  ratios in wastewater due to both, strong competition with other water constituents and its limited effect on radical exposure has also been documented in previous studies on non-membrane based peroxone treatment (Hübner et al., 2015b). This is further complicated in membrane contactors by the dynamics within the modules. In Figure 8, a hypothesized dissolved ozone concentration from wall to wall is visualized for the peroxone process at the hollow fiber entrance and exit, based on previous illustrations of fast ozone reactions (Jansen, 2005). In the influent, excess hydrogen peroxide reacts fast ( $2 < Ha < E_\infty$ ) with ozone to form OH-radicals, so that no ozone reaches the bulk liquid. In this hypothetical scenario, the hydrogen peroxide is depleted at a specific fiber length and ozone is distributed into the bulk liquid (considering a feed water without additional significant ozone consumers). Thus, fiber diameter, flow path length or residence time, concentrations of ozone gas and hydrogen peroxide may strongly impact OH-radical and ozone exposure.

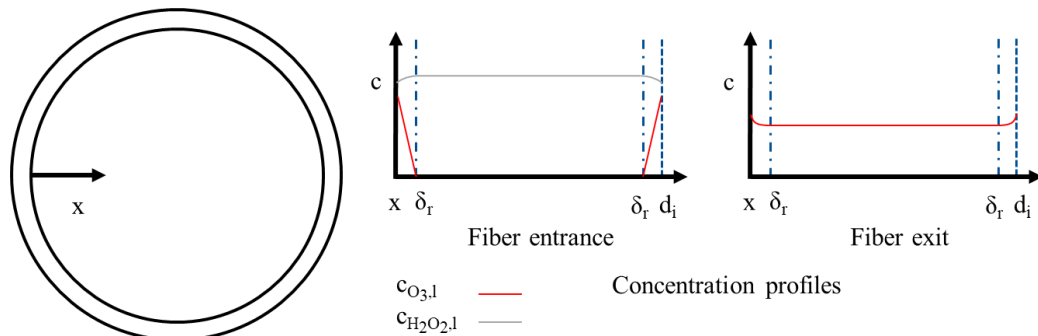


Figure 8: Hypothesized dissolved ozone and peroxide concentration at the fiber entrance and exit with water of low reactivity and hydrogen peroxide as feed during peroxone treatment (concentration profiles adopted from Jansen (2005) and modified).

Accordingly, Stylianou et al. (2018b) observed lower radical exposure with a larger fiber diameter for treatment of surface water with a single tube  $\alpha-Al_2O_3$  ozone membrane contacting unit coupled with peroxide addition, which was explained by the less efficient mixing of ozone with peroxide. Merle et al. (2017) applied an ozone membrane contactor for peroxone treatment with the objective to minimize bromate concentrations in treated ground- and lake water at low gaseous ozone concentration of

$0.5 - 10 \text{ g m}^{-3}$ . The membrane module contained 40 PTFE hollow fibers with an inner diameter of 0.45 mm. The best OH-radical exposure with the lowest bromate formation was observed with ozone gas concentrations of  $0.5 \text{ g m}^{-3}$ , peroxide concentration of  $5.67 \text{ mg L}^{-1}$  and a residence time of approximately five minutes. This finding may be explained by the illustration in Figure 8: If the residence time is longer, the hydrogen peroxide is scavenged earlier and causes an increase of ozone exposure closer to the fiber exit. Thus, an excessive peroxide concentration coupled with a shorter residence time reduces the ozone concentration in the liquid bulk drastically. Additionally, a lower ozone gas concentration leads to a lower interfacial ozone concentration (if operated with an open end) and thus a reduced ozone mass transfer enhancement.

## **4.8 Implications for designing large-scale applications**

### **4.8.1 Efficient design and operation of modules**

Due to the lack of operating large-scale systems, tested lab-scale modules are used to assess the suitability of ozone contactors for future module design. Among existing gas-liquid membrane contactor geometries such as flat sheet, spiral wound, rotating annular, or tubular membranes, only hollow fiber, single tube and flat sheet contactors were considered for ozone membrane contacting so far. Polymeric flat sheet membranes were used for laboratory mass transfer analysis and as well suggested for upscaling (Phattaranawik et al., 2005; Pines et al., 2005). One advantage of flat sheet membranes for experimental studies is the availability of several membrane materials, as sheets can be easily exchanged in a set-up. Their specific surface area, however, is lower compared to hollow fiber modules, which were investigated in most ozone membrane contacting studies. Generally, hollow fiber modules for membrane contacting received large attention by researchers due to their high surface area per volume and other advantages and were extensively reviewed for various applications (Bazhenov et al., 2018; Gabelman and Hwang, 1999; Mansourizadeh and Ismail, 2009; Pabby and Sastre, 2013). Thus, there is much experience in operating such membrane contacting systems at large-scale (Klaassen et al., 2005).

Analogous to heat exchange, the countercurrent operation (Figure 9) offers an overall higher concentration difference, and is thus preferred over parallel flow in most studies. The hollow fiber modules employed for ozonation in the reviewed studies contained between 10 to 375 fibers and were all operated with water flowing on the lumen side and gas on the shell side in a countercurrent mode (Atcharyawut et al., 2009; Bamperng et al., 2010; Jansen et al., 2005; Merle et al., 2017; Noda et al., 2002). For inorganic membranes, which were studied as single tubes, a multichannel module is proposed for larger applications (Stylianou et al., 2016). In these multichannel membrane modules as

used for filtration, a substantially larger channel diameter from 1 up to 146 mm can be expected (Lee et al., 2015a), compared to polymeric hollow fiber modules with a diameter typically below 1 mm. This may limit the use of currently available ceramic filtration units for ozone membrane contacting.

To reduce waste of excess gas, Janknecht et al. (2001) recycled the ozone/oxygen mixture back to the ozone generator after desiccation. This has not been done in other experimental set-ups discussed here but may be a promising strategy to minimize energy- and material-related costs. The modification of the membrane shape in order to create more turbulence is another optimization strategy. Recently, helical PTFE fibers were suggested by Sabelfeld and Geißen (2019) as alternative to straight fibers. The comparison of simulated mass transfer in straight fibers and experimentally determined mass transfer in helical fibers indicates an enhancement factor between 3 and approximately 6.75 due to the increased turbulences in the helical configuration. To our knowledge, other improved hollow fiber module designs such as cross flow mode with water flowing on the shell side and baffles added to increase turbulence, as known from other applications (Gabelman and Hwang, 1999), have not been tested so far.

Few studies are addressing the transfer of knowledge gained in lab-scale experiments to design large-scale processes with high treatment efficiency. The term efficiency describes the establishment of a desired ozone and/or OH-radical exposure with the lowest possible energy consumption and investment costs for the equipment and membrane material. This includes the use of most ozone generated. In lab-scale membrane modules, where all analyzed data comes from, only a small fraction of the generated ozone enters the liquid phase. For a large-scale system, planners have to select how to produce ozone (and hydrogen peroxide, in case of peroxone treatment), and how to size membrane modules. Pines et al. (2005) used Eq. 4 with a log-mean concentration driving force and experimentally determined K values to demonstrate design of a large-scale ozone membrane contacting system with 99% gas transfer efficiency ( $3,785 \text{ m}^3 \text{ d}^{-1}$ , liquid ozone concentration is  $2 \text{ mg l}^{-1}$ ). Their suggested hollow fiber module is open-ended, contains fibers of 1.8 mm inner diameter, has a total membrane area of  $300 \text{ m}^2$ , and a volume of  $0.15 \text{ m}^3$ . In this simple calculation approach, no chemical reaction and the resulting enhancement is included, and the selection of module geometry is based on other lab-scale experiments (Noda et al., 2002) with no further consideration of favorable conditions.

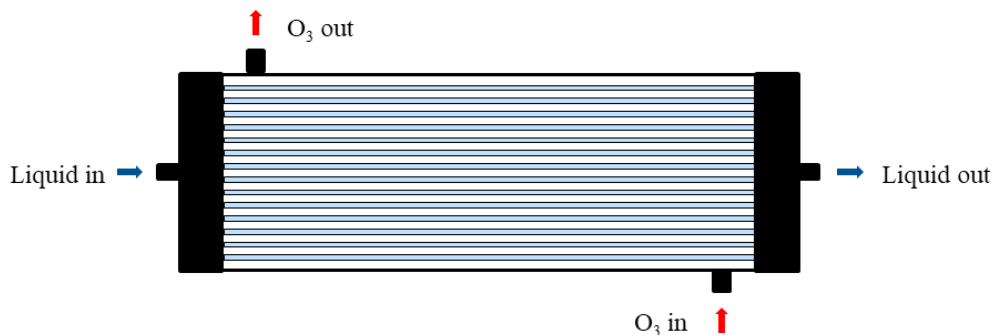


Figure 9: Typical ozone membrane contacting configuration in a circular module with the liquid flowing on the lumen side and gas on the shell side.

As could be shown in previous sections (4.5.2 and 4.6), PTFE or PVDF hollow fibers with diameters below 1 mm are well-suited for a hypothetical large-scale ozonation process with regards to material stability, oxidant exposure, and mass transfer coefficients. However, decreasing the fiber diameters not only increases mass transfer coefficients and thereby reduces required membrane surface areas, it also increases the required pressure to establish a certain liquid velocity and the desirable plug-flow conditions. It may also lead to clogging if suspended solids are in the water and fiber diameters are small. Pines et al. (2005) simply calculated the required module length based on pre-defined fiber diameter and number of fibers, which are not optimized for long-term operation at large-scale. More sophisticated iterative design procedures, which optimize investment costs and continuous energy consumption with respect to hydraulics, technical ozone gas production requirements, and mass transfer are needed for future design of full-scale membrane ozone contactors. The adoption of existing solutions for other processes, e.g., the metaheuristic optimization of heat exchangers may provide a potential solution (Patel et al., 2019). For instance, the genetic algorithm has been used to find optimized design parameters for shell-and-tube heat exchangers (Guo et al., 2009; Selbaş et al., 2006).

Another parameter which is challenging to adapt for large-scale applications is the mass transfer enhancement (section 4.7). The enhancement factor by theory depends on the interfacial ozone concentration  $c_{O_3, \text{int}}$  (Eq. 16) which would change largely due to the partial ozone gas pressure drop on the gas-side of the system when  $> 90\%$  of generated ozone are transferred into the liquid phase. This also applies to peroxone treatment, where enhancement would change largely over the fiber length especially for sub-stoichiometric peroxide doses (Figure 8). For most ozone applications, where ozone depletion is not dominated by a single chemical, the reactivity of water is hard to characterize. Reaction kinetics of ozone in natural and wastewaters have been described before (Elovitz and von Gunten, 1999; Nöthe et al., 2009), but were never translated into enhancement factors for membrane contactors. Nevertheless, enhancement should be considered in future studies

dealing with ozone membrane contacting (especially for peroxone treatment) to prevent significant overestimation of the required membrane area.

#### 4.8.2 Comparison to standard injection methods

In contrast to ozone membrane contacting, mass transfer in any bubble forming gas-liquid exchanger can only be determined as lumped parameter  $k_1 a$  (volumetric mass transfer coefficient) with liquid-side mass transfer coefficient  $k_1$  and specific surface area  $a$ , as the surface area of the bubbles is largely unknown. This parameter allows direct comparison of ozone membrane contacting and other ozone transfer technologies with regards to mass transfer per time in a given volume (Gottschalk et al., 2010; Pines et al., 2005). The volumetric mass transfer coefficient  $K a_s$  of gas-liquid membrane contactors with overall mass transfer coefficient  $K$  and internal specific surface area  $a_s$  is valid independent of the scale as the upscaling can be achieved by the addition of modules with well-known characteristics. For ozone membrane contactors,  $K a_s$  values were calculated from collected mass transfer coefficients and visualized as log-boxplot (Figure 10).

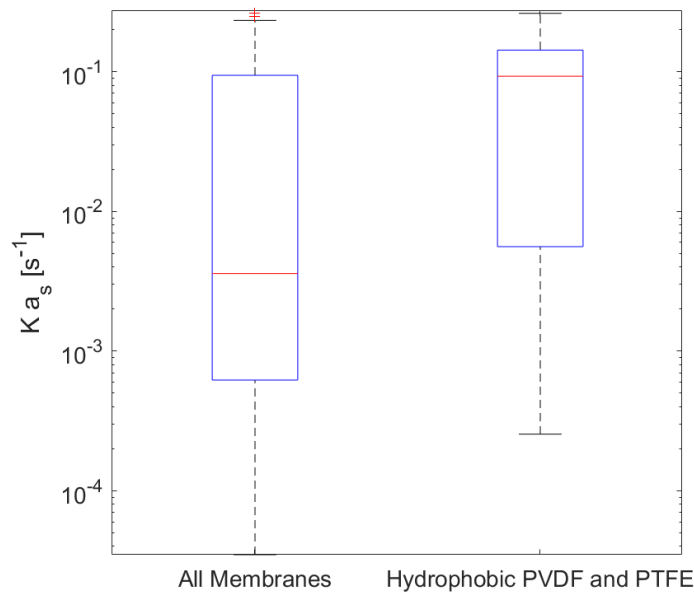


Figure 10: Experimental  $K a_s$  values for all membranes ( $n=108$ ) and for hydrophobic PVDF and PTFE membranes only ( $n=55$ , as well included in the dataset on the left side).

The specific internal surface areas in the included modules ranged from 512.82 to 8,000  $m^{-1}$ . As expected, there is a strong variation of  $K a_s$  values, since  $K$  in the original data set varied over several orders of magnitude. This is related to the differences discussed in section 4.5.2 and 4.6. Hence, the minimum and maximum  $K a_s$  values of  $3.49 \cdot 10^{-5} s^{-1}$  and  $2.6 \cdot 10^{-1} s^{-1}$  for the data set from all membranes represent extreme conditions. Values between 25<sup>th</sup> and 75<sup>th</sup> percentile range from  $6.21 \cdot 10^{-4}$  to  $9.4 \cdot 10^{-2} s^{-1}$ . If

only hydrophobic PVDF and PTFE membranes are considered, the same percentile range is from  $5.60 \cdot 10^{-3} \text{ s}^{-1}$  to  $1.43 \cdot 10^{-1} \text{ s}^{-1}$  with a median value of  $9.29 \cdot 10^{-2} \text{ s}^{-1}$  (Figure 10). In case of bubble columns, the height of the column, injection type, gas velocity and the liquid velocity impact the mass transfer coefficient. As tested columns differ largely in geometry and were operated differently, only a range of  $k_1$  can be considered for comparison. Biń et al. (2001) determined values between  $3 \cdot 10^{-3} \text{ s}^{-1}$  -  $2 \cdot 10^{-2} \text{ s}^{-1}$  for a co-current bubble column with a height of 5.5 m and a diameter of 0.15 m. In these experiments, the liquid flow rate varied from 0.1 to  $0.45 \text{ m}^3 \text{ h}^{-1}$ . Similar  $k_1$  values of approximately  $5 \cdot 10^{-3}$  -  $1.4 \cdot 10^{-2} \text{ s}^{-1}$  were achieved in another experimental study with a column of the same diameter and a height of 2.5 m., operated with longer residence times of 111 - 480 s and a flow rate from 0.3 to  $1.32 \text{ m}^3 \text{ h}^{-1}$  (Roustan et al., 1996). Both studies worked with porous ozone distributors.

Venturi injection is another method to transfer ozone at high rates with efficiencies larger than 90%. For full-scale applications, gaseous ozone is often applied in side streams followed by injection into the main stream in static mixers (El-Din and Smith, 2003; Schulz and Prendiville, 1993). Compared to gas-liquid membrane contactors, ozone gas transfer in venturi injection is much more controlled by gas velocity. In an optimized design with multiple venturi injection points, Baawain et al. (2011) determined  $k_1$  values between approximately  $7 \cdot 10^{-2}$  and  $3 \cdot 10^{-1} \text{ s}^{-1}$  for ozonation at a much higher liquid flow rate of  $36 \text{ m}^3 \text{ h}^{-1}$ . This corresponds to the upper part of collected ozone membrane contacting data. These results demonstrate that investigated gas-liquid membrane contacting devices can achieve similar or even higher mass transfer in the same volume as some bubble columns but are in the same size range as an exemplary large-scale venturi injector with multiple injection points.

This comparison does not consider other potential benefits or drawbacks of hollow fiber gas-liquid contactors such as the gas transfer efficiency, which can be controlled in ozone membrane contacting, or the energy demand, for instance from pumping, which highly depends on system-specific pressure drops. Additionally, limited knowledge on lifetime of membrane materials adds uncertainty to this comparison (section 4.4). On the positive side, direct injection of ozone into the liquid stream coupled with hydrogen peroxide as suggested for ozone membrane contacting could potentially allow a very controlled treatment of specific water matrices and minimize undesired by-products (Merle et al., 2017). However, side-stream venturi injection is much more established, including operational experience and manufacturing companies (Schulz and Prendiville, 1993). From the data compared, it cannot be stated that ozone membrane contacting generally offers the advantage of higher volumetric mass transfer coefficients and superior mass transfer performances. A full economic comparison is necessary which should be based on the specific energy required to transfer a certain amount of ozone to

1 m<sup>3</sup> of water in a certain time period. This also must include some assumptions on investment costs and lifetime as well as requirements for subsequent retention volume and degassing.

## 4.9 Conclusions

This review discusses advances in developing ozone membrane contacting applications for water and wastewater treatment. Major outcomes are briefly summarized herein.

- Except PTFE, all polymeric membranes used for ozone membrane contacting reportedly change their properties if exposed continuously to ozone. The continuous exposure will result in comparably fast material breakdown of PP or long-term decline of mass transfer of PVDF. The long-term durability of PDMS membranes is unknown, but structural changes are to be expected.
- Inorganic membranes were modified with various surfactants to create hydrophobic surfaces. Both, long-chained fluorosilanes and trichloromethylsilane were successfully used to achieve large contact-angles of water droplets on the modified membrane surface. The ozone stability of the functionalized layer of this approach has not been investigated.
- Reported ozone mass transfer coefficients in pure water agree well with calculated values (Lévêque solution) if the values are comparably high. Values for PTFE and hydrophobic PVDF membranes agree much better with calculations than PDMS, hydrophilic PVDF or  $\alpha$ -Al<sub>2</sub>O<sub>3</sub> membranes, potentially due to significant, but unknown membrane resistances.
- Investigated hydrophobic PVDF and PTFE membranes show superior ozone mass transfer compared to other membrane materials. It can be assumed that this is related to smaller membrane diameters and lower membrane resistance, which becomes most relevant at high liquid velocities.
- A difficulty for upscaling of lab-scale results using mass transfer enhancement theory to design membrane areas are suspected concentration changes over fiber length, induced by unknown reactivity of combined reactants and the large gas-side pressure drop along the fiber. The enhancement by H<sub>2</sub>O<sub>2</sub> during peroxone treatment has not been investigated systematically so far.
- Volumetric mass transfer coefficients of investigated lab-scale membrane modules range from  $3.49 \cdot 10^{-5} \text{ s}^{-1}$  to  $2.6 \cdot 10^{-1} \text{ s}^{-1}$ . Volumetric mass transfer in PTFE and hydrophobic PVDF modules is higher than in bubble columns and comparable to a highly optimized venturi injection system.



- A full economic comparison must include detailed cost considerations, as pumping energy, ozone transfer energy and investment costs may differ largely. It is suggested that there is unused potential to optimize design of ozone membrane contactors as fiber diameters and module length impact hydraulic pressure drop and mass transfer.

#### **4.10 Acknowledgement**

This work was performed within the German-Israeli cooperation project “ISCO<sub>3</sub>” funded by the German Federal Ministry of Education and Research (BMBF) and the Ministry of Science and Technology (MOST) from Israel, funding codes 02WIL1523 and 3-15878.

## 5 GROUNDWATER REMEDIATION BY IN-SITU MEMBRANE OZONATION: REMOVAL OF ALIPHATIC 1,4-DIOXANE AND MONOCYCLIC AROMATIC HYDROCARBONS

The following chapter presents investigations related to **research objective 2 (hypotheses 2.1 and 2.2)**: *Evaluate the operation of ozone-releasing gas-liquid membrane contactors for ISCO applications with different contaminant types and porous media effects.*

This chapter has been published with some editorial changes as follows:

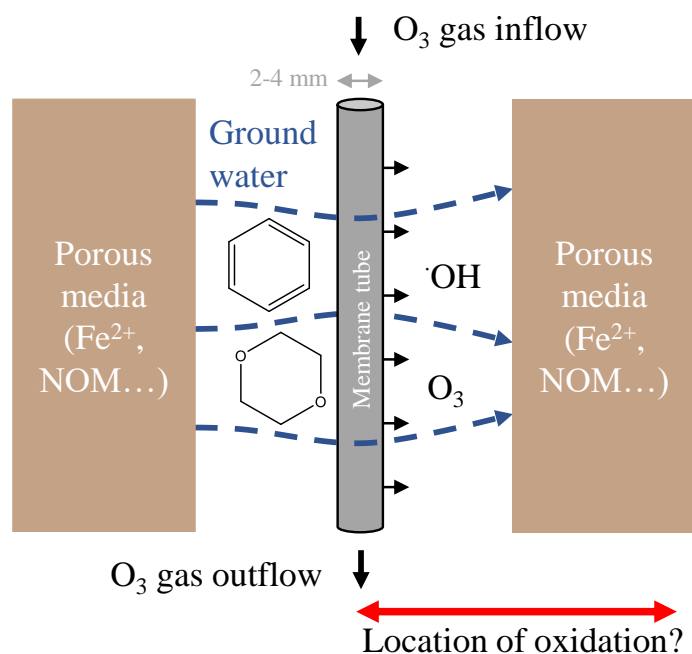
*Bein, Emil; Pasquazzo, Giulia; Dawas, Anwar; Yechezkel, Yinon; Zucker, Ines; Drewes, Jörg E.; Hübner, Uwe (2024): Groundwater remediation by in-situ membrane ozonation: Removal of aliphatic 1,4-dioxane and monocyclic aromatic hydrocarbons. In: Journal of Environmental Chemical Engineering 93 (10), 111945. DOI: 10.1016/j.jece.2024.111945.*

Author contributions: Emil Bein: Conceptualization, Methodology, Formal analysis, Investigation, Software, Writing – Original Draft, Writing – Review & Editing, Giulia Pasquazzo: Formal analysis, Investigation, Writing – Review & Editing, Anwar Dawas: Writing – Review & Editing, Yinon Yechezkel: Writing – Review & Editing, Ines Zucker: Funding acquisition, Writing - Review & Editing, Jörg E. Drewes: Funding acquisition, Writing - Review & Editing, Uwe Hübner: Conceptualization, Methodology, Supervision, Funding acquisition, Writing – Review & Editing

### 5.1 Abstract

Groundwater contamination by widespread and persistent organic compounds requires extensive treatment efforts, for example by in-situ chemical oxidation (ISCO). In this study, we investigated ozone mass transfer and removal mechanisms of ozone-resistant monocyclic aromatic and non-aromatic compounds in a novel in-situ treatment method using ozone-permeable membranes as reactive barrier. Initial batch experiments confirmed fast depletion of ozone in presence of sub-stoichiometric benzoic acid (BA), in contrast to the non-aromatic 1,4-dioxane (DIOX), where ozone depleted much slower. Simulated in-situ membrane ozonation treatment of contaminated groundwater led to lower removal of 5 mg L<sup>-1</sup> BA (52.7%) compared to DIOX (60.6 %). Inhibited removal

of BA compared to additional batch experiments could be explained by quick depletion of ozone by reactive intermediates on the membrane surface. Surprisingly, reactive porous media did not lead to substantial changes of in-situ DIOX oxidation, although a stronger impact of the media on DIOX oxidation was hypothesized. Furthermore, experimental ozone mass transfer coefficients were determined ( $3.94 \cdot 10^{-7} - 3.12 \cdot 10^{-6} \text{ m s}^{-1}$ ) and compared to modeled values for different membrane types (polydimethylsiloxane and polytetrafluoroethylene). Finally, a mathematical model based on mass transfer data was developed to support upscaling efforts. We concluded that contaminant properties are crucial for the feasibility assessment of in-situ ozone membrane treatment technology.



**Keywords:** Groundwater remediation; in-situ chemical oxidation; membrane contactors; ozonation

## 5.2 Introduction

In-situ chemical oxidation (ISCO) for remediation of contaminated groundwater is a widely applied type of treatment technology, where different oxidants, such as ozone (O<sub>3</sub>), permanganate (MnO<sub>4</sub><sup>-</sup>), persulfate salts (S<sub>2</sub>O<sub>8</sub><sup>2-</sup>, HSO<sub>5</sub><sup>-</sup>), hydrogen peroxide, or a combination of different oxidants are injected into the groundwater to remove persistent and toxic contaminants (Krembs et al., 2010; Siegrist et al., 2011; Watts and Teel, 2006). Ozonation alone or the combination of ozone with hydrogen peroxide (“peroxone”) are among the most common treatment technologies, where the formation of highly powerful hydroxyl radicals (·OH) in combination with direct ozone reactions oxidize a wide range of organic contaminants (e.g., aromatic and aliphatic compounds with various reactive functional groups such as amines), and can lead to successful remediation of sites

contaminated with monocyclic aromatic hydrocarbon (Krembs et al., 2010; Nimmer et al., 2000). Challenges associated with in-situ ozonation, however, can be found with the injection method as gaseous ozone needs to be dissolved as efficiently as possible and problems such as gas channeling may inhibit the proper distribution of dissolved ozone in sparging operations (Clayton, 1998; Siegrist et al., 2011). Additionally, substantial consumption of ozone by soil constituents may limit the travel distance and make the zone of influence of sparging wells difficult to predict. This is also the case for potential  $\cdot\text{OH}$  formation through interactions of ozone with metals or organic matter (Lim et al., 2002; Ying et al., 2021). Volatile organic chemicals present another issue when they are pushed to the unsaturated soil during ozone gas injection and require further treatment and attention (Siegrist et al., 2011).

An alternative to ozone bubble diffusion that may overcome some of the discussed challenges constitutes the use of gas-liquid membrane contactors, where gas- and liquid-phases are separated by a gas-permeable membrane and ozone is released by direct dissolution at the membrane surface (Bein et al., 2021; Gabelman and Hwang, 1999; Pabby and Sastre, 2013). Such ozone membrane contactors were previously discussed for ex-situ treatment of surface water, groundwater, and wastewater with different research goals, e.g. bromate minimization and mass transfer modeling (Kämmler et al., 2022; Stylianou et al., 2018b; Zoumpouli et al., 2018). Hollow fiber membrane modules and long wounded membrane tubes of varying diameters (<1 mm up to several mm) have been investigated for in-situ hydrogen and oxygen release, which are aimed to cover a contaminated cross-section by creating large surface area (Chaplin et al., 2009; Edstrom et al., 2005; Fang et al., 2002; Fang et al., 2004; Patterson et al., 2002; Patterson et al., 2004; Schnobrich et al., 2007). This was done, for example, with the intention to stimulate biological degradation of nitrate and trichloroethene with  $\text{H}_2$ , or atrazine removal with  $\text{O}_2$ . Recently, polydimethylsiloxane (PDMS) membranes were tested for ozone release to form a permeable reactive barrier (PRB), with chemical reactions taking place in proximity of the membrane (Dawas et al., 2023). However, the removal of relevant organic contaminants at slow flow velocities with reactive porous media as well as a realistic engineering design approach for a scale up of such an ozone injection system has not been demonstrated yet.

In this study, we used two structurally different model contaminants, benzoic acid (BA) and 1,4-dioxane (DIOX), to investigate—to our knowledge the first time—the effect of contaminant properties and porous media on in-situ removal efficiency using ozone membrane contactors. Furthermore, experimentally determined mass transfer coefficients were used to characterize ozone mass transfer and assess feasibility of large-scale treatment. BA is not a typical groundwater pollutant, but it can be used to simulate reaction mechanisms during ozonation due to its stabilized aromatic ring, structurally

similar to BTEX (benzene, toluene, ethylbenzene, and xylene isomers) (Bein et al., 2023a). DIOX is a heterocyclic ether and emerging groundwater pollutant, whose extraordinary persistence and accumulation in natural water bodies has raised great concern (Adamson et al., 2014; Adamson et al., 2015). While both compounds are practically not reactive with ozone itself ( $k_{O_3}$  of 1.2 and  $0.32 \text{ M}^{-1} \text{ s}^{-1}$ , Hoigné and Bader (1983a)), reactions of  $\cdot\text{OH}$  with BA (as a representative of monocyclic aromatics,  $k_{OH} = 4.3 \cdot 10^9 \text{ M}^{-1} \text{ s}^{-1}$ , Buxton et al. (1988)) generate ozone-reactive intermediates that further consume ozone, accelerate its decomposition, and initiate radical chain reactions if the BA concentration is high enough (Huang et al., 2015; Wang et al., 2022c). DIOX, contrarily, forms no such known intermediates and therefore its removal by ozone is expected to be much more reliant on the factors that impact  $\cdot\text{OH}$  production ( $k_{OH} = 2.8 \cdot 10^9 \text{ M}^{-1} \text{ s}^{-1}$ , Buxton et al. (1988)). These are on the one hand the allowed reaction time due to slow  $\cdot\text{OH}$  formation in natural water with low DOC (Acero and von Gunten, 2001), and on the other hand accelerating or inhibiting factors for radical formation such as ozone-soil reactions (Ying et al., 2021). Therefore, we hypothesize that removal of DIOX in a cross flow PRB with ozone-releasing membranes is heavily impacted by the nature of porous media after passing the barrier. BA, in contrast, may be quickly consumed due to the described self-enhanced decomposition, and ozone-consuming soil layers have a limited effect due to immediate consumption of released ozone.

Within the scope of this study, we first investigated the effect of accelerated ozone consumption in presence of BA in direct comparison to DIOX in batch experiments with natural water. In a second step, removal of BA and DIOX during simulated ozone delivery by PDMS membranes was compared at the same liquid flow velocity. Experiments were conducted with different layers of porous media—that are either inert or reactive with ozone—as well as natural soil. This was compared to removal of BA and DIOX at different ozone doses. Third, we characterized ozone mass transfer through a membrane PRB using two membrane materials and different flow velocities. Finally, we were able to make design considerations for upscaling using a simple numerical model and highlight limitations and potential applications of this technology.

## 5.3 Materials and methods

### 5.3.1 Chemicals and reagents

All used chemicals, their purities, and the suppliers are listed in the supplemental information (SI), Table 8. Solutions for experiments were freshly prepared on the days of experiments by dissolving contaminants and other desired constituents, either in ultrapure water with phosphate buffer (pH 7), or in freshly withdrawn non-chlorinated tap water (TW, typical withdrawal pH = 7.6-7.7,  $\text{HCO}_3^- = 333 \text{ mg L}^{-1}$ ,  $\text{TOC} < 1 \text{ mg C L}^{-1}$ ).

## 5.3.2 Ozone batch experiments

### 5.3.2.1 Ozone consumption in presence of contaminants

Batch experiments to demonstrate enhanced ozone decomposition in presence of BA compared to DIOX at the conditions of this study were performed by adding ozone stock solution containing approximately 1 mM dissolved ozone to magnetically stirred batches with 500 mL total volume in 1 L borosilicate bottles. 5 mL sample were withdrawn for ozone analysis after fixed time intervals using a dispenser (Carl Roth, Germany) that was sealing the bottle during the experiments. Ozone stock solution was produced from pure oxygen using a bench-scale ozone system that included a BMT 803 BT ozone generator and a BMT 964 gas analyzer (BMT Messtechnik GmbH, Germany), where ozone gas was injected via bubble diffusion into a cooled glass reactor filled with ultrapure water, and stock solution withdrawn by a peristaltic pump. Stoichiometric ratios of 2:1, 10:1, and 20:1 (O<sub>3</sub>:contaminant) were achieved with a constant target ozone dosage of approximately 81.2 μM for BA and 113.5 μM for DIOX experiments, and variable BA and DIOX concentrations of 40.9, 8.2, and 4.1 μM for BA and 56.7, 11.3, and 5.7 μM for DIOX, corresponding to 5, 1 and 0.5 mg L<sup>-1</sup>. Solutions were prepared with tap water (TW) that was diluted by ultrapure water by a constant factor of 0.8 (80% TW, 20 % UPW) due to the addition of ozone stock solution and contaminant spiking.

### 5.3.2.2 Compound removal depending on dissolved ozone dose

Additional batch experiments to investigate removal of BA/DIOX were conducted in the same water matrix, where a variable amount of ozone stock solution was added to complete 50 mL / 100 mL amber batches containing 5 mg L<sup>-1</sup> DIOX or BA. The closed batches were slowly stirred for 1 hour and 48 minutes before sampling, which corresponds to the expected travel and reaction time in the membrane ozonation system at 150 cm d<sup>-1</sup> average liquid flow velocity to compare removal under similar conditions. Samples were analyzed for residual ozone and then quenched with 1 mM sodium thiosulfate (Na<sub>2</sub>S<sub>2</sub>O<sub>3</sub>) to stop the reaction after the desired reaction time. Further information can be found in the SI, 10.3.3.

## 5.3.3 Membrane-based ozone delivery

Cross-flow gas-liquid membrane contacting experiments were performed with a customized cylindrical stainless steel reactor with 15 cm inner diameter and a height of approximately 32 cm. The membrane tubes were fixed on a stainless steel perforated support at a height of 17.9 cm (Figure 11). The bottom section (up to approximately 15 cm) of the reactor was filled with 3 mm diameter glass beads (VWR, USA) to improve the homogeneity of the flow. The feed solution was pumped through PTFE tubing into

the reactor by a gear pump and the flow rate was monitored with a DK 800 Krohne rotameter (Krohne Messtechnik GmbH, Germany). The average flow velocity was defined as the measured flow rate divided by the cross-sectional area of the reactor. A needle valve was installed after the reactor to slightly adjust the pressure in the system by partial closure of this valve until no bubble formation was observed for porous PTFE membranes. No adjustment was required for PDMS membranes.

Ozone was produced with the same system as in section 5.3.2, which was connected to the membrane with PTFE tubing. The system also included a magnetic valve, which either directs the gas stream to the membrane system or to a catalytic destruction unit. Ozone gas concentrations, membrane types, and the water matrix were adjusted based on the type of experiment and are specified in the respective protocols below.

Two different membrane materials were used throughout the experiments: (1) PDMS (DOW Corning, Silastic, USA), purchased from Cole Parmer (Germany) with an inner and outer diameter of 1.98 and 3.18 mm cut to a length of 2.59 m (Zoumpouli et al., 2018), and (2) expanded PTFE (FluorTex GmbH, Germany) with a porosity of 50% and an inner and outer diameter of 2.8 and 3.8 mm cut to a length of 2 m. The tube lengths corresponded to approximately the same membrane surface area, considering the logarithmic average of inner and outer diameter.

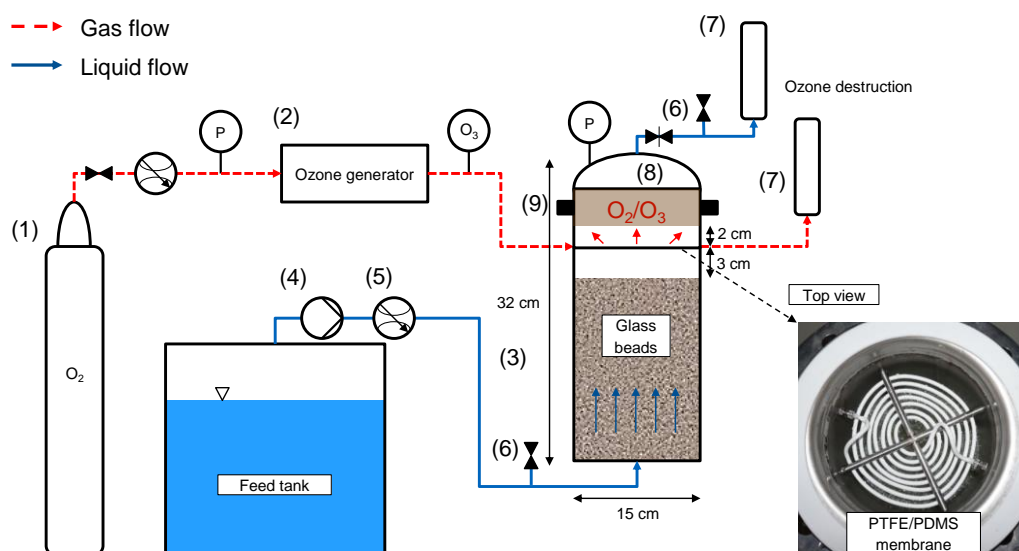


Figure 11: Experimental set-up for ozone membrane contacting experiments in cross flow mode. Single components: (1) Oxygen gas cylinder; (2) Ozone generator with integrated pressure and flow control; (3) Stainless steel reactor filled with glass beads; (4) Gear pump; (5) Flow meter; (6) Sampling port (and needle valve); (7) Catalytic ozone gas destruction; (8) Optional soil layer; (9) Flange for opening the reactor.

### 5.3.4 In-situ oxidation of BA and DIOX

In-situ oxidation experiments with BA and DIOX were performed using the experimental set-up displayed in Figure 11 with an installed customized stainless steel tray to hold a porous media layer approximately 2 cm above the membrane holder, which was passed by the ozonated water. The tray contained different types of porous media: (1) Baked technical sand (BS, 400° C for 4 h), (2) catalytic MnO<sub>2</sub> for ozone destruction (MNO-92, GAWU GmbH, Germany), and (3) the standard soil A2.1 (LUF A Speyer, Germany) that contains 0.55% organic carbon and various metals (SI, Table 9). The tray contained 200 g of material, unless otherwise specified. Only the PDMS membrane type was used in these experiments. BA and DIOX (5 mg L<sup>-1</sup>) were always spiked into 11 L of freshly withdrawn TW. The average flow velocity of 150 cm d<sup>-1</sup> was kept constant for this type of experiment and the ozone gas concentration was set to 200 g Nm<sup>-3</sup> at a gas flow rate of approximately 0.2 NL min<sup>-1</sup>. Samples for DIOX/BA quantification and dissolved ozone concentrations were withdrawn at the effluent sampling port every 21 min and 44 s, which corresponds to 0.2 empty bed volumes treated (EBVT), defined by the volume from membrane tube to sampling port. The samples for BA/DIOX quantification were immediately mixed with 1 mM Na<sub>2</sub>S<sub>2</sub>O<sub>3</sub> to remove residual ozone. Removal of contaminants (BA and DIOX) was calculated using the feed solution concentration (sample taken at the beginning of the experiment) and the effluent concentrations after each time step.

### 5.3.5 Experimental mass transfer estimations

Mass transfer of PTFE and PDMS membranes was determined separately in different liquid velocities using a customized probe compound method. Briefly, removal of probe compounds at trace concentrations (Table 6) was used to calculate the overall ozone exposure from the point of ozone release at the membrane until the sampling port. Assuming that ozone is the only relevant reactant with the respective compound due to suppression of hydroxyl radical exposures by using the scavenger tertiary butanol (t-BuOH), one can state that

$$\ln\left(\frac{c_{p,t}}{c_{p,0}}\right) = -k_{O_3} \int_0^t [O_3] dt \quad \text{Eq. 19}$$

where  $c_{p,t}$  is the concentration of the probe compound at the sampling port (at time  $t$ ),  $c_{p,0}$  the concentration of the same compound in the feed tank,  $k_{O_3}$  the second order reaction rate constant (M<sup>-1</sup> s<sup>-1</sup>) of the probe compound (Table 6) with ozone at pH 7, and  $\int_0^t [O_3] dt$  the ozone exposure after contact time  $t$  (here the theoretical travel time of water from membrane to sampling port). Assuming that ozone decomposition inside the reactor is



unaffected by probe compounds due to their negligible concentrations  $< 10 \mu\text{g L}^{-1}$ , the ozone concentration may be described by a pseudo first-order kinetic

$$[O_3] = [O_3]_0 e^{-k_d t} \quad \text{Eq. 20}$$

where  $[O_3]_0$  is the ozone concentration at  $t = 0$ ,  $k_d$  the first-order rate constant for ozone decay  $[\text{s}^{-1}]$ . By integrating this equation over  $t$ , ozone exposure can also be expressed as

$$\int_0^t [O_3] dt = \int_0^t [O_3]_0 e^{-k_d t} dt. \quad \text{Eq. 21}$$

Rearrangement and integration of this equation leads to

$$[O_3]_0 = \left( \int_0^t [O_3] dt \right) k_d (1 - e^{-k_d t})^{-1}. \quad \text{Eq. 22}$$

Ozone exposure determined by the probe compound approach (Eq. 19) can be used to calculate the ozone concentration at  $t=0$  (Eq. 22), which is then used for the calculation of ozone mass transfer coefficients  $K$ , according to the procedure used by Karakurt-Fischer et al. (2020) for oxygen, which is also explained in detail in the SI, 10.3.4.

The unknown ozone decay  $k_d$  was determined by measuring residual ozone concentrations at the sampling port in all experiments (different flow velocities and membranes) and fitting  $k_d$  so that there is a maximum correlation of measured sampling port concentrations and calculated reactor effluent concentrations based on the ozone exposure, determined by using Eq. 20 and 21 (SI, 10.3.5).

Table 6: Second-order reaction rate constants of probe compounds used in this study.

Compound	$k_{O_3}$ (pH 7) ( $\text{M}^{-1} \text{s}^{-1}$ )	Reference
Primidone	1	Real et al. 2009
Iopromide	<0.8	Huber et al. 2003
Ibuprofen	9.6	Huber et al. 2003
Gabapentin	13.7	Bein et al. 2023b
Benzotriazole	142	Estimated <sup>a</sup>
Atenolol	$1.7 \cdot 10^3$	Benner et al. 2008
Carbamazepine	$3 \cdot 10^5$	Huber et al. 2003

<sup>a</sup> Calculated with  $pK_a$  of 8.37 and reaction rate constants 35 and  $2650 \text{ M}^{-1} \text{ s}^{-1}$  of the two species (von Sonntag and von Gunten, 2012).

Experiments were conducted with 15 L feed solutions that were freshly prepared on each day by diluting probe compounds ( $5 \mu\text{g L}^{-1}$ ),  $t\text{-BuOH}$  (50 mM), and pH 7 phosphate buffer (5 mM) in ultrapure water. First, the reactor was filled with feed solution, then the flow rate was adjusted accordingly to achieve average reactor flow velocities of  $136 - 978 \text{ cm d}^{-1}$  ( $1.57 \cdot 10^{-5} - 1.13 \cdot 10^{-4} \text{ m s}^{-1}$ ). After achieving a stable flow rate, the ozone gas stream was fed into the membrane tube at a concentration of  $100 \text{ g Nm}^{-3}$  and a gas flow rate of approximately  $0.2 \text{ L min}^{-1}$  and the timer was started. Samples were taken from the feed tank and three times from the sampling port at the reactor effluent after

reaching steady-state, which was defined as the time after approximately three EBVT. In addition to samples for the probe compounds, dissolved ozone concentrations were determined at the outlet using a modified indigo method (section 5.3.7). All experiments were performed with the same membrane material in randomized order.

### 5.3.6 Modeling of mass transfer rates

In addition to experiments, K values for membrane mass transfer to groundwater flow were also estimated using a dimensionless correlation established by Fang et al. (2002), depending on membrane, gas, and liquid properties. Mass transfer coefficients of this correlation were integrated in a mathematical model that simulates ozone transfer of a long membrane tube into a groundwater current based on mass balances in finite sections including the partial ozone pressure drop on the gas side (SI, 10.3.9).

### 5.3.7 Analytical methods

BA was analyzed using an Agilent 1260 Infinity II HPLC-DAD system with the same gradient method that was previously described (Bein et al., 2023a). Briefly, samples were injected at a volume of 50  $\mu\text{L}$  and separated on an XSelect HSS C18 column (2.1 x 100 mm, 3.5  $\mu\text{m}$  particle size) at a flow rate of 0.6  $\text{mL min}^{-1}$ , with 0.1% formic acid in  $\text{H}_2\text{O}$  and 100% acetonitrile as solvents. Calibration standards ranged from 0.5 to 10  $\text{mg L}^{-1}$  for these experiments.

DIOX was analyzed using an Agilent 7980 gas chromatograph with Agilent 7697A headspace auto-sampling module coupled with flame ionization detection (HS-GC/FID, Agilent, USA). Compound separation was performed on a 30 m column (0.32 mm inner diameter, 1.80  $\mu\text{m}$  film thickness, DB-624, Agilent, USA) with nitrogen as carrier gas. The initial oven temperature of 40  $^{\circ}\text{C}$  was kept for 3 min and increased by 12.5  $^{\circ}\text{C min}^{-1}$  to 250  $^{\circ}\text{C}$  and maintained there for 3 min. 10 mL of sample was filled into a 20 mL headspace vial containing 0.5 g sodium sulfate. The calibration standards ranged from 0.5 to 10  $\text{mg L}^{-1}$ . More details can be found in the SI, 10.3.2.

Probe compounds listed in Table 6 were quantified with a SCIEX TripleQ mass spectrometer coupled with a KNAUER PLATINBLUE UHPLC for compound separation. An XSelect HSS C18 (particle size 2.5  $\mu\text{m}$ ; 2.1 x 100 mm) column was employed for separating compounds with a gradient method (Waters, USA). Compounds were detected in positive ESI mode with 0.2% formic acid in  $\text{H}_2\text{O}$  (A) and 100% acetonitrile as solvents, except for ibuprofen, which was detected in negative ESI. In this case, 0.1% acetic acid in  $\text{H}_2\text{O}$  was used for A instead. Further details on sample preparation and the LC-MS/MS method can be found in Müller et al. (2017).

The concentration of dissolved ozone in batch experiments was measured using a modified indigo method (Bader and Hoigné, 1981) with Indigo carmine (610 nm, 19,000 M<sup>-1</sup> cm<sup>-1</sup>), first in order to adjust ozone stock solution volumes added to batches and, second, to follow ozone decay.

## 5.4 Results

### 5.4.1 Ozone decomposition in presence of BA and DIOX

Initial batch experiments confirmed accelerated decomposition of ozone in presence of BA as function of its concentration compared to DIOX oxidation (Figure 12). Immediate (< 30 s) and complete ozone consumption (ca. 73 μM) was observed with 40.9 μM initial BA (5 mg L<sup>-1</sup>). At lower BA concentrations of 8.2 μM and 4.1 μM, more than 92% and 48% of dissolved ozone was removed after 10 min with ozone in excess by a factor of 10 and 20. This confirms a highly over-stoichiometric ozone consumption despite the extremely low direct reactivity of BA with ozone ( $k_{O_3} = 1.2 \text{ M}^{-1} \text{ s}^{-1}$ , Hoigné and Bader (1983a)). To prove that this mechanism is also relevant for monocyclic aromatic groundwater contaminants, we conducted additional ozone decomposition tests with toluene in the same water matrix. A similar pattern was observed with toluene, where small concentrations (< 1 mg L<sup>-1</sup>) decompose a large portion of added ozone after 10 min (SI, 10.3.6). It has to be noted that the TW composition (alkalinity, metals, DOC) may slightly fluctuate over time, however, one batch of withdrawn water was used for this set of experiments and pH remained constant (7.6-7.7) throughout all experiments. Accelerated and simultaneous decomposition of BA and ozone depletion has already been reported for acidic conditions (pH 2.3), where the low abundance of hydroxide ions (OH<sup>-</sup>) results in less formation of hydroxyl radicals via ozone-water interactions and therefore slows down the reaction (Huang et al., 2015). In their study, Huang et al. (2015) could also show that BA is ozone-resistant in presence of the radical-scavenger t-BuOH. An even faster process can be expected at neutral pH due to the higher abundance of hydroxide ions, which are reacting with ozone to form radical species.

The observed pattern of accelerated decomposition with ozone can be explained by the well-known formation of ·OH radicals during ozonation of activated aromatic compounds such as phenol or municipal wastewater DOC in general (Buffle and von Gunten, 2006; Nöthe et al., 2009; von Sonntag and von Gunten, 2012). Phenolic intermediates such as salicylic acid may cause formation of other reactive oxygen species (HO<sub>2</sub>·, O<sub>3</sub><sup>-</sup>) while reacting with ozone, which eventually promotes radical chain reactions and leads to more ·OH formation as part of the ozone decay in water (Ramseier and von Gunten, 2009; von Gunten, 2003). Recently, Wang et al. (2022c) detected H<sub>2</sub>O<sub>2</sub> during ozonation of both BA and its hydroxylated intermediates, which is an indication of a

further breakdown of carbon double bonds by the Criegee mechanism (Criegee, 1975). Hence,  $\cdot\text{OH}$  production to accelerate the removal of BA can be caused by follow-up reactions of ozone with  $\text{H}_2\text{O}_2$  but also through direct interaction of ozone with phenolic intermediates.

In contrast, addition of DIOX had no noteworthy effect on ozone decay, independent of the amount of DIOX added (Figure 12). The average ozone decay of 31.5 % after 10 min in the experiments containing 11.3  $\mu\text{M}$  was only slightly more than in the control without contaminant addition (28.4 %). Similar to BA, DIOX is practically ozone-resistant with a second-order rate constant of  $0.32 \text{ M}^{-1} \text{ s}^{-1}$  (Hoigné and Bader, 1983a) and no ozone consumption was expected due to the absence of unsaturated carbon or other electron-rich moieties that react fast with ozone, e.g., secondary or tertiary amines (Lim et al., 2019). Even though these findings are based on previously known mechanisms, this direct comparison is to our knowledge the first of its kind in an applied groundwater remediation context and highlights how ozone consumption by intermediate products can affect treatment of structurally differing groups of ozone-resistant contaminants.

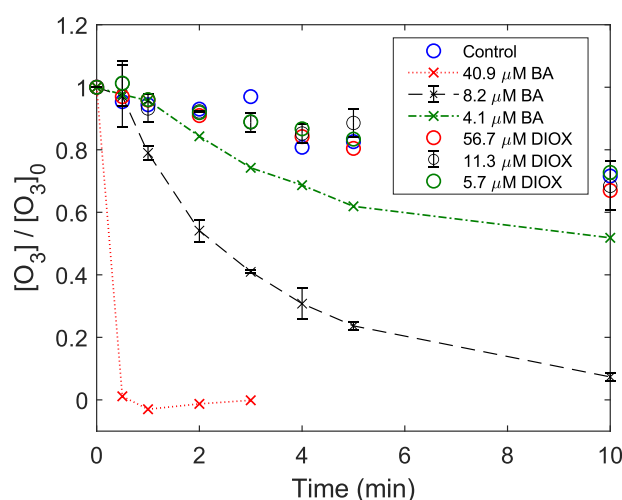


Figure 12: Ozone consumption in presence of different BA and DIOX concentrations in TW (pH 7.6-7.7). “Control” refers to the same experiment without spiked contaminant. Ozone decomposition with 8.2  $\mu\text{M}$  BA and 11.3  $\mu\text{M}$  DIOX ( $1 \text{ mg L}^{-1}$ ) has been obtained as triplicates ( $n=3$ ), the remaining data from single experiments ( $n=1$ ). Actual initial dissolved ozone concentrations were  $75.2 \pm 4.0 \mu\text{M}$  in BA and  $111.0 \pm 5.8 \mu\text{M}$  in DIOX experiments.

## 5.4.2 In-situ ozonation of BA and DIOX

### 5.4.2.1 Effects of different porous media layers on removal

In-situ ozonation of the two structurally different contaminants (BA and DIOX) was simulated with a 2.59 m PDMS membrane tube at  $150 \text{ cm d}^{-1}$  average flow velocity with different porous media layers installed after the membrane injection. The porous media layers represent organic-free porous media with relatively low reactivity (BS), catalytic

ozone consumption without hydroxyl radical generation (MNO-92), and natural soil (A2.1, finite and catalytic ozone consumption). A steady-state removal of both compounds was achieved after 1-2 empty bed volumes treated (EBVT) in the prevailing flow conditions, with approximately 55 - 75 % elimination for DIOX and about 50 % for BA, respectively (Figure 13a and b). Minor initial effects of DIOX adsorption onto porous media layers MNO-92 and A2.1 were observed, however, strong agreement of removal with other experiments from 0.4 BVT until the end (3.2 EBVT) indicate that this is not a lasting effect and does not impact removal after 2-3 EBVT (Figure 13a).

Different porous media (MNO-92, A2.1) did not cause substantial reduction or increase of contaminant removal in case of DIOX, compared to the reference BS system (Figure 13a). A minor reduction of DIOX removal with 1,400 g MNO-92 compared to BS was observed (55.1 vs. 60.6%). In contrast, effluent dissolved ozone concentrations changed for different layers, well in line with the initial assumption that both, installed MNO-92 and A2.1, consume ozone (Figure 13c). Expectedly, the BS layer led to the highest dissolved ozone concentration at the effluent, even though some reactivity can still be expected due to the heterogeneous nature of technical sand. The largest amount of MNO-92 (1,400 g) completely removed dissolved ozone after the membrane tube and we expected this ozone destruction to follow a non-radical pathway, as previous work demonstrated no effect on  $UV_{254}$ -absorbance if this material is used to remove ozone from ozonated wastewater (Schneider et al., 2016), and we also observed inhibition of DIOX oxidation in control batch experiments with MNO-92 added (SI, 10.3.3). Generally, removal of DIOX in presence of ozone can be largely attributed to formation of  $\cdot OH$  due to reactions of ozone with hydroxide, where the initial reaction proceeds with a rate constant of  $70 \text{ M}^{-1} \text{ s}^{-1}$  (von Gunten, 2003). However, since ozone-water-interactions were limited to the travel time from the membrane tube to the MNO-92 layer, the limited effect of the enhanced ozone decomposition on DIOX removal is surprising and an indication that most of the  $\cdot OH$  radical formation and reaction took place in close proximity to the membrane barrier. Due to the ozone quenching at the sampling port, final DIOX removal in the BS experiment in fact may be slightly higher if the reaction would have been allowed to proceed. However, as can be shown with batch experiments (section 5.4.2.2), residual dissolved ozone concentrations of  $30 \text{ }\mu\text{M}$  could only oxidize a small fraction of  $5 \text{ mg L}^{-1}$  ( $56.7 \text{ }\mu\text{M}$ ) DIOX.

Steady-state partial removal of ozone was also observed for A2.1 in DIOX experiments (Figure 13c), most likely related to catalytically active metal constituents of the natural soil such as iron ( $4.5 \text{ g kg}^{-1}$ , Table 9) that are known to substantially affect catalytic ozone consumption (Lim et al., 2002; Ying et al., 2021). Permanent ozone decomposition with installed A2.1 took place very similarly as with the same amount of

MNO-92 (200 g). The effluent ozone concentrations after both layers were only about 42% of what was measured for BS, which demonstrates the high level of ozone decomposition in a natural system (A2.1). This does not seem to cause higher removal of DIOX by species formed in reactions of ozone and soil, however, it was not possible to assess the ozone-soil interaction of this particular soil type in this study.

As expected, practically no dissolved ozone was detected in the reactor effluent in all experiments performed with BA (SI, 10.3.7) and removal of BA agreed very well in the experiments with BS, MNO-92, and A2.1, averaging around  $52.7 \pm 1.0$ ,  $52.2 \pm 0.6$ , and  $49 \pm 1.9$  % removal (average of the last four steady state concentrations). Mixing  $5 \text{ mg L}^{-1}$  ( $40.9 \text{ }\mu\text{M}$ ) BA with  $73.0 \text{ }\mu\text{M}$  ozone in solution caused complete ozone consumption within seconds, as discussed in section 5.4.1, thus a complete decomposition of ozone can be assumed for membrane experiments before the water reaches the porous media layer. It is noteworthy that more DIOX than BA was removed with a BS layer (60.6% vs. 52.7%), even though it can be considered more recalcitrant during ozonation because there is no comparable self-enhanced removal (section 5.4.1), a key feature of BA and other monocyclic aromatics such as toluene (Wang et al. (2022c), Huang et al. (2015), 10.3.6). This confirms that the rapid reaction of intermediates during ozonation of monocyclic aromatics not only increased the reaction kinetics, but also enhances decomposition of ozone, which is then not available for the oxidation of target (parent) chemicals.

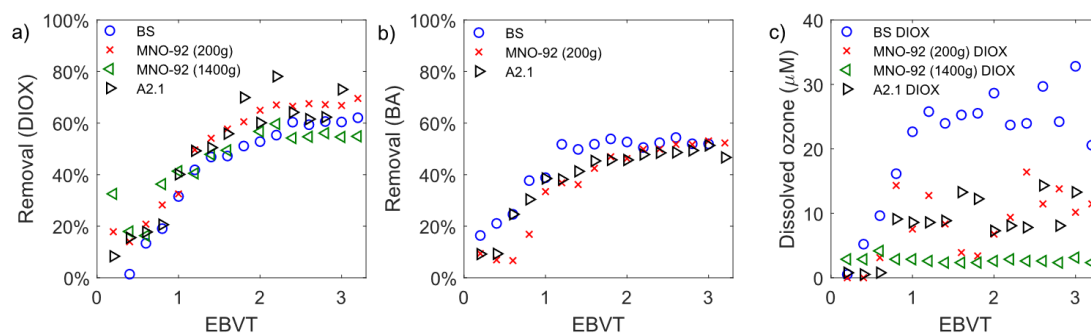


Figure 13: Removal of DIOX (a) and BA (b) as measured in the effluent of the membrane ozonation reactor as function of the empty bed volumes treated (EBVT) with different porous media layers installed ( $n=1$ ). Actual concentrations in the feed were  $5.34 \pm 0.17 \text{ mg L}^{-1}$  (DIOX) and  $5.16 \pm 0.19 \text{ mg L}^{-1}$  (BA). Ozone gas concentration was  $200 \text{ g Nm}^{-3}$  and the liquid flow velocity was  $150 \text{ cm d}^{-1}$  in all experiments. c) Dissolved ozone concentration in the reactor effluent in all DIOX experiments.

#### 5.4.2.2 Effect of ozone injection type on removal

Another series of batch experiments was performed to gain further understanding of the relationship between membrane mass transfer of ozone and contaminant removal. The same water matrix and reaction time was approximated (residual ozone was quenched after 0.75/1 EBVT, SI, 10.3.3) to compare removal of BA and DIOX observed in

membrane ozonation with direct addition of dissolved ozone (Figure 14a). The ozone doses were ranging from 23 to 232  $\mu\text{M}$ . The impact of DIOX and ozone losses to the ambient was also checked for batches with DIOX by ozonating batches with different volumes (i.e., different headspaces) and without ozone addition. Volatile losses of DIOX in these tests were marginal (<5%) and these effects can largely be excluded (SI, 10.3.3).

A consistently higher removal of BA compared to DIOX was observed for the same amount of ozone consumed (Figure 14a), which is the opposite trend as for the experiment with in-situ membrane-based ozone delivery (section 5.4.2.1, Figure 13). Measured residual dissolved ozone for variable ozone doses, however, indicated that only  $59.5 \pm 6.6$  % of the added ozone was consumed after 1 EBVT in DIOX batch experiments (SI, 10.3.3). This results in an ozone consumption ranging from 22 to 139  $\mu\text{M}$  for a DIOX removal between 9 and 68%, making DIOX removal per  $\mu\text{M}$  ozone dose consumption lower than BA oxidation for all ozone doses in batch experiments (Figure 14a). Interestingly, residual dissolved ozone concentrations in the batches with comparable removal of DIOX were much higher (>50  $\mu\text{M}$ ) than what was observed in membrane ozonation (20-35  $\mu\text{M}$ ) (SI, 10.3.3), which is in alignment with the observation of fast DIOX oxidation close to the membrane surface (section 5.4.2.1). The apparent stoichiometry of the reaction was on average 0.25 M BA and 0.28 M DIOX removed per M ozone consumed.

An observed removal over 50 % of 5  $\text{mg L}^{-1}$  (56.7  $\mu\text{M}$ ) DIOX using ozonation with doses between 6 and 11  $\text{mg L}^{-1}$  can be considered high compared to other studies, where lower concentrations of DIOX ( $\ll 1 \text{ mg L}^{-1}$ ) were ozonated only for a few minutes (Andaluri and Suri, 2017) or DIOX was spiked into a secondary treated wastewater effluent (Vatankhah et al., 2019). This is most likely related to the long reaction time (>1 h) in this study without substantial ozone consumers and hydroxyl radical scavengers.

The observed inhibition of BA removal in membrane experiments compared to batch experiments can be explained by the reaction-limiting steps in the two systems: In the self-enhanced removal mechanism of BA during batch experiments, initial  $\cdot\text{OH}$  formation by the chain of ozone reactions in water is taking place with dissolved ozone in excess, which is involving intermediate products such as  $\text{HO}_2^-$ ,  $\text{O}_2^-$ , and  $\text{O}_3^-$ . Thus, a large amount of  $\cdot\text{OH}$  can be formed in a short time period of a few seconds. In contrast to batch experiments, a steady but smaller amount of ozone is released during membrane ozonation and, additionally, PDMS membrane resistance is a factor that cannot be neglected. This is also apparent in the direct comparison with PTFE membranes (Bein et al., 2021; Zoumpouli et al., 2018). Even if mass transfer is enhanced via a reduced ozone concentration at the liquid side of the membrane, specifically PDMS is limited by the maximum diffusion of ozone through the material, i.e. the membrane resistance (Dawas

et al., 2023). Therefore, fast ozone consumption within the gas-liquid boundary layer near the membrane surface can be expected in water containing BA. The mechanism is illustrated in Figure 14, where in Step 1  $\cdot\text{OH}$  radicals are produced by reactions of released ozone and hydroxide, leading to immediate attack of BA. After transformation of BA into hydroxylated intermediates in the gas-liquid boundary layer near the PDMS membrane, these intermediates will quickly react with several ozone molecules, producing even more radicals (Step 2).

Assuming that the presence of DIOX did not cause any major changes to mass transfer (no direct reactions with ozone), we can roughly estimate that 110 – 140  $\mu\text{M}$  ozone was consumed to achieve observed DIOX removal of roughly 60% in the simulated groundwater based on ozone consumption vs. DIOX removal. This is compared and discussed further in the following section using experimental mass transfer data that was determined for different flow velocities.

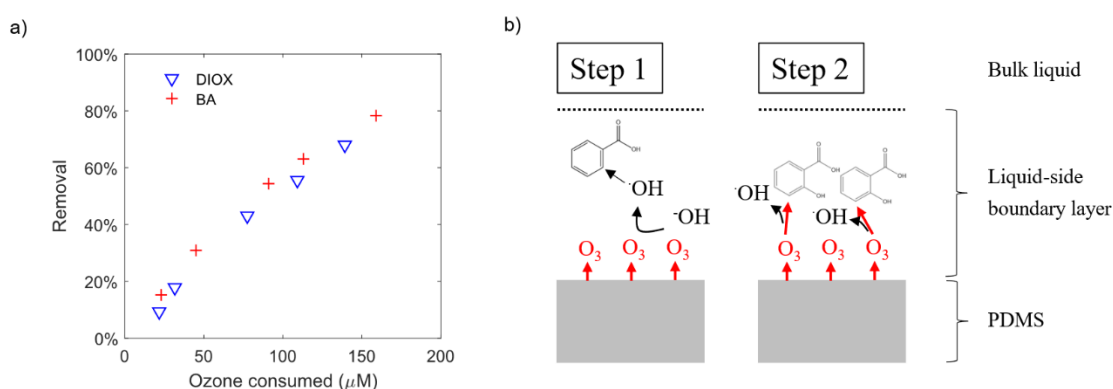


Figure 14: a) Removal of DIOX and BA ( $5 \text{ mg L}^{-1}$ ) in batch experiments conducted with tap water and ozone stock solution. The reaction time corresponds to 1 EBVT (DIOX) and 0.75 EBVT (BA). b) Illustration of fast reactions in the liquid-side boundary layer of the PDMS membrane, based on the film theory (Sirkar, 1992) and ozone decomposition and reaction with BA (von Gunten, 2003; Wang et al., 2022c).

### 5.4.3 Mass transfer estimations

#### 5.4.3.1 Experimental mass transfer coefficients

We evaluated the ozone mass transfer to assess if ozone injection at low groundwater flow velocities can be described correctly with established design equations from literature (Bein et al., 2021). Additionally, we wanted to compare removal of BA and DIOX with membrane mass transfer to evaluate options for designing membrane systems that meet remediation goals. The removal of probe compounds at trace concentrations was used to calculate the ozone exposure for two membrane materials (PTFE and PDMS) from the point of ozone injection to the sampling port for average flow velocities of 136



to  $978 \text{ cm d}^{-1}$  (Figure 15a and b). Due to the trace concentrations of less than  $10 \mu\text{g L}^{-1}$ , mass transfer enhancement can be excluded, which is typically reported for concentrations of several  $\text{mg L}^{-1}$  of highly ozone-reactive substances (Phattaranawik et al., 2005; Zhang and Wang, 2011). Additionally, t-BuOH addition (50 mM) suppressed hydroxyl radical reactions, resulting in no primidone removal for the highest liquid velocities and small removal for lower velocities, where a correction of  $\cdot\text{OH}$  exposure was applied to the ozone exposure (SI, 10.3.8).

The calculated exposure differed between the probe compounds that had deviating reactivities with ozone, where gabapentin and ibuprofen are slow reactants ( $< 20 \text{ M}^{-1} \text{ s}^{-1}$ ), and benzotriazole and atenolol faster reactants (Table 6). Carbamazepine and iopromide were excluded for the data analysis because they were fully depleted, or removal did not allow accurate calculation of ozone exposure values (SI, 10.3.8). Calculated exposure for slowly reacting compounds is much higher than for atenolol and benzotriazole throughout the entire data set, and this deviation becomes smaller with rising liquid velocity. For example,  $\int [O_3] dt$  for the lowest velocity (PTFE) was over 3.3 times higher if calculated with gabapentin vs. benzotriazole, and still about 2.4 times higher for the highest flow velocity (Figure 15a). A similar effect was observed during ozonation of secondary treated effluents, where calculated ozone exposure increased with decreasing second-order ozone-reactivity of probe compounds (Hübner et al., 2013). An explanation could be the sensitivity of fast reacting compounds towards imperfect hydraulics and mixing, similar to disinfection considerations where the actual exposure (usually called CT) differs from the theoretical exposure (Wols et al., 2010). Statistical analysis comparing measured and calculated effluent ozone concentrations (based on exposure) shows the highest agreement with exposure measured using gabapentin as a probe compound, which was therefore used for mass transfer calculations (SI, 10.3.5).

Mass transfer coefficients obtained by the procedure outlined in 10.3.4 (SI) ranged from  $4.39 \cdot 10^{-7}$  to  $3.12 \cdot 10^{-6} \text{ m s}^{-1}$  (PTFE) and from  $3.94 \cdot 10^{-7}$  to  $2.04 \cdot 10^{-6} \text{ m s}^{-1}$  (PDMS), with consistently higher mass transfer through the PTFE membrane (Figure 15c). This is in line with previous data, where the PDMS membrane wall resistance was discussed as main reason for the difference (Bein et al., 2021). Additionally, an increase of mass transfer coefficients with increasing Reynolds number (largely representing liquid velocity) is observed, which is caused by an enlarged ozone concentration gradient from gas phase to liquid boundary layer and has been described by dimensionless correlations for multiple geometries (Gabelman and Hwang, 1999; Wickramasinghe et al., 1992).

We included mass transfer coefficients originating from such a dimensionless correlation in Figure 15c to compare and further validate the obtained mass transfer data. Fang et al. (2002) established this correlation with a comparable set-up in groundwater-

like flow conditions ( $8.6 - 12,973 \text{ cm d}^{-1}$ ) for  $\text{H}_2$  delivery using different hydrophobic porous membranes with substantially smaller diameters ( $390\text{-}300 \mu\text{m}$ ). Furthermore, this correlation was used in different studies to estimate the  $\text{H}_2$  and  $\text{O}_2$  membrane mass transfer rate into porous media, but to our knowledge never applied for ozone mass transfer (Agarwal et al., 2005; Chaplin et al., 2009; Schnobrich et al., 2007). Although mass transfer coefficients obtained here are in the same order of magnitude as the values originating from the correlation, there remains a substantial deviation, especially for low flow velocities (Figure 15c). Additionally, the dimensionless correlation suggests an opposite trend ( $K_{\text{PDMS}} > K_{\text{PTFE}}$ ) compared to the experimentally determined mass transfer and previously reported correlations. This can be explained by the specific membranes used in this study, where the smaller membrane diameter of PDMS ( $3.18 \text{ mm}$  vs.  $3.8 \text{ mm}$ ) is expected to cause better mass transfer compared to PTFE membranes (based on the correlation of  $Sh$ ,  $Re$ , and  $Sc$ , Figure 5c).

If the mass transfer correlation by Fang et al. (2002) is used to calculate the mass transfer rate and estimate the amount of ozone transferred by the PDMS membrane in the conditions of BA/DIOX experiments (section 5.4.2.1), an ozone dose of  $82 \mu\text{M}$  is forecasted in these flow conditions at  $20 \text{ }^\circ\text{C}$  (Eq. S6-S8, SI). This is lower than the projected  $110 - 140 \mu\text{M}$  for DIOX removal (Figure 14a) but nevertheless provides a conservative first estimation for design considerations. The experimentally determined mass transfer coefficients are even lower, which could be caused by different ozone decomposition kinetics along the reactor, adding uncertainty to the ozone exposure and thus calculated initial ozone concentrations needed for this approach (SI, 10.3.4 and 10.3.8). This complements the finding that porous media layers do not have the expected effect on DIOX removal and supports the assumption that even in case of DIOX most of the oxidation takes place in proximity of the membrane surface.

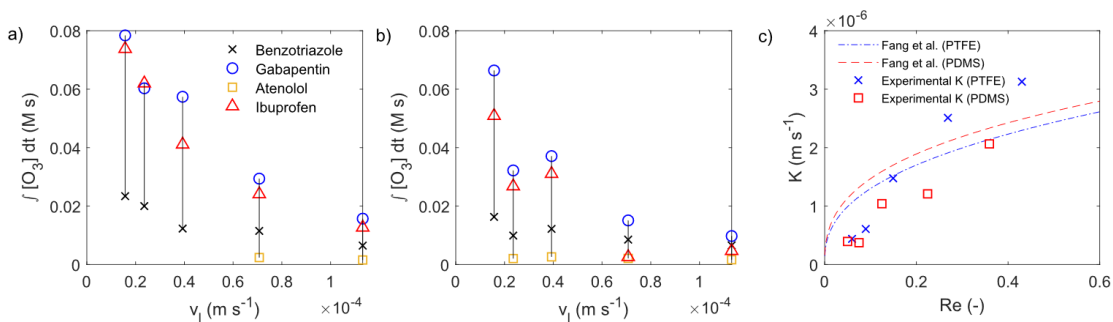


Figure 15: Ozone exposure in pH 7 phosphate buffer as function of liquid velocity, calculated with different probe compounds. a) PTFE, b) PDMS, c) Experimental mass transfer coefficients according to the novel procedure compared to the empirical correlation  $Sh = 0.824 Re^{0.39} Sc^{0.33}$ , developed by Fang et al. (2002) for  $0.0004 < Re < 0.6$ . The legend in a) also applies to b).

### 5.4.3.2 Modeling of a large scale remediation scenario

With knowledge on mass transfer efficiency and how ozone transferred translates to contaminant removal, further considerations regarding the applicability of this technology are possible. While the effect of ozone-consuming intermediates may enhance breakdown of monocyclic aromatic hydrocarbon towards simpler structures (Bein et al., 2023a), it is expected to limit the effectivity as PRB for the parent compounds, as in the tested scenarios all ozone is consumed at the membrane wall. Results for the aliphatic chemical DIOX are much more promising. Soil layers do not cause major removal inhibitions and a large portion of reactions is taking place near the membrane; these can be seen as beneficial mechanisms.

A mathematical model was developed and used to demonstrate feasibility and implications for a real contaminant scenario (SI, 10.3.9). It is based on the mass transfer coefficients by Fang et al. (2002) that were previously also used to estimate  $H_2$  transfer in field studies (Chaplin et al., 2009; Edstrom et al., 2005). In an exemplary cross-sectional plume of  $5 \times 1$  m ( $A_{\text{plume}} = 5 \text{ m}^2$ ) with 50% soil porosity and  $10 \text{ cm d}^{-1}$  effective groundwater flow velocity, a PDMS membrane tube of 94.3 m would be needed to deliver a dose of  $5 \text{ mg L}^{-1}$  ( $104 \text{ }\mu\text{M}$ ) dissolved ozone over the entire cross-section (Figure 16a). This assumes an ozone gas concentration of  $190 \text{ g m}^{-3}$ , a gas flow of  $0.1 \text{ L min}^{-1}$ , a temperature of  $15 \text{ }^\circ\text{C}$ , and a mass transfer coefficient of  $4.18 \cdot 10^{-7} \text{ m s}^{-1}$ . Such settings result in a comparably short tube length ( $<100$  m) but only a low percentage of the ozone gas fed into the tube is delivered into the groundwater (4.6 %, Figure 16b). The aim of this engineering design, however, should be to maximize the ozone gas exploitation. This could be achieved by reducing the gas flow rate from 0.1 to 0.0075 or 0.005  $\text{L min}^{-1}$ , where ozone transfer efficiencies rise to 61 or 91.6%, respectively. The resulting trade-off is a prolonged tube length (248.8 m for  $0.005 \text{ L min}^{-1}$ ), as the partial pressure drop on the gas side reduces the overall concentration gradient and therefore the average flux  $J_{\text{mean}}$  (Figure 16b).  $J_{\text{mean}}$  was calculated as the average of mass transfer rates in every finite membrane piece using Eq. S6 (SI) with the gas- and liquid-side concentrations, and the mass transfer coefficient, divided by the membrane area. They range from 0.0073 to  $0.0193 \text{ mg m}^{-2} \text{ s}^{-1}$  in these scenarios.

The modeling approach demonstrates that the design of such a system must be elaborated for an efficient ozone gas use and requires adaptation for hydraulic conditions and the required ozone dose that needs to be delivered. Further experimental validation may allow a final assessment on the effectivity and scalability of the technology. Especially the geological and engineering prerequisites for installing a PRB consisting of membranes, as for example demonstrated by Patterson et al. (2004), are not covered in this work.

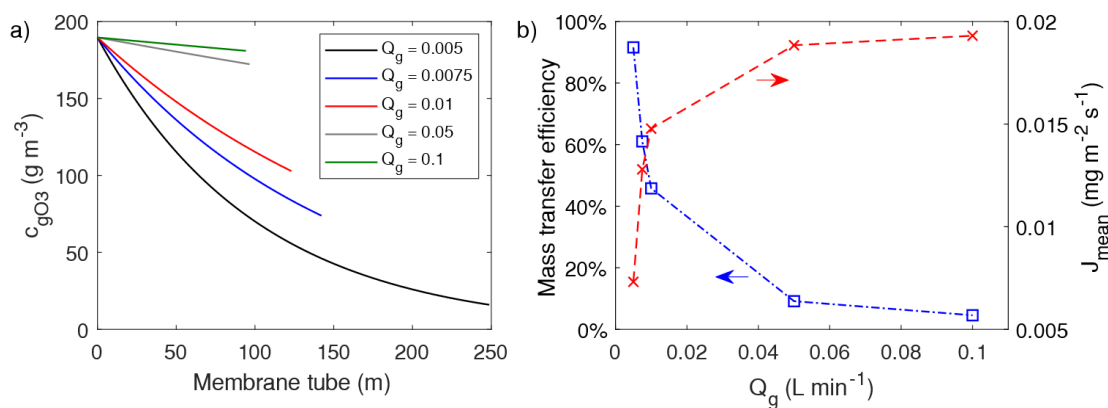


Figure 16: Modeling results for the case study with a  $5 \times 1$  m contaminated cross-section. a) Change of ozone gas concentration in the PDMS tube, depending on the gas flow rate  $Q_g$  in  $L\ min^{-1}$ . b) Resulting mass transfer efficiency (% of ozone gas used, blue squares) and the ozone flux averaged over the membrane tube length (red crosses).

## 5.5 Conclusions

A novel membrane-based method for in-situ ozonation was tested in this study in order to gain insights into contaminant removal based on contaminants' and porous media properties. The tested PDMS membrane tube was found capable of diffusing ozone sufficiently in order to decompose BA and DIOX by more than 50% in flow slightly faster than groundwater ( $150\ cm\ d^{-1}$ ). Higher removal should therefore be feasible in groundwater velocities of  $10\ cm\ d^{-1}$  or lower due to the smaller volumes to be treated. Removal of DIOX was—against the initial expectation—not largely affected by ozone-consuming porous media layers, indicating that most radical-driven oxidation reactions took place near the membrane, even though porous media layers affected the dissolved ozone concentrations in the effluent. This makes it a promising reactive barrier approach for DIOX removal. Conversely, in-situ ozonation of BA as representative monocyclic aromatic was adversely affected by the quick ozone consumption that was caused by ozone-reactive hydroxylated intermediates formed from the reaction of BA with hydroxyl radicals. These reactions seem to cause complete ozone decomposition near the PDMS membrane surface without ozone mass transfer into the bulk liquid, which reduces overall BA removal compared to batch experiments. This enhanced ozone decomposition was additionally confirmed for the ozonation of toluene, suggesting the limited use of in-situ membrane ozonation for remediation of contaminated sites with monocyclic aromatics.

Mass transfer modeling enabled the quantification of the strong effect of gas-settings, especially the gas flow rate on dimensioning the membrane tube. The installation of a membrane tube  $>100$  m was required for a comparably small cross-section of  $5\ m^2$  in our example to achieve a high ozone transfer efficiency, highlighting that more excavation and general gas injection site preparation may be required than for well sparging

operation. Overall, the results open the door for further investigation and assessment of this technology as PRB, as major limitations but also promising fields of application could be demonstrated.

## **5.6 Acknowledgement**

This study was performed within the German-Israeli cooperation project “ISCO<sub>3</sub>”, which was funded by the German Federal Ministry of Education and Research (BMBF) and the Ministry of Science and Technology (MOST) of Israel, funding codes 02WIL1523 and 3-15878. We would like to thank Erin Kim for her experimental support.

## 6 ADVANCED OXIDATION PROCESSES FOR REMOVAL OF MONOCYCLIC AROMATIC HYDROCARBON FROM WATER: EFFECTS OF O<sub>3</sub>/H<sub>2</sub>O<sub>2</sub> AND UV/H<sub>2</sub>O<sub>2</sub> TREATMENT ON PRODUCT FORMATION AND BIOLOGICAL POST-TREATMENT

The following chapter presents investigations related to *research objective 3 (hypotheses 3.1 and 3.2)*: *Investigate the potential synergies of different reactive oxygen species in ozone-based advanced oxidation processes (O<sub>3</sub>/H<sub>2</sub>O<sub>2</sub>) on the transformation of monocyclic aromatic hydrocarbon.*

This chapter has been published with some editorial changes as follows:

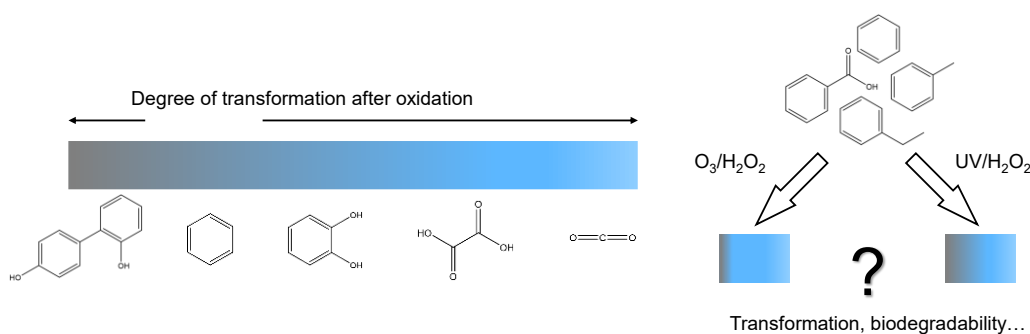
*Bein, Emil; Seiwert, Bettina; Reemtsma, Thorsten; Drewes, Jörg E.; Hübner, Uwe (2023): Advanced oxidation processes for removal of monocyclic aromatic hydrocarbon from water: Effects of O<sub>3</sub>/H<sub>2</sub>O<sub>2</sub> and UV/H<sub>2</sub>O<sub>2</sub> treatment on product formation and biological post-treatment. In: Journal of Hazardous Materials 188 (2-3), 131066. DOI: 10.1016/j.jhazmat.2023.131066.*

Author contributions: Emil Bein: Conceptualization, Methodology, Formal analysis, Investigation, Writing – Original Draft, Writing – Review & Editing, Bettina Seiwert: Investigation, Formal analysis, Writing – Review & Editing, Thorsten Reemtsma: Resources, Writing – Review & Editing, Jörg E. Drewes: Resources, Funding acquisition, Writing - Review & Editing, Uwe Hübner: Conceptualization, Methodology, Supervision, Funding acquisition, Writing – Review & Editing

### 6.1 Abstract

Several oxidative treatment technologies, such as ozonation or Fenton reaction, have been studied and applied to remove monocyclic hydroaromatic carbon from water. Despite decades of application, little seems to be known about formation of transformation products while employing different ozone- or 'OH-based treatment methods and their fate in biodegradation. In this study, we demonstrate that O<sub>3</sub>/H<sub>2</sub>O<sub>2</sub> treatment of benzene, toluene, ethylbenzene (BTE), and benzoic acid (BA) leads to less hydroxylated aromatic transformation products compared to UV/H<sub>2</sub>O<sub>2</sub> as reference system – this at a similar 'OH exposure and parent compound removal efficiency. Aerobic

biodegradation tests after oxidation of 0.15 mM BA (12.6 mg C L<sup>-1</sup> theoretical DOC) revealed that a less biodegradable DOC fraction >4 mg C L<sup>-1</sup> was formed in both oxidative treatments compared to the BA control. No advantage of ozonation over UV/H<sub>2</sub>O<sub>2</sub> treatment was observed in terms of mineralization capabilities, however, we detected less transformation products after oxidation and biodegradation using high-resolution mass spectrometry. Biodegradation of BA that was not oxidized was more complete with minimal organic residual. Overall, the study provides new insights into the oxidation of monocyclic aromatics and raises questions regarding the biodegradability of oxidation products, which is relevant for several treatment applications.



**Keywords:** Advanced oxidation processes; monocyclic aromatic carbon; reaction kinetics; ozone; hydroxyl radicals.

## 6.2 Introduction

Monocyclic aromatic hydrocarbons, most importantly BTEX (benzene, toluene, ethylbenzene, o-, p-, and m-xylene), are abundant, toxic groundwater contaminants that show high resistivity towards powerful oxidants such as ozone due to their aromatic ring without activating group (Hoigné and Bader, 1983a; von Sonntag and von Gunten, 2012). Various AOPs have been proposed in the past to achieve an efficient removal of BTEX compounds from contaminated water (Bustillo-Lecompte et al., 2018; Dutschke et al., 2022; Fernandes et al., 2019a; Fernandes et al., 2019b; Garoma et al., 2008; Kasprzyk-Hordern et al., 2005; Rayaroth et al., 2023; Yang et al., 2020). For in-situ treatment of BTEX contamination, ozonation by sparging gas into wells is a state-of-the-art field-scale groundwater remediation technology (Krembs et al., 2010; Nimmer et al., 2000; Siegrist et al., 2011). Due to the low direct reactivity of BTEX with ozone, oxidation efficiency relies on the in-situ generation of <sup>•</sup>OH from the reaction of ozone with the soil matrix or simultaneously injected hydrogen peroxide. Depending on the concentration, self-enhanced removal may occur due to radicals produced by reactions of hydroxylated intermediates with ozone, as it has been shown for benzoic acid (BA) (Huang et al., 2015).

Important criteria to study the efficacy of oxidative treatment are the enhanced removal of target contaminants compared to other tested treatment methods, but also the required energy input (Katsoyiannis et al., 2011; Miklos et al., 2019; Sgroi et al., 2021). However, complete mineralization is extremely energy-intensive and rarely achieved in oxidative treatment and, hence, the formation of transformation products (TPs) appears unavoidable. Therefore, ozonation – which is a very established process in advanced water treatment – is often coupled with biological post-treatment for lowering DOC and removing TPs of micropollutants in treated effluent (Itzel et al., 2020; Schollée et al., 2018). Generally, energy reductions are also postulated for coupling of other AOPs, such as electrochemical Fenton and photo-Fenton processes, with biological post-treatment due to the suspected formation of more readily biodegradable intermediates (Huang et al., 2017; Oller et al., 2011). Biodegradability of intermediates is also relevant for in-situ groundwater remediation, as mineralization of remaining organic carbon is desired but difficult to achieve with chemical oxidation only, requiring coupling strategies of biological and chemical treatment (Sutton et al., 2011).

In this study, we investigate the transformation of monocyclic aromatics, namely benzene, toluene, ethylbenzene (BTE) and benzoic acid (BA) during O<sub>3</sub>/H<sub>2</sub>O<sub>2</sub> and UV/H<sub>2</sub>O<sub>2</sub> treatment. These target contaminants have been proven prone to ·OH attack with reported second-order rate constants >10<sup>9</sup>M<sup>-1</sup> s<sup>-1</sup> (Buxton et al., 1988), leading to hydroxylated (i.e., phenolic) TPs: For instance, phenol and o-, p- and m-cresol have been reported as TPs in different UV-based AOPs (UV/NO<sub>3</sub><sup>-</sup> and UV/TiO<sub>2</sub>) of benzene and toluene as result of H-abstraction reactions (Hatipoglu et al., 2010; Park and Choi, 2005). For toluene and ethylbenzene, other aromatic structures resulting from ·OH attack (H-abstraction) at the methyl and ethyl group were detected (Cui et al., 2017; Hatipoglu et al., 2010).

We hypothesize that an oxidation process including both, ozone and ·OH production, will have synergistic effects for treating monocyclic aromatic hydrocarbons based on known reaction pathways of hydroxylated intermediates. Phenol, the major product of benzene oxidation with ·OH (Park and Choi, 2005), is highly reactive with ozone (10.4.3, Table 15, Figure 40). It can be directly transformed to aliphatic acids such as cis,cis-muconic acid by ring-cleavage or to other intermediates with intact ring structure, for instance catechol and p-benzoquinone (Mvula and von Sonntag, 2003; Ramseier and von Gunten, 2009). All of these compounds are further reacting with ozone, eventually giving rise to small products with low ozone reactivity such as oxalic and formic acid. Similar mechanisms and reactivities are expected for toluene, ethylbenzene and BA due to their structural similarity and the formation of hydroxylated products that are reactive with ozone. A different composition of intermediates can be expected in AOPs with ·OH as



major oxidant (such as UV/H<sub>2</sub>O<sub>2</sub>) due to the absence of ozone. This rapid breakdown of monocyclic aromatic compounds to aliphatic products in ozone-based AOPs is expected to enhance aerobic biodegradation and mineralization of oxidation TPs by microbial communities in the aquifer.

The aim of this investigation was to determine differences of O<sub>3</sub>/H<sub>2</sub>O<sub>2</sub> (“peroxone”) and UV/H<sub>2</sub>O<sub>2</sub> AOPs for transformation of mostly ozone- and photo-resistant monocyclic aromatic hydrocarbons. We also study the effect of different oxidative treatments on subsequent biodegradation of dissolved organic matter for BA. Due to assumed similarities of BA and BTE, BA may serve as good model compound for biological post-treatment as it is non-volatile and therefore more suitable to assess the degree of mineralization.

## 6.3 Materials and methods

### 6.3.1 Chemicals and reagents

The purity of all quantified organic compounds was higher than 98%. Used chemicals are listed in the SI, Table 8. Experimental solutions for BTE experiments were freshly prepared by directly diluting BTE into pH 7 phosphate buffer solution (PBS) with a final concentration of 10 mM on the days of experiments. Concentrated PBS (0.5 M) was prepared with NaH<sub>2</sub>PO<sub>4</sub>·2H<sub>2</sub>O and Na<sub>2</sub>HPO<sub>4</sub> in ultrapure water (UPW). The final pH was then adjusted by adding either phosphoric acid or sodium hydroxide. 20 mM H<sub>2</sub>O<sub>2</sub> stock solutions were freshly prepared from 30% stabilized H<sub>2</sub>O<sub>2</sub> (VWR Chemicals) on each day and added accordingly.

### 6.3.2 Oxidation experiments

#### 6.3.2.1 O<sub>3</sub>/H<sub>2</sub>O<sub>2</sub> process for BTE treatment

BTE were oxidized in closed recirculation experiments using a gas-liquid membrane contactor in counter-current flow for O<sub>3</sub>/H<sub>2</sub>O<sub>2</sub> treatment (Figure 17a). Experimental setups are designed to allow direct comparisons of BTE removal during both AOPs as function of ·OH exposures by avoiding losses due to volatilization. They are not intended to optimize the treatment efficiency, neither with respect to treatment time nor oxidant dose. All materials in contact with the solution were made of PTFE, PVDF, PEEK, glass, or stainless steel.

The ozone membrane contacting unit consisted of a glass column with 22 cm inner diameter that was equipped with gas-tight in- and outlets for gas- and liquid-streams (Bühler Technologies GmbH, Germany). Porous PTFE (FluorTex GmbH, Germany) was

chosen as membrane material due to its high ozone-resistance and mass transfer (Bein et al., 2021). The 25.5 cm membrane tube was installed inside the glass column and had an inner diameter of 2.8 mm, a wall thickness of 0.5 mm, and a porosity of 50%. Ozone gas with a concentration of 200 g Nm<sup>-3</sup> was generated by a BMT 803 BT ozone generator, analyzed by a BMT 964 analyzer (BMT Messtechnik GmbH, Germany) and inserted at a flow rate of approximately 0.25 NL min<sup>-1</sup> from top to bottom of the glass column. The liquid was pumped from bottom to top through the membrane tube (Figure 17a, counter-current configuration). A needle valve was used to control liquid-side pressure to achieve bubble-free ozonation, where ozone directly diffuses into the gas-liquid boundary layer in proximity to the membrane surface (Bein et al., 2021).

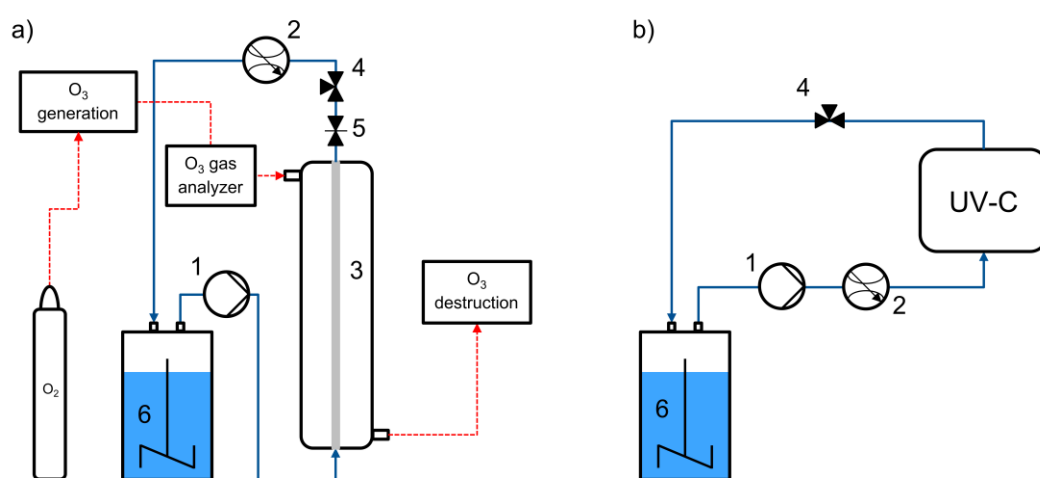


Figure 17: Experimental set-ups for recirculation experiments: a) ozone membrane contacting, b) UV-C irradiation. 1: gear pump, 2: flow meter, 3: PTFE membrane, 4: sampling port, 5: needle valve, 6: stirred feed solution.

For every ozone membrane contacting experiment, a 0.6 L solution was prepared containing 10 mM PBS (pH 7), 0.1  $\mu$ M pCBA, 30 mg L<sup>-1</sup> H<sub>2</sub>O<sub>2</sub> (0.88 mM), and BTE (0.12-0.25 mM). BTE concentrations varied considerably among experiments due to the applied procedure to prepare solution, which is discussed in section 6.4. The solution was transferred to a closed glass bottle of the same volume to keep the gas-liquid contact area and volatility losses low. The constantly stirred solution was pumped through the recirculation set-up at a flow rate of 6.5 L h<sup>-1</sup> that was controlled by a DK 800 Krohne rotameter (Krohne Messtechnik GmbH, Germany). This corresponds to approximately 0.3 m s<sup>-1</sup> liquid flow velocity in the membrane and a theoretical ozone mass transfer coefficient of 1.77·10<sup>-5</sup> m s<sup>-1</sup> (L  v  que solution, without chemical reaction). 20 mL samples plus 20 mL sample port flush were withdrawn from a three-way valve after different recirculated volumes. The time after one volume recirculated was defined as volume of the solution divided by the liquid flow rate. Sampling times were corrected for volume removed accordingly. The first 20 mL sample was taken from the bottle prior to

start. 9.4 mL of sample were filled immediately into headspace (HS) vials, prepared for GC-FID analysis according to the analytical method, and quickly sealed to avoid further losses. An aliquot of the sample was directly analyzed for UV/Vis absorbance. The remainder was quenched with 1 mM Na<sub>2</sub>S<sub>2</sub>O<sub>3</sub> to remove any remaining O<sub>3</sub> or H<sub>2</sub>O<sub>2</sub> pending further analysis.

### 6.3.2.2 UV/H<sub>2</sub>O<sub>2</sub> process for BTE treatment

UV/H<sub>2</sub>O<sub>2</sub> treatment and sampling was performed analogously using a UV-C flow-through reactor with the same water matrix as in ozonation experiments with 1.1 L feed solution at a flow rate of 10 L h<sup>-1</sup> (Figure 17b). Additionally, photo-resistant probe compounds carbamazepine (CBZ), gabapentin (GBP), and primidone (PRI) were added at trace concentrations of 0.05 (CBZ) and 0.1 μM (GBP, PRI) instead of pCBA (Miklos et al., 2018a). pCBA could not be used as probe compound in UV-based treatment due to its decay in a control experiment without H<sub>2</sub>O<sub>2</sub>. A discussion on the probe compound selection can be found in the SI, section 10.4.1. UV-C light was emitted using a 10W LP mercury lamp in a stainless-steel flow-through system (Purion GmbH, Germany) with an irradiated reactor volume of approximately 105 mL.

### 6.3.2.3 Oxidative treatment of BA

Oxidation of 0.15 mM BA prior to biodegradation experiments was conducted in diluted natural water instead of PBS. Tap water (TW) of an approximate pH of 7.7 and DOC < 1 mg C L<sup>-1</sup> was chosen as natural buffer system and diluted with UPW at a ratio of 1:2.85 TW:UPW to achieve the same water matrix for all samples during ozonation and UV/H<sub>2</sub>O<sub>2</sub> treatment. For UV/H<sub>2</sub>O<sub>2</sub> experiments, the UV-C set-up described in 6.3.2.2 was used. Sample volumes were increased to 200 mL (plus 20 mL sample port flush) with a total recirculation volume of 1.5 L. Withdrawn samples were also quenched with 1 mM Na<sub>2</sub>S<sub>2</sub>O<sub>3</sub> and stored at -20 °C after taking samples for BA and TOC until subsequent biodegradation experiments. TOC samples were acidified with two droplets 32% HCl (≤ pH 2) and stored at 4°C prior to analysis.

As BA is non-volatile, O<sub>3</sub>/H<sub>2</sub>O<sub>2</sub> treatment was performed in batch experiments with addition of pre-defined amounts of ozone stock solution and H<sub>2</sub>O<sub>2</sub> in a molar ratio of 2:1 followed by short stirring (<1 min). Ozone stock solutions of approximately 52 mg L<sup>-1</sup> were produced with the ozone generator described in section 2.2.1 in a cooled (4 °C) 2.5 L glass reactor with a porous bubble diffuser that was constantly supplied with gaseous ozone. The applied ozone doses ranged from 0.1 to 0.7 mM. ·OH exposure in O<sub>3</sub>/H<sub>2</sub>O<sub>2</sub> batch experiments was determined using PRI instead of pCBA that also agreed closely with UV/H<sub>2</sub>O<sub>2</sub> data.

### 6.3.3 Aerobic biodegradation experiments

Initial biodegradation was assessed in batch experiments by inoculating 60 mL samples with 10 g sand (wet weight) from the top layer of a biological sand filtration column, continuously fed with aerated wastewater treatment plant effluent from top to bottom for more than 6 weeks before experiments. The sand was homogenized and carefully washed with TW on a 200 µm stainless steel sieve to remove remaining wastewater. Inoculated batches (250 mL amber glass bottles) were closed with perforated lids, shaken at 125 rpm for 6 days, and 6 mL samples for DOC analysis were taken several times. Oxic conditions (>7 mg L<sup>-1</sup> dissolved oxygen) were confirmed by daily measurements using flow-through cells, where sample was pumped through using a plastic syringe (FTC-PSt3, Presens, Germany). For abiotic control experiments, three times 10 g biologically active sand was placed in amber bottles for shake tests and autoclaved to demonstrate inhibited biological activity.

Samples for DOC analysis were immediately filtered through 0.45 µm cellulose acetate filters that were pre-rinsed with 200 mL UPW and approximately 0.5 mL of sample. Samples were diluted with UPW (DF 0.167) and acidified as for TOC analysis. Biodegradation tests were performed in triplicates for each sample taken from oxidation experiments. The selected samples for biodegradation experiments are specified in 6.4.3.2 and 10.4.2.

### 6.3.4 Analytical methods

BTE were measured by an Agilent 7980 GC gas chromatograph with headspace auto-sampling module coupled with flame ionization detection (HS-GC/FID). Compound separation was performed on a 30 m column with 0.32 mm inner diameter and 1.80 µm film thickness (DB-624, Agilent, USA), using nitrogen as carrier gas. The initial oven temperature of 40 °C was kept for 3 min and increased by 12.5 °C min<sup>-1</sup> to 250 °C. Detailed instrument settings are listed in the SI, Table 17. Calibration standards (1-50 mg L<sup>-1</sup>) were prepared from a BTE stock solution in MeOH, which was added to headspace vials, filled up to 0.6 mL MeOH and mixed with 9.5 mL UPW and 0.5 g sodium sulfate. Accordingly, 9.4 mL samples + 0.1 mL UPW were mixed with 0.6 mL MeOH instead of the calibration standard, and the same amount of salt was added.

BTE TPs and BA were analyzed using an Agilent 1260 Infinity II high performance liquid chromatography system with diode array detector (HPLC-DAD). Two separate methods were applied: phenol, o-cresol and o-ethylphenol (0.1-5 mg L<sup>-1</sup>) were separated on an XSelect HSS C18 column (2.1 x 100 mm, 3.5 µm particle size) at a flow rate of 0.5 mL min<sup>-1</sup>, using a gradient method with H<sub>2</sub>O and acetonitrile (ACN) as solvents. All of

the three compounds were detected at 275 nm. Wavelength scans were performed in parallel to confirm the compounds via retention time and spectrum. BA (0.25-10 mg L<sup>-1</sup>) was detected using the same system but at a flow rate of 0.6 mL/min (0.1% formic acid in H<sub>2</sub>O and ACN), at 238 nm. The injection volume was 50 µL for both methods. Further details are listed in the SI, Table 18.

Quantitation of ·OH probe compound candidates PRI, CBZ, and GBP was performed with an LC-MS/MS system in scheduled MRM mode (positive ESI) using isotope labelled standard (IS) correction (0.0025 – 10 µg/L). The system is composed of a SCIEX Triple Quad 6500 mass spectrometer (SCIEX, USA) coupled with a Knauer PLATINBLUE UHPLC (Knauer, Germany) and an XSelect HSS T3 (particle size 2.5 µm; 2.1 x 100 mm) column (Waters, USA). More details on the method can be found in Müller et al. (2017). pCBA (m/z 111) was analyzed similarly with internal standard correction (pCBA d4) in negative ESI mode with 0.1% acetic acid in H<sub>2</sub>O and ACN as solvents and a modified gradient.

TOC/DOC (0.1-10 mg C L<sup>-1</sup>) was analyzed on a VarioTOC TOC/DOC analyzer (Elementar, Germany). Organic carbon in chemical oxidation experiments was determined as TOC (analysis without filtration) and in biodegradation experiments as DOC. However, no noteworthy differences between TOC and DOC became apparent in pre-tests, thus we assumed TOC≈DOC. UV spectra were recorded using a Hach DR6000 UV/Vis spectrophotometer (200-800 nm). Excitation emission matrices (EEMs) were obtained by an Aqualog (HORIBA Jobin Yvon, Germany). EEM samples were filtered as for DOC analysis and diluted 1:13. Obtained EEM data was modified including corrections for inner filter effects, Rayleigh masking, and Raman normalization (Bahram et al., 2006).

An identification of chemical structures of oxidation products in BA experiments was undertaken using RPLC-HRMS screening, following the method described by Seiwert et al. (2021). Briefly, screenings were performed with an ACQUITY UPLC system connected to a XEVO G2 XS TOF MS equipped with an electrospray ionization source (Waters, USA). In addition, a fluorescence detector was connected and set to regions identified in EEMs (290/410 nm and 320/450 nm). Contrary to Seiwert et al. (2021), ACN was used as solvent B instead of MeOH. All relevant compounds were identified in negative ESI. Sum formulas of peaks were identified based on exact mass and structures proposed where applicable. Further details can be found in the SI, Table 19.

## 6.4 Results

### 6.4.1 Removal kinetics during O<sub>3</sub>/H<sub>2</sub>O<sub>2</sub> and UV/H<sub>2</sub>O<sub>2</sub> treatment

Oxidative treatment of BTE in neutral PBS led to similar partial removal of all three contaminants (SI, Figure 41). By the end of the treatment, between 60 and 70% of BTE were removed in both processes. To achieve this removal in the ozone membrane contactor, the treated solution was circulated 50 times, compared to 5 times during UV/H<sub>2</sub>O<sub>2</sub> treatment. This is a consequence of the comparably small ozone dose transferred in the short (25.5 cm) single tube contactor if compared to larger hollow fiber membrane modules used in some previous works (Leiknes et al., 2005; Zhang et al., 2017).

Removal of ozone- and UV-resistant probe compounds was used to determine  $\cdot\text{OH}$  exposures during O<sub>3</sub>/H<sub>2</sub>O<sub>2</sub> and UV/H<sub>2</sub>O<sub>2</sub> treatment and compare both oxidative treatments on the basis of similar  $\cdot\text{OH}$  exposures (Figure 18). The  $\cdot\text{OH}$  exposure values were calculated using second-order reaction rate kinetics with reported rate constants of probe compounds, as discussed previously (e.g., Rosenfeldt et al. (2006) and Wunsch et al. (2021)). The final selection of two probe compounds (CBZ for UV/H<sub>2</sub>O<sub>2</sub> and pCBA for O<sub>3</sub>/H<sub>2</sub>O<sub>2</sub>) resulted in good agreement of contaminant removal kinetics for both, BTE and BA experiments with a more pronounced deviation of the two treatment processes in case of BA experiments (SI, 10.4.1). Data point scattering in BTE experiments was observed for all three compounds and is most likely related to sampling and analysis of the volatile substances. PRI with a reported rate constant of  $6.7 \cdot 10^9 \text{ M}^{-1} \text{ s}^{-1}$  (Real et al., 2009) led to similar results as pCBA for BA ozonation experiments, confirming that both are suitable probe compounds for measuring  $\cdot\text{OH}$  exposure during ozonation (Figure 21).

For further validation, second-order rate constants were determined from the slope of the linear fit of O<sub>3</sub>/H<sub>2</sub>O<sub>2</sub> data points in Figure 18a and b as  $7.7 \cdot 10^9 \text{ M}^{-1} \text{ s}^{-1}$  for benzene ( $7.4 \cdot 10^9 \text{ M}^{-1} \text{ s}^{-1}$  for UV/H<sub>2</sub>O<sub>2</sub>) and  $5.6 \cdot 10^9 \text{ M}^{-1} \text{ s}^{-1}$  for BA ( $6.3 \cdot 10^9 \text{ M}^{-1} \text{ s}^{-1}$  for UV/H<sub>2</sub>O<sub>2</sub>), respectively. These values are in close agreement with previously reported respective values of  $7.8 \cdot 10^9 \text{ M}^{-1} \text{ s}^{-1}$  (Schuler and Albarran, 2002) and  $5.9 \cdot 10^9 \text{ M}^{-1} \text{ s}^{-1}$  (Buxton et al., 1988). Rate constants of toluene and ethylbenzene are very similar to that of benzene (SI, Figure 42). These results confirm the plausibility of calculated  $\cdot\text{OH}$  exposures. Moreover, they indicate that  $\cdot\text{OH}$  oxidation is the major removal mechanism for BTE, and volatilization, ozonolysis, or photolysis were insignificant.

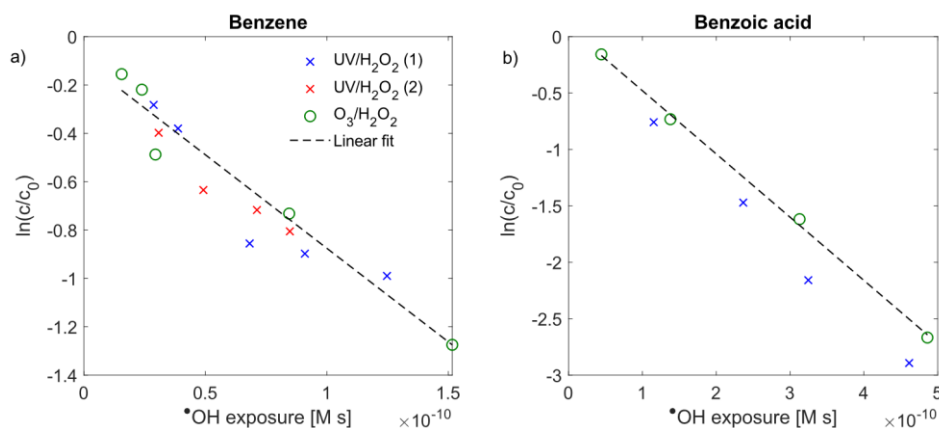


Figure 18: Removal of (a) benzene during BTE oxidation experiments and (b) BA during separate experiments as function of  $\cdot\text{OH}$  exposure. Displayed linear fits were calculated with O<sub>3</sub>/H<sub>2</sub>O<sub>2</sub> data points. The shown UV/H<sub>2</sub>O<sub>2</sub> experiment with BA was performed in diluted TW instead of PBS.

## 6.4.2 Product formation during BTE oxidation

### 6.4.2.1 Hydroxylated transformation products

HPLC-DAD analysis of treated samples confirmed a constant formation of the hydroxylated TPs phenol, o-cresol and o-ethylphenol in UV/H<sub>2</sub>O<sub>2</sub> treatment (Figure 19). Interestingly, the observed yield of o-ethylphenol from ethylbenzene ( $20.6 \pm 2.6\%$ ) was much higher than of phenol ( $2.2 \pm 1.0\%$ ) and o-cresol ( $4.1 \pm 0.6\%$ ) from benzene and toluene, respectively. In contrast, none of the three compounds were found in samples treated with O<sub>3</sub>/H<sub>2</sub>O<sub>2</sub> (lowest point of calibration 0.0011-0.00082 mM or 0.1 mg L<sup>-1</sup>), likely due to direct reaction with ozone present at the boundary layer of the ozone membrane contactor, where compounds such as phenol are quickly oxidized via electron transfer and formation of ozone adduct intermediates (Ramseier and von Gunten, 2009). This also indicates that enough ozone was available to directly oxidize intermediates, while simultaneous  $\cdot\text{OH}$  production occurs through reactions with H<sub>2</sub>O<sub>2</sub> (Merényi et al., 2010) and potentially through the reactions with phenolic intermediates (Huang et al., 2015). Contrarily, formation rates of these TPs in UV/H<sub>2</sub>O<sub>2</sub> treatment must be higher than any subsequent decay, either by radicals or photolysis, as long as BTE are still present in larger amounts, which was the case in all experiments. Direct photolysis of intermediates and resulting production of other reactive oxygen species during UV-irradiation cannot be excluded, but has been reported for phenol only for much longer exposure times of several hours or substantially stronger UV-lamps (e.g., 500 W), and can therefore only be a minor contribution in the experimental conditions of the study (Alapi and Dombi, 2007; Chun et al., 2000).

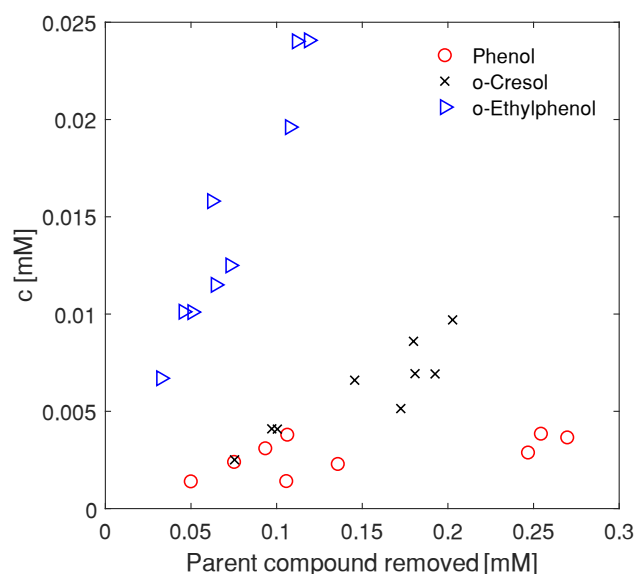


Figure 19: Concentration of hydroxylated TPs over the course of UV/H<sub>2</sub>O<sub>2</sub> treatment. Parent compounds: benzene (phenol), toluene (o-cresol), ethylbenzene (o-ethylphenol).

The formation of hydroxylated TPs in the  $\cdot\text{OH}$ -based process is in accordance with previous literature findings. The yield of o-cresol during photochemical oxidation of 1.4 mM toluene reported by Hatipoglu et al. (2010) was 30.5% and 77.5% for all cresol isomers. Less than 10% of initial toluene was transformed in this experiment, which may explain the comparably high yield and the absence of other TPs. Cui et al. (2017) degraded 1 mM ethylbenzene using a modified Fenton reaction, where  $\cdot\text{OH}$  was demonstrated to be the main reactant by scavenger control experiments. Besides o-, m- and p-ethylphenol, they also found acetophenone and  $\beta$ -phenylethanol as TPs, suggesting that  $\cdot\text{OH}$  may also abstract hydrogen at the ethyl moiety with subsequent oxygen attachment. A corresponding reaction with toluene may lead to benzaldehyde or BA. These compounds were not addressed analytically in this experiment though. The absence or low quantity of the analyzed hydroxylated TPs in O<sub>3</sub>/H<sub>2</sub>O<sub>2</sub> treatment demonstrates the effect of ozone exposure, leading to immediate transformation of hydroxylated TPs of BTE.

#### 6.4.2.2 Change of Absorbance

UV/vis absorbance spectra were recorded to check for formation of absorbance peaks characteristic for different types of organic carbon with conjugated  $\pi$ -electron systems. Absorbance increased during both treatments in the UV range (Figure 20a, SI, Figure 43). This differs from wastewater ozonation, where UV-absorbance is reduced while conjugated  $\pi$ -electron systems in aromatic and olefinic compounds are decomposed by ring-cleavage and the Criegee mechanism (Criegee, 1975; Lamsal et al., 2011; Nöthe et al., 2009; Wenk et al., 2013). Indeed, a stronger increase was observed for UV/H<sub>2</sub>O<sub>2</sub>



treatment with two pronounced peaks at 275 and 350 nm that were absent during O<sub>3</sub>/H<sub>2</sub>O<sub>2</sub> treatment. This is highlighted by changes of absorbance at selected wavelengths (275 nm/350 nm, Figure 20b and c versus  $\cdot$ OH exposures. Although initial concentrations were different, the qualitative comparison shows that larger wavelengths are only absorbed in the samples treated with UV/H<sub>2</sub>O<sub>2</sub>, which also resulted in visible color formation. Similar differences between the two treatments were also observed for BA (SI, Figure 44).

The stronger absorbance increase of samples treated with UV/H<sub>2</sub>O<sub>2</sub> at 275 nm (Figure 20b) is attributed to hydroxylated or di-hydroxylated compounds that show maximum absorbance at 260-280 nm and are abundant in these samples (see section 6.4.2.1). At the end of UV/H<sub>2</sub>O<sub>2</sub> treatment, an absorbance of 0.786 was measured compared to only 0.176 in case of O<sub>3</sub>/H<sub>2</sub>O<sub>2</sub>. As single-hydroxylated TPs were not detected in case of O<sub>3</sub>/H<sub>2</sub>O<sub>2</sub>, the observed rise is either caused by lower concentrations or the absorbance of other compounds.

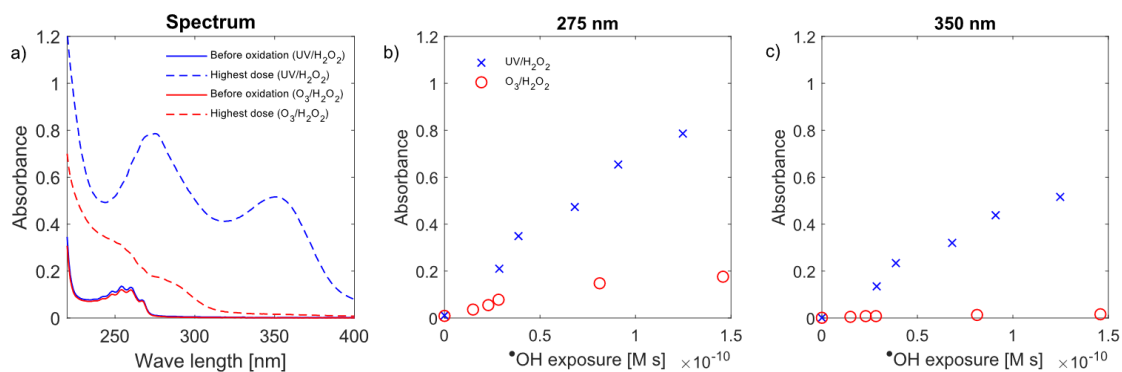


Figure 20: Absorbance change over the whole spectrum during oxidative treatment (a), and for selected wavelengths as a function of  $\cdot$ OH exposure (b,c). Initial BTE concentrations were 0.43/0.28/0.18 mM (UV/H<sub>2</sub>O<sub>2</sub>) and 0.25/0.25/0.12 mM (O<sub>3</sub>/H<sub>2</sub>O<sub>2</sub>) (see also SI, Table 20-Table 23).

The other distinct absorbance increase during UV/H<sub>2</sub>O<sub>2</sub> treatment for larger wavelengths, most notably at 350 nm (Figure 20c), may occur by formation of a large diversity of other hydroxylated aromatic or other structures with intact  $\pi$ -electron systems, for example p-benzoquinone, which also absorbs strongly between 300 and 500 nm (Nagakura and Kuboyama, 1954). Due to its fast reaction with ozone (SI, Table 15), the absence in the respective spectrum would be plausible. Another possibility is the highly concentration-dependent polymerization of aromatic rings that has been observed for phenol during pulsed radiolysis at a much higher concentration of 0.02 M (1.88 g L<sup>-1</sup>) (Ye and Schuler, 1989). A similar reaction is described for aniline at a concentration of 150 mg L<sup>-1</sup> (Shang and Yu, 2002). The potential for the formation of such dimers or even polymers will be discussed further in 6.4.3 for BA.

### 6.4.3 Coupling chemical oxidation and biodegradation

#### 6.4.3.1 O<sub>3</sub>/H<sub>2</sub>O<sub>2</sub> and UV/H<sub>2</sub>O<sub>2</sub> treatment of BA

Oxidative treatment resulted in reduction of BA concentration up to 94% depending on the 'OH exposure, but only minor mineralization, expressed as reduction of TOC (Figure 21a). TOC decreased by approximately 2.6 mg C L<sup>-1</sup> in both processes by applying the highest doses. Initial BA concentrations were very similar (17.85 and 17.16 mg L<sup>-1</sup>), but initial TOC was slightly elevated in UV/H<sub>2</sub>O<sub>2</sub> treatment (ca. + 2 mg C L<sup>-1</sup>). The initial BA concentration (17.85 mg L<sup>-1</sup>) in the O<sub>3</sub>/H<sub>2</sub>O<sub>2</sub> control sample corresponds to a theoretical TOC of 12.3 mg C L<sup>-1</sup>, which is in good agreement with the measured TOC of 13 mg C L<sup>-1</sup> confirming that BA is the major organic carbon source in the samples with only minor contributions of natural organic matter in the used TW.

UV/vis spectra were recorded for each oxidative step (SI, Figure 44). Analogously to BTE oxidation, an increase of absorbance was observed for both, UV/H<sub>2</sub>O<sub>2</sub> and O<sub>3</sub>/H<sub>2</sub>O<sub>2</sub> treatment of BA. Color formation occurred, also indicated by absorbance increases for 400 nm and larger. Interestingly, colorization was more apparent during ozonation of BA as for BTE. Such color formation, expressed as increased absorption at 420 nm during ozonation of BA, was already reported by Shang and Yu (2002), who did not further elaborate the formation of individual TPs. However, they detected increased toxicity for low ozone doses.

#### 6.4.3.2 Aerobic microbial degradation

Samples highlighted with number codes in Figure 5a were used for biodegradation experiments in triplicates (Figure 21b). Oxidized samples (1a and 1b) exhibited a strong reduction of DOC after two days. However, biodegradation stopped after approximately three days and the DOC content remained above 4 mg L<sup>-1</sup> until day 6. Contrarily, DOC present in the BA sample not treated with oxidants (0a) was removed to concentrations below 2 mg L<sup>-1</sup> after 6 days (Figure 21b). Similar results were observed in replicate experiments with samples (0b), (1b) and (2a) (SI, Figure 39). Only after five days a minor reduction of DOC could be observed in control experiments with autoclaved sand, which may be related to regrowth of bacteria as experiments were not conducted under sterile conditions. It demonstrates that removal of DOC in the first three days of biodegradation tests was not related to sorption effects (Figure 21b). Differences between UV/H<sub>2</sub>O<sub>2</sub> and O<sub>3</sub>/H<sub>2</sub>O<sub>2</sub> treatment were small and did not support the hypothesis that the ozone-based AOP improves rapid biodegradation compared to the UV-based AOP of BA.

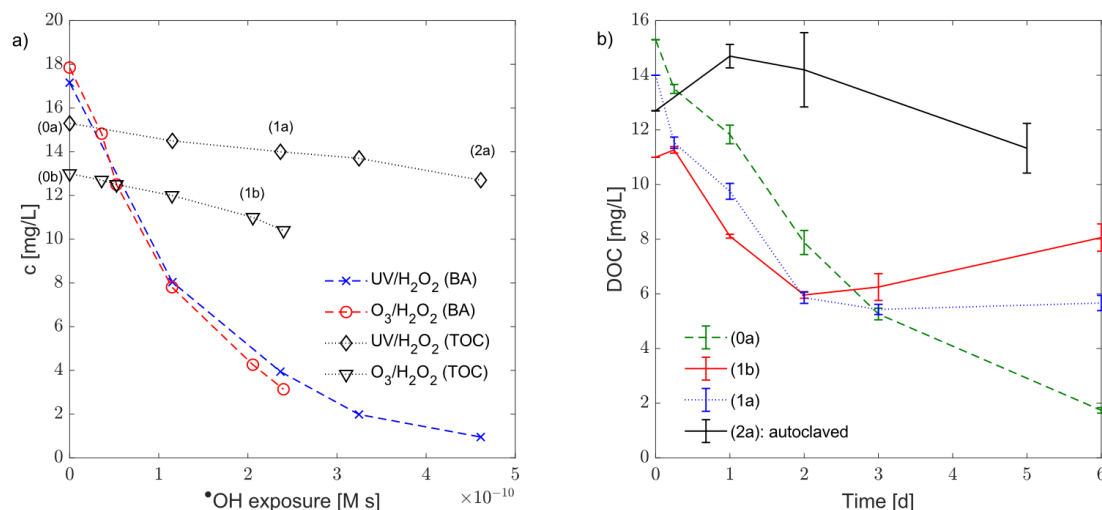


Figure 21: Chemical oxidation of BA and subsequent biodegradation. a) Changes of BA concentrations and TOC vs.  $\cdot\text{OH}$  radical exposure. b) Degradation of DOC in shaken batches of selected samples withdrawn in oxidation experiments. Standard deviations originate from DOC data of three individual batches containing the same water matrix ( $n=3$ ). TOC from a) was taken as initial value. The shaker was temporarily interrupted on day 5-6 (samples 0a and 1a) with dissolved oxygen levels staying well above  $7 \text{ mg L}^{-1}$  during that time. Data of more batches is visualized in Figure 39 (SI).

The reduced biodegradability of the DOC after oxidation contradicts previous studies on ozonation of treated wastewater with subsequent biological post-treatment (Hübner et al., 2012). It indicates that overall biodegradability of TPs should be considered in more detail, especially when combining AOPs with biological treatment for industrial or groundwater applications, where only a few contaminants may dominate the organic water constituents. For instance, Pariente et al. (2008) concluded that photo-Fenton oxidation improved aerobic biodegradability of treated BA ( $150 \text{ mg L}^{-1}$ ), expressed as faster reduction of COD in biological shake flask tests after oxidation compared to untreated BA. However, sum parameters such as COD or BOD<sub>5</sub> might have a limited meaning, as they do not fully indicate, if refractory compounds have been formed. Additionally, they continued oxidative treatment after BA was fully removed, which may improve biodegradability but is also energy intensive.

#### 6.4.3.3 Analysis of transformation products after oxidation and after biodegradation

In order to investigate refractory compounds after biodegradation, excitation emission matrices (EEMs) were recorded before and after oxidation, and after biodegradation. UV/H<sub>2</sub>O<sub>2</sub> treatment led to a substantial increase in fluorescence with two maximum regions at approximately 290/410 nm (peak 1) and 320/450 nm (peak 2) (Figure 22). Peak 1 is very similar to what has been reported previously for *o*-hydroxybenzoic acid (salicylic acid) (Ni et al., 2006). After biodegradation a weaker signal (22-24 Raman units before, 6-7 after) could be found for the latter peak, which

indicates that larger, fluorescing molecules remained present to some degree as refractory DOC. The same can be observed for O<sub>3</sub>/H<sub>2</sub>O<sub>2</sub>, where only peak 2 (320/450 nm) was formed and also remained present with weaker intensity after biodegradation (SI, Figure 45).

To gain further insights into the nature of this recalcitrant organic carbon, we coupled LC-high-resolution mass spectrometry (LC-HRMS) with fluorescence detection. LC-HRMS with fluorescence detection of 290/410 and 320/450 nm revealed that UV/H<sub>2</sub>O<sub>2</sub> treatment (sample 1a) caused formation of a wide array of different TPs. Overall, 15 TPs were identified based on signal intensity, and sum formulas were determined using exact masses with a maximal mass error of 5 ppm (Figure 23, Table 25, SI). TP138 could be identified as salicylic acid by retention time comparison with a purchased standard. The TPs 154a, 154b (C<sub>7</sub>H<sub>6</sub>O<sub>4</sub>) and 170 (C<sub>7</sub>H<sub>6</sub>O<sub>5</sub>) are likely other expected di- and tri-hydroxylated products from BA oxidation. TPs 168, 172a, 172b and 184 were only formed in UV/H<sub>2</sub>O<sub>2</sub> treatment and might represent quinones that are also known intermediates from ozonation of phenol (Ramseier and von Gunten, 2009). Additionally, very polar TPs likely containing a hydroxyl and a sulfate group (TP234a, b, and c with sum formula C<sub>7</sub>H<sub>6</sub>O<sub>7</sub>S) were detected that may be products of radical reactions of the aromatic ring with sulfate present in the TW. TPs containing nitrogen as unwanted and potentially toxic side-products could not be identified, but their formation may occur in water with higher nitrite or nitrate concentrations (Rayaroth et al., 2022).

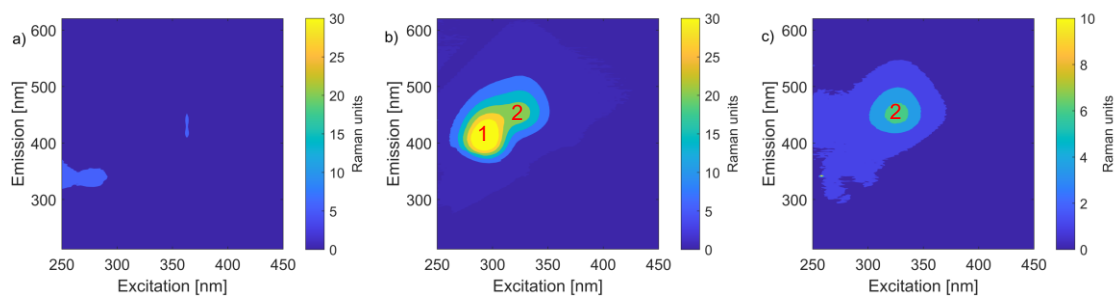


Figure 22: EEMs (a) before UV/H<sub>2</sub>O<sub>2</sub> oxidation (0a), (b) after oxidation (1a), and (c) after biodegradation (1a).

The fluorescence measurement over the whole LC-HRMS method confirmed that the first of the two fluorescence maximum regions (290/410 nm) seen in EEMs of UV/H<sub>2</sub>O<sub>2</sub> samples can be linked to salicylic acid (TP138) at RT 5.16 min. This hydroxylated TP is being formed especially during UV/H<sub>2</sub>O<sub>2</sub> treatment (as discussed in 6.4.2.1 for BTE) and is also present in smaller quantities after O<sub>3</sub>/H<sub>2</sub>O<sub>2</sub> treatment (Figure 51: Fluorescence (320/450 nm) in the first 6 min of the HRMS run of (1b) before (purple line) and after biological degradation (green line).Figure 51, SI). The fluorescence of peak region 2 (320/450 nm) was visible in all samples in the first 4-5 min of the chromatogram and can

generally be assigned to the identified more polar TPs (Figure 49-Figure 52, SI). Interestingly, the fluorescence signal was present even where no peaks were identified, suggesting that a large number of TPs with low abundance were formed that are not included in this list. The signal was substantially weakened after biodegradation compared to after AOP treatment, but still at much higher intensity than in the control samples without oxidative treatment, before and after biodegradation.

In contrast, a limited number of TPs was detected in the ozonated sample (1b), which is attributed to the reactivity of activated aromatic rings with ozone (Figure 23b). Within the group of identified TPs, only the sulfate-containing TP234a and a trace of TP138 was still found in both samples (1a and 1b) after biodegradation. No dimers or other polymers, that were already reported for ozonation of aniline and phenol, were found in this analysis (Shang and Yu, 2002; Ye and Schuler, 1989). Dimers and polymers were expected to be retained even longer than the parent compound on the reversed-phase column, but no respective mass and fluorescence signals were observed in the relevant time period. Nevertheless, it cannot be excluded that dimers and polymers remained undetected due to ionization problems during MS measurements or the low concentration of isomeric substances in the samples. Furthermore, very polar compounds, such as short-chained organic acids would not be detected in this HPLC-method due to limited retention on the column.

In accordance with DOC data (Figure 21b), BA in samples without oxidation (0a and 0b) was biodegraded completely with almost no detectable TPs after biodegradation. Only weak signals of TP138 in both, and TP166 and TP170 in (0b) could be detected (Figure 23). This confirms that aerobic biodegradation of the parent compound was more complete in this experimental set-up.

The transferability of the results of initial biodegradation to real groundwater contamination scenarios must be evaluated with care: first, the effect of microbial adaptation is not fully taken into account here, thus it is possible that similar biodegradation of oxidized vs. not oxidized samples can be achieved if the microbial community is pre-exposed and adapted. Second, a direct transfer of BA biodegradation to BTEX is not possible due to different toxicity thresholds that may inhibit microbiological activity in a fundamentally different way, although past research has shown that certain bacteria strains can handle hundred or more mg L<sup>-1</sup> BTEX (El-Naas et al., 2014; Wolicka et al., 2009; Xin et al., 2013).

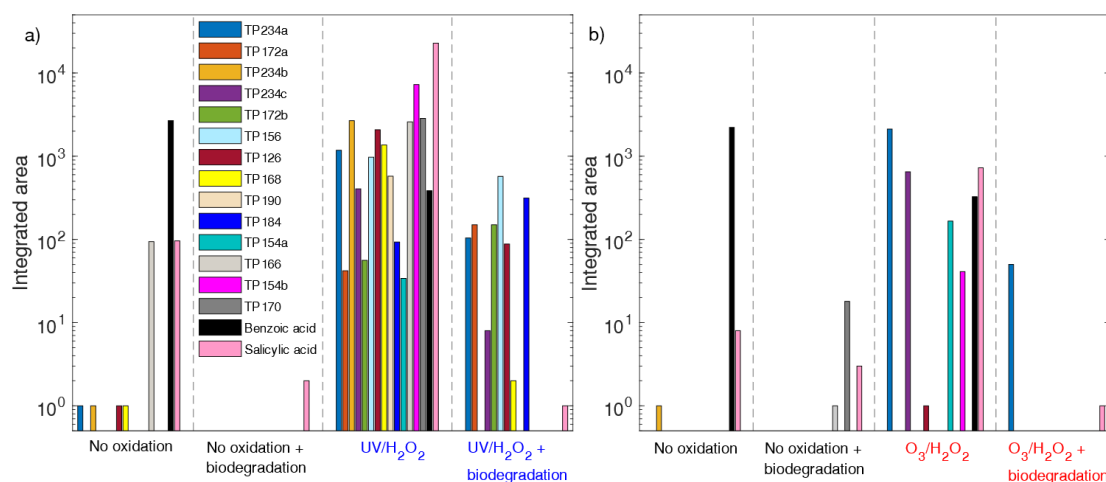


Figure 23: Integrated peak areas of identified TPs, grouped by retention time, before and after biological degradation for samples treated with a) UV/H<sub>2</sub>O<sub>2</sub> (sample 1a), and b) O<sub>3</sub>/H<sub>2</sub>O<sub>2</sub> (sample 1b), and the respective control samples without chemical oxidation (0a and 0b).

Nevertheless, we conclude that the benefits of AOPs compared to aerobic biological treatment, for instance stimulated by passive oxygen release (Chapman et al., 1997), should be re-assessed for removal of monocyclic aromatics with respect to BA results. This is especially the case for in-situ groundwater remediation scenarios with several mg L<sup>-1</sup> contaminant, where full mineralization by chemical oxidation cannot be guaranteed due to limited process control. For instance, Yang et al. (2020) suggested the use of persulfate or H<sub>2</sub>O<sub>2</sub> with Fe<sup>2+</sup> for in-situ oxidation of BTEX. They observed a substantial but not always complete removal of their contaminants in column studies with soil, thus it would be worth looking closer at the remaining dissolved organic compounds. We therefore recommend checking for color and fluorescence increases, which are parameters comparably easy to measure.

## 6.5 Conclusions

O<sub>3</sub>/H<sub>2</sub>O<sub>2</sub> and UV/H<sub>2</sub>O<sub>2</sub> AOPs are viable technologies for the oxidation of monocyclic aromatics BTE and BA if removal of target contaminants from treated water is the main objective. DOC removal in both processes was at maximum 20% for removal of BA up to 94%, and multiple organic TPs were formed. The detection of absorbance changes and quantification of hydroxylated TPs in BTE and BA oxidation experiments indicate that some intermediates are oxidized more efficiently during O<sub>3</sub>/H<sub>2</sub>O<sub>2</sub> treatment. This confirms hypothesized synergies of ozone and ·OH exposure in a direct comparison. Nevertheless, absorbance of UV and visible light increased in both treatment processes, where only partial oxidation was investigated. Additionally, results from biodegradation experiments with BA and TPs provide strong evidence that coupling both AOPs with biological post-treatment is not beneficial for fast, complete mineralization compared to

direct biotransformation of the parent compound. Higher oxidant exposures, potentially multiple times higher than needed for removal of parent compounds, are required to achieve a more complete mineralization. Further research is needed to assess the toxicological relevance of the remaining organics, as well as a potential microbial adaptation for improved mineralization of TPs during long-term exposure. In this context, evaluation of field sites with in-situ chemical oxidation of BTEX may provide valuable information.

## **6.6 Acknowledgement**

This study was funded by the German Federal Ministry of Education and Research (BMBF), funding code 02WIL1523. We would like to thank Dr. Oliver Knoop for his help with GC-FID method development and analysis, Kristina Mraz for her help with BTE experiments, Carl Witthöft for his help with biodegradation tests, and Myriam Reif for analyzing TOC/DOC.

## 7 A NOVEL CATALYTIC FILTRATION PROCESS USING $\text{MnO}_2$ @SAND AND PEROXYMONOSULFATE FOR UNSELECTIVE REMOVAL OF ORGANIC CONTAMINANTS FROM WATER

The following chapter presents investigations related to *research objective 4 (hypothesis 4.1): Explore catalytic oxidation processes for unselective removal of organic contaminants.*

This chapter has been published with some editorial changes as follows:

*Bein, Emil; Yechezkel, Yinon; Zucker, Ines; Drewes, Jörg E.; Hübner, Uwe (2023): A novel catalytic filtration process using  $\text{MnO}_2$ @sand and peroxymonosulfate for unselective removal of organic contaminants from water. In: Chemical Engineering Journal 476, 146636. DOI: 10.1016/j.cej.2023.146636.*

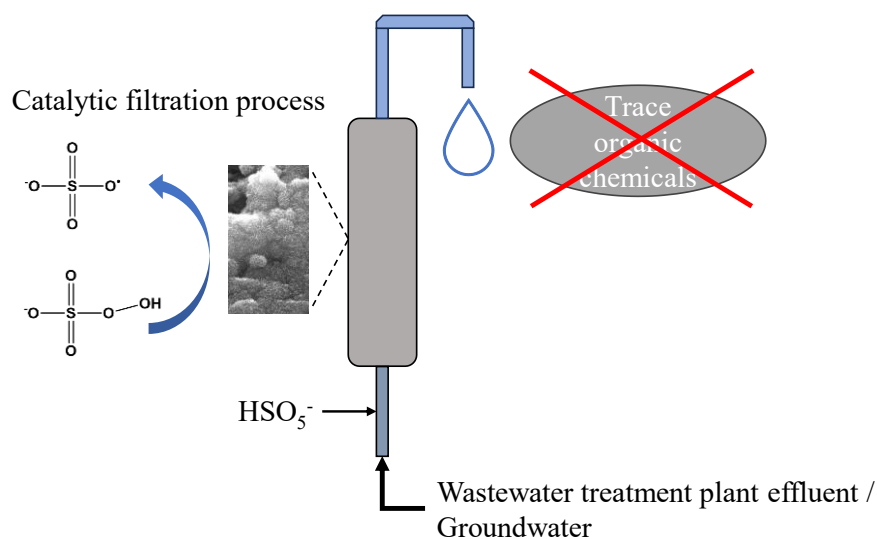
Author contributions: Emil Bein: Conceptualization, Methodology, Formal analysis, Investigation, Writing – Original Draft, Writing – Review & Editing, Yinon Yechezkel: Formal analysis, Investigation, Writing – Review & Editing, Ines Zucker: Funding acquisition, Writing - Review & Editing, Jörg E. Drewes: Funding acquisition, Writing - Review & Editing, Uwe Hübner: Conceptualization, Methodology, Supervision, Funding acquisition, Writing – Review & Editing

### 7.1 Abstract

Multiple catalytic oxidation processes involving new synthesized materials have recently been examined to replace conventional oxidative treatment methods for water purification, but upscaling and demonstration stages are mostly lacking, which hinders their practical implementation. In this study, we introduce a novel catalytic process where peroxymonosulfate (PMS) is activated by  $\text{MnO}_2$  surfaces that are attached on natural sand as part of a catalytic filtration column (CFC). PMS decomposition in the CFC was stable during steady-state filter operation with different natural waters (tap water and secondary effluent) and sulfate radicals were identified as main radical species. Complete oxidation (>99%) of 10 mg  $\text{L}^{-1}$  rhodamine B in tap water could be achieved with PMS concentrations as low as 0.2 mM and a residence time of less than 3 min. Furthermore, unselective oxidation of various recalcitrant and environmentally-relevant trace organic



chemicals (e.g., carbamazepine, sulfamethoxazole, and benzotriazole) was achieved with 0.6 mM PMS in tap water and secondary effluent, proving the robustness of the process in presence of multiple organic and inorganic constituents. Future investigations are needed to optimize the CFC process for specific applications and confirm its operation in real-world water matrices and to study sustainability aspects. Overall, this study demonstrates the potential of the CFC process to be implemented as a practical nano-enabled water treatment and offers a framework for next steps to be taken before upscaling. It provides important performance data that can be used as reference for future proposals of scalable catalytic oxidation water treatment technology.



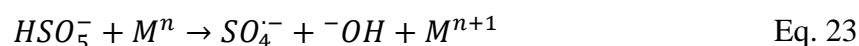
**Keywords:** Catalytic oxidation; PMS activation; sulfate radicals; advanced water treatment; chemicals of emerging concern

## 7.2 Introduction

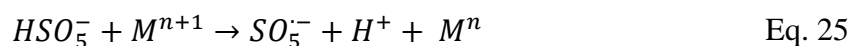
Advanced oxidation processes (AOPs) include a large variety of water treatment processes, where—according to a wide definition—powerful radicals such as hydroxyl ( $\text{OH}^{\bullet}$ ), sulfate ( $\text{SO}_4^{\bullet-}$ ), or chlorine ( $\text{Cl}^{\bullet}$ ) radicals are generated in-situ to oxidize recalcitrant organic chemicals (Miklos et al., 2018b). In heterogeneous catalytic AOPs, pollutants are oxidized through the activation of dissolved oxidants, e.g.,  $\text{O}_3$  (Yu et al., 2020),  $\text{H}_2\text{O}_2$  (Xie et al., 2019; Xu et al., 2021b), or persulfate salts (peroxymonosulfate, peroxydisulfate) (Kohantorabi et al., 2021; Oh et al., 2016; Oh and Lim, 2019) in a catalytic surface reaction. In recent years, persulfate salt activation has gained attraction as an alternative to  $\text{O}_3$ - and  $\text{H}_2\text{O}_2$ -based treatment technologies (Lee et al., 2020).

In particular, activation of peroxymonosulfate ( $\text{HSO}_5^-$ , PMS) has been studied intensively with various catalytic materials, e.g.,  $\text{MnO}_2$  of different crystallinity and

morphology (Huang et al., 2019; Huang and Zhang, 2019; Khan et al., 2018; Saputra et al., 2013),  $\text{Cu}_2\text{O}$  (Li et al., 2020), or rare compounds such as lanthanum (La) or cobalt (Co) (Lin et al., 2017a; Marinescu et al., 2018; Zhang et al., 2022). PMS is generally considered more suitable than peroxydisulfate (PDS) for catalytic processes due to its good reactivity with various transition metals, which is linked to its asymmetrical structure (Anipsitakis and Dionysiou, 2004; Lee et al., 2020). Both  $\text{SO}_4^{\cdot-}$  and  $\cdot\text{OH}$  can potentially be formed in such a reaction of PMS with the transition metal (M) by an electron-transfer reaction (Kohantorabi et al., 2021):



A simultaneous reduction of  $\text{M}^{n+1}$  has been postulated for reactions of some transition metals such as Mn, Co, and La with PMS (Anipsitakis and Dionysiou, 2004; Lin et al., 2017b):



While some studies provide evidence for the generation of powerful radicals ( $\cdot\text{OH}$ ,  $\text{SO}_4^{\cdot-}$ ) during catalytic PMS activation that can transform a broad range of organic contaminants (Ahn et al., 2019; Chen et al., 2019; Guan et al., 2020), others reported catalyst-specific removal of certain contaminants with electron-rich moieties (i.e., activated aromatic rings) by the generation of singlet oxygen ( $^1\text{O}_2$ ) (Gao et al., 2019; Shahzad et al., 2020) or even by a non-radical mechanism following a catalyst-mediated electron transfer from contaminant to oxidant (Ahn et al., 2016; Li et al., 2020; Zhang et al., 2022). Hence, the characteristics of the catalyst material seem to determine if PMS activation leads to unselective ( $\cdot\text{OH}$ ,  $\text{SO}_4^{\cdot-}$ ) or more selective ( $^1\text{O}_2$ , mediated electron transfer) reactive species or mechanisms. Whether or not a new process with high specificity towards individual contaminants can constitute an actual alternative in the context of water treatment and in which specific applications is subject to an ongoing scholarly debate (Kohantorabi et al., 2021; Lee et al., 2020; Yan et al., 2023; Yang et al., 2021).

For the abatement of trace organic chemicals (TOrcs) during drinking water treatment and advanced wastewater treatment (and reuse), processes and process combinations are needed that can remove a broad range of chemicals with different characteristics.  $\text{SO}_4^{\cdot-}$ -based oxidation shows high promise in this regard because  $\text{SO}_4^{\cdot-}$  reacts less selectively than  $\text{O}_3$  with relevant target contaminants, but it is more stable in water compared to  $\cdot\text{OH}$  (Miklos et al., 2019; Nihemaiti et al., 2018). Furthermore, catalytic AOPs can be operated with comparably low on-site energy input and do not generate waste streams, which makes them suitable solutions especially for decentralized, smaller plants (Hodges et al., 2018). In our view, the main research need linked to

catalytic AOPs is the development of scalable treatment processes that can achieve similar or better performance, and/or a reduced carbon or energy footprint compared to state-of-the-art systems (Hübner et al., 2022; Miklos et al., 2018b; von Gunten, 2018).

Despite the substantial progress made with synthesis of effective catalysts in recent years, some of the most important obstacles for upscaling catalytic AOPs as part of an advanced water treatment scheme have not been fully solved, or are even rarely addressed (Mauter et al., 2018), where we want to name four key milestones: (1) The engineering challenge of full-scale reactor design, as many lab-scale studies demonstrated catalytic effects with fine powders that would need to be fully retained to avoid leaching of toxic metals and prolong the lifetime of the process, (2) the reduction of oxidant doses to levels that are competitive and comparable to existing processes, typically well below 1 mM, (3) the proof that the catalyst works reliably for long time periods in continuous operation, and (4) the demonstration of reactivity with all relevant contaminants in a realistic water matrix, which also may contain several scavengers and promoters.

In this contribution, we address these challenges through employing a “catalytic filtration column” (CFC) with a facile-to-synthesize and highly reactive  $\text{MnO}_2$  nanostructured material that is immobilized on sand ( $\text{MnO}_2$ @sand).  $\text{MnO}_2$  is a frequently tested nanomaterial for catalytic PMS activation with well-described characteristics and synthesis conditions, and, therefore, was chosen as promising candidate for further upscaling efforts (Chen et al., 2019; Deng et al., 2017b; Khan et al., 2018; Saputra et al., 2013). The catalyst immobilization and subsequent operation in a CFC will enable effective liquid to solid mass transfer and facilitate upscaling of the catalytic oxidation process, a critical step that is rarely taken in catalytic oxidation studies. We followed a proposed framework to assess the suitability of the catalytic process (Hübner et al., 2022), which includes characterization of the material, demonstration of lasting oxidant decomposition without catalyst leaching, a general performance assessment using the well-known model pollutant rhodamine B (Rh-B), and, ultimately, a demonstration that the process can remove relevant TOxCs occurring in natural water systems.

## 7.3 Materials and methods

### 7.3.1 Synthesis of $\text{MnO}_2$ @sand

$\text{MnO}_2$ @sand was produced using a modified hydrothermal synthesis method for the production of  $\alpha$ - $\text{MnO}_2$ , based on Nawaz et al. (2015) and Luo et al. (2008). In this work, 0.25 M  $\text{KMnO}_4$  (VWR chemicals, analytical grade) and 1 M  $\text{HCl}$  (32%, Merck, analytical grade) were mixed in 40 mL ultrapure water (UPW, total volume) as precursor solution in an open batch (Figure 24a). This solution was transferred to a 100 mL stainless steel

PTFE-lined autoclave that contained 40 g of washed technical sand (0.2-2.5 mm grain size, 10.5.1). The mixture was gently stirred manually, the autoclave closed, and placed into an oven at 160 °C for 14 hours. After cooling down at room temperature,  $\text{MnO}_2$ @sand was collected and rinsed thoroughly with DI water on a 200  $\mu\text{m}$  stainless steel sieve, then dried at 105° C for at least 12 hours before storage and further use.  $\text{MnO}_2$  suspension that was not attached to sand was collected separately from  $\text{MnO}_2$ @sand and washed with UPW in three centrifugation cycles (15 min, 3000 rpm) for further analysis.

### 7.3.2 Material characterization

Scanning electron microscopy (SEM) was used to study the morphology of catalyst particles, both attached and not attached to the sand (Quanta 200 FEG, FEI, USA). The samples ( $\text{MnO}_2$ @sand,  $\text{MnO}_2$  powder) were placed on an SEM knob using conductive carbon tape. For the  $\text{MnO}_2$  powder, droplets of a suspension were evaporated on cleansed silicon wafers. X-ray diffraction (XRD) patterns were obtained with a Bruker D8 Discover diffractometer (Bruker, USA) ranging from 10 to 80 °  $2\theta$  with 0.02°  $2\theta$  s<sup>-1</sup> scan speed. The accelerating voltage applied to the copper anode was 40 kV and the emission current 40 mA. X-Ray photoelectron spectroscopy (XPS) was performed using an ESCALAB QXi system (Thermo Scientific, USA) with dual beam compensation and a spot size of 650  $\mu\text{m}$ . In order to quantify the Mn coating,  $\text{MnO}_2$  on sand was dissolved in ascorbic acid (Charbonnet et al., 2018). Therefore, 20 mL of 30 mM ascorbic acid was added to 0.5 g coated sand in triplicates and the Mn concentration in the solutions was determined by atomic absorption spectroscopy (AAS).

### 7.3.3 Catalytic oxidation experiments

Catalytic oxidation experiments were conducted using 35 g of coated sand filled into a glass column of 32 cm length and 1 cm inner diameter as a CFC that was connected to a gear pump and a feed bottle (Figure 24b). For control experiments, the column was filled with 35 g of the same sand material without coating but the same pre-treatment (i.e., washing and sieving).

Contaminant removal experiments were carried out with (1) Rh-B in tap water (TW), (2) TOrCs in TW, and (3) TOrCs in secondary effluent (WW). Before each oxidation experiment, the target amount of PMS (“Oxone”, 307.38 g mol<sup>-1</sup>, Thermo Scientific) was dissolved in the required volume of water, contaminant(s) were spiked, and the feed bottle was connected to the CFC (Figure 24b). Rh-B (Acros organics, >98% purity) was added from a 2 g L<sup>-1</sup> stock solution (varying dilution factors) and TOrCs from a 200-600  $\mu\text{g L}^{-1}$  stock solution mixture with a dilution factor of 0.002 (TOrCs in the stock solution were dissolved in ultrapure water). The solution volume in the CFC was initially exchanged

with feed solution at a flow rate of  $20\text{--}40\text{ mL min}^{-1}$  for approximately 5 min. Afterwards, the CFC was operated at steady-state flow conditions, where solution was pumped once through the CFC with  $5\text{ mL min}^{-1}$  in all experiments. Samples were taken before the start of operation from the feed bottle and in triplicates from the CFC effluent after 60 min of steady-state operation to assess removal of PMS and contaminants. After each experiment (approximately 75 min), an additional sample was taken from the feed bottle to check for direct PMS reactivity with contaminants. All samples intended for TOxCs quantitation were immediately mixed with  $1\text{ mM Na}_2\text{S}_2\text{O}_3$  (Merck, analytical grade) to remove residual PMS.

An initial longevity test analyzing PMS decomposition was performed over 9.5 h with newly synthesized material. The material used here was pre-exposed to  $0.6\text{ mM PMS}$  in TW for additional two hours beforehand at a flow rate of  $5\text{ mL min}^{-1}$  (i.e.,  $2+9.5\text{ h}$ ). In addition to measurement of PMS concentrations, solution pH and Mn leaching from the active nanocomposite were analyzed. Each effluent sample was withdrawn over 6 minutes to collect the required volume for analysis, and the start of sampling was treated as sampling time in the data analysis. The influent PMS concentration was measured at the beginning and at the end of each experiment to monitor PMS decomposition in the feed container. More details on the used catalyst batches (CFC1, 2, and 3) can be found in the supplemental information (SI), 10.5.2.

Experiments were conducted in TW of slightly alkaline pH ( $7.6\text{--}8.15$ ) with a typical bicarbonate concentration of  $333\text{ mg/L}$  and a  $\text{TOC} < 1\text{ mg C L}^{-1}$ , unless otherwise noted. This water matrix was chosen to mimic a realistic carbonate-buffer system (see SI, 10.5.4, for an extensive water characterization). Secondary treated effluent (WW) from the Wastewater Treatment Plant Garching ( $31,000\text{ PE}$ ) was withdrawn freshly on the day of experiments and analyzed for dissolved organic carbon (DOC),  $\text{NO}_2^-$ , and  $\text{NO}_3^-$ . WW was used as obtained without additional pre-treatment, and PMS solutions were prepared similar to TW.

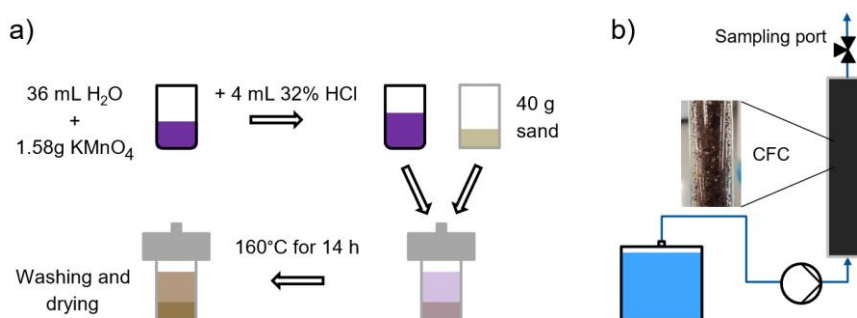


Figure 24: a)  $\text{MnO}_2$ @sand synthesis procedure, and b) experimental set-up used for longevity and contaminant removal experiments.

### 7.3.4 Analytical methods

PMS was analyzed spectrophotometrically using a Shimadzu UV1900 spectrophotometer (Shimadzu, Japan) by oxidation of iodide ions. Briefly, 1 mL of an aqueous solution containing  $100 \text{ g L}^{-1}$  potassium iodide (Merck, analytical grade) and  $5 \text{ g L}^{-1}$  sodium bicarbonate (Carl Roth, >99%) (Wacławek et al., 2015) was mixed with in total 1 mL UPW and sample containing PMS. This mixture was shortly vortexed, and absorbance was analyzed at 395 nm after more than 20 min. PMS was thereafter quantified using a linear calibration curve ( $2.5 - 50 \text{ mg L}^{-1}$ ). Rh-B removal was measured on the same instrument as absorbance decrease at 554 nm wavelength immediately after the samples were withdrawn without additional treatment.

A total of 22 TOrCs were analyzed using an Agilent 1260 Infinity II HPLC system coupled with a SCIEX 6500 TripleQ mass spectrometer in ESI positive mode (HPLC-MS/MS), following the procedure described in Müller et al. (2017). Before storage and analysis, samples were quenched with 1 mM  $\text{Na}_2\text{S}_2\text{O}_3$  (VWR Chemicals, analytical grade), mixed with internal standard solution, vortexed, and finally filtered through  $0.22 \mu\text{m}$  PVDF filters. WW DOC was analyzed by a varioTOC Cube (Elementar, Germany) after filtration through cellulose acetate membrane filters with a pore size of  $0.45 \mu\text{m}$  (Altmann Analytik, Germany).  $\text{NO}_3^-$  and  $\text{NO}_2^-$  were quantified using test kits from Hach (LCK340, LCK341). Mn concentrations for coating quantities and leaching studies were determined by flame AAS (AA240FS, Agilent, USA) with and without graphite furnace after acidification of samples with 1%  $\text{HNO}_3$ .

## 7.4 Results

### 7.4.1 Characteristics of $\text{MnO}_2$ @sand

SEM micrographs of the synthesis products reveal different morphologies for the  $\text{MnO}_2$  deposited onto sand ( $\text{MnO}_2$ @sand) compared to the unattached (suspended)  $\text{MnO}_2$  that did not grow on the sand surface (Figure 25a-d). Suspended  $\text{MnO}_2$  particles had a wire-shape of up to  $2\text{-}3 \mu\text{m}$  length (Figure 25a). This wire-like morphology was previously shown for  $\alpha\text{-MnO}_2$  (Nawaz et al., 2015; Saputra et al., 2013; Zucker et al., 2019). The aimed crystallinity of the unattached nanoparticle is confirmed by the obtained XRD pattern, which matches a data base record of  $\alpha\text{-MnO}_2$  (JCPDS 044-0141, Figure 25e).

Supported  $\text{MnO}_2$  (i.e.,  $\text{MnO}_2$ @sand), however, consisted of smaller rod- and wire-like morphologies (Figure 25b-d, 10.5.3, SI), but also a much finer flower-like morphology (Figure 25d). The length and width of these attached structures decreased

compared to the wires of suspended  $\text{MnO}_2$  (Figure 25a), to sizes smaller than  $1 \mu\text{m}$ . Different morphologies in the same synthesis batch due to growth of the nanomaterial on the sand may be caused by the different nucleation and crystal growth on the very heterogeneous sand surface (Thanh et al., 2014). This is an indication that the choice of support materials to be coated may lead to changes in morphological structures (Borovik et al., 2020). It was not possible to obtain XRD patterns of the coated surfaces due to the strong signal of the support material compared to the thin layer of the coating, even when different sample preparation methods were tried, including ultrasound detachment strategies and  $\text{MnO}_2$ @sand crushing techniques. However, presence of  $\text{MnO}_2$  on the surface was detected by XPS spectra, where the  $\text{Mn}2\text{p}3$  peak contained a “shoulder” at ca. 643 e.V. in all samples that is characteristic for  $\text{MnO}_2$  based on reference spectra, indicating a high share of the  $\text{Mn}^{4+}$  oxidation state, whereas smaller quantities of  $\text{Mn}^{3+}$  ( $\text{Mn}_2\text{O}_3$ ) and  $\text{Mn}^{2+}$  ( $\text{MnO}$ ) may be present (Biesinger et al., 2011) (Figure 25g, Figure 56). Furthermore, in such synthesis conditions (pressure, temperature, precursor type, and concentration) we expect similar crystallinity on the surface and in suspension despite the varying morphologies obtained (Nawaz et al., 2015).

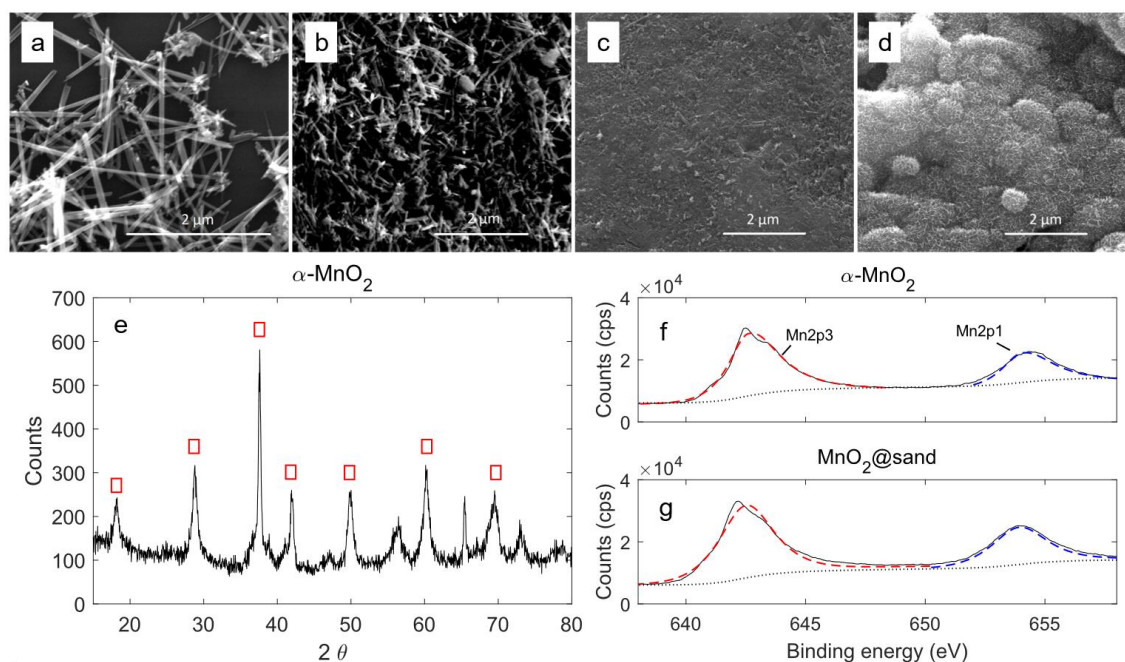


Figure 25: (a) SEM micrographs of suspended  $\alpha\text{-MnO}_2$ , and (b-d) different morphologies observed for  $\text{MnO}_2$  deposited onto sand ( $\text{MnO}_2$ @sand). All shown morphologies were found on one sand grain. (e) XRD pattern of suspended  $\alpha\text{-MnO}_2$ , red rectangles indicate a match with JCPDS 044-0141. (f) XPS spectrum of suspended  $\alpha\text{-MnO}_2$ , (g) XPS spectrum of  $\text{MnO}_2$ @sand.

No apparent change of the oxidation state of  $\text{MnO}_2$  ( $\text{Mn}2\text{p}3$ ,  $\text{Mn}2\text{p}1$ ) on the coated surface was observed with XPS analysis compared to suspended  $\alpha\text{-MnO}_2$  in the same synthesis batch (Figure 25f-g). These comparable XPS spectra are evidence of the presence of  $\text{MnO}_2$  on the coated sand surface. Potassium ( $\text{K}^+$ ) was also found in C1 XPS

scans of all samples (SI, Figure 56), which is part of the precursor solution and might have been incorporated in the  $\alpha$ - $\text{MnO}_2$  2x1 tunnel structures (Chen et al., 2018; Robinson et al., 2013). Additionally, a direct comparison of used and freshly prepared  $\text{MnO}_2$ @sand shows no change of the oxidation state after several hours of exposure to PMS, indicating a high level of catalytic stability and suggesting that reactions with PMS involve a complete redox cycle (i.e., oxidation/reduction of  $\text{Mn}^{3+}/\text{Mn}^{4+}$ ) as described by Eq. 23-25 (SI, Figure 56). More data on elemental surface composition and pictures of the coated material can be found in the SI, 10.5.3.

#### 7.4.2 PMS decomposition and process stability

Monitoring PMS decomposition in presence of  $\text{MnO}_2$ @sand over 9.5 h (after a 2 h separate pre-exposure experiment) without contaminants exhibited an initial period of increasing decomposition performance until steady-state conditions were reached after 390 min, where PMS removal was stable at about 90% (Figure 26a). The initial feed solution had to be replaced after 360 min and the experiment was re-started as described in section 7.3.3. Negligible PMS decomposition was observed in the feed solution (0.61 mM before start and 0.6 mM at  $t = 360$  min). In a control experiment with 35 g sand without catalyst in the same column set-up, PMS removal below 10% was observed over 120 min (SI, Figure 59). Reproducibility of the synthesis and thus PMS activation performance was confirmed by a similar PMS decomposition of about 90% in the same conditions using another synthesized CFC (SI, 10.5.2).  $\text{MnO}_2$ @sand did not change its oxidation state following exposure to PMS compared to fresh  $\text{MnO}_2$ @sand, which largely excludes irreversible reactions with  $\text{MnO}_2$  that could cause the initial period of changing PMS decomposition (section 7.4.1). The initial performance changes could also not be attributed to initial Mn leaching, which may, for example, lead to a change of available active sites. Mn, however, was barely detected in the effluent between  $<5 \mu\text{g L}^{-1}$  and  $13 \mu\text{g L}^{-1}$  in the first 300 min of the experiment (Figure 26a). Thus, no conclusion can be drawn about the reasons for the observed performance increase in the first hours of the experiments.

In contrast to our results, a strong decrease in oxidation performance has been observed previously in catalyst recycling batch experiments with PMS/ $\text{MnO}_2$ , where used suspended catalyst was separated and re-used (Huang et al., 2020; Saputra et al., 2013; Wang et al., 2015). The established lasting PMS decomposition in absence of major organic contamination is a strong indication that the CFC/PMS system generates radical species, and PMS is not removed through previously reported mediated electron transfer (Zhang et al., 2022). A distinct feature of such mechanism would be that PMS only decomposes in presence of contaminants, because electrons are directly transferred from



an organic compound to PMS via the metal oxide catalyst (Lee et al., 2020; Shen et al., 2022). Mediated electron transfer has also been reported for  $\alpha\text{-MnO}_2$  that was synthesized with a different synthesis protocol as used here, which highlights that differently synthesized  $\text{MnO}_2$  may result in strongly differing activation mechanisms (Shen et al., 2022).

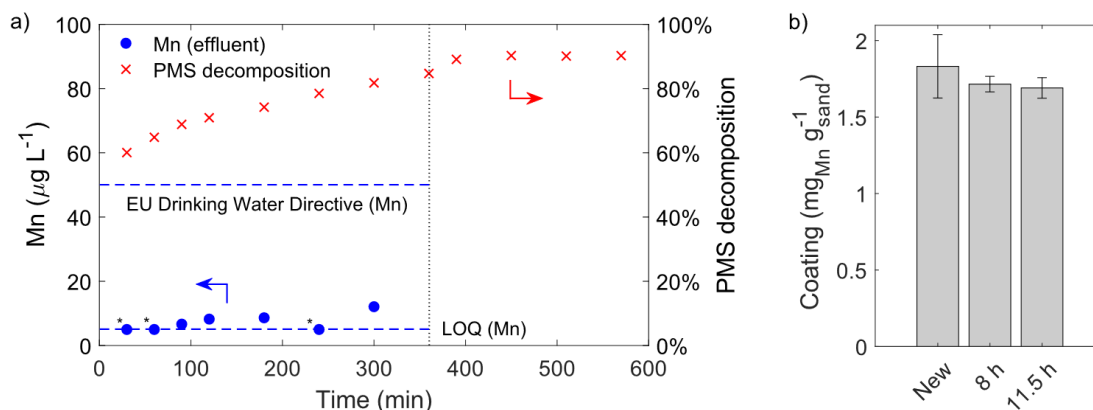


Figure 26: a) PMS decomposition and Mn leaching test of a newly synthesized catalytic column (CFC3) with 0.6 mM PMS in TW. Asterisks indicate if Mn was below the LOQ of  $5 \mu\text{g L}^{-1}$ . The vertical line at 360 min indicates the replacement of the feed solution. 0.61 mM PMS was in the feed solution before the experiment and 0.6 mM by the time of replacement (360 min). The replacement solution had a PMS concentration of 0.6 mM with no noteworthy changes over 230 min. b) Change of Mn coating after different hours of total operation (here including the pre-exposure).

The short- to mid-term stability of attached Mn and the process in general was further assessed by quantifying the coating of freshly prepared material with material operated in steady-state ( $5 \text{ mL min}^{-1}$ , 0.6 mM PMS in TW) for in total 8 and 11.5 h (Figure 26b). Initially,  $1.83 \pm 0.21 \text{ mg}_{\text{Mn}} \text{ g}^{-1}_{\text{sand}}$  were attached to newly synthesized (washed) material, which slightly reduces to  $1.72 \pm 0.05$  after 8 h and to  $1.69 \pm 0.07 \text{ mg}_{\text{Mn}} \text{ g}^{-1}_{\text{sand}}$  after 11.5 h. The differences of coating quantities after different time steps were small and statistically insignificant (t-test,  $\alpha = 0.05$ ). Although there is no experimental evidence of long-term process stability in this study, the CFC proved capable of steady radical generation with a similar amount of water ( $> 2 \text{ L}$ ) passing through as in a recently proposed  $\text{Cu-C}_3\text{N}_4$  Fenton filter for  $\text{H}_2\text{O}_2$  activation (Xu et al., 2021b). Overall, the  $\text{MnO}_2$ @sand CFC demonstrated promise for future long-term operation studies with continuous oxidation over several days to weeks.

### 7.4.3 Rhodamine B decomposition

Decomposition of the textile dye Rh-B ( $10 \text{ mg L}^{-1}$  spiked in TW) was investigated due to its frequent previous use in testing of catalytic PMS activation processes and therefore good comparability (Chen et al., 2019; Lin et al., 2017a; Marinescu et al., 2018). With estimated contact times of 2.2 min, Rh-B was already removed by approximately

72.3 and 86.4 % with comparably low PMS doses of 0.06 and 0.12 mM after 60 min of steady-state operation of the CFC (Figure 27a). The applied doses  $\geq 0.2$  mM PMS led to complete decolorization ( $>99\%$ ). Adsorption of Rh-B to the  $\text{MnO}_2$ @sand (PMS = 0 mM) was negligible (2%) in a control experiment without PMS (Figure 27a). As shown previously, (initial) adsorption can be a substantial contribution to removal of Rh-B in catalytic oxidation experiments (Huang et al., 2020; Peng et al., 2020). Another control experiment with the sand column (without coating) and 0.6 mM PMS showed 1% PMS (Figure 27b) and 21% Rh-B decomposition (SI, 10.5.5), which is similar to the direct PMS reaction observed in the feed bottle. Hence, it can be concluded that Rh-B decomposition occurred due to catalytic reactions of PMS in the CFC. While PMS was decomposed below the LOQ (0.016 mM or  $5 \text{ mg L}^{-1}$ ) for doses below 0.6 mM, the decomposition in the experiment with 0.6 mM PMS was about 94%, which is similar to the steady-state decomposition without Rh-B as shown in the longevity test (Figure 26a). This is another indication that PMS decomposition is unaffected by the presence of a contaminant in the water matrix.

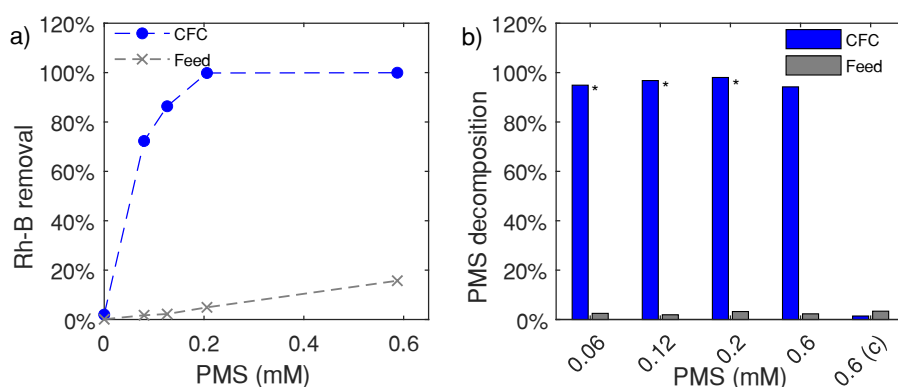


Figure 27: a) Dependence of Rh-B removal on PMS feed solution concentrations. "CFC" is the removal in the catalyst column, calculated based on the initial PMS/Rh-B feed concentration. "Feed" is the Rh-B removal in the feed bottle after ca. 75 min due to direct PMS reactions. Each data point represents one steady-state column experiment. b) PMS decomposition for different feed solution concentrations and the control (c) with 35 g washed sand. Asterisks indicate that removal was estimated using LOQ/4 as effluent concentration as PMS was below LOQ.

Assuming that decolorization of Rh-B is approximately equal to a reduction of Rh-B concentration, 0.19 M and 0.14 M Rh-B were decomposed per 1 M PMS in experiments with 0.06 and 0.12 mM PMS, respectively. This implies an even higher share of PMS led to powerful oxidants because multiple reactions with transformation products may occur simultaneous to Rh-B removal. An experiment with 50 mM tertiary butanol (TBA) as selective  $\cdot\text{OH}$  scavenger ( $k_{\text{OH}} = 6 \cdot 10^8 \text{ M}^{-1} \text{ s}^{-1}$  (Wolfenden and Willson, 1982) vs.  $k_{\text{SO}_4} = 8.9 \cdot 10^5 \text{ M}^{-1} \text{ s}^{-1}$  (George et al., 2001)) and 0.12 mM PMS, however, leads to the assumption that most of the Rh-B is oxidized by  $\text{SO}_4^{\cdot-}$ , because 77.2% of Rh-B were still

removed in the absence of  $\cdot\text{OH}$  (SI, 10.5.6). The potential involvement of  $\cdot\text{OH}/\text{SO}_4^{\cdot-}$ , and  $^1\text{O}_2$  is discussed further in section 7.4.4 and the SI, 10.5.8.

A comparison of different catalysts and catalytic processes is challenged by the fact that often only first-order reaction kinetics in batch experiments are reported or can be derived from the data. With differing effective surface areas, catalyst concentrations, water matrices, and contaminant types and concentrations, these kinetic terms should be interpreted with care. In an attempt to compare our results with a range of catalytic PMS AOPs, we analyzed the stoichiometric ratio of  $[\text{PMS}]_0:[\text{Rh-B}]_0$  from different studies needed to achieve a Rh-B removal of  $>90\%$  in batch experiments (SI, Table 33). The  $[\text{PMS}]_0:[\text{Rh-B}]_0$  ratio of 9.6 in this study is comparable to best performing catalysts from literature, such as a graphene-Co composite ( $[\text{PMS}]_0:[\text{Rh-B}]_0 = 4.0$ ) used by Marinescu et al. (2018). In our experiments, Rh-B was decomposed in a natural buffer system, which has an additional impact due to scavenging/promoting effects. Furthermore, Rh-B decomposition in the CFC occurs in less than 3 min and therefore much faster than in the other studies, probably due to the comparably high catalyst dose of  $6.2 \text{ g L}^{-1}$  (estimated, Table 33). In the chosen experimental design, we can immediately exclude the existence of unwanted side effects, such as excessive permanent Mn-leaching (SI, Table 32), blocking of active sites by adsorption of intermediates (Huang et al., 2020), and fast depletion of catalyst activity, as all data were gathered in independent steady-state operation experiments.

#### 7.4.4 Reactivity with a wide range of contaminants in TW and WW

While removal of Rh-B provided a good indication for the generation of reactive species, it only has limited meaning for the applicability of this process for removal of TOrCs in drinking water and wastewater, which requires an unselective attack of various compounds with different characteristics. Such a proof should be obtained since many selective catalytic PMS activation mechanisms have been reported in the recent past (Cui et al., 2022; Lee et al., 2020; Zhang et al., 2022). The 22 TOrCs spiked in TW and WW represent a broad variety of different chemical structures, such as (activated and deactivated) aromatic rings, primary, secondary or tertiary amines, triazoles, olefins, and more (see SI, 10.5.7 for a full list of compounds). Overall, 20 and 13 out of the 22 measured TOrCs were removed by more than 80% in TW and WW, respectively. 12 compounds showed substantial direct reactivity with PMS ( $>20\%$  decay in feed bottle) in TW and 9 in WW (SI, Table 35 and Table 36). However, removal of these substances was strongly enhanced in the CFC, mostly to levels below the limit of quantification. 10 compounds were completely resistant to PMS exposure in both TW and WW and, therefore, their removal can be attributed to reactive species from catalytic PMS

activation (Figure 28a and b). Among these PMS-resistant compounds, adsorption was only relevant for climbazole and 4-,5-methylbenzotriazole (SI, Figure 60). Tris(2-chloroethyl) phosphate (TCEP) was the only compound for which no removal was observed at all, which is consistent with its low reactivity with  $\cdot\text{OH}$  and  $\text{SO}_4^{\cdot-}$  reported in previous studies (Miklos et al., 2019; Watts and Linden, 2009). Other compounds with a comparably low reactivity with  $\text{SO}_4^{\cdot-}$  ( $<10^9 \text{ M}^{-1} \text{ s}^{-1}$ ), such as primidone, phenytoin, or benzotriazole (Nihemaiti et al., 2018) were removed by  $>80\%$  in TW, but substantial inhibitory effects of the WW matrix ( $9.8 \pm 3.5 \text{ mg C L}^{-1}$  DOC,  $12.1 \pm 1.5 \text{ mg L}^{-1}$   $\text{NO}_3^-$ ,  $0.10 \pm 0.07 \text{ mg L}^{-1}$   $\text{NO}_2^-$ , pH 7.67) reduced removal to 24, 22 and 34% in WW (Figure 28b).

PMS decomposition in TW ( $90.4 \pm 2.2 \%$ ) was comparable to experiments discussed in sections 0 and 0, confirming the reproducibility of the shown performance data. For WW, however, we observed a moderate inhibition of PMS decomposition in steady-state operation ( $67.4 \pm 7.2 \%$ ) with more variability, probably caused by the fluctuating water quality as WWTP effluent samples were taken on three different days (Figure 28c). In addition, a slightly stronger direct decomposition of PMS of approximately 4% occurred in the feed bottle (Figure 28c, SI, Table 37). Based on these observations, it can be concluded that the decreased performance of the CFC process in WW is not only related to the higher radical scavenging, but also induced by an inhibition of the catalytic activation/decomposition of PMS. The inhibitory effect on the CFC process did not increase over time and may be related to multiple dissolved or suspended compounds interacting with the material packed in CFC. By extending the column or reducing the flow rate, a higher removal may be achieved with the same PMS concentration of 0.6 mM, assuming that the inhibition is steady and not increasing. Nevertheless, radical scavenging by organic and inorganic constituents would most likely not lead to a removal of the same extent as in TW. Process optimization (i.e., PMS dosing, residence time) followed by long-term operation with WW are required next steps to validate the suitability of the process, identify potential adverse effects, and determine operation and maintenance procedures such as column backwash or chemical regeneration.

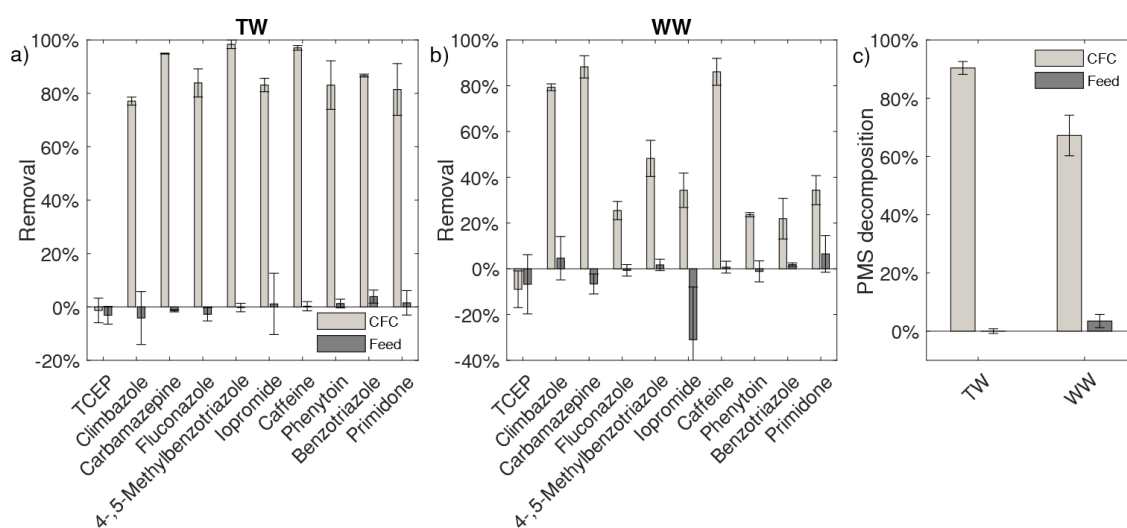


Figure 28: Removal of TOrCs without observed direct PMS reactivity in TW (a) and WW (b) based on three independent experiments for each water matrix ( $n=3$ ). “CFC” refers to the removal observed in the column and “Feed” to the removal observed in the feed bottle from start to end of the experiment (ca. 75 min). c) PMS (0.6 mM) decomposition in the same experiments.

The moderate selectivity of this process, where compounds with electron-donating functional groups, such as carbamazepine ( $\text{C}=\text{C}$ ), amisulpride ( $-\text{NH}_2$ ), or diclofenac ( $-\text{NH}-$ ), are readily removed (SI, Table 35 and Table 36), points to a substantial involvement of sulfate radicals (Ye et al., 2017). A regression analysis was used to assess the potential contribution of  $\cdot\text{OH}$  and  $\text{SO}_4^{\cdot-}$ . The regression was performed with ln-normalized removal of six compounds, that neither adsorbed on surfaces nor showed any substantial direct reaction with PMS, and their reported second-order reaction rate constants with  $\cdot\text{OH}$  and  $\text{SO}_4^{\cdot-}$  as input parameters (see SI, 10.5.8 for further methodological details and outcomes). As a result, we determined  $\cdot\text{OH}$  and  $\text{SO}_4^{\cdot-}$  exposures for every experiment because exposures are largely affected by radical scavenging from the water matrix. The calculated compound removal with these exposures was compared to measured data in Figure 29a. As control, the regression was performed with the assumption of negligible  $\cdot\text{OH}$  exposure (Figure 29b) and negligible  $\text{SO}_4^{\cdot-}$  contribution (Figure 29c). Overall, results of the regression analysis suggest that removal of all TOrCs is best explained by reactions with  $\text{SO}_4^{\cdot-}$  ( $R^2 = 0.74 \pm 0.01$  in TW,  $R^2 = 0.70 \pm 0.02$  in WW), where minor  $\cdot\text{OH}$  contribution cannot be ruled out (SI, 10.5.8). Regression with  $\cdot\text{OH}$  radical reactions only correlated poorly ( $R^2 = 0.36 \pm 0.09$  in TW and  $0.08 \pm 0.005$  in WW). This is in agreement with the Rh-B scavenging experiment, which showed almost the same removal in presence of 50 mM TBA as  $\cdot\text{OH}$  scavenger compared to the experiment without TBA (section 7.4.2). Potential minor contributions of, for example,  $^1\text{O}_2$  cannot be excluded. However, its second order reactivity with compounds such as diclofenac, sulfamethoxazole, and primidone is several orders of

magnitude lower than with  $\text{SO}_4^{\cdot-}$  (Yan et al., 2023), while being substantially more short-lived in water ( $\approx 2.8$  vs. 30-40  $\mu\text{s}$  (Ghanbari and Moradi, 2017; Lee et al., 2020)).

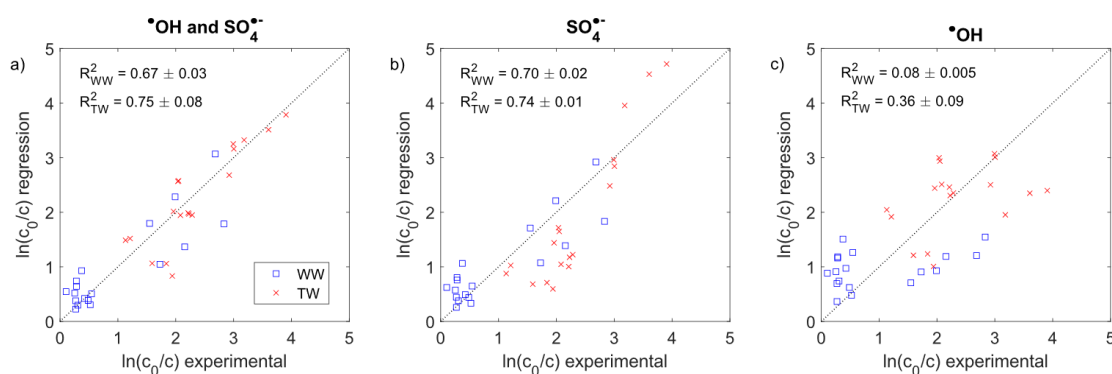


Figure 29: Correlation of experimentally observed removal of six TOxCs and the removal based on (multivariate) linear regression with their reported second order reaction rate constants. Regression was performed a) with  $\cdot\text{OH}$  and  $\text{SO}_4^{\cdot-}$ , b) only  $\text{SO}_4^{\cdot-}$ , and c) only  $\cdot\text{OH}$ .

#### 7.4.5 Benchmarking the CFC process as potential drinking water or advanced wastewater treatment step

Overall, the presented data show effective removal of TOxCs without significant performance losses during mid-term operation for  $>10$  h. Combined with the cost-effective synthesis procedure and platform (filtration sand), and the simple process design as a media filter with a PMS dosing station, the CFC process represents a promising alternative for organic contaminant removal in drinking water treatment, e.g., surface water, or as part of a multiple barrier advanced water treatment system, e.g., agricultural reuse of wastewater.

As a next step, energy demand and costs of the CFC process should be assessed in comparison to a typically applied benchmark process for a potential application. Hübner et al. (2022) proposed a three-step procedure to (1) describe treatment application and select suitable benchmark processes, (2) assess and optimize treatment performance in real water matrix, and, finally, (3) compare energy and cost efficiency. Identification of the treatment application includes the description of the water matrix, the identification of relevant contaminants, as well as the definition of treatment goals. We demonstrate how to apply the proposed framework for the two cases of drinking water and advanced wastewater treatment.

In drinking water treatment, objectives for TOxCs removal depend on occurrence levels in specific water works. State-of-the-art benchmarks for comparison of drinking water treatment technologies could be UV/ $\text{H}_2\text{O}_2$  and  $\text{O}_3/\text{H}_2\text{O}_2$  AOPs due to their low by-product formation potential (most importantly  $\text{BrO}_3^-$ ) and unselective reactions with a variety of different chemicals (von Gunten, 2018). All investigated compounds except of

TCEP were largely removed (>75%) with the CFC process. While (initial) effectivity of the CFC process is demonstrated with the data of this study, additional experiments are needed to optimize the performance for a site-specific case study, proof long-term stability over months of operation, and evaluate other process-related advantages or disadvantages. In particular, one challenge in drinking water treatment could be the salt release caused by PMS addition ( $\text{KHSO}_5 \cdot 0.5\text{KHSO}_4 \cdot 0.5\text{K}_2\text{SO}_4$ ), where potentially 2.5 M  $\text{K}^+$  and 1-2 M  $\text{SO}_4^{2-}$  (depending on the reactions of sulfate radicals with organics) are released per 1 M PMS added. While sulfate concentrations of maximum 115.3 mg  $\text{L}^{-1}$  for 0.6 mM PMS release may not be critical, potassium levels and its implications should also be evaluated carefully. A co-benefit of UV- and  $\text{O}_3$ -based oxidation is the parallel disinfection. Recent studies demonstrated effective inactivation of pathogens by  $\text{SO}_4^{\cdot-}$  (Xiao et al., 2020; Zhou et al., 2023), but additional experiments out of the scope of this study are required to assess disinfection in the CFC process.

Treatment goals for the removal of TOxCs from secondary effluents were recently proposed by the European Commission in a draft of a revised Urban Waste Water Treatment Directive (European Commission, 2022). The draft defines a minimum average removal of 80% for at least four compounds selected from category 1 (amilsulpride, carbamazepine, citalopram, clarithromycin, diclofenac, hydrochlorothiazide, metoprolol, and venlafaxine) and two compounds from category 2 (benzotriazole, candesartan, irbesartan, and the sum of 4- and 5-methylbenzotriazole). In the tested secondary effluent of the WWTP Garching, CFC operation with approximately 0.4 mM PMS decomposition achieved average removal of 74.70 % for the compounds carbamazepine, citalopram, diclofenac, metoprolol, benzotriazole, and 4- and 5-methylbenzotriazole, and average removal by 68.8% for all 22 measured TOxCs. This constitutes a comparable performance as reported for the ozonation step (as potential benchmark) in advanced wastewater treatment (Bourgin et al., 2018). As discussed for drinking water treatment, further experiments are needed to optimize the process and demonstrate long-term process stability. The observed performance in secondary effluent does also not include potential for optimization by pre-treatment and technological (i.e., sensor-based) possibilities to adjust PMS dosing on fluctuating water quality.

Next steps for a comparison of the CFC vs. other competitive systems in drinking water (UV- or  $\text{O}_3$ -based AOPs) and advanced wastewater treatment (ozonation, activated carbon) would include a full analysis of arising costs (chemical consumption, catalyst synthesis, energy) for full-scale operation. This comparison also needs to consider other process-related potential drawbacks such as the expected elevated salt release ( $\text{K}^+$ ,  $\text{SO}_4^{2-}$ ) or a lifetime limitation of the column, as too short lifetimes would severely affect implementation strategies. The simple upscaling of the CFC process as a media filter with

dosing of PMS allows a direct comparison and offers a path towards implementation using the presented framework.

## 7.5 Conclusions

In this study, we were able to report successful treatment of environmentally relevant contaminants in a fixed bed catalytic system ( $\text{MnO}_2$ @sand), introduced as “catalytic filtration column” (CFC). The main outcomes are summarized herein:

- Our modified hydrothermal synthesis method resulted in stable attachment of  $\text{MnO}_2$  on the sand surface with a large variety of different morphologies, where XPS analysis confirmed both presence of  $\text{MnO}_2$  and no changes of the oxidation state after reactions with PMS.
- The CFC was capable of decomposing 0.6 mM PMS in TW (near-neutral pH) over several hours of operation (9.5h +) with no apparent decline of performance.
- An estimated amount of 0.14-0.19 M Rh-B was oxidized per 1 M PMS, which does not include reactions with multiple transformation products and demonstrates a high process efficiency (i.e., conversion of PMS into radicals).
- A large variety of TOrCs was removed by more than 80% in TW and WW, where a statistical analysis suggests that sulfate radicals ( $\text{SO}_4^{\cdot-}$ )—besides direct PMS reactions in the feed container—were the main cause of breakdown.
- Alternative mechanisms, i.e., mediated electron transfer or generation of less powerful radicals, can largely be ruled out due to PMS decomposition in absence of organics and unselective reactivity.
- The process met several criteria, such as low oxidant doses needed, scalability, and effectivity, allowing future investigations for potential applications. Issues to be addressed for the next phase were proposed and include pre-treatment optimization, by-product formation, inactivation of pathogens, and an analysis of treatment costs to proceed with the outlined framework for novel AOPs.

## 7.6 Acknowledgement

This study was performed within the German-Israeli cooperation project “ISCO<sub>3</sub>”, which was funded by the German Federal Ministry of Education and Research (BMBF) and the Israeli Ministry of Science and Technology (MOST) with the funding codes 02WIL1523 and 3-15878. Funding of a research stay of Emil Bein at Tel Aviv University



(TAU) by the German-Israeli Young Scientists Exchange Program (YSEP) is gratefully acknowledged. We would like to thank Dr. David Levy (TAU) and Dr. Pini Shekhter (TAU) for XRD and XPS measurements. Furthermore, we would like to thank Kristina Mraz (TUM) for her help with catalytic oxidation experiments, and Wolfgang Schröder (TUM) and Myriam Reif (TUM) for analyzing tap water quality parameters.

## 8 DISCUSSION AND FUTURE RESEARCH NEEDS

Organic groundwater contamination remains a challenge to be addressed by innovative treatment approaches and an enhanced understanding of reaction chemistry. This dissertation project investigated two novel oxidative technologies that could be installed for ISCO treatment.

The first part of this dissertation explored the potential of gas-liquid membrane contactors for in-situ groundwater remediation using ozone gas. First, existing knowledge on gas-liquid membrane contactors for ozone release in water and wastewater treatment was organized and data analysis tools were used to quantify the mass transfer performance of several membrane materials (*research objective 1*). Second, bench-scale experiments were used to study the performance of PTFE and PDMS membrane materials for ozone release for treatment of the model compounds benzoic acid (BA) and 1,4-dioxane (DIOX) (*research objective 2*). Third, synergistic effects of ozone-based treatment were investigated in relation to UV/H<sub>2</sub>O<sub>2</sub> treatment, where ·OH radicals are produced in absence of ozone. This was combined with a study on biodegradability of remaining DOC after chemical oxidation (*research objective 3*). In the second part of this dissertation, a novel PMS-activation process including an immobilized catalyst was developed and tested merely with a focus on the general mechanism and robustness in different water matrices (*research objective 4*). Therefore, this discussion chapter is divided as follows: (i) feasibility of membrane-based treatment with ozone is critically assessed based on the literature review and experimental results (chapters 4 and 5), (ii) results of chapter 6 are discussed in context of the challenge of coupling chemical oxidation with subsequent biodegradation, and (iii) the road ahead of catalytic PMS activation for groundwater remediation and other treatment applications (chapter 7).

### 8.1 The applicability of gas-liquid membrane contactors for in-situ ozonation of contaminated groundwater

#### 8.1.1 The challenge of material stability and mass transfer

The aim of *research objective 1* was to review membrane materials and analyze mass transfer data in order to gain an understanding of favorable conditions for passive (i.e., diffusion-driven) ozone release in water. The review revealed several critical roadblocks and challenges, as well as opportunities of the technology. First of all, ozone is an extremely difficult gas to work with, as it will attack – one way or another – any materials

and reduce their lifetime. For example, fast material failures with PP membranes were reported, even though there is an absence of unsaturated carbon bonds or other functional groups that are typically directly attacked by ozone. Compared to the gas phase, ozone-reactions in water lead to  $\cdot\text{OH}$ , which is aggressive against most polymers. Fluorinated polymers PTFE and PVDF seem to be the most logical and durable choice as fluorinated carbon cannot be easily degraded by oxidative treatment, although even in case of these materials, property changes have been observed (section 4.4.1). However, recent results suggest that also PTFE exhibited severe material failures after 40 hours of operation (Schmitt et al., 2022). No reliable lifetime could previously be identified for PDMS but operation was possible without major problems for testing purposes over several hours (Zoumpouli et al., 2018). Also, in the experimental section of this dissertation no noteworthy material failures, such as excessive penetration of water into the gas-phase, were observed with both PTFE and PDMS membranes. This speaks for the possibility to achieve lasting stability for duration of groundwater remediation and to proceed with testing in a real treatment scenario. However, a long-term operation study was not conducted and this constitutes a major uncertainty that could not be resolved here. It is recommended to expect material failures in a long-term operation and establish a monitoring system for failures, which would for example result in increased gas flow resistance on the gas phase due to water leakage. Additionally, a technical solution to replace membrane material in this case should be planned ahead. This comparison does not include environmental implications, where the use of PTFE can be considered harmful due to the energy-intensive production and toxicity aspects compared to other polymers (Schwarz et al., 2021).

A second challenge is predicting and establishing a satisfying mass transfer rate of ozone from gas to liquid phase. Mass transfer, as pointed out in chapter 4, is not only strongly dependent on material properties, but also mostly on liquid flow velocities. Only the fast exchange of saturated liquid volumes on the membrane surface with fresh water can result in a high concentration gradient at the gas-liquid boundary layer. The literature data analysis could show that mass transfer can be well predicted using dimensionless correlations especially for high mass transfer coefficients that were mostly observed for PTFE/PVDF at high liquid velocities ( $>10^{-2} \text{ m s}^{-1}$ ). For lower mass transfer coefficients ( $<10^{-6} \text{ m s}^{-1}$ ) and other materials such as PDMS, however, other aspects such as membrane wall resistance need to be considered and also lead to substantial reduction of experimental mass transfer compared to calculated values. To maximize ozone mass transfer, membrane module design proved critical, with small membrane tube diameters  $<1 \text{ mm}$  being most favorable as a large membrane surface area can be achieved in small overall volumes. As it was pointed out in chapter 4, mathematical/numerical tools such as genetic algorithm could be used to formalize and customize membrane module designs

for the respective application and provide a powerful opportunity to further improve the engineering design with a focus on energy efficiency and treatment effectivity. It should be emphasized that high mass transfer rates do not mean that a maximum of produced ozone is effectively brought into the liquid phase, which needs to be considered in membrane geometry designs and is elaborated in more detail in 8.1.2.

### 8.1.2 Transfer to ISCO applications

Previous studies dealt with drinking water and wastewater applications, where one or several membrane modules are intended to deliver ozone to a pumped water stream. For in-situ groundwater remediation applications, however, the membrane geometries and gas flow configurations need to be adjusted to the respective conditions. Specifically, one has to consider basically negligible movements of water bodies ( $<100 \text{ cm d}^{-1}$ ) and the presence of ozone consumers such as SOM or solid metal oxides in the surroundings. Active technologies, i.e., well sparging, will create movement through gas injection and bubbles moving up and into the porous media, potentially causing gas clogging, which may not be the case in membrane-based operation. In *research objective 2*, therefore, the operation of gas-liquid membrane contactors in ISCO was evaluated in bench-scale experiments with different contamination scenarios and porous media types. For contamination, we chose the two model pollutants for their chemical properties: BA and DIOX (Figure 30). Ozonation of aromatic compounds generates  $\cdot\text{OH}$  radicals that can further enhance the removal of the target contaminant, which was previously called “self-enhanced ozonation” in a detailed investigation on BA decomposition in ozonation (Huang et al., 2015). Results from BA suggest that aromatic compounds that are present in high concentrations of several  $\text{mg L}^{-1}$ , which is typical for groundwater contamination scenarios, may undergo rapid decomposition in presence of ozone via a chain of reactions, where hydrogen abstraction reactions with  $\cdot\text{OH}$  lead to hydroxylated compounds. These react with ozone, forming more  $\cdot\text{OH}$ . In contrast, DIOX is composed of C-C and C-O single bonds that make it highly unreactive with ozone and also intermediates are not expected to react with ozone due to the absence of any reactive functional groups.

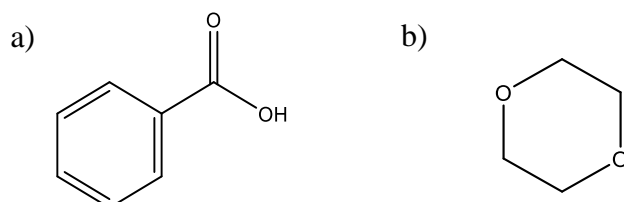


Figure 30: Structural formulas of a) benzoic acid (BA) and b) 1,4-dioxane (DIOX).

It was aimed to test the practical implications of the contaminant properties with *hypothesis 2.1: Removal of benzoic acid (concentrations  $\geq 5 \text{ mg L}^{-1}$ ) as monocyclic aromatic compound is not affected by ozone-reactions with different subsequent porous*

media layers in membrane-based ISCO treatment with ozone due to fast reactions of aromatic intermediate products in proximity of the point of ozone release, whereas removal of aliphatic 1,4-dioxane changes by soil properties due to the promoting or inhibiting effects of ozone-soil reactions. The expectation in the experimental investigation was that the reaction with BA as monocyclic aromatic representative would take place near the membrane and not be affected by reactive soil layer, which could be quantified by measuring residual dissolved ozone concentrations after treatment and measurement of BA removal. In comparison, higher residual dissolved ozone concentrations and varying removal were expected for the control contaminant DIOX. Removal of BA was in fact very similar in different soil layer configurations ( $52.7 \pm 1.0$ ,  $52.2 \pm 0.6$ , and  $49 \pm 1.9$  %), where MNO-92 material was chosen for rapid and radical-free ozone destruction (Schneider et al., 2016) and a natural soil layer for more realistic conditions. No ozone was detected in the effluent as compared to DIOX experiments, which provided additional evidence that the reactions of BA TPs with ozone proceeded rapidly. For DIOX, surprisingly, porous media layers did not have distinguishable effects on removal based on four independently carried out experiments. Dissolved ozone concentrations in the reactor effluent indicated ozone consumption by porous media layers nevertheless. This leads to a **partial acceptance** of *hypothesis 2.1* for BA, however, not in case of DIOX.

What also became apparent in these experiments is that efficiency of BA removal is reduced compared to batch experiments with ideal mixing conditions with ozone. This can be explained by the limited ozone distribution due to the slow release of the gas-liquid membrane contactor vs. fast injection of dissolved ozone. This is pointing to severe drawbacks of gas-liquid membrane contactor usage for ozone release in ISCO operations, where monocyclic aromatics are present. For example, treatment of groundwater containing several  $\text{mg L}^{-1}$  of BTEX could lead to a similarly suppressed spatial distribution of ozone. Unfortunately, reaching steady-state groundwater-like conditions while diffusing ozone requires an extensive and time-consuming experimental campaign. Therefore, it was not possible to investigate more contaminant types and concentrations and soil layers. Moreover, performance at very low velocities such as  $10 \text{ cm d}^{-1}$  or lower could not be tested, because this would require continuous operation of the ozonation system for several days to generate a single data point. However, in the author's opinion, more experimental efforts are not needed for a first assessment of applicability of the membrane-based ISCO treatment approach, because the quantities, i.e., required membrane tubing and realistic removal of contaminants could be demonstrated (described in 5.4.3.2 and 5.5).

By testing *Hypothesis 2.2*, experimental and calculated mass transfer coefficients were compared: *Ozone membrane mass transfer in simulated groundwater flow conditions can*

be accurately predicted ( $\leq 20\%$  difference) using empirical dimensionless correlations set up for different gases and membrane materials. This comparison is important to assess if the modeled values are sufficient to predict mass transfer, which is a crucial step for engineering design of a field-scale treatment. A maximum difference of 20% was defined as acceptable between calculated and experimental mass transfer coefficients. Calculated mass transfer coefficients were based on a dimensionless correlation developed by Fang et al. (2002) for hydrogen release to groundwater in a similar Reynolds number regime ( $Re < 1$ ) and gas-liquid membrane contacting set-up as in this study. Mass transfer coefficients were experimentally determined for flow velocities from 136 to 978  $\text{cm d}^{-1}$  (section 5.4.3.1), which is slightly higher than typical groundwater flow for practical reasons. A novel probe compound approach was used to estimate ozone exposure, which was then converted to dissolved ozone concentrations after the membrane contactor. Subsequently, this was converted to mass transfer coefficients. This method was developed to overcome enormous difficulties in reliably quantifying ozone membrane mass transfer in creeping flow conditions. The problem of using effluent dissolved ozone concentrations for the calculation of mass transfer was previously recognized, however, ozone decay was considered marginal in experimental set-ups with high liquid flow velocities that result in residence times of several seconds (Leiknes et al., 2005; Sabelfeld and Geißen, 2019). In the tested conditions of this dissertation, residence times reached values  $>1$  h. Shortening this time by taking samples closer to the membrane was not possible for the following two reasons: 1) Creeping flow conditions result in non-ideal mixing and sampling in close proximity of the membrane may not represent the actual averaged dissolved ozone concentration. 2) Withdrawal of water samples in very slowly moving water severely disturbs the flow regime as a significant share of the water flowing is taken out and may therefore reduce the accuracy of results.

As demonstrated in section 5.4.3.1, it was possible to obtain mass transfer coefficients (K) using the probe compound procedure. A comparison of K values for different flow velocities is summarized in Table 7. As can be seen, the experimental and calculated values differ substantially in most cases and differences exceed the set 20% acceptable threshold in 8 out of 10 data points. Thus, **hypothesis 2.2 is rejected**.

Table 7: Direct comparison of in section 5.4.3.1 calculated and experimentally determined K and the difference based on  $K_{\text{cal}}/K_{\text{exp}}$  for PTFE and PDMS membranes.

$v_l$ ( $\text{cm d}^{-1}$ )	PTFE			PDMS		
	$K_{\text{exp}}$ ( $\text{m s}^{-1}$ )	$K_{\text{cal}}$ ( $\text{m s}^{-1}$ )	Diff.	$K_{\text{exp}}$ ( $\text{m s}^{-1}$ )	$K_{\text{cal}}$ ( $\text{m s}^{-1}$ )	Diff.
136	4.39E-07	1.05E-06	58.24%	3.95E-07	1.12E-06	64.86%
204	6.08E-07	1.23E-06	50.63%	3.74E-07	1.31E-06	71.37%
340	1.48E-06	1.50E-06	1.80%	1.04E-06	1.58E-06	34.00%
611	2.51E-06	1.89E-06	-32.75%	1.21E-06	1.95E-06	38.09%
978	3.13E-06	2.27E-06	-37.73%	2.06E-06	2.31E-06	10.71%

Some aspects of this analysis, however, should be elaborated further. It must be emphasized that the probe compound approach in this hypothesis testing was used as control, and additional validation of this method could not be conducted as part of this work. Some problems with this approach, especially the calculated ozone decay rate, are discussed in detail in chapter 5.3.5. Nevertheless, the transfer of the dimensionless correlation that was used for calculation of  $K$  from hydrogen to ozone worked well in the sense that  $K$  resulted in the same order of magnitude in both approaches, allowing a preliminary estimation of mass transfer for the tested flow conditions. In fact, by comparing mass transfer calculation results, batch experiments, and in-situ membrane ozonation experiments, it was found that the amount of ozone that was expected to be released ( $88 \mu\text{M}$ ) was similar to the amount of ozone needed for DIOX removal ( $110\text{-}140 \mu\text{M}$ ). More data would be needed to complete the assessment how accurate the projection of ozone release by the membranes would be in various flow conditions and also water matrices, as a clearly differing correlation of liquid velocity (expressed as  $Re$ ) and mass transfer coefficients ( $K$ ) was found especially in case of PTFE (Figure 15). Water properties are already considered by including temperature-dependent gas solubility. Henry's constant (i.e., solubility) is impacted by pH or the presence of ions, which in turn could additionally change ozone mass transfer. This is not discussed further in the thesis. The correlation approach and the developed numerical method that includes gas-side pressure drop may be sufficient to estimate the amount of membrane material required to deliver the required ozone dose, considering a generous safety factor.

With the dimensioning tool, a realistic assessment of treatment in field scale can be taken. It must be emphasized that large amounts of membrane material would be required to transfer substantial amounts of ozone to a contaminated cross section. One problem is the previously mentioned (2.1.4) difficulty in using the ozone gas efficiently. If ozone gas is delivered to membrane tubes with open ends and subsequent destruction of residual ozone, some portion is continuously wasted. This aspect is considered by our modeling tool by calculating partial gas pressure drops in the gas phase. The reader is referred to the hypothetical case study that is simulated in 5.4.3.2, where over 200 m of membrane tube are required to achieve an average dissolved ozone concentration of  $5 \text{ mg L}^{-1}$  in a  $5 \times 1 \text{ m}$  contaminated cross-section at a realistic groundwater flow velocity of  $10 \text{ cm d}^{-1}$  and by using over 90 % of the generated ozone gas. In one of the previous field scale studies,  $\text{H}_2$  was delivered via membranes placed in wells for microbial denitrification and problems with distributing sufficient gas were mentioned (Chaplin et al., 2009). Chaplin et al. (2009) also concluded, based on numerical modeling, that more than one of the used modules would be needed in one flow path (i.e., two wells in a row) to actually meet the electron donor requirement, indicating difficulties in achieving the required targets of gas dissolution. One suggested solution would be the design of a PRB that is substantially

more permeable than the surrounding soil to force the water flow through. The PRB would require excavation work and would most likely be more labor-intensive than drilling borewells for module installation. A follow-up lab-scale investigation should look into removal of an indicator contaminant using different geometries such as borewells or PRBs of different widths to shed light on these design issues for practical applications.

The dissolution of stable gases (unlike ozone) has the key advantage that gas bottles can be stored on-site and no external energy source is required for operation. The membranes can be pressurized in dead-end operation (end of the tubes is sealed). In case of ozone, on-site production is required and storage options are limited. Additionally, closed end operation is complicated because typically ozone gas is brought to its final use immediately after generation. Therefore, open-end configurations were only considered in this dissertation, where residual ozone gas leaves the membrane tube after being pumped through. The open-end configuration is easy to set up, however, in closed operation, much higher partial ozone gas pressures could be achieved by concentrating ozone in a storage solution and it may eventually be easier to exploit most of the produced ozone. There is a report on using an ozone storage tank with a compressor before guiding the gas to the membrane module (Kaprra et al., 2020). This could also be a solution for dead-end operation in an ISCO case.

Overall, the author must state that the experimental set-ups chosen in this work could not demonstrate substantial advantages using gas-liquid membrane contactors for ISCO ozone treatment over other treatment methods and operational challenges were identified. Furthermore, some of the previously mentioned (section 2.1.4) expected advantages over gas sparging such as reduced release of VOC could not be tested, as this would require a completely different experimental set-up. Fundamental knowledge on operating ozone-diffusing membranes could be gained with regard to contaminant properties and ozone consumption by soil. The author recommends a set-up closer to field scale geometries for further testing.

## **8.2 Coupling chemical and biological transformation of monocyclic aromatic hydrocarbon—Tackling the unknowns**

Ozone treatment is often favored in advanced wastewater treatment for the dual role of dissolved  $O_3$  as direct reactant and generator of hydroxyl radicals via both, interactions with water and organic matter. Both reactive species ( $O_3$  and  $\cdot OH$ ) are also present in treatment of groundwater polluted with monocyclic aromatic hydrocarbons. As elaborated in detail in chapter 6, H-abstraction reactions in processes involving  $\cdot OH$  can quickly result in formation of hydroxylated TPs, which are in turn highly reactive with ozone. In *research objective 3*, the potential synergies of the mentioned reactive oxygen



species in ozone-based AOPs (here  $O_3/H_2O_2$ ) on chemical and biological transformation of monocyclic aromatic hydrocarbon were investigated by conducting chemical oxidation and aerobic biodegradation experiments, coupled with different analytical tools.

With **Hypothesis 3.1**, the assumption was tested that in comparable conditions (i.e., similar  $\cdot OH$  exposure), less stable hydroxylated TPs would be formed in the  $O_3/H_2O_2$  AOP compared to the control process UV/ $H_2O_2$  (*Oxidation of monocyclic aromatic hydrocarbon using  $O_3/H_2O_2$  treatment leads to less formation of hydroxylated aromatic transformation products compared to UV/ $H_2O_2$  treatment if compounds are exposed similarly to hydroxyl radicals*). First, probe compounds were tested in both processes to ensure reliable measurement of  $\cdot OH$  exposure (section 6.4.2). After comparability of the two processes was confirmed by verifying that  $\cdot OH$  is the main driver of the first step of the oxidation based on second order reaction kinetics, hydroxylated TP formation was analyzed for benzene, toluene, and ethylbenzene (BTE). In conclusion, substantial formation of single-hydroxylated TPs phenol, o-cresol, and o-ethylphenol could be confirmed for UV/ $H_2O_2$ , whereas these compounds stayed below the LOQ in the ozone-based process. Thus, **hypothesis 3.1 can be accepted**.

In the second **hypothesis 3.2**, it was tested whether ozone-based treatment improves biodegradability of remaining DOC compared to UV/ $H_2O_2$  at similar  $\cdot OH$  exposure of the non-volatile model compound BA: *If benzoic acid as monocyclic aromatic model compound is similarly removed by  $O_3/H_2O_2$  and UV/ $H_2O_2$  treatment, remaining DOC is mineralized better after the ozone-based treatment in subsequent aerobic biodegradation tests*. This was assessed by shake batch biodegradation experiments, where several chemically oxidized and not oxidized (i.e., BA without further treatment) samples were mixed with inoculated sand and samples were taken over seven days. Analytical tools included measurement of DOC as direct indicator of mineralization, and also high-resolution MS of samples before and after biodegradation to gain insights in the nature of persistent and biodegradable TPs. The analysis revealed that both oxidative processes (UV/ $H_2O_2$  and  $O_3/H_2O_2$ ) generated a similar fraction of less biodegradable DOC ( $>4 \text{ mg C L}^{-1}$ ) that remained constant between days 3-7. Contrarily, the samples that were not oxidized showed almost complete removal of DOC from BA at the same time. Therefore, **hypothesis 3.2 is rejected**.

While testing **hypothesis 3.1** led to the expected outcome based on the reaction chemistry of both tested AOPs, the outcome of **hypothesis 3.2** contradicts previous studies, which were mainly conducted in secondary WWTP effluent, and requires further discussion and investigation. WWTP effluent DOC is a highly site-dependent complex mixture of natural organic matter (e.g., humic substances), residuals of the previous treatment process such as cell fragments that are considered dissolved ( $<0.45 \mu\text{m}$ ), and

other substances released through anthropogenic activities (Michael-Kordatou et al., 2015). Past experience shows that ozonation of such DOC (surface water or wastewater) generally leads to an enrichment of shorter and more oxygen-rich compounds, for example aldehydes and carboxylic acids, that are well biodegradable (Hübner et al., 2012; Lim et al., 2022; Phan et al., 2021). However, especially in case of micropollutants with complex structures that are often purely synthetic, there are exceptions of this assumption (Hübner et al., 2015a).

The aromatic model pollutant BA chosen in this work was expected to be similarly broken down by ozonation as natural organic matter and the remaining DOC, thus, expected to be more biodegradable. The employed high-resolution MS analysis confirmed that an incomplete elimination of the parent compound BA with concentration reductions of ca. 70-90% led to a high abundance of hydroxylated but still fully aromatic TPs in case of UV/H<sub>2</sub>O<sub>2</sub>. Much less of these compounds were seen in O<sub>3</sub>/H<sub>2</sub>O<sub>2</sub> treatment. DOC removal, however, was similarly low in both processes. Fluorescence measurements, both as a straightforward analysis of the sample (excitation emission matrix, EEM) and also coupled to high-resolution MS, proved to be a very useful additional parameter, as it similarly described the presence of many aromatic TPs: high fluorescence was detected in the samples after UV/H<sub>2</sub>O<sub>2</sub> treatment, and substantially lower fluorescence was detected after O<sub>3</sub>/H<sub>2</sub>O<sub>2</sub> treatment in the respective regions. The fluorescence could be largely attributed to the identified aromatic TPs, where a variety of TPs likely containing new functional groups such as sulfonate was detected (e.g., TP234a, TP234b, and TP190), pointing towards radical interactions with the natural water matrix. As fluorescence and signal intensities of aromatic TPs were much lower in O<sub>3</sub>/H<sub>2</sub>O<sub>2</sub>, the nature of this fraction could not be fully revealed, despite the similar magnitude of DOC as for UV/H<sub>2</sub>O<sub>2</sub> samples. This is on the one hand an analytical issue, as shorter and smaller organic fractions are harder to reliably analyze or even quantify in a complex matrix. On the other hand, the conducted shake batch tests do not provide a complete picture on how adaptation of microbial communities would further improve biodegradability. A soil passage that is continuously fed with the ozonated substrate may in the end contain the microbial communities capable of better utilizing the organic compounds. Follow-up investigations should therefore consider comparing DOC removal in inoculated sand columns that were equilibrated with the oxidized/not oxidized water matrix for several weeks, as done for surface water and wastewater AOP/biodegradation studies (Wünsch et al., 2019). The approach of sole bioremediation by inoculation or stimulating redox conditions could easily be incorporated in such study designs. However, it must be noted that one reason of limited data on VOC biodegradation and chemical oxidation in comparative assessments is the volatility that makes experimental

design more complicated and must be considered for AOP but also redox condition alteration operations.

In the author's opinion, many unknowns remain in order to fully understand positive or adverse effects of chemical oxidation on biodegradability of different compound groups, where novel analytical tools or a thoughtful use of established technologies can shed further light on. Especially a focus on parameters that quantify oxygen demand (BOD<sub>5</sub>, COD) has very limited meaning, as formation of persistent compounds is completely left out (Pariante et al., 2008; Phan et al., 2021). A parameter that would be very easy and cost-efficient to measure in ISCO field studies is fluorescence (i.e., EEMs), where certain peak regions could indicate incomplete transformation of monocyclic aromatic hydrocarbon. Initial absorbance and fluorescence increases are to be expected for BTEX and their TPs in chemical oxidation operations, as shown in this work (sections 6.4.2.2 and 6.4.3.1) and previous studies (Peng et al., 2018; Shang and Yu, 2002). Fluorescence intensity reductions in certain EEM peak regions belonging to biodegradable chemical substances or the steady existence of a peak region representing more persistent compounds could enable analysis of field sites with very limited effort. Additionally, advanced tools such as high-resolution MS and also size-exclusion chromatography – organic carbon detection (LC-OCD) could help identifying recalcitrant fractions (Huber et al., 2011).

### 8.3 Catalytic oxidation for water decontamination

#### 8.3.1 PMS-activation—A feasible treatment alternative?

In the last part of this dissertation (chapter 7), a new catalyst immobilization approach was introduced that aimed to allow PMS activation and oxidation of contaminants in a fixed bed without additional catalyst retention measures. The objective was to explore potential for unselective contaminant oxidation (*research objective 4*). *Hypothesis 4.1* tests whether the catalytic process could generate sulfate radicals that would be available for unselective oxidation of a variety of organic contaminants in natural water: *A newly synthesized immobilized MnO<sub>2</sub> catalyst activates pre-dosed PMS to form sulfate radicals for unselective oxidation*. Besides extensive material characterization and longevity performance assessments, a focus, therefore, was to observe the decomposition/oxidation of various compounds to prove with high certainty that there is unselective oxidation. In this work, removal of 22 spiked TOxCs (ca. 1 µg L<sup>-1</sup>) was chosen because of the large variety of functional groups (e.g., aromatic, olefinic, amine) and largely known reactivity with radicals, and the relevance in the context of advanced wastewater treatment. The high removal of various compounds makes it easy to compare with other state-of-the-art AOP technologies such as ozonation for water treatment applications and is especially

interesting for cases where the advantages of catalytic AOPs could play out (e.g., no external energy input required). Overall, the process with the chosen parameters, i.e., catalyst amount, residence time, and PMS dosing, was capable of removing more than 50 % of compounds by more than 80 % in wastewater and groundwater (tap water). Several other more recalcitrant compounds to ozone or sulfate radicals, such as primidone or iopromide, were partially oxidized (<80 %), indicating that higher PMS doses and longer catalyst contact times could also achieve their complete removal.

Compared to studies where only a handful of compounds is tested in catalytic processes, the large variety of TOxCs and their known properties could be exploited to use second-order reactivities for an alternative method to identify radical species (section 7.4.4). Exposure to sulfate and hydroxyl radicals was determined using multivariate linear regression and the agreement of compound removal based on the regression was compared with experimentally observed removal. Overall, high correlation coefficients  $R^2 = 0.7$  and  $R^2 = 0.74$  could be determined for exclusive sulfate radical reactions of compounds in wastewater and groundwater, respectively. This agreed much better than any major involvement of  $\cdot\text{OH}$  ( $R^2 < 0.4$ , Figure 29). Involvement of other reactive oxygen species such as singlet oxygen can largely be excluded due to the overall much lower reactivity with most organic compounds, for example sulfamethoxazole or primidone (Lee et al., 2020; Yan et al., 2023). Based on these findings, ***hypothesis 4.1 can be accepted.***

The potential as ISCO PRB but also as part of an advanced water treatment train can be considered high based on the promising oxidation results of various compounds and functional groups. Concerning ISCO treatment, removal of for example BTEX compounds should generally be feasible based on the second-order reactivity of these compounds with sulfate radicals (Table 2) and previous research works with BTEX and persulfate (Kambhu et al., 2012; Liang et al., 2008). Persulfate (most commonly  $\text{S}_2\text{O}_8^{2-}$ ) has already become an acknowledged groundwater remediation technology (Huling and Pivetz, 2006; Siegrist et al., 2011). In case of the catalytic activation material approach, however, success of the technology depends on the technical options and hydrogeologic conditions to allow the installation of a PRB, where contaminated water is forced through, plus the ability to inject PMS solutions which will distribute well along the PRB. This is a similar challenge as for gas-liquid membrane contactors for dissolved ozone delivery. A lab-scale set-up simulating PMS injection and a PRB could help in that regard, where tracer tests can also support the decision-making for PMS injection techniques.

### 8.3.2 Future research needs in the field of catalytic oxidation

Catalytic oxidation for water treatment is a very dynamic research field with a large amount of publications every year. This includes, besides activation of PMS, also  $O_3$ ,  $H_2O_2$ , and PDS. Although new materials are being introduced almost on a daily basis and some very promising results have been reported, it is important to take a step back and identify critical roadblocks that have not been solved so far.

#### *1. Accurate description of reactive oxygen species involved.*

There is a growing body of literature dealing with and claiming that the reactive oxygen species singlet oxygen ( $^1O_2$ ) or superoxide radical ( $O_2^{\cdot-}$ ) can play important roles in various treatment processes (Gao et al., 2019; Li et al., 2019b; Nawaz et al., 2015; Zhu et al., 2019). The first problem is the reliable identification of the species involved in oxidative treatment. Scavenging experiments are known to have pitfalls, as they can interfere with the reaction chemistry of oxidant and water. For example, t-BuOH is a good  $\cdot OH$  scavenger, however, also slows down ozone decay in water (Guo et al., 2021b; Wang and Yu, 2022) and scavengers for other species such as l-histidine for  $^1O_2$  suffer from other previously discussed drawbacks (section 2.2.1). The second problem is that, given these species are actually responsible for removal of contaminants in tested conditions, their broad applicability is highly questionable, as convincingly pointed out by Lee et al. (2020) (limited ability of  $^1O_2$  to mineralize DOC, low reactivity with compounds tested). In this dissertation, these problems were addressed by a simple, however, strikingly novel approach: removing contaminants at realistic concentration in a realistic water matrix, where a lot of reference data from other more established processes (e.g.,  $O_3$  or UV/ $H_2O_2$ ) is available. This allowed us to correlate this compound removal with known second-order reactivity in a continuous flow through experiment. The key advantage is, besides comparability to standard processes, that some common experimental difficulties can be avoided. For example, testing a process exclusively with activated aromatic compounds such as bisphenol A or nitrophenol to describe reactive species may not provide a full picture on potential use of the process with other compounds. Overall, more standardization of experimental designs is crucial. For example, the use of pCBA as  $\cdot OH$  radical probe compound has become standard in AOP research (Rosenfeldt et al., 2006; von Sonntag and von Gunten, 2012). Such standard practices can hardly be found in catalytic AOP research and this matter urgently needs to be addressed to allow a comparison of existing materials with new materials that are continuously introduced with potential that is hard to assess. One step forward may be the implementation of plausibility tests, e.g., comparing scavenging experiments with probe compound removal experiments and EPR data.

## 2. *Engineering of a process that has upscaling potential*

As pointed out in chapter 7 and in section 2.2.2, upscaling potentials should already be included while conceptualizing fundamental research, and this is mostly related to immobilization or catalyst retention approaches. A good example is the work of Xu et al. (2021b), where catalyst development and fundamental testing was accompanied by the complete design of a treatment train where contaminated water gets purified in continuous flow. The containing information, i.e., residence time, oxidant dosing, expected treatment efficiency, and required post- or pre-treatment, is crucial for any further steps. The focus on testing novel catalysts in batch experiments with suspensions is a logical first step, however, the author proposes a focus shift towards critical application-oriented testing and comparison of the existing catalyst materials. As demonstrated in this dissertation, a material with known catalytic reactivity could be synthesized and immobilized, and insights on applicability of the process (longevity, selectivity, water matrix effects) could be gained. This does not exclude further optimization of the material and the process, however, was not the focus here. Furthermore, many scientific questions that are heavily investigated and crucial for further assessing established processes, such as biodegradability of oxidized organic matter, TP formation, unwanted side-products like bromate or NDMA (Lutze et al., 2015; Szczuka et al., 2020), cannot really be investigated in the standard design typically chosen (batch experiment with removal of a model contaminant in artificial buffer solution).

## 3. *“Honest” economic comparisons can only be achieved by calculating radical generation efficiencies*

Batch experiments are suitable to produce fundamental, general information, e.g., that oxidation takes place and what oxidant doses are needed to achieve certain contaminant removal. However, some of the experimental designs chosen do not really allow economic comparisons, and valid comparisons are – in the author’s opinion – largely dependent on formation efficiencies of the desired reactive oxygen species. For instance, catalytic ozonation studies frequently test removal of compounds in direct ozone injection bubble reactors (Gonçalves et al., 2012; Nawaz et al., 2015; Ponnusamy et al., 2021) and relate removal to the treatment time. If the catalyst performs better in the time of ozone bubble injection, this does not necessarily mean that the underlying reaction mechanism leads to more produced radicals per mol ozone, but could also just be an artefact of the experimental design, where breakdown of ozone is accelerated and therefore more ozone stays in the water instead of leaving the reactor via the off-gas. There are other examples, where such mass balances have been calculated and in fact better removal efficiencies were determined for largely ozone-resistant compounds such as ibuprofen or pCBA (Guo et al., 2021a; He et al., 2021). Similarly, for PMS/PDS or

other Fenton-like processes with  $\text{H}_2\text{O}_2$ , a statement on the actual radical formation efficiency is rare. Why is this so important for economic comparisons? For more established processes such as UV/ $\text{H}_2\text{O}_2$  or UV/PDS, the mechanism of radical generation is known and the external UV source, for instance, adds energy besides the chemical energy in the used substances. If a new catalytic process is introduced and claimed to be advantageous because there is no need of additional activation energy, the argument would be flawed if the radical yield would only be 50% or less. The stoichiometric information of how many moles  $\text{H}_2\text{O}_2$ /PMS/PDS are consumed per mole degraded contaminant is, however, rarely provided or discussed (Li et al., 2021; Wang et al., 2015; Wolters et al., 2022; Yu et al., 2014).

In conclusion, there exist much more uncertainties than certainties regarding the future application of nanomaterials and other catalysts for catalytic oxidation water treatment processes on larger scale. The respective part of this dissertation (chapter 7) aimed to move the experimental design towards a more application-oriented engineering and this in the author's opinion heavily needed, because, similarly as for ozonation or other AOPs, more relevant scientific and practical questions will most likely pose challenges for successful implementation.

## 9 OVERALL CONCLUSION AND OUTLOOK

This thesis addressed fundamental research questions around ISCO technologies, but also aimed to advance knowledge on technology solutions and their application. In the first part, gas-liquid membrane contactors for ozone delivery were introduced (chapter 4), their effectivity investigated in ISCO operations (chapter 5), and TP formation in ozone-based AOPs analyzed (chapter 6). In the second part, a catalytic PMS activation process was introduced (chapter 7). In this section, the author would like to provide some final thoughts on the overall outcomes and the future steps to be taken.

It could be shown that gas-liquid membrane technology is interesting for in-situ groundwater remediation due to the high level of processes control, as ozone is directly dissolved at a defined gas-liquid interface. Modeling tools, therefore, can be a good basis for dimensioning such a system. However, they may only be effective in a PRB, requiring moving water to some extent, as the ozone travel distance in groundwater is limited. Adverse effects observed with monocyclic aromatics make this technology less attractive for BTEX contamination cases, but it showed potential for aliphatic compounds (here 1,4-dioxane). Future studies dealing with ozone membrane contactors for groundwater treatment should therefore carefully review, if the roadblocks identified in this work could also pose a problem in their application and if economic feasibility with materials and excavation works is given. The aforementioned optimization of injection geometry (borewells vs. curtain, section 8.1.2) seems the logical next step in lab scale studies. ISCO studies face the fundamental problem that technologies cannot be well compared because each site is highly individual and therefore the performance largely site-dependent. If the next steps are promising, a scale-up is a necessity to even be able for a full comparison to other ISCO technologies. Aside from that, this technology is also studied for other drinking water and wastewater applications, and there is a much greater potential for module geometry and mass transfer optimization using known mass transfer relationships and new algorithm-based methods.

Analyzing TP formation and persistence constitutes an important part of AOP research of high global interest. It is especially relevant because of the ongoing introduction of new substances on the market and unknown effects on the environment. In this thesis, the issue of choosing good analytical frameworks could be highlighted. Residual organic matter is often overlooked not only in ISCO processes, but also various other cases. Even though groundwater remediation may not be the research field receiving



the highest attention at the moment, critical aspects on TP formation should still be researched. For some parameters, e.g., fluorescence measurements, gathering of data at field sites could be a feasible task and compared to lab-scale oxidation experiments. Coupling research methodologies and expertise in environmental chemistry with groundwater remediation technology development could enable valuable synergies in this regard.

Lastly, the potential of catalytic processes for PMS activation could be demonstrated here, as removal of groundwater contaminants is efficiently achieved with sulfate radicals. But the efforts in this thesis can only be seen as a tiny part of a larger picture. A full understanding on how catalytic activation works and even a comprehensive framework on how to investigate it is still missing. The results are promising enough to test the immobilized MnO<sub>2</sub> in a field-scale application (ISCO or other water treatment purposes) after a careful reconsideration of potential side-effects and products, e.g., manganese leaching or by-product formation. This has to be taken seriously while introducing novel processes and materials. The list of critical issues in section 8.3.2 can and should be used as guidance and basis for a scientific discussion on future research needs in the field of catalytic oxidation in water treatment.

## 10 APPENDIX

### 10.1 List of publications

#### Research articles (peer-reviewed)

1. Bein, Emil; Zucker, Ines; Drewes, Jörg E.; Hübner, Uwe (2021): *Ozone membrane contactors for water and wastewater treatment: A critical review on materials selection, mass transfer and process design*. In: *Chemical Engineering Journal* 413 (18), 127393. DOI: 10.1016/j.cej.2020.127393.
2. Bein, Emil; Pasquazzo, Giulia; Dawas, Anwar; Yecheskel, Yinon; Zucker, Ines; Drewes, Jörg E.; Hübner, Uwe (2024): *Groundwater remediation by in-situ membrane ozonation: Removal of aliphatic 1,4-dioxane and monocyclic aromatic hydrocarbons*. In: *Journal of Environmental Chemical Engineering* 93 (10), 111945. DOI: 10.1016/j.jece.2024.111945.
3. Bein, Emil; Seiwert, Bettina; Reemtsma, Thorsten; Drewes, Jörg E.; Hübner, Uwe (2023): *Advanced oxidation processes for removal of monocyclic aromatic hydrocarbon from water: Effects of O<sub>3</sub>/H<sub>2</sub>O<sub>2</sub> and UV/H<sub>2</sub>O<sub>2</sub> treatment on product formation and biological post-treatment*. In: *Journal of Hazardous Materials* 188 (2-3), 131066. DOI: 10.1016/j.jhazmat.2023.131066.
4. Bein, Emil; Yecheskel, Yinon; Zucker, Ines; Drewes, Jörg E.; Hübner, Uwe (2023): *A novel catalytic filtration process using MnO<sub>2</sub>@sand and peroxymonosulfate for unselective removal of organic contaminants from water*. In: *Chemical Engineering Journal* 476, 146636. DOI: 10.1016/j.cej.2023.146636.

#### Additional research articles (peer-reviewed)

1. Bein, Emil; Sierra Olea, Millaray; Petersen, Sophie; Drewes, Jörg E.; Hübner, Uwe (2023): *Ozonation of Gabapentin in Water—Investigating Reaction Kinetics and Transformation Mechanisms of a Primary Amine Using Isotopically Labeled Ozone*. In: *Environ. Sci. Technol.* DOI: 10.1021/acs.est.2c06709.
2. Sierra-Olea, Millaray; Kölle, Simon; Bein, Emil; Reemtsma, Thorsten; Lechtenfeld, Oliver J.; Hübner, Uwe (2023): *Isotopically labeled ozone: A new approach to elucidate the formation of ozonation products*. In: *Water Research* 233, 119740. DOI: 10.1016/j.watres.2023.119740.
3. Dawas, Anwar; Yecheskel, Yinon; Bein, Emil; Hübner, Uwe; Zucker, Ines (2023): *Passive Ozone Injection through Gas-Permeable Membranes for Advanced In Situ Groundwater Remediation*. In: *ACS ES&T Engineering*. DOI: 10.1021/acsestengg.2c00395.

**Conference talks**

1. *Bein, Emil; Drewes, Jörg E.; Hübner, Uwe (June 2022): Advanced oxidation of benzene, toluene, and ethylbenzene in water: Synergistic effects of O<sub>3</sub>/H<sub>2</sub>O<sub>2</sub> compared to UV/H<sub>2</sub>O<sub>2</sub> treatment, 12<sup>th</sup> Micropol and Ecohazard Conference, Santiago de Compostela.*
2. *Bein, Emil; Yechezkel, Yinon; Zucker, Ines; Drewes, Jörg E.; Hübner, Uwe (May 2023): Test von immobilisiertem MnO<sub>2</sub> in einer katalytischen Filtrationssäule zur PMS-Aktivierung für die weitergehende Abwasserbehandlung. Jahrestagung der Wasserchemischen Gesellschaft vom 15. bis 17. Mai 2023, Augsburg.*

**Conference posters**

*Bein, Emil; Drewes, Jörg E.; Hübner, Uwe (May 2021): Experimentelle Bestimmung und Modellierung von passivem, membranbasiertem Sauerstoff- und Ozoneintrag in eine Grundwasserströmung zur in-situ Sanierung, Jahrestagung der Wasserchemischen Gesellschaft vom 10. bis 12. Mai 2021.*

## 10.2 List of supervised student theses

### Master theses

1. *Petersen, Sophie: Ozonation of gabapentin: Reaction kinetics and the formation of transformation products in an aqueous environment.*
2. *Pasquazzo, Giulia: Investigation of the removal of benzoic acid and 1,4-dioxane in a simulated groundwater flow environment via ozonation using a PDMS gas-liquid membrane contactor.*
3. *Kim, Erin: Determination of ozone exposure and mass transfer for gas-liquid membrane contactors through the removal of trace organic compounds.*

### Study projects

1. *Andalib, Afrina: Analyzing mass transfer efficiency and hydroxyl radical exposure for porous and non-porous membrane contactors applied for in-situ ozonation and peroxone treatment of groundwater flow.*
2. *Kim, Erin: Fundamental mass transfer analysis of oxygen and ozone delivery to groundwater.*
3. *Contreras Vomend, Mario: Assessment of the catalytic activity of manganese dioxide and iron(III) oxide-hydroxide via the formation of hydroxyl radicals for their use in heterogeneous catalytic ozonation.*

### Bachelor theses

1. *Duraku, Erzen: Grundwassersanierung durch membrangestützten In-situ-Gaseintrag — Umsetzung und Wirksamkeit.*
2. *Witthöft, Carl: Investigating biological degradation of transformation products after oxidative treatment of benzoic acid by ozone/hydrogen peroxide and UV/peroxide.*

## 10.3 Supplementary information for Chapter 5

### 10.3.1 Chemicals and reagents

Table 8: List of compounds used throughout this study.

Substance	Purity / concentration	Manufacturer / brand
Ibuprofen	>98%	Sigma-Aldrich
Atenolol	>98%	Sigma-Aldrich
Benzotriazole	99%	Alfa Aesar
Primidone	98%	Sigma-Aldrich
Carbamazepine	98%	Sigma-Aldrich
Gabapentin	99.8%	Sigma-Aldrich
C <sub>4</sub> H <sub>10</sub> O (t-BuOH)	99%	Carl Roth
Na <sub>2</sub> S <sub>2</sub> O <sub>3</sub> ·5H <sub>2</sub> O	99.5%	VWR Chemicals
H <sub>3</sub> PO <sub>4</sub>	85%	Supelco
NaOH	32%	Merck
NaH <sub>2</sub> PO <sub>4</sub> ·2H <sub>2</sub> O	>99%	Merck
Na <sub>2</sub> HPO <sub>4</sub>	>99%	Merck
Indigo carmine	80%	Carl Roth
1,4-Dioxane	99.8% (anhydrous)	Thermo scientific
Benzoic acid	>99.5%	Supelco
Toluene	99.8%	Sigma-Aldrich

Table 9: Standard soil (A2.1) characteristics.

Parameter	Soil A2.1	Source
Organic carbon (% C)	0.55 ± 0.1	LUFA Speyer (2023)
Nitrogen (% N)	0.06 ± 0.01	LUFA Speyer (2023)
pH value (0.01 M CaCl <sub>2</sub> )	4.6 ± 0.1	LUFA Speyer (2023)
Cation exchange capacity (meq/100g)	2.9 ± 0.2	LUFA Speyer (2023)
Aluminum (mg/kg)	3383 ± 148	Aqua regia analysis of soil sample
Iron (mg/kg)	4477 ± 29	Aqua regia analysis of soil sample
Copper (mg/kg)	16.4 ± 0.2	Aqua regia analysis of soil sample
Manganese (mg/kg)	217 ± 2.5	Aqua regia analysis of soil sample

### 10.3.2 Analytical methods

Table 10: Details of HSGC-FID method for 1,4-dioxane quantification.

Headspace settings	
Equilibration time	20 min
Oven temperature	95 °C
Transfer line temperature	220 °C
Loop temperature	155 °C
Gas chromatograph settings	
Gas flow	3 mL/min
Septum purge flow	3 mL/min
Total flow	9 mL/min
Makeup flow	25 mL/min
Air flow	400 mL/min
Split ratio	1:1
Inlet temperature	250 °C
FID gas flow	30 mL/min H <sub>2</sub>
FID temperature	250 °C

### 10.3.3 Text S1: Batch experiments to compare DIOX and BA removal with ozone membrane contacting experiments

As shown in the manuscript, the reaction of 40.9  $\mu\text{M}$  BA with ozone proceeds within seconds and highly over-stoichiometric, and therefore any other effects that become relevant over longer time intervals can be ruled out for the ozone doses applied. As BA was consumed by maximum 80% in the shown batch experiments (Figure 4a), ozone must be completely depleted within seconds to a few minutes. To compare removal of DIOX and BA on the basis of consumed ozone, the measured dissolved ozone after 1 EBVT was taken to calculate the consumed ozone in case of DIOX and removal was plotted as function of consumed ozone (Figure 14). This confirms that even when only consumed ozone is considered, BA removal is more efficient in batch experiments vs. membrane ozonation experiments. For completeness, residual dissolved ozone concentration measured in DIOX experiments is shown in Figure 31b.

The reaction of DIOX with  $\cdot\text{OH}$  is governed by the conversion of ozone to  $\cdot\text{OH}$  in natural slightly alkaline water without additional promotion and thus proceeds slowly. Therefore, effects such as DIOX and/or ozone loss to the atmosphere need to be addressed. We additionally tested batch experiments in 100 mL amber bottles of the same kind and first ozonated samples with a sample volume of 50 mL, therefore 50 mL of volume remains free in the closed vials (0.75 EBVT). This was also the default volume for BA. Additionally, we scaled the sample volume to 100 mL for DIOX experiments to see if there is a change and indeed, removal efficiency is increased by 10-20% in 100 mL batches, where the gas phase is reduced to an absolute minimum (Figure 32). Therefore, experiments with DIOX were performed with 100 mL solutions for 1 EBVT for the comparison between BA and DIOX.

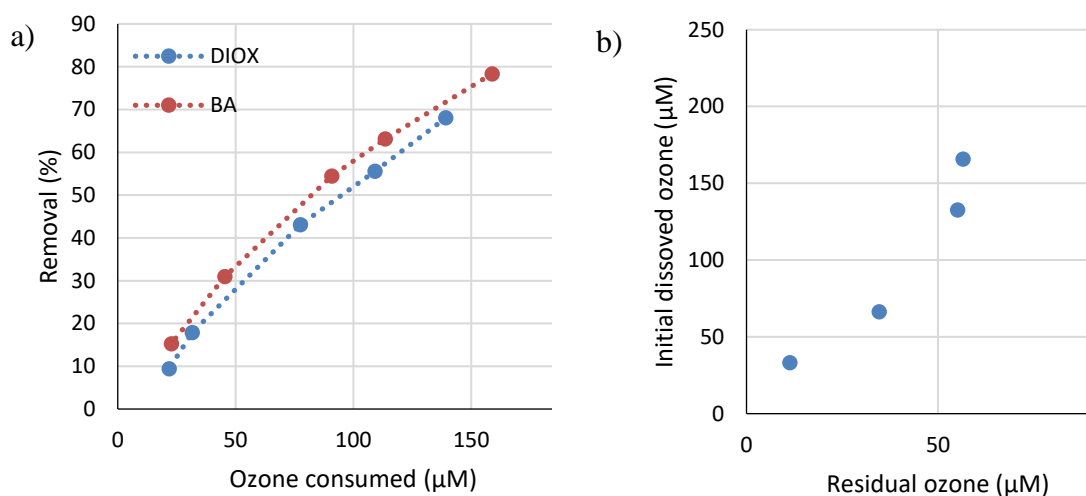


Figure 31: a) Removal of DIOX and BA in batch experiments as function of consumed ozone (assuming 100% consumption in BA batches). b) Residual dissolved ozone concentration after the experiment vs. the initial dissolved ozone concentrations for DIOX experiments.

Several additional control experiments were performed to check for volatile losses and the effect of MNO-92 on the oxidation performance with ozone (Table 11). If a solution with DIOX without any ozone is stirred, DIOX loss in the time 0.75 EBVT is about 2.3% and therefore minimal. Based on this, we also assume that volatilization in all of the experiments play a minimal role in an experimental time between 1 and 4 hours. Furthermore, we performed batch ozonation tests, where we added 2 g of MNO-92 to see if there is any catalytic inhibition or enhancement of the oxidation, and we can see a slightly increased but still minor removal without ozone (3.1 %), and clearly inhibited removal in presence of ozone, if compared to the dose-removal relationship in Figure 32.

Table 11: Additional data on removal of DIOX in control experiments.

Sample	O <sub>3</sub> dose (μM)	Removal DIOX
DIOX control after 0.75 EBVT (50 mL)	0	2.3%
DIOX control with 2 g MNO-92 after 0.75 EBVT (50 mL)	0	3.1%
DIOX ozonation with 2 g MNO-92 after 0.75 EBVT (50 mL)	109	26%
DIOX ozonation with 2 g MNO-92 after 0.75 EBVT (50 mL)	191	42%

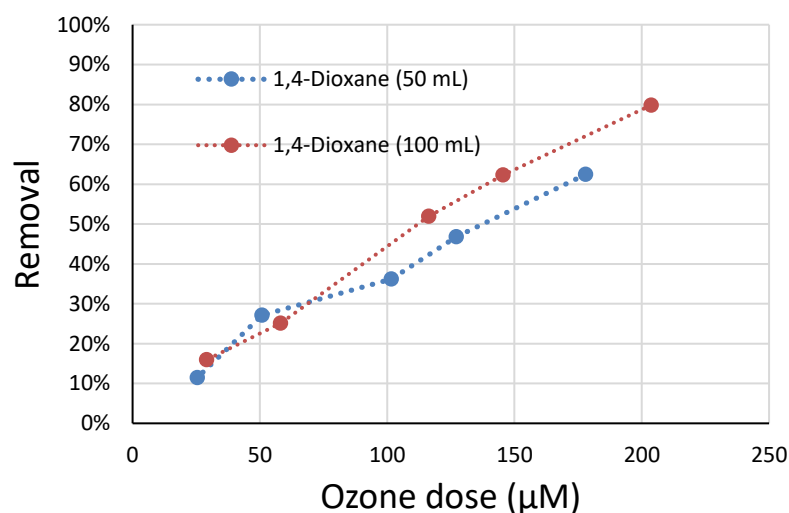


Figure 32: Removal of DIOX as function of ozone dose in batch experiments with two different solution volumes.

### 10.3.4 Text S2: Detailed procedure to obtain experimental mass transfer coefficients

The procedure to calculate the mass transfer coefficient is partly described in Karakurt-Fischer et al. (2020) for oxygen and originally taken and modified from Orgill et al. (2019). The mass transfer rate  $N$  ( $\text{mg s}^{-1}$ ) in a gas-liquid membrane contactor can be calculated in three different ways:

$$N = A K \Delta c \quad (S1)$$

$$N = Q_l (c_{l,out} - c_{l,in}) \quad (S2)$$

$$N = Q_g (c_{g,in} - c_{g,out}) \quad (S3)$$

Eq. S1 describes the mass transfer rate based on the mass transfer coefficient  $K$ , membrane surface area  $A$  and characteristic concentration difference  $\Delta c$ . Eq. S2 is the mass balance on the liquid side, where  $Q_l$  is the liquid flow rate, and  $c_{l,out}$  and  $c_{l,in}$  are the volumetrically averaged in- and outflow dissolved ozone concentrations ( $c_{l,in}$  is always assumed to be 0). Eq. S3 is the mass balance on the gas side where  $Q_g$  is the gas flow rate and  $c_{g,out}$  and  $c_{g,in}$  the ozone gas concentration at the in- and outflow.  $c_{g,in}$  and  $Q_g$  are fixed at certain values ( $c_{g,in} = 100 \pm 1 \text{ g/Nm}^3$ ,  $Q_g = 0.2 \text{ L/min}$ ) and recorded by the ozone system, respectively the ozone gas analyzer.  $\Delta c$  in Eq. S1 depends on the gas-liquid membrane contactor geometry and is therefore different for both geometries investigated in this study. For the cross flow geometry,  $\Delta c_{cr}$  is defined as

$$\Delta c_{cr} = \frac{(c_{sat,in} - c_{sat,out})}{\ln\left(\frac{c_{sat,in} - c_{l,av}}{c_{sat,out} - c_{l,av}}\right)} \quad (S4)$$

as proposed by Côté et al. (1989). In difference to the original equation, the average of in and outflow liquid concentrations  $c_{l,av}$  is taken instead of  $c_{l,out}$ , as proposed for low  $Re$  and flow velocities by Fang et al. (2002).  $c_{sat,in}$  and  $c_{sat,out}$  are saturation concentrations in equilibrium of gas- and liquid phase at the membrane in- and outlet and are equal to the partial gas pressure (bar) of ozone at the respective location divided by the Henry's constant ( $\text{m}^3 \text{ bar mg}^{-1}$ ). To obtain  $K$  (cross flow), the following steps were taken:

1. Calculation of  $[O_3]_0$  according to the procedure outlined in this publication's section 2.3.2 with  $k_d$  as determined by the procedure described in Text S3.
2. Calculation of  $N$  using Eq. S2 and including the known  $Q_l$  and  $c_{l,out}$  ( $= [O_3]_0$ )
3. Insertion of  $N$  into Eq. S3 to calculate  $c_{g,out}$
4. Conversion of  $c_{g,in}$  and  $c_{g,out}$  into  $c_{sat,in}$  and  $c_{sat,out}$ . Therefore,  $c_{g,in}$  and  $c_{g,out}$  are first converted into partial gas pressure using the ideal gas law and ambient temperature that was recorded for each experiment and then divided by the Henry constant of ozone in water ( $0.0001 \text{ mol}/(\text{m}^3 \text{ Pa})$ ) (Sander, 2015)).
5. Finally,  $\Delta c_{cr}$  is calculated and inserted into Eq. S1 together with the known  $A$  and  $N$  from step 2. This equation can be solved for  $K$ .



### 10.3.5 Text S3: Determination of ozone decay $k_d$ from membrane to sampling port

A procedure was developed to estimate the ozone decay ( $k_d$ ,  $s^{-1}$ ) inside the reactor with the specific water matrix used in the mass transfer experiments. This was done by finding the best agreement of ozone exposure, ozone decay, and effluent dissolved ozone concentrations, measured for different flow velocities and membranes. In detail, ozone exposure (Table 13), calculated with different probe compounds, was inserted into Eq. 22 to obtain the initial concentration ( $c_0$ ). This was performed for overall 10,000  $k_d$  values ranging from  $10^{-3}$  to  $10^{-6}$   $s^{-1}$  for exposures based on gabapentin, ibuprofen, and benzotriazole removal. For every entry of this array consisting of 10,000 values ( $c_0$ ), the concentration ( $c_{calc}$ ) at the sampling port was calculated using this initial concentration and the respective  $k_d$ . Since this concentration at the sampling port was also measured, these two values were compared by calculating the coefficient of correlation ( $r$ ), as can be seen in Figure 33b. The highest agreement of calculated and measured sampling port concentrations ( $r = 0.95$ ) was achieved with gabapentin and a  $k_d$  of  $1.355 \cdot 10^{-4}$   $s^{-1}$  (Figure 33a). This was done without experiment two, because including this point led to much worse agreement of all data points ( $r < 0.8$ ) and was considered an outlier. The calculated  $c_0$  using the  $k_d$  with the highest agreement was used as liquid-side ozone concentration inside of the reactor and mass transfer coefficients were calculated with these values.

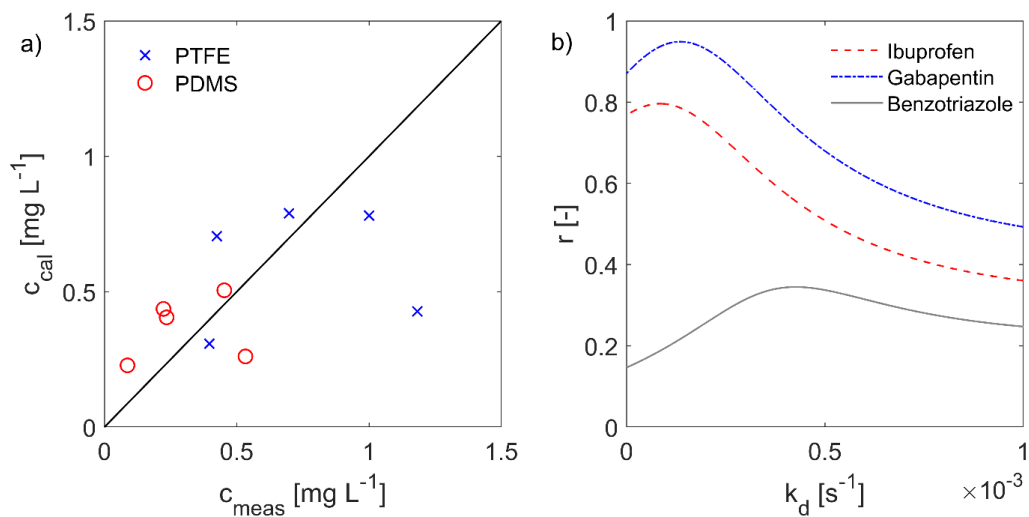
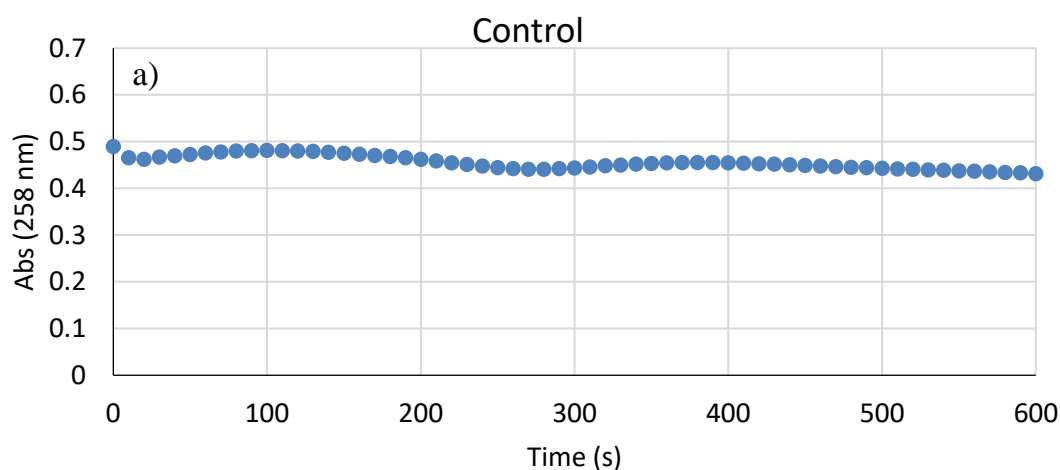


Figure 33: a) Comparison of measured ( $c_{meas}$ ) and calculated ( $c_{cal}$ ) concentrations at the effluent sampling port of the cross flow experimental set-up for different flow rates (1 - 7.2  $L h^{-1}$ ).  $c_{cal}$  was determined using  $k_d$  with the highest Pearson correlation coefficient  $r$  ( $1.36 \cdot 10^{-4}$   $s^{-1}$ ). b)  $r$  of  $c_{cal}$  and  $c_{meas}$  between  $1 \cdot 10^{-9}$   $s^{-1} < k_d < 1 \cdot 10^{-3}$   $s^{-1}$ .

### 10.3.6 Text S4: Ozone decomposition in presence of toluene

Ozone decomposition in presence of toluene was demonstrated in modified batch experiments, where 0.0082 mM toluene and a target concentration of 0.164 mM dissolved ozone are mixed in the same water matrix as used in the other batch experiments. First, toluene was added from a freshly prepared 50 mg L<sup>-1</sup> stock solution and then ozone stock solution of a concentration of 58.5 mg L<sup>-1</sup> was added, resulting in an actual dose of 0.2 mM. The reaction was directly monitored in a quartz glass cuvette of 1 cm path length, placed in a UV1900 Shimadzu double beam spectrophotometer (with UPW reference). The absorbance was measured at 258 nm every 10 seconds for 10 min. Absorbance of toluene without ozone was below 0.1, thus the majority of absorbance is originating from ozone. As can be seen, the addition of toluene leads to a similar ozone consumption as for BA (Figure 34b and c).

Absorbance in the control sample was reduced by less than 20 % after 10 min, with some fluctuations that might be related to minor bubble formation and the fact that the batch is not stirred and therefore mixing is not ideal (Figure 34a). In contrast, a much faster kinetic can be observed if 0.0082 mM toluene is added (Figure 34b and c), where absorbance reduces from initial values of 0.4277 and 0.441 to 0.2378 and 0.1786 after 10 min. This is the case even though toluene ozonation can lead to intermediates that are absorbing strongly in this wavelength region (Bein et al., 2023a). This is an additional proof that the choice of BA as model pollutant was justified, and similar acceleration mechanisms can be expected in case of other monocyclic aromatics such as BTEX.



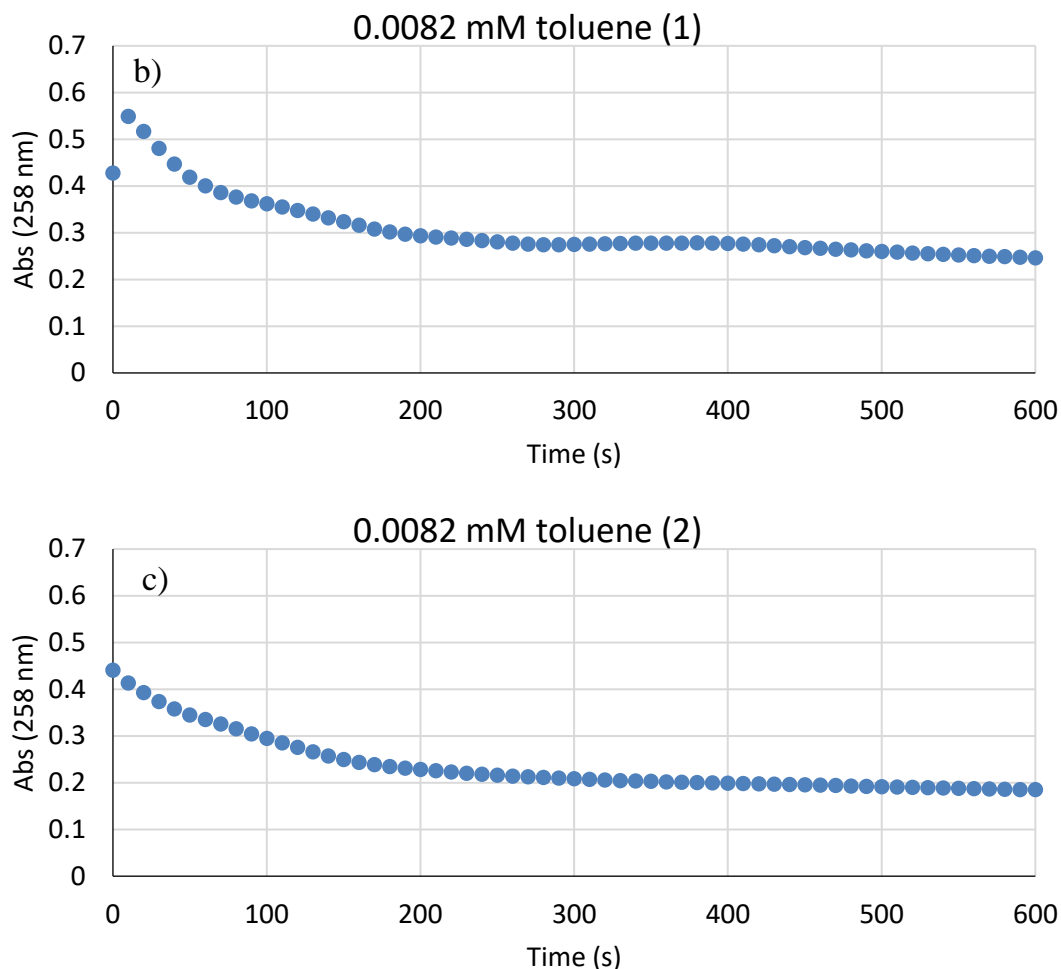


Figure 34: Absorbance change (258 nm) over time as directly measured in the measurement cell for a control without toluene (a) and two repetitions with 0.0082 mM toluene (b, c).

### 10.3.7 Text S5: Dissolved ozone measurements during BA in-situ ozonation experiments

Values measured with the indigo method in BA experiments were close to zero, if directly compared to Indigo data shown in the manuscript's Figure 13c, where ozone reaches concentrations of 20-30  $\mu\text{M}$  for BS (DIOX). A small ozone concentration is observed in this data, which may be caused by minor human error in the preparation of the indigo standards or other interference/reactions in the photometric method that cannot fully explained here.

Table 12: Indigo measurements in the effluent of experiments with BA and different porous media layers.

EBVT	BS ( $\text{O}_3$ in $\mu\text{M}$ )	200 g MNO-92 ( $\text{O}_3$ in $\mu\text{M}$ )	A2.1 ( $\text{O}_3$ in $\mu\text{M}$ )
0.2	2.08	0.52	1.82
0.4	2.08	0.52	2.08
0.6	2.60	1.04	3.65
0.8	2.60	1.04	3.65
1	2.60	1.04	4.17
1.2	2.86	1.04	4.17

1.4	2.86	1.56	3.12
1.6	2.86	1.04	4.17
1.8	2.60	0.78	3.91
2	2.86	0.52	3.65
2.2	2.08	0.26	3.65
2.4	2.34	0.52	3.39
2.6	2.60	0.52	3.39
2.8	1.30	0.52	3.39
3	1.30	0.00	3.12
3.2	1.82	-0.26	2.86

### 10.3.8 Text S6: Ozone exposure data and its handling

As discussed in methods section 4.5.1, removal of probe compounds was used to calculate ozone exposure with Eq. 20 in the manuscript. Primidone and iopromide are practically ozone-resistant probe compounds that were used to control the effectivity of radical scavenging with 50 mM t-BuOH. However, we noticed that iopromide was partially removed in most data sets, while primidone was partially removed in experiments with slow velocities and therefore high ozone exposure (Table 13 and Table 14). Therefore, we used primidone data to calculate the  $\cdot\text{OH}$  exposure with a rate constant of  $6.7 \cdot 10^9 \text{ M}^{-1} \text{ s}^{-1}$  (Real et al., 2009), wherever primidone removal was higher than 5 % (marked in red) and corrected the ozone exposure by removal expected from hydroxyl radical contribution with the known second order rate constants of these compounds (here denoted “O<sub>3</sub> cExp”). In Table 14 there is a summary of the calculated and measured dissolved ozone concentration at the sampling port (c1\_calc and c1\_meas) and the mass transfer coefficient resulting from the calculated c<sub>0</sub> with gabapentin exposure data.

Table 13: Ozone exposure calculated with probe compound removal.

Experiment	Benzotriazole				Primidone		Iopromide		Gabapentin				Atenolol				Ibuprofen			
	c_in (ng/l)	c_out (ng/l)	O <sub>3</sub> Exp (Ms)	O <sub>3</sub> cExp (Ms)	c_in (ng/l)	c_out (ng/l)	Exp OH (Ms)	c_in (ng/l)	c_out (ng/l)	O <sub>3</sub> Exp (Ms)	O <sub>3</sub> cExp (Ms)	c_in (ng/l)	c_out (ng/l)	O <sub>3</sub> Exp (M s)	O <sub>3</sub> cExp (Ms)	c_in (ng/l)	c_out (ng/l)	O <sub>3</sub> Exp (Ms)	O <sub>3</sub> cExp (Ms)	
1	5664	52	3.25E-02	2.34E-02	5290	4080	3.88E-11	4539	2825	4647	1119	1.042E-01	7.84E-02	n.a.	n.a.	6984	2581	1.037E-01	7.3804E-02	
2	5924	110	2.76E-02	2.00E-02	5081	4145	3.04E-11	4338	3253	4627	1540	8.054E-02	6.03E-02	n.a.	n.a.	6874	3027	8.542E-02	6.2004E-02	
3	5650	477	1.71E-02	1.23E-02	5242	4529	2.18E-11	4404	3524	4700	1759	7.193E-02	5.74E-02	n.a.	n.a.	6356	3645	5.791E-02	4.1097E-02	
4	5685	1076	1.15E-02	1.15E-02	5293	5077	6.23E-12	n.a.	n.a.	4799	3211	2.941E-02	2.94E-02	4765	83	6696	5313	2.409E-02	2.4094E-02	
5	5741	2253	6.48E-03	6.48E-03	5317	5202	3.28E-12	4341	4095	4807	3877	1.574E-02	1.57E-02	5039	353	4830	4276	1.268E-02	1.2682E-02	
6	5233	206	2.24E-02	1.63E-02	4792	4071	2.43E-11	3906	3131	4370	1413	8.265E-02	6.64E-02	4345	n.a.	4178	2141	6.965E-02	5.0897E-02	
7	5116	722	1.36E-02	9.91E-03	4800	4379	1.37E-11	4087	3740	4396	2500	4.131E-02	3.22E-02	4299	105	4352	3040	3.736E-02	2.6797E-02	
8	5873	1013	1.22E-02	1.22E-02	5331	5075	7.34E-12	4377	3955	4724	2845	3.713E-02	3.71E-02	5018	57	5273	3914	3.104E-02	3.1043E-02	
9	5910	1725	8.53E-03	8.53E-03	5410	5229	5.09E-12	4423	4332	4763	3875	1.510E-02	1.51E-02	4920	136	4915	4794	2.601E-03	2.6009E-03	
10	5241	2032	6.56E-03	6.56E-03	4650	4810	-5.05E-12	4021	4057	4326	3786	9.751E-03	9.75E-03	4172	251	4339	4148	4.679E-03	4.6791E-03	

Table 14: Experimental conditions and calculated parameters for probe compound removal experiments.

Experiment	Experimental conditions						Calculated initial concentration / mass transfer				
	Q1 (l/h)	v1 (cm/d)	t-but (mM)	O3 (g/m3)	Membr.	t_contact (s)	c_0_calc (mg/l)	K (m/s)	Re (-)	c1_meas (mg/l)	c1_calc
1	1	136	50	100	PTFE	7207.56	0.8178	4.392E-07	0.0597	0.397	0.30791
2	1.5	204	50	100	PTFE	4805.04	0.8197	6.08091E-07	0.0896	1.183	0.427412
3	2.5	340	50	100	PTFE	2883.02	1.1545	1.47636E-06	0.1493	1.000	0.781118
4	4.5	611	50	100	PTFE	1601.68	0.9806	2.50983E-06	0.2688	0.698	0.789263
5	7.2	978	50	100	PTFE	1001.05	0.8072	3.1279E-06	0.4301	0.425	0.704797
6	1	136	50	100	PDMS	7207.56	0.6933	3.94792E-07	0.0499	0.533	0.261037
7	1.5	204	50	100	PDMS	4805.04	0.4374	3.73994E-07	0.0749	0.087	0.228068
8	2.5	340	50	100	PDMS	2883.02	0.7467	1.04091E-06	0.1248	0.453	0.505217
9	4.5	611	50	100	PDMS	1601.68	0.5036	1.2093E-06	0.2246	0.235	0.4053
10	7.2	978	50	100	PDMS	1001.05	0.5000	2.06425E-06	0.3593	0.223	0.436575

### 10.3.9 Text S7: Estimation of ozone mass transfer with dimensionless correlations and numerical modeling

Mass transfer coefficients for the liquid side  $k_l$  can be calculated through dimensionless correlations for any gas type if the membrane dimensions, gas diffusivity (as diffusion coefficient,  $D_{O_3} = 1.76 \cdot 10^{-9} \text{ m}^2 \text{ s}^{-1}$ ), and liquid flow velocity (variable) and viscosity  $1.0272 \cdot 10^{-6} \text{ m}^2/\text{s}$  of the water are known. The following correlation was taken from Fang et al. (2002):

$$Sh = 0.824 Re^{0.39} Sc^{0.33} \quad (S5)$$

Definitions of the individual dimensionless numbers can be found in Fang et al. (2002) and Bein et al. (2021). In addition to this, membrane resistance was included in the same way as in Bein et al. (2021) with an ozone permeability  $P_{mO_3} = 1.05 \cdot 10^{-12} \text{ mol}/(\text{m s Pa})$  (Berry et al., 2017; Dingemans et al., 2008), which results in an individual membrane mass transfer  $k_m$  of  $2.063 \cdot 10^{-5} \text{ m/s}$  for a membrane wall thickness of 0.5975 mm. Mass transfer resistance on the gas side was calculated with the correlation also used by Sabelfeld and Geißen (2019) but resulted in a contribution of less than 0.1 %, and is not discussed further here.

Based on the assumption that the correlation by Fang et al. (2002) is accurate, we developed a simple numerical modeling tool for the estimation of ozone mass transfer, including the reducing ozone gas concentration with increasing tube length, using the same mass balances as in Text S2, however only describing mass the transfer rate  $N_i$  through a finite piece of membrane ( $dA$ ):

$$N_i = dA K \Delta c \quad (S6)$$

$$N_i = Q_{l,i} (c_{l,out,i} - c_{l,in,i}) \quad (S7)$$

$$N_i = Q_g (c_{g,i} - c_{g,i+1}) \quad (S8)$$

where  $N_i$  is the ozone mass transfer rate for the element “i” ( $\text{g s}^{-1}$ ),  $K$  the mass transfer coefficient that is assumed to be independent of other parameters at steady-state flow,  $\Delta c$  the characteristic concentration difference between gas- and liquid phase (Eq. S4),  $Q_{l,i}$  the horizontal liquid flow rate of water passing the finite membrane tube piece,  $c_{l,out,i}$  the liquid side concentration after passing the membrane and  $c_{l,in,i}$  before the membrane (set to 0 because of absence of ozone in natural water).  $dA$  is the logarithmic average of  $d_{in}$  and  $d_{out}$  of the membrane times the finite tube length  $dl$  and  $\pi$  (Figure 35).  $Q_{l,i}$  is defined as the water flow rate passing the finite membrane piece at the flow velocity near the membrane, where the finite cross-sectional area  $dA_i$  is defined by the so-called penetration depth  $p_d$  according to Fang et al. (2004).  $p_d$  is the square root of the ozone diffusion coefficient in water times the residence time at the membrane (defined as

$d_{out}/v_l$ ).  $dA_1$  in this model is assumed to be  $2p_d \cdot dl$ . The liquid velocity  $v_l$  here is the average velocity in proximity of the membrane. This is assuming that the membrane is surrounded by a free water body without porous media and that the effective groundwater velocity ( $v_{l,e}$ ) in porous media is equal to the velocity near the membrane. In reality, there might be more deviation between the effective groundwater velocity and the velocity near the membrane. This needs to be evaluated and adjusted for the respective treatment scenarios.

The numerical computation proceeds as follows for each consecutive step:

1. Set a start value for  $N_i$  (e.g., 0.0000001 g/s)
2. Calculate  $c_{l,out,i}$  with Eq. S7.
3. Calculate  $c_{g,out,i}$  with  $c_{g,in,i}$  and  $Q_g$  (Eq. S8).
4. Convert  $c_{g,out}$  and  $c_{g,in}$  into  $c_{sat,in}$  and  $c_{sat,out}$  with the ideal gas law and the Henry constant.
5. Calculate  $\Delta c$  with values obtained in 2. and 4.
6. Calculate the new mass transfer rate ( $N_i$ ) with Eq. S6.
7. Jump back to 2. and continue until convergence is reached (e.g., difference between new  $N$  and  $N$  from previous step smaller than 0.1%).
8. Move to the next step ( $i+1$ ): reset of  $N$  to start value,  $c_{g,out,i} = c_{g,in,i+1}$ .

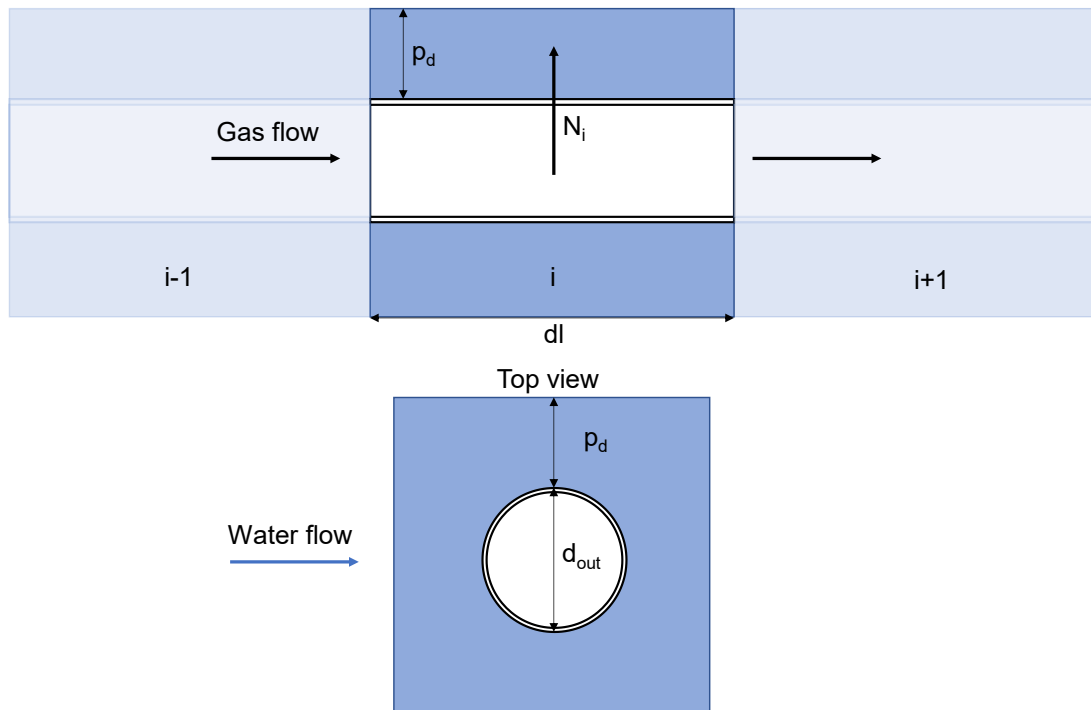


Figure 35: Schematic of the finite membrane piece and its dimensions. Water is flowing perpendicular to the membrane, as shown in the top view display.



## 10.4 Supplementary information for Chapter 6

### 10.4.1 Text S1: Selection of hydroxyl radical probe compounds

Overall, four different probe compounds were tested: para-chlorobenzoic acid (pCBA) and primidone (PRI) for  $O_3/H_2O_2$ , and PRI, carbamazepine (CBZ), and gabapentin (GBP) for UV/ $H_2O_2$  treatment. Compounds were chosen based on their ozone-resistance for ozone-based treatment and photo-resistance in case of UV/ $H_2O_2$  treatment, as reported previously (Miklos et al., 2018a; Real et al., 2009). Additionally, pCBA is a well-established standard probe compound for both processes (Pereira et al., 2007; Rosenfeldt et al., 2006; von Sonntag and von Gunten, 2012). pCBA ( $5 \cdot 10^9 \text{ M}^{-1} \text{ s}^{-1}$ ) and PRI ( $6.7 \cdot 10^9 \text{ M}^{-1} \text{ s}^{-1}$ ) both led to similar results in ozonation experiments and were therefore both considered applicable, as discussed in the manuscript's sections 3.1 and 3.3.2. pCBA, however, could not be used as probe compound in UV/ $H_2O_2$ , because it substantially decayed in UV light in a control experiment with BA and no  $H_2O_2$  added, although it is considered a suitable photo-resistant probe compound for UV/ $H_2O_2$  studies (Figure 36).

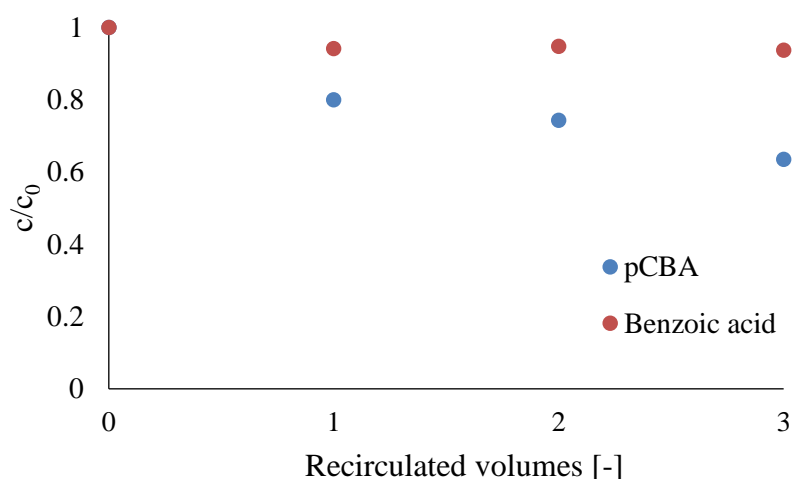


Figure 36: Photolytic decay of 0.1  $\mu\text{M}$  pCBA in a UV-C control experiment with 10 mg/L BA and no  $H_2O_2$  added.

PRI, GBP and CBZ were photo-resistant in a UV control experiment (Figure 38), but calculation of  $\cdot\text{OH}$  exposures from PRI and GBP in UV/ $H_2O_2$  experiments sharply reduced agreement with ozone-based BTE transformation and resulted in much higher second order reaction rate constants of BTE compared to reported values (Figure 37). Calculated  $\cdot\text{OH}$  exposures and contaminant removal during UV/ $H_2O_2$  matched reasonably with the ozone-based process if CBZ was used with a rate constant of  $5.85 \cdot 10^9 \text{ M}^{-1} \text{ s}^{-1}$  (Pereira et al., 2007), expressed as close agreement of second order reaction rate constants of BTE with literature data (discussed in section 3.1). This was the case, even though strongly deviating second order reaction rate constants of  $5.85 \cdot 10^9$  (Pereira et al., 2007),  $8.8 \cdot 10^9$  (Huber et al., 2003) or  $9.5 \cdot 10^9 \text{ M}^{-1} \text{ s}^{-1}$  (Wols et al., 2013) were determined

independently for reactions of CBZ with  $\cdot\text{OH}$ . All of the aforementioned observations demonstrate general difficulties in reliably quantifying  $\cdot\text{OH}$ . Obviously, the selection of reaction rate constants can considerably affect calculated exposure in such a sensitive comparison.

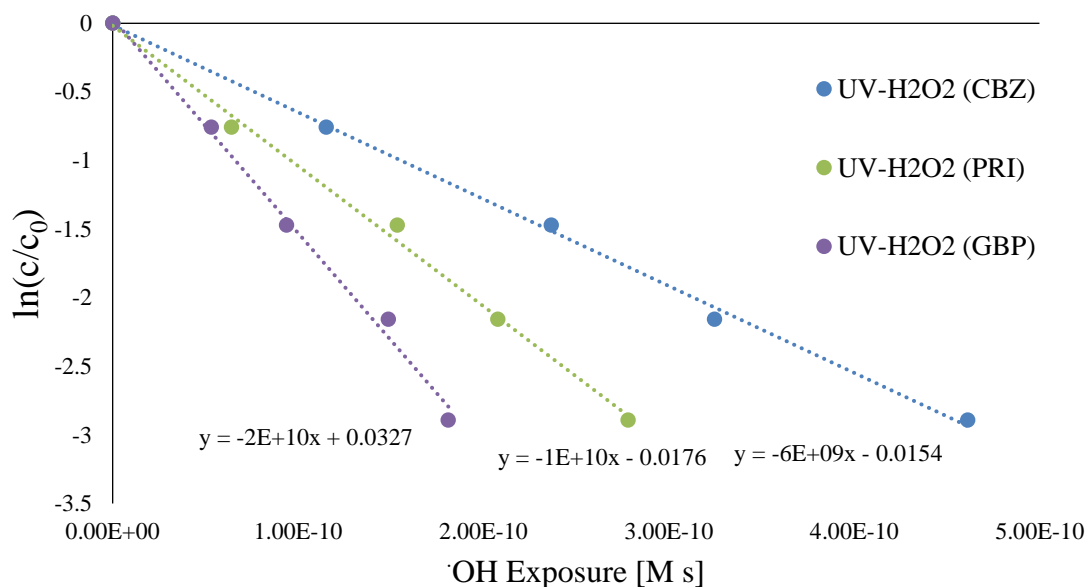


Figure 37: Comparison of linearized BA removal vs.  $\cdot\text{OH}$  exposure in UV/ $\text{H}_2\text{O}_2$  treatment, if calculated either using PRI ( $6.7 \cdot 10^9 \text{ M}^{-1} \text{ s}^{-1}$  Real et al. (2009)), GBP ( $9.1 \cdot 10^9 \text{ M}^{-1} \text{ s}^{-1}$  Lee et al. (2014)), or CBZ ( $5.85 \cdot 10^9 \text{ M}^{-1} \text{ s}^{-1}$  Pereira et al. (2007)) in case of UV/ $\text{H}_2\text{O}_2$ . The slopes of the different exposure data sets indicate that CBZ agrees best, both with ozonation experiments but also with the reported rate constants of benzoic acid and BTE.

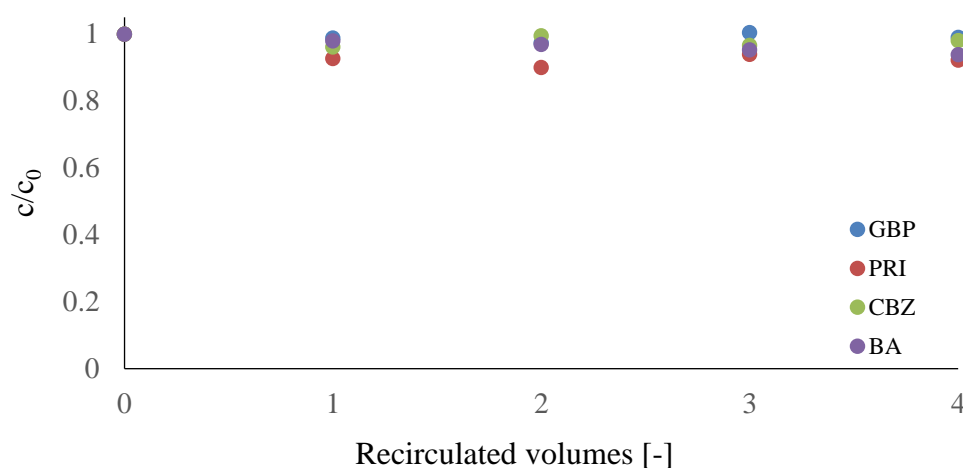


Figure 38: Control experiment with  $0.1 \mu\text{M}$  GBP, PRI and CBZ ( $0.05 \mu\text{M}$ ) with  $10 \text{ mg/L}$  BA and no  $\text{H}_2\text{O}_2$  added, exposed to UV-C light as in the oxidation experiments to demonstrate photo-resistance.

### 10.4.2 Text S2: Further notes on biodegradation experiments with biological sand

Overall, 21 individual batches were treated in two sets of experiments (seven triplicates). Samples (0a), (1a) and (2b) were in set 1, (0b), (3a) and (2a) in set 2. For each of the two sets, a sample of biological sand was taken from the wastewater-conditioned sand filter for inoculation of the individual batches, which also explains different mineralization rates if the two sets are directly compared. In set two, some increase of DOC was observed in the last three days (Figure 21 and Figure 39), which may be due to the release of DOC by bacteria in the decline stage, where available substrate is limited. However, the general behavior is very comparable, as in both sets the DOC of oxidated samples stay well above the BA control.

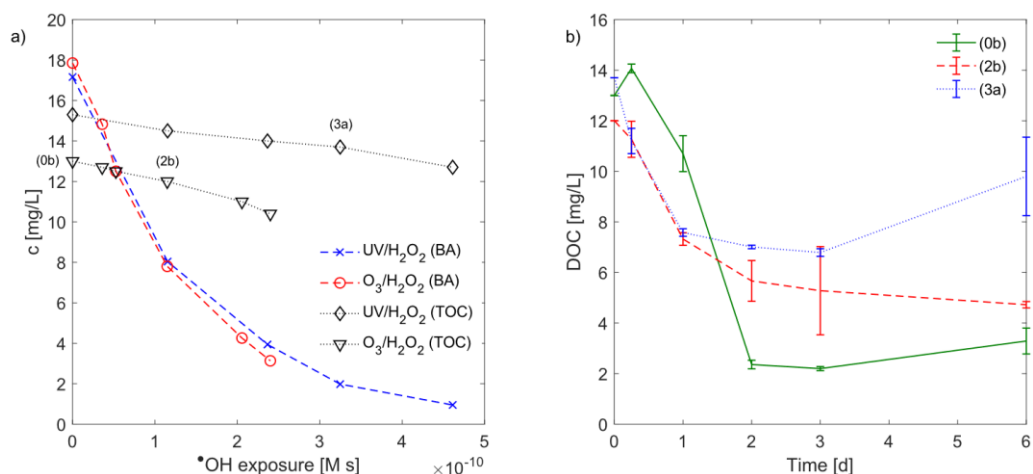


Figure 39: a) Changes of BA concentrations and TOC vs.  $\cdot\text{OH}$  radical exposure. b) additional biological degradation batch tests (b).

## 10.4.3 Reaction rate constants

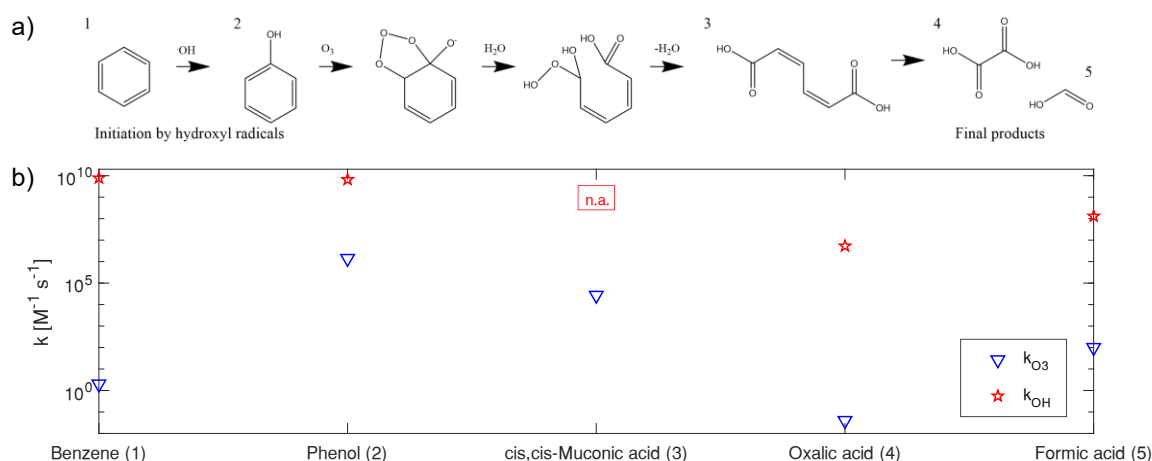


Figure 40: a) Proposed transformation pathway of benzene with first attack of  $\cdot\text{OH}$  and subsequent ozone attack, resulting in short-chained aliphatic compounds (phenol ozonation adapted from Ramseier and von Gunten (2009)). Other intermediate products such as catechol or benzoquinone may form, and quantities may change depending on the ozone:benzene stoichiometry. b) Demonstration of increased reactivity of intermediates with ozone. Sources of reported reaction rate constants can be found in Table 15.

Table 15: Second order reaction rate constants of benzene, phenol and reported TPs in ozonation of phenol with ozone and  $\cdot\text{OH}$  radicals.

Compound	$k_{\text{O}_3}$ [ $\text{M}^{-1} \text{s}^{-1}$ ]	$k_{\text{OH}}$ [ $\text{M}^{-1} \text{s}^{-1}$ ]	References
Benzene	2	$7.8 \cdot 10^9$	Hoigné and Bader (1983a) / Schuler and Albarran (2002)
Phenol	$\approx 1.4 \cdot 10^6$ <sup>a</sup>	$6.6 \cdot 10^9$	von Sonntag and von Gunten (2012) / Buxton et al. (1988)
Catechol	$5.2 \cdot 10^5$	$1.1 \cdot 10^{10}$	Mvula and von Sonntag (2003) / Buxton et al. (1988)
p-Benzoquinone	$2.5 \cdot 10^3$	$1.2 \cdot 10^9$	Mvula and von Sonntag (2003) / Buxton et al. (1988)
cis,cis-Muconic acid	$2.7 \cdot 10^4$	n.a.	Leitzke and von Sonntag (2009)
Oxalic acid	$\leq 4 \cdot 10^{-2}$	$5.3 \cdot 10^6$	Hoigné and Bader (1983b) / Sehested et al. (1971)
Formic acid	$\approx 100$ <sup>b</sup>	$1.3 \cdot 10^8$	Hoigné and Bader (1983b) / Buxton et al. (1988)

<sup>a</sup> Estimated for pH 7 using experimental rate constants of protonated ( $1.3 \cdot 10^3 \text{ M}^{-1} \text{ s}^{-1}$ ) and deprotonated ( $1.4 \cdot 10^9 \text{ M}^{-1} \text{ s}^{-1}$ ) species and  $\text{pK}_a$  10. <sup>b</sup> Estimated for pH 7 using experimental rate constants of protonated ( $5 \text{ M}^{-1} \text{ s}^{-1}$ ) and deprotonated ( $100 \text{ M}^{-1} \text{ s}^{-1}$ ) species and  $\text{pK}_a$  3.75.

## 10.4.4 Chemicals and reagents

Table 16: List of all chemical substances used in experiments.

Substance	Purity / concentration	Manufacturer / brand	Country
Benzene	99.8%	Sigma-Aldrich	Germany / USA
Toluene	99.9%	Supelco	Germany / USA
Ethylbenzene	99.8%	Acros Organics	USA
Phenol	100%	VWR Chemicals	USA
o-Cresol	99.8%	Sigma-Aldrich	Germany / USA
o-Ethylphenol	99%	Sigma-Aldrich	Germany / USA
Benzoic acid	>99.5%	Supelco	Germany / USA
Primidone	98%	Sigma-Aldrich	Germany / USA
p-Chlorobenzoic acid	99.6%	LGC/Dr. Ehrenstorfer	Germany
Salicylic acid	>99.0%	Sigma-Aldrich	Germany / USA
Carbamazepine	98%	Sigma-Aldrich	Germany / USA
Gabapentin	99.8%	Sigma-Aldrich	Germany / USA
H <sub>2</sub> O <sub>2</sub> (stabilized)	30%	VWR Chemicals	USA
Na <sub>2</sub> S <sub>2</sub> O <sub>3</sub> ·5H <sub>2</sub> O	99.5%	VWR Chemicals	USA
H <sub>3</sub> PO <sub>4</sub>	85%	Supelco	Germany / USA
NaOH	32%	Merck	Germany
NaH <sub>2</sub> PO <sub>4</sub> ·2H <sub>2</sub> O	>99%	Merck	Germany
Na <sub>2</sub> HPO <sub>4</sub>	>99%	Merck	Germany

## 10.4.5 Analytical methods

Table 17: Instrument settings of Agilent 7980 GC and Agilent 7697A HS module.

Headspace settings	
Equilibration time	30 min
Oven temperature	90 °C
Transfer line temperature	195 °C
Loop temperature	150 °C
Gas chromatograph settings	
Gas flow (N <sub>2</sub> )	3 mL/min
Septum purge flow	3 mL/min
Total flow	36 mL/min
Split ratio	10:1
Inlet temperature	250 °C
Makeup flow (N <sub>2</sub> )	25 mL/min
Air flow	400 mL/min
FID gas flow	30 mL/min H <sub>2</sub>
FID temperature	250 °C

Table 18: HPLC-UV methods for detection of phenol, o-cresol, and o-ethylphenol and benzoic acid.

Settings / steps	Phenol, o-cresol, and o-ethylphenol	Benzoic acid
Solvents	A: H <sub>2</sub> O, B: ACN (gradient method)	A: H <sub>2</sub> O (+0.1% formic acid), B: ACN (gradient method)
Flow rate	0.5 mL/min	0.6 mL/min
Injection volume	50 µL	50 µL
Separation column	XSelect HSS C18 (Waters, USA)	XSelect HSS C18 (Waters, USA)
Sample preparation	Immediate analysis, no filtration or dilution	Filtration through 0.22µm PVDF filters, storage in the fridge, dilution with UPW according to calibration

Applied gradient	0 min 2 % B, 11 – 13 min 100% B, 14 – 18 min 2% B	0 min 2 % B, 10 – 11 min 100% B, 13 – 16 min 2% B
Calibration	0.1-5 mg/L	0.25-10 mg/L
Wave length	275 nm	238 nm

Table 19: UPLC-TOF methods for detection of TPs of benzoic acid.

Settings / steps	Suspect/Non-Target-Screening
Solvents	A: H <sub>2</sub> O, 0.1% FA B: ACN, 0.1 % FA (gradient method)
Flow rate	0.45 mL/min
Injection volume	10 µL
Separation column	ACQUITY UPLC HSS T3 column (100 x 2.1, 1.7 µm) (Waters, USA)
Sample preparation	Filtration through 0.22µm PVDF filters, centrifugation
Applied gradient	0–0.25 min, 2% B; 12.25–15 min, 99% B; 15.1–17 min, 98% B
UPLC	ACQUITY UPLC system (Waters, USA)
Detector	Fluorescence detector (set to the identified regions (290/410 and 320/450))
Mass spectrometer	XEVO G2XS equipped with an electrospray ionization source (Waters, USA)
Source temperature	140 °C
Desolvation temperature	550 °C
Sampling cone voltage	20 V
Gases	Nitrogen and argon were used as cone and collision gases. The desolvation gas flow was 950 L h <sup>-1</sup>
Source offset	50 V
Capillary voltage	0.7 kV in positive ion mode and -1. kV in negative ion mode
Scan time	0.15 s
m/z range	m/z 50 to m/z 1200
Detection mode	MSe: One dataset contained low-collision-energy data (4 eV, MS, effectively the accurate mass of precursors) and the second dataset elevated-collision-energy data (15–35 eV, MSE, all of the fragments)
Data evaluation	MassLynx, MarkerLynx, TargetLynx

## 10.4.6 Experimental data tables

Table 20: Results of O<sub>3</sub>/H<sub>2</sub>O<sub>2</sub> membrane ozonation experiment.

CT	Benzene			Toluene			Ethylbenzene			OH [M s]	Transformation products [mM]		
	c [mM]	c/c <sub>0</sub>	ln(c/c <sub>0</sub> )	c [mM]	c/c <sub>0</sub>	ln(c/c <sub>0</sub> )	c [mM]	c/c <sub>0</sub>	ln(c/c <sub>0</sub> )		Phenol	o-Cresol	o-Ethylphenol
0	0.25	1.00		0.25	1.00		0.12	1.00		0.00E+00	<0.0011	<0.00092	<0.00082
2	0.22	0.86	-0.16	0.21	0.86	-0.15	0.11	0.92	-0.08	1.55E-11	<0.0011	<0.00092	<0.00082
5	0.20	0.80	-0.22	0.20	0.81	-0.22	0.11	0.87	-0.13	2.29E-11	<0.0011	<0.00092	<0.00082
10	0.15	0.61	-0.49	0.15	0.60	-0.51	0.08	0.63	-0.46	2.83E-11	<0.0011	<0.00092	<0.00082
30	0.12	0.48	-0.73	0.12	0.47	-0.75	0.06	0.50	-0.69	8.12E-11	<0.0011	<0.00092	<0.00082
50	0.07	0.28	-1.27	0.07	0.27	-1.31	0.03	0.28	-1.27	1.46E-10	<0.0011	<0.00092	<0.00082

Table 21: Results of UV/H<sub>2</sub>O<sub>2</sub> experiment (1).

CT	Benzene			Toluene			Ethylbenzene			OH [M s]	Transformation products [mM]		
	c [mM]	c/c <sub>0</sub>	ln(c/c <sub>0</sub> )	c [mM]	c/c <sub>0</sub>	ln(c/c <sub>0</sub> )	c [mM]	c/c <sub>0</sub>	ln(c/c <sub>0</sub> )		Phenol	o-Cresol	o-Ethylphenol
0	0.43	1.00		0.28	1.00		0.18	1.00		0.00E+00	<0.0011	<0.00092	<0.00082
1	0.32	0.75	-0.28	0.21	0.73	-0.31	0.13	0.74	-0.30	2.87E-11	0.0014	0.0025	0.0101
2	0.29	0.68	-0.38	0.18	0.64	-0.44	0.12	0.65	-0.43	3.87E-11	0.0023	0.0041	0.0158
3	0.18	0.43	-0.86	0.11	0.39	-0.95	0.07	0.40	-0.93	6.82E-11	0.0029	0.0051	0.0196
4	0.17	0.41	-0.90	0.10	0.36	-1.02	0.07	0.37	-0.99	9.10E-11	0.0039	0.0069	0.0240
5	0.16	0.37	-0.99	0.09	0.32	-1.15	0.06	0.33	-1.10	1.25E-10	0.0037	0.0069	0.0241

Table 22: Results of UV/H<sub>2</sub>O<sub>2</sub> experiment (2).

CT	Benzene			Toluene			Ethylbenzene			OH [M s]	Transformation products [mM]		
	c [mM]	c/c <sub>0</sub>	ln(c/c <sub>0</sub> )	c [mM]	c/c <sub>0</sub>	ln(c/c <sub>0</sub> )	c [mM]	c/c <sub>0</sub>	ln(c/c <sub>0</sub> )		Phenol	o-Cresol	o-Ethylphenol
0	0.49	1.00	0.00	0.32	1.00		0.22	1.00		0.00E+00	n.a.	n.a.	n.a.
1	0.33	0.67	-0.40	0.21	0.64	-0.45	0.14	0.63	-0.46	3.08E-11	n.a.	n.a.	n.a.
2	0.26	0.53	-0.63	0.16	0.49	-0.70	0.11	0.50	-0.70	4.92E-11	n.a.	n.a.	n.a.
3	0.24	0.49	-0.72	0.14	0.45	-0.81	0.10	0.45	-0.81	7.12E-11	n.a.	n.a.	n.a.
4	0.22	0.45	-0.81	0.13	0.40	-0.91	0.09	0.40	-0.91	8.48E-11	n.a.	n.a.	n.a.

Table 23: Results of UV/H<sub>2</sub>O<sub>2</sub> experiment (3).

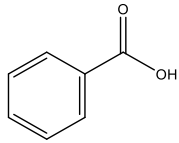
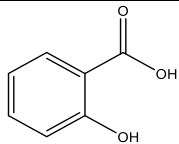
CT	Benzene			Toluene			Ethylbenzene			OH [M s]	Transformation products [mM]		
	c [mM]	c/c <sub>0</sub>	ln(c/c <sub>0</sub> )	c [mM]	c/c <sub>0</sub>	ln(c/c <sub>0</sub> )	c [mM]	c/c <sub>0</sub>	ln(c/c <sub>0</sub> )		Phenol	o-Cresol	o-Ethylphenol
0	0.17	1.00		0.31	1.00		0.11	1.00		n.a.	<0.0011	<0.00092	<0.00082
1	0.12	0.71	-0.34	0.21	0.68	-0.38	0.08	0.71	-0.34	n.a.	0.0014	0.0041	0.0067
2	0.10	0.57	-0.57	0.16	0.52	-0.65	0.06	0.55	-0.59	n.a.	0.0024	0.0066	0.0101
3	0.08	0.46	-0.77	0.13	0.41	-0.89	0.05	0.43	-0.83	n.a.	0.0031	0.0086	0.0115
4	0.07	0.39	-0.95	0.10	0.34	-1.09	0.04	0.36	-1.02	n.a.	0.0038	0.0097	0.0125

Table 24: Results of BA biological degradation experiments (DOC).

d	0a			1a			2b			0b			1b			2a		
	c (mg/L)	Std	c/c0	c (mg/L)	Std	c/c0	c (mg/L)	Std	c/c0	c (mg/L)	Std	c/c0	c (mg/L)	Std	c/c0	c (mg/L)	Std	c/c0
0	15.30	0.00	1.00	14.00	0.00	1.00	10.40	0.00	1.00	13.00		1.00	11.00		1.00	13.70		1.00
0.25	13.50	0.16	0.88	11.53	0.21	0.82	11.27	0.71	1.08	14.07	0.17	1.08	11.27	0.12	1.02	11.20	0.50	0.82
1	11.83	0.34	0.77	9.75	0.29	0.70	7.32	0.25	0.70	10.70	0.71	0.82	8.11	0.07	0.74	7.58	0.15	0.55
2	7.88	0.44	0.52	5.86	0.21	0.42	5.67	0.81	0.54	2.36	0.17	0.18	5.96	0.12	0.54	7.01	0.07	0.51
3	5.26	0.21	0.34	5.43	0.19	0.39	5.28	1.74	0.51	2.20	0.08	0.17	6.25	0.49	0.57	6.79	0.15	0.50
6	1.74	0.10	0.11	5.67	0.28	0.40	4.73	0.12	0.45	3.29	0.51	0.25	8.06	0.50	0.73	9.80	1.55	0.72



Table 25: Summary of identified compounds in HRMS analysis with proposed structure (if possible), time, and integrated peak area.

Sum formula	Difference to benzoic acid / structure	Detected exact mass in negative ESI mode	Determined mass error (ppm)	Time [min]	Integrated peak area												
					(0a)	(0a) biol.	(0b)	(0b) biol.	(1a)	(1a) biol.	(2a)	(2a) biol.	(1b)	(1b) biol.	(2b)	(2b) biol.	
C <sub>7</sub> H <sub>5</sub> O <sub>2</sub> S (TP234a)	Benzoic acid + SO <sub>2</sub> + 2O	m/z 232.9764	3.4 ppm	0.96	1	-	-	-	-	1179	104	1863	86	2120	50	2556	127
C <sub>7</sub> H <sub>6</sub> O <sub>2</sub> (TP172a)	Benzoic acid + H <sub>2</sub> O + 2O	m/z 171.0296	1.8 ppm	1.26	-	-	-	-	-	42	150	43	420	-	-	-	-
C <sub>7</sub> H <sub>5</sub> O <sub>2</sub> S (TP234b)	Benzoic acid + SO <sub>2</sub> + 2O	m/z 232.9766	4.3 ppm	1.29	1	-	1	-	-	2671	-	2375	-	-	-	-	-
C <sub>7</sub> H <sub>5</sub> O <sub>2</sub> S (TP234c)	Benzoic acid + SO <sub>2</sub> + 2O	m/z 232.9766	4.3 ppm	1.63	-	-	-	-	-	405	8	797	5	649	-	717	12
C <sub>7</sub> H <sub>6</sub> O <sub>2</sub> (TP172b)	Benzoic acid + H <sub>2</sub> O + 2O	m/z 171.0293	3.5 ppm	1.88	-	-	-	-	-	56	150	74	370	-	-	-	-
C <sub>7</sub> H <sub>6</sub> O <sub>2</sub> (TP156)	Benzoic acid + H <sub>2</sub> O + O	m/z 155.0347	1.9 ppm	2.3	-	-	-	-	-	972	571	654	5	-	-	-	-
C <sub>7</sub> H <sub>4</sub> O <sub>2</sub> (TP126)	Benzoic acid - CO <sub>2</sub> + 3O	m/z 125.0239	4.8 ppm	2.53	1	-	-	-	-	2080	88	817	2	1	-	4	-
C <sub>7</sub> H <sub>4</sub> O <sub>2</sub> (TP168)	Benzoic acid - 2H + 3O	m/z 166.9984	2.4 ppm	2.87	1	-	-	-	-	1365	2	1819	-	-	-	-	-
C <sub>7</sub> H <sub>4</sub> O <sub>2</sub> S (TP190)	Benzoic acid - CO <sub>2</sub> + SO <sub>2</sub> + O	m/z 188.9864	3.2 ppm	3.01	-	-	-	-	-	575	-	574	-	-	-	-	-
C <sub>7</sub> H <sub>4</sub> O <sub>2</sub> (TP184)	Benzoic acid - 2H + 4O	m/z 182.9937	3.8 ppm	3.17	-	-	-	-	-	93	314	166	24	-	-	-	-
C <sub>7</sub> H <sub>6</sub> O <sub>2</sub> (TP154a)	Benzoic acid + 2O	m/z 153.0192	2.6 ppm	3.41	-	-	-	-	-	34	-	432	-	166	-	254	-
C <sub>7</sub> H <sub>4</sub> O <sub>2</sub> (TP166)	Benzoic acid + CO <sub>2</sub>	m/z 165.0194	3.6 ppm	3.56	94	-	-	1	-	2585	-	-	6	-	-	28	2
C <sub>7</sub> H <sub>6</sub> O <sub>2</sub> (TP154b)	Benzoic acid + 2O	m/z 153.0194	3.9 ppm	3.77	-	-	-	-	-	7257	-	9255	2	41	-	113	-
C <sub>7</sub> H <sub>4</sub> O <sub>2</sub> (TP170)	Benzoic acid + 3O	m/z 169.0145	4.7 ppm	3.81	-	-	-	18	-	2850	-	2944	-	-	-	-	5
C <sub>7</sub> H <sub>6</sub> O <sub>2</sub> (benzoic acid)		m/z 121.0290	0 ppm	4.92	2677	-	2216	-	-	385	-	105	-	326	-	825	-
C <sub>7</sub> H <sub>6</sub> O <sub>2</sub> (TP138, salicylic acid)		137.0247	5.8 ppm	5.16	96	2	8	3	-	22822	1	17987	2	725	1	2087	1

## 10.4.7 Additional result figures

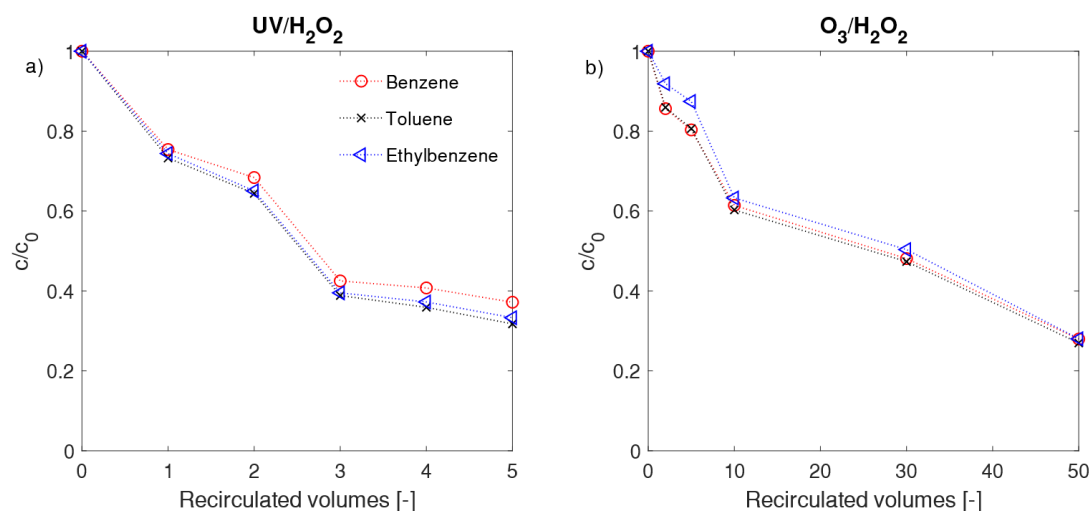


Figure 41: Removal of BTE as function of recirculated volumes in both oxidative treatment processes. Initial concentrations of BTE were 0.42/0.28/0.18 mM in the displayed UV/H<sub>2</sub>O<sub>2</sub> experiment (a), and 0.25/0.25/0.12 mM in the O<sub>3</sub>/H<sub>2</sub>O<sub>2</sub> experiment. Variations of initial BTE concentrations are observed due to losses during solution preparation.

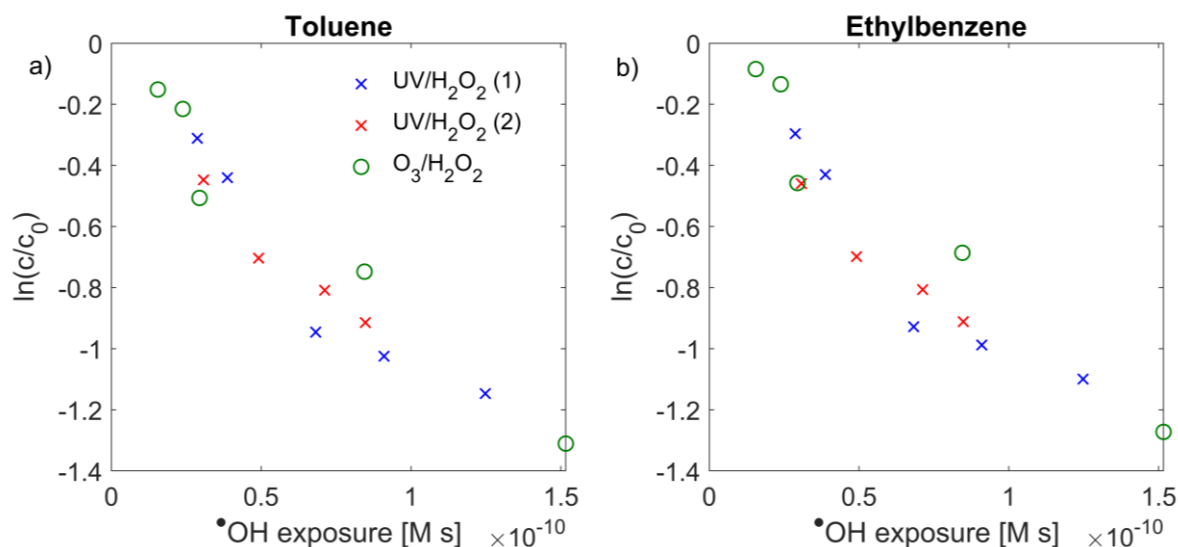


Figure 42: Removal of (a) toluene in BTE oxidation experiments and (b) ethylbenzene (same experiments) as function of  $\cdot\text{OH}$  exposure. Second order reaction rate constants based on this data were  $8.6 \cdot 10^9 \text{ M}^{-1} \text{ s}^{-1}$  or  $8.3 \cdot 10^9 \text{ M}^{-1} \text{ s}^{-1}$  for toluene and  $8.2 \cdot 10^9 \text{ M}^{-1} \text{ s}^{-1}$  or  $8.5 \cdot 10^9 \text{ M}^{-1} \text{ s}^{-1}$  for ethylbenzene, if either UV/H<sub>2</sub>O<sub>2</sub> or O<sub>3</sub>/H<sub>2</sub>O<sub>2</sub> data is used. This agrees closely with  $8.1 \cdot 10^9 \text{ M}^{-1} \text{ s}^{-1}$  (Schuler and Albarran, 2002), and  $7.5 \cdot 10^9 \text{ M}^{-1} \text{ s}^{-1}$  (Buxton et al., 1988) as reported in the literature.

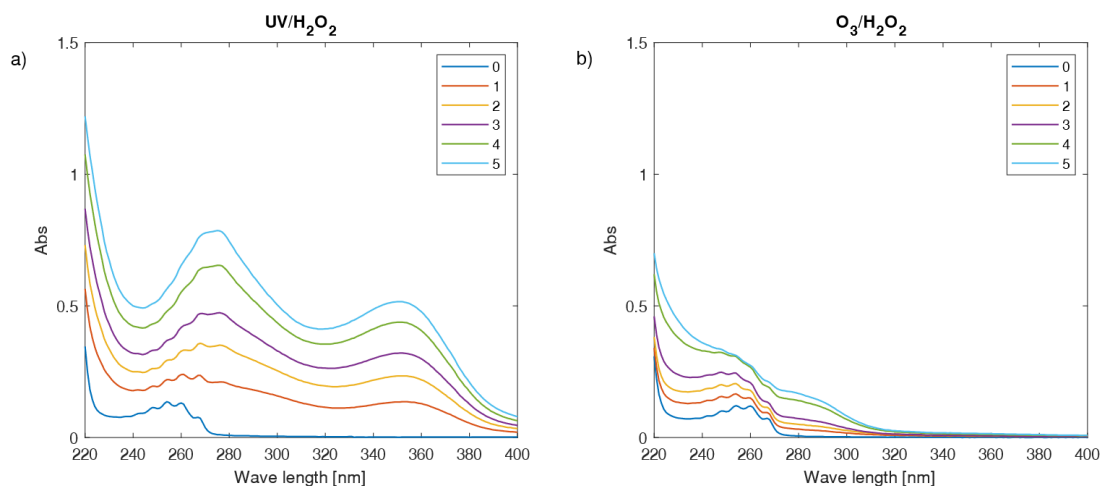


Figure 43: UV spectra of BTE oxidation experiments,  $O_3/H_2O_2$  (a), and  $UV/H_2O_2$  (b). Numbers indicate the steps of oxidation (0 is no oxidation, the highest number is the highest dose).

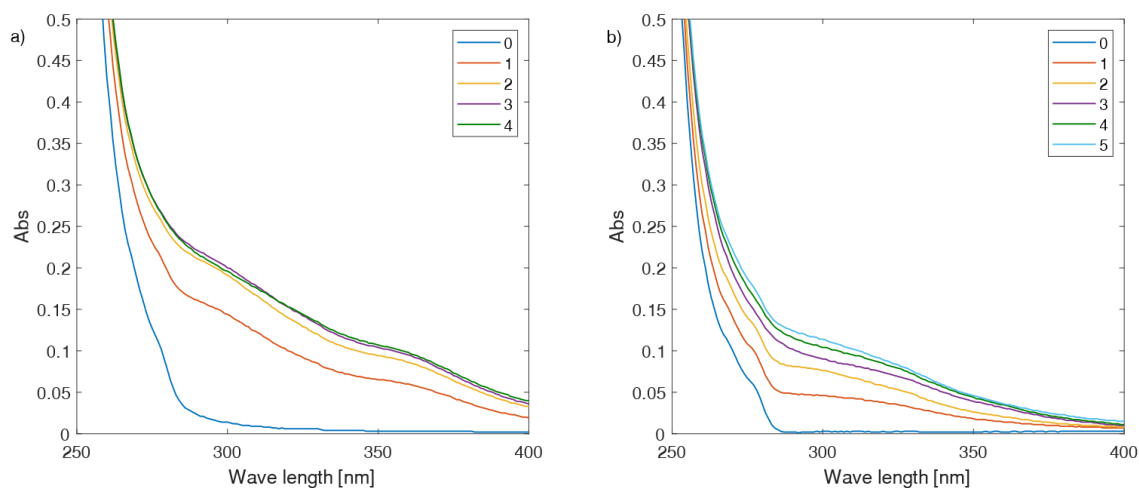


Figure 44: UV spectra of BA oxidation experiments for biological treatment,  $UV/H_2O_2$  (a), and  $O_3/H_2O_2$  (b). Numbers indicate the steps of oxidation (0 is no oxidation, the highest number is the highest dose).

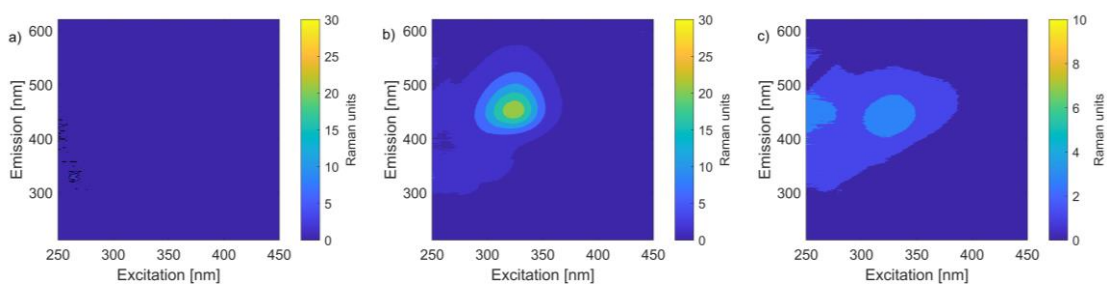


Figure 45: EEMs (a) before  $O_3/H_2O_2$  oxidation (0b), (b) after oxidation (1b), after biological degradation (1b).

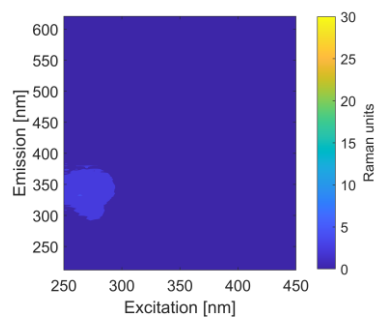


Figure 46. EEM after biological degradation of BA (sample (0a), not chemically oxidated).

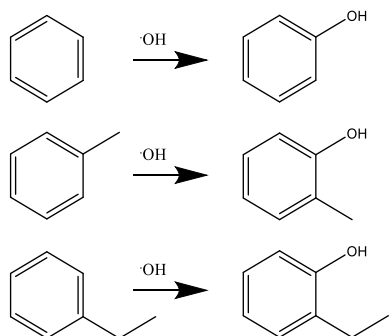


Figure 47: Transformation of BTE to phenol, o-cresol, and o-ethylphenol.

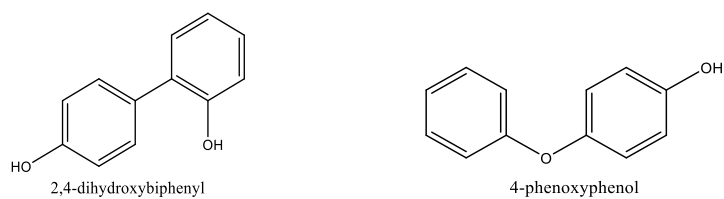


Figure 48: Exemplary products from phenol ozonation, as observed by Ye and Schuler (1989).

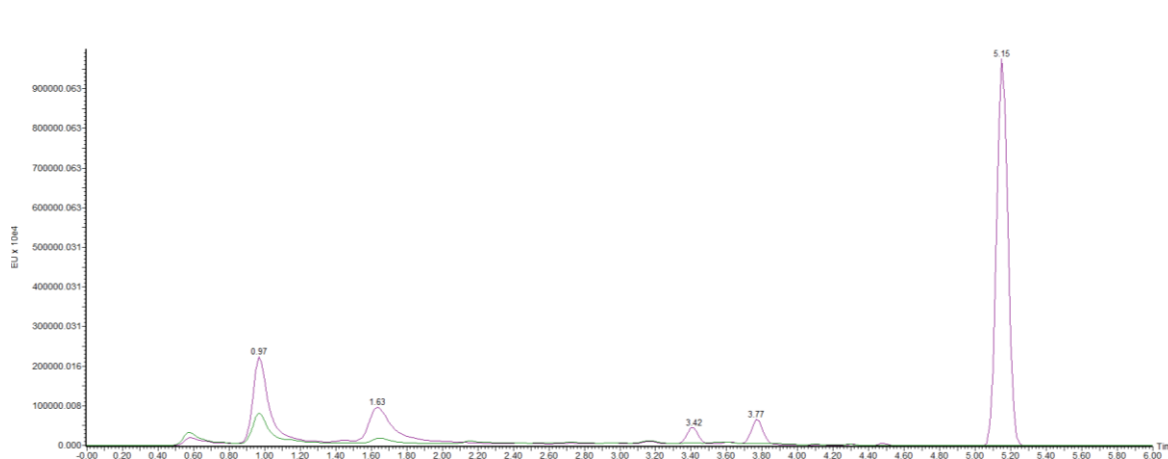


Figure 49: Fluorescence (320/450 nm) in the first 6 min of the HRMS run of (1a) before (purple line) and after biological degradation (green line).

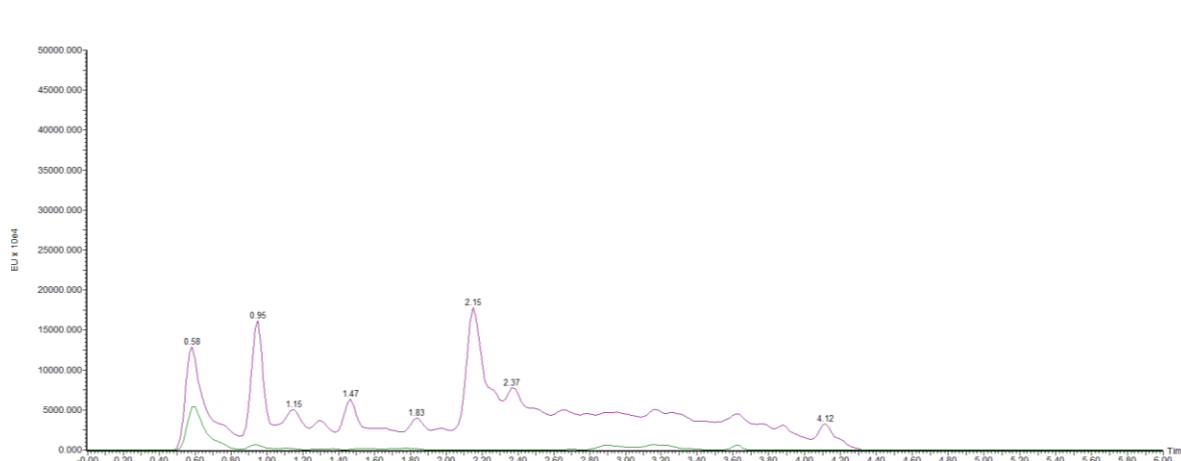


Figure 50: Fluorescence (320/450 nm) in the first 6 min of the HRMS run of (0a) before (purple line) and after biological degradation (green line).

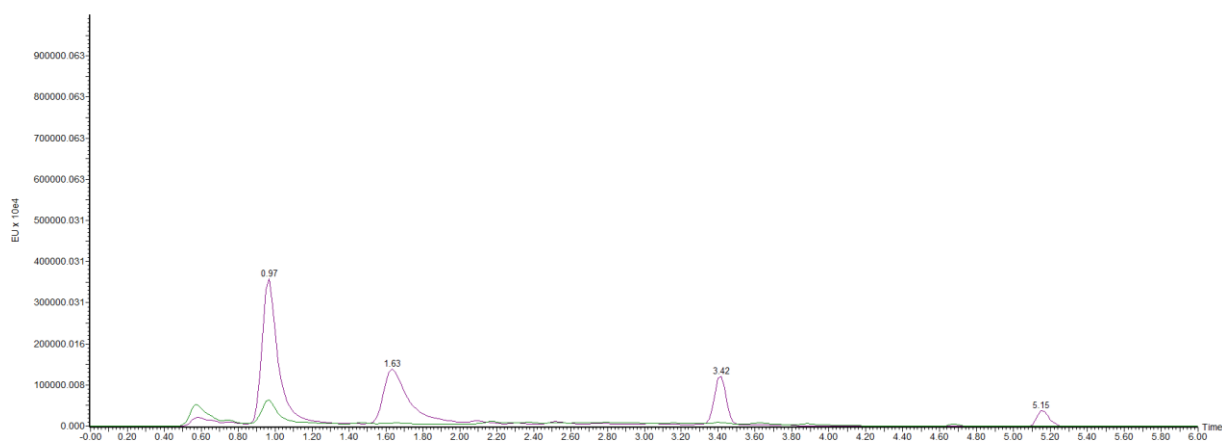


Figure 51: Fluorescence (320/450 nm) in the first 6 min of the HRMS run of (1b) before (purple line) and after biological degradation (green line).

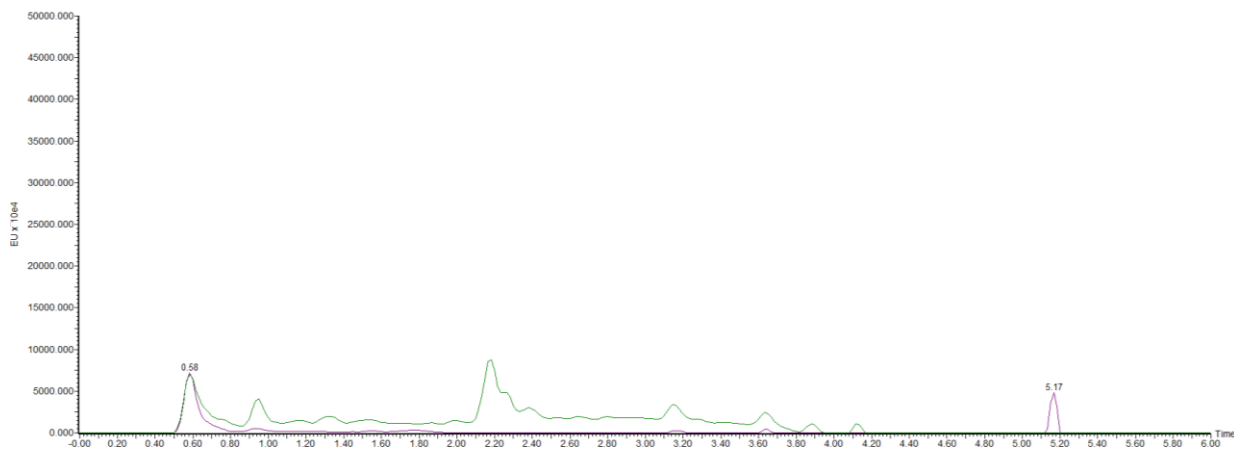


Figure 52: Fluorescence (320/450 nm) in the first 6 min of the HRMS run of (0b) before (purple line) and after biological degradation (green line).



Figure 53: Fluorescence (290/410 nm) in the first 6 min of the HRMS run of (1a) before biological degradation (green line).

## 10.5 Supplementary information for Chapter 7

### 10.5.1 Text S1: Detailed explanation of sand pre-treatment and properties

The technical sand used was originally intended for a sand filtration system and washed thoroughly with DI water on a 200  $\mu\text{m}$  stainless sieve to remove fine particles. Afterwards, the sand was soaked in a 1 M HCl solution for ca. one hour, then rinsed with DI water one more time. After washing, the sand was dried at 105  $^{\circ}\text{C}$  (>12 h) before further usage. A sieve analysis ( $n=2$ ) was performed to obtain the particle size distribution as decisive factor for the coating quantity and the specific surface area of the granular material (Table 26). The vast majority of the sand has an average diameter between 0.5 and 1 mm, enabling stable operation in the used column setup.

Table 26: Particle size distribution of washed sand used for synthesis. The sum of shown percentages is not exactly 100% as this is the mean value of two analyses.

Size range (mm)	Weight percent
<0.200	0.00
0.200-0.315	0.20
0.315-0.500	5.05
0.500-0.710	33.40
0.710-1.000	55.40
1.000-2.500	5.90
>2.500	0.00

### 10.5.2 Text S2: Characterization of different synthesized catalyst batches and their use in the experiments

Overall, three batches of coated sand (40g) were synthesized with the protocol outlined in the article (section 2.1), here labeled CFC1, CFC2 and CFC3 (Table 27). Their coating quantities and other properties were determined with the 5 g of material not used in the column experiments (35 g), as described in the article's section 2.2. The values were very similar in the first two batches and elevated in batch 3 (CFC3).

Table 27: Overview on different synthesized batches and their use in experiments.

Synthesized batch	Coating of new material ( $\text{mg}_{\text{Mn}} \text{g}^{-1}_{\text{sand}}$ )	Experiments
CFC1	$1.24 \pm 0.11$	TOrCs adsorption test
CFC2	$1.18 \pm 0.19$	Rh-B removal (except 0.12 mM PMS and Rh-B adsorption); TOrCs TW and WW tests; XRD; SEM; XPS
CFC3	$1.83 \pm 0.21$	Longevity test; Rh-B removal (0.12 mM PMS, 0 mM PMS)

This, however, did not lead to a different steady-state removal of 0.6 mM PMS in TW compared to CFC2, which always fluctuated around 90% in different experiments. Since CFCs showed initial changes in PMS decomposition, the columns for removal experiments were only used after demonstrating longevity and therefore steady-state PMS decomposition. In Figure 54 this initial inhibition can be seen for CFC2 which was used for Rh-B and TOrCs experiments.

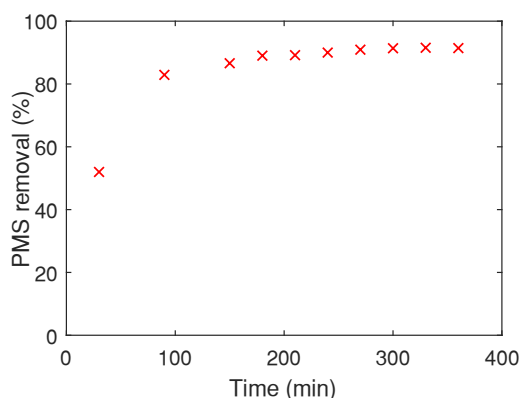


Figure 54: Test of long-term PMS decomposition of CFC2 that was used for Rh-B and TOrCs experiments after the shown exposure.

Compared to the longevity test of CFC3, steady-state was reached faster after already ca. 200 min (with <2 h pre-exposure to PMS before start of the experiment). After the longevity tests, the steady-state PMS decomposition of 90% was already reached in less than 60 min, and we assumed stable operation after this time which is well beyond the theoretical residence time in the system at a flow rate of 5 mL min<sup>-1</sup>.

### 10.5.3 Text S3: Additional material characterization results

Most SEM images were obtained using CFC2 grains that were used for experiments with Rh-B and TOrCs. This was done to capture mostly morphologies that are solidly attached and stable in presence of oxidants. In Figure 55a-c more images of used CFC2 are shown. In Figure 55a, the wire-type morphology seems to be grown as unordered coating, while the flower-like morphology can be seen in Figure 55b. Some of the  $\alpha$ -MnO<sub>2</sub> wires that were synthesized in the same batch were found in the flower-like morphology as well. In Figure 55c, a transition between the two morphologies a and b can be seen. In Figure 55d, new CFC2 is shown, where the morphology more corresponds to what is displayed in the article in Figure 25. Figure 56 Figure 56: Mn2p and C1 XPS scans of new MnO<sub>2</sub>@sand (a, b), used MnO<sub>2</sub>@sand (c, d), and unattached  $\alpha$ -MnO<sub>2</sub> powder (e, f). shows more XPS data, Figure 57 EDS elemental composition results of coated sand, and Figure 58 a comparison of coated and pristine sand.



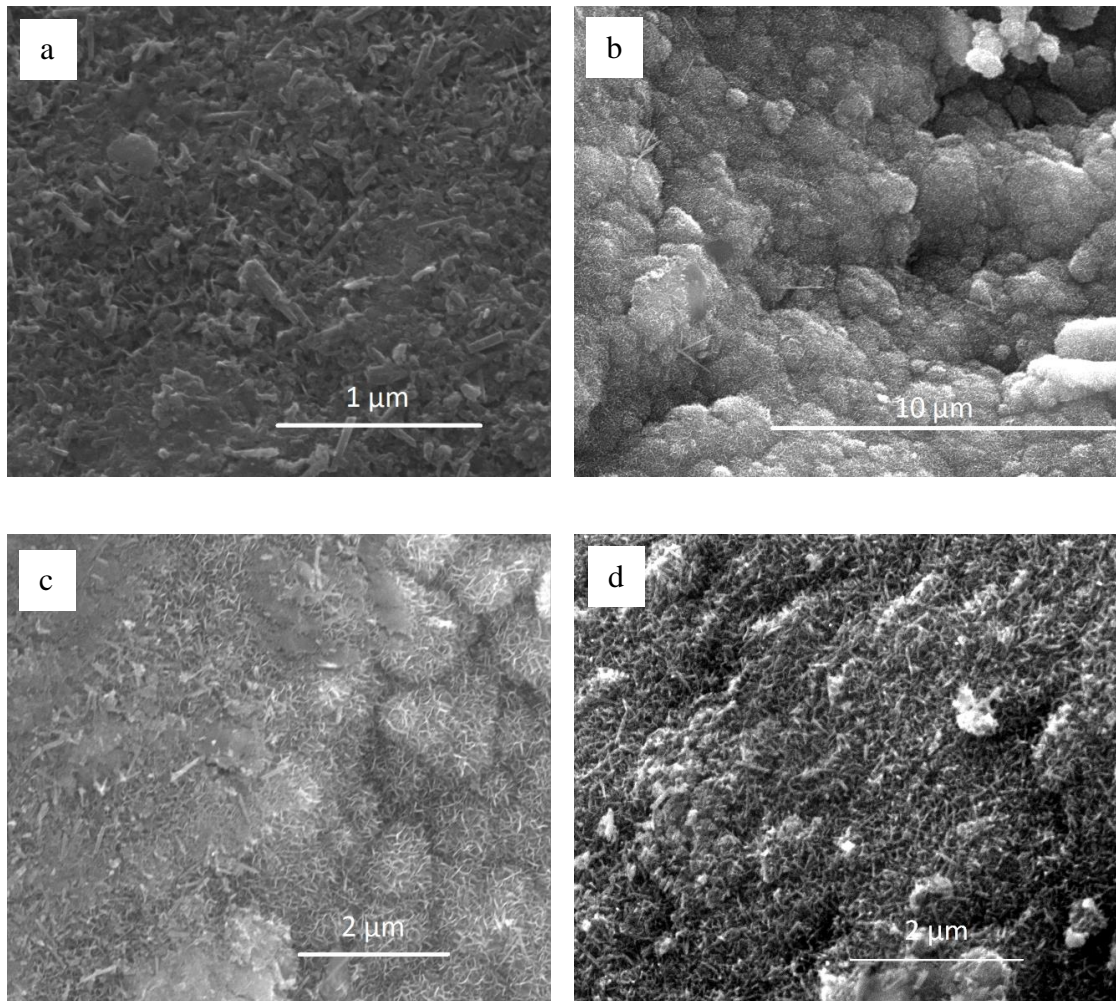


Figure 55: Additional SEM images of the coating of used CFC2 (a,b and c) and new CFC2 (d).

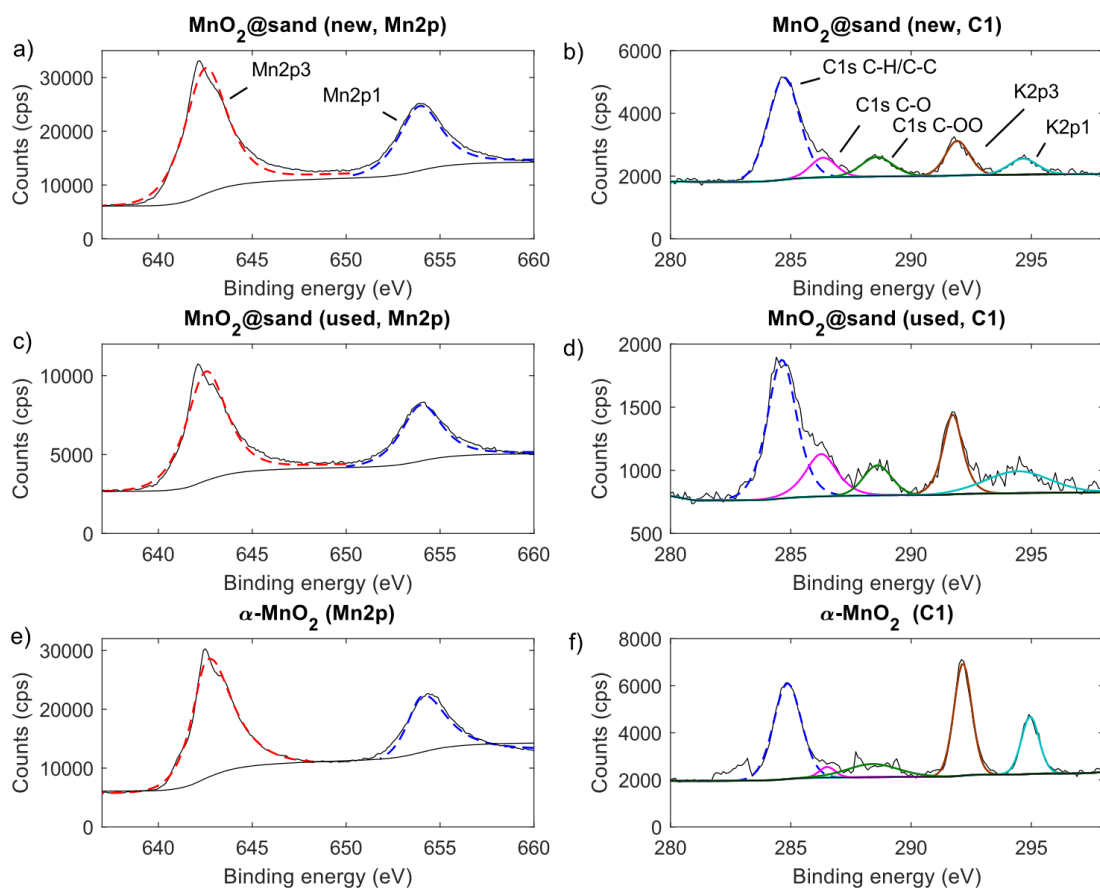
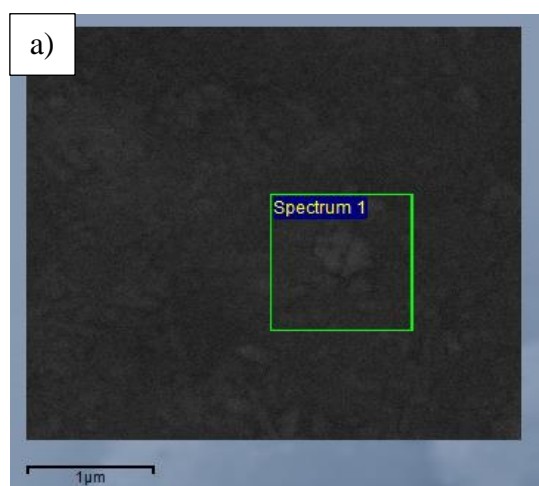


Figure 56: Mn2p and C1 XPS scans of new MnO<sub>2</sub>@sand (a, b), used MnO<sub>2</sub>@sand (c, d), and unattached α-MnO<sub>2</sub> powder (e, f).



Element	Atomic%
O	74.69
Si	23.95
K	0.06
Cr	0.73
Mn	0.57

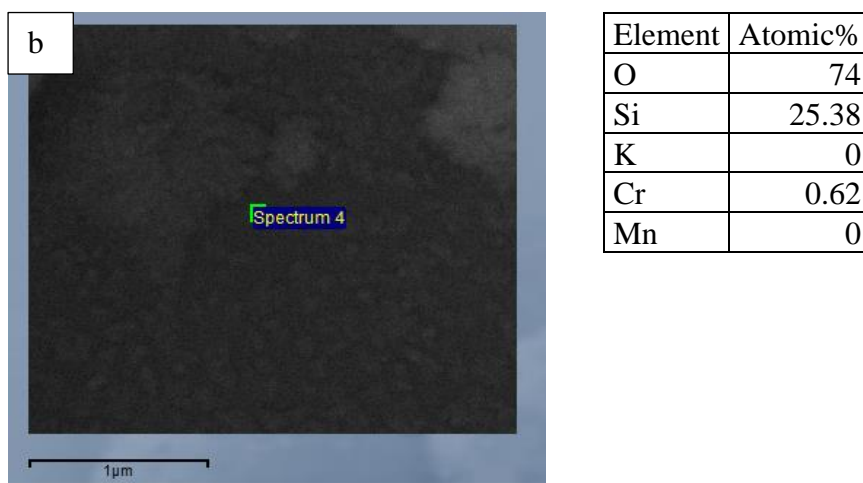


Figure 57: EDS analysis results of coated material ( $\text{MnO}_2$ @sand), a) coating area, b) blank area on the same sand grain with no coating based on SEM micrographs.

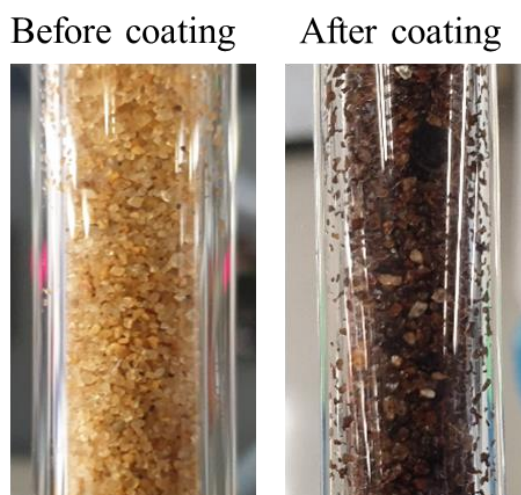


Figure 58: Comparison of sand placed in the column used for experiments before and after the hydrothermal synthesis coating.

#### 10.5.4 Text S4: Additional data on used tap water and catalyst longevity experiments

The longevity test and other tests denoted with “TW” were performed with PMS, dissolved in tap water, originating from a local groundwater well. The TW contained typical amounts of alkalinity and ions and traces of metal cations such as potassium and iron (Table 28). It had a pH of between 7.6 and 8.15 during the first 360 min of the longevity test, as shown in

Table 29. Some of the small pH increase of the first samples may be caused by minor changes in the carbonate buffer system by gas exchange in the sample bottles.

Table 28: Water quality parameters of a representative tap water (TW) sample withdrawn during the time of experiments.

Parameter	Unit	Analysis results
Calcium	mg/L	68.4
Chloride Cl <sup>-</sup>	mg/L	22.8
CO <sub>2</sub> (dissolved)	mg/L	12.6
Iron	µg/L	55.2
HCO <sub>3</sub> <sup>-</sup>	mg/L	333
Potassium	mg/L	1.04
Copper	µg/L	-
Sodium	mg/L	34
Nitrate (NO <sub>3</sub> <sup>-</sup> )	mg/L	0.253
Sulfat (SO <sub>4</sub> <sup>2-</sup> )	mg/L	42.2
TOC	mg C/L	0.595

Table 29: pH measurement of inflow and outflow in the longevity test.

Time (min)	pH
Inflow sample	8.11
30	7.92
60	7.89
90	7.94
120	7.85
180	7.82
240	7.73
300	7.72
360	7.64

### 10.5.5 Text S5: Sand control experiments

#### *Longevity test*

A supplemental control experiment with 35 g technical sand without coating in the column was performed in the same manner as the longevity test but only for 120 min to demonstrate the limited removal of PMS. A stable, low removal (<10%) can be concluded (Figure 59), which may be caused either by the other system components or by traces of metals found in the natural filtration sand used.

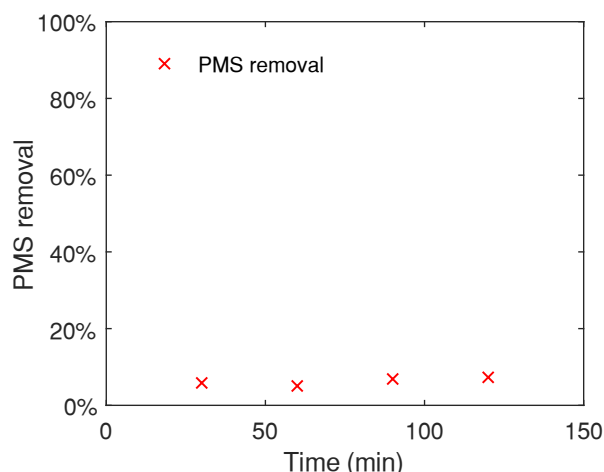


Figure 59: Control experiment with 35 g sand, as used for synthesis of coated sand material. Removal of 0.58 mM PMS was well below 10% over 120 min.

### *Rh-B removal*

An additional control experiment was performed to test removal of Rh-B in the same manner as the Rh-B experiments with the CFC, however, with technical sand without coating. Three outflow samples were withdrawn after 60 min of steady-state operation. Similar to the CFC experiment with 0.6 mM PMS, a relevant direct reaction with PMS led to 22% removal of Rh-B in the feed bottle and a similar removal was observed in the column outflow (Table 30). PMS decomposition was similarly small as observed in the longevity control (Figure 59).

Table 30: Removal of Rh-B in a control experiment with 0.6 mM PMS and 10 mg L<sup>-1</sup> Rh-B.

Sample	Rh-B removal	PMS removal
Feed after experiment (ca. 75 min)	22%	3.4%
Outflow (averaged three samples)	21%	1.4%

## 10.5.6 Text S6: Additional data on Rh-B oxidation experiments

### *Hydroxyl radical scavenging*

A hydroxyl radical scavenging experiment was conducted with 0.12 mM PMS, 10 mg L<sup>-1</sup> Rh-B and 50 mM tertiary butanol (TBA) in TW. TBA reacts with hydroxyl radicals ( $\cdot\text{OH}$ ) with a rate constant of  $6 \cdot 10^8 \text{ M}^{-1} \text{ s}^{-1}$  (Wolfenden and Willson, 1982), which is three orders of magnitude higher than for sulfate radicals ( $4\text{-}9.1 \cdot 10^5 \text{ M}^{-1} \text{ s}^{-1}$  (Neta et al., 1988)). In presence of TBA, removal of Rh-B remained on a high level (77.2%, Table 31) compared to the same experiment without TBA (86.4 %, Figure 27). This is a clear indication that hydroxyl radicals are not the main reaction partner in the Rh-B removal

mechanism. PMS removal is slightly inhibited compared to the experiment without TBA, suggesting that there is some interaction between PMS, the catalyst, and TBA.

Table 31: Removal of Rh-B in a control experiment with 0.12 mM PMS, 10 mg L<sup>-1</sup> Rh-B and 50 mM TBA.

Sample	Rh-B removal	PMS removal
Feed after experiment (ca. 75 min)	1.8 %	1.7 %
Outflow (averaged three samples)	77.2 %	82.0 %

### Leaching of Mn in Rh-B experiments

In addition to data displayed in the article, effluent of the column (CFC) was analyzed for Mn leaching using flame AAS detection without graphite furnace (LOQ=50 µg L<sup>-1</sup>) during the discussed Rh-B oxidation experiments (Table 32, except 0.12 mM). No manganese was observed above this threshold, which is in accordance with the longevity test.

Table 32: Measured Mn concentrations in the inflow and effluent of various different experiments.

Water matrix	Mn (µg L <sup>-1</sup> ) feed bottle	Mn (µg L <sup>-1</sup> ) column effluent (steady-state >60 min)
10 mg L <sup>-1</sup> RhB + 0.06 mM PMS in TW	<50	<50
10 mg L <sup>-1</sup> RhB + 0.2 mM PMS in TW	<50	<50
10 mg L <sup>-1</sup> RhB + 0.6 mM PMS in TW	<50	<50

### Comparison of Rh-B removal in this study to other published catalyst studies

Table 33: Comparison of different PMS:Rh-B ratios used in selected studies to achieve a Rh-B removal of >90%.

Catalyst material	[PMS] <sub>0</sub> : [Rh-B] <sub>0</sub>	[PMS] <sub>0</sub> (mM)	[Rh-B] <sub>0</sub> (mM)	Removal of Rh-B (%)	Initial pH	Catalyst concentration (g L <sup>-1</sup> )	Reaction time (min)	Study
CuO-CeO <sub>2</sub>	16.0	1.60	0.100	>98%	7 <sup>c</sup>	0.4	60	Li et al., 2019b
CoFe <sub>2</sub> O <sub>4</sub> /ordered mesoporous carbon	7.2	1.50	0.209	>90%	n.a.	0.05	60	Deng et al., 2017a
MnO <sub>2</sub> /MnFe <sub>2</sub> O <sub>4</sub>	935.0	1.95	0.002	>98%	7 <sup>c</sup>	0.6	15	Chen et al., 2019
Cu/ZSM5 (zeolite base)	18.7	0.20	0.021	>95%	7 <sup>c</sup>	1	60	Ji et al., 2014
rGO-CoPc (reduced graphene oxide, cobalt phtalocyanine)	4.0	0.1	0.025	>99%	n.a.	0.5	9	Marinescu et al., 2018

MnO <sub>2</sub> @sand	9.6	0.20	0.021	>99%	7.6- 8.15	6.2 <sup>b</sup>	2.2 <sup>a</sup>	This study
------------------------	-----	------	-------	------	--------------	------------------	------------------	------------

<sup>a</sup> Reaction time = residence time, assumption based on porosity/density of used technical sand, neglecting the effect of coating on density/porosity. <sup>b</sup> Estimation based on coating ( $\text{mg}_{\text{Mn}} \text{g}^{-1}_{\text{sand}}$ ) converted into MnO<sub>2</sub> and related to the effective pore volume of the column. <sup>c</sup> pH adjusted to 7 by acid/base, but no stabilizing buffer added.

### 10.5.7 Text S7: Detailed results of TOrCs removal and CFC adsorption behavior

A test was carried out to identify compounds among the 22 TOrCs that are (partly) removed in the column by different mechanisms than direct reactions with PMS, most importantly adsorption. Therefore, the removal experiment was repeated in TW with the spiked TOrCs mix but without addition of PMS. Three samples were taken after 60 min. The test results show that only for the compounds climbazole, 4-,5-methylbenzotriazole, venlafaxine, citalopram and amisulpride adsorption is observed >10%, while all other compounds remain on a similar level in the CFC effluent. Among these, venlafaxine, citalopram and amisulpride additionally reacted directly with PMS and further in the CFC column via PMS activation, thus their removal can also be expected in case of an adsorption breakthrough (Table 34, Table 35).

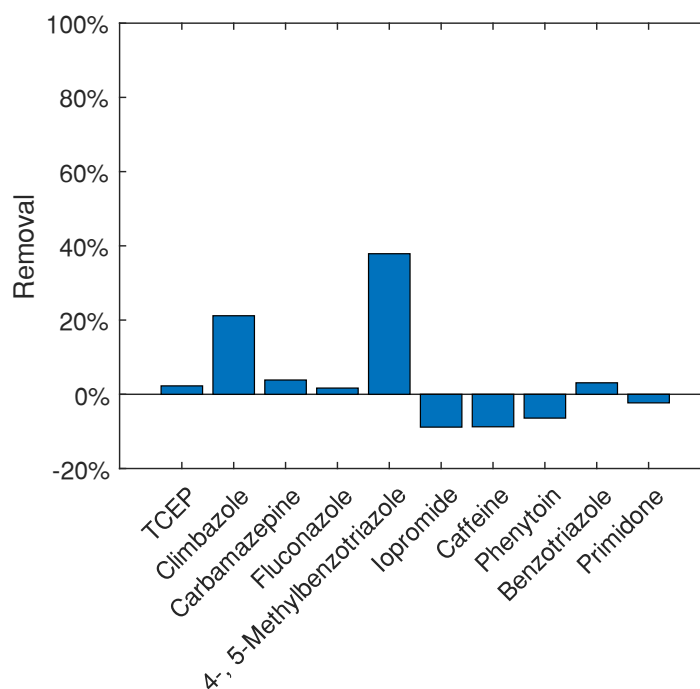


Figure 60: Adsorption test results (TW, no PMS) of compounds that are not directly reacting with PMS.

Table 34: Adsorption test results (TW, no PMS) of all analyzed compounds. Adsorption &gt;10% is highlighted in red color.

Compound	Removal in column
TCEP	2.27%
Climbazole	21.17%
Carbamazepine	3.85%
Fluconazole	1.68%
4-, 5-Methylbenzotriazole	37.88%
Iopromide	-8.85%
Caffeine	-8.75%
Phenytoin	-6.41%
Benzotriazole	3.10%
Primidone	-2.31%
Atenolol	3.29%
Metoprolol	2.12%
Sotalol	3.55%
Tramadol	0.88%
Venlafaxine	18.75%
Sulfamethoxazole	8.50%
Diclofenac	6.04%
Trimethoprim	5.64%
Antipyrine	-5.30%
Citalopram	91.71%
Amisulpride	17.05%
Gabapentin	5.13%
4-Formylaminoantipyrin	2.16%

Table 35: Removal of TORCs (WW, 0.6 mM PMS, n=3). The removal is related to the feed concentration before the start of the experiment. Removal higher than 20 % via direct PMS reaction is highlighted in red.

Compound	Removal in feed bottle (direct PMS reaction, ca. 75 min)	Column effluent	LOQ <sup>a</sup> (ng/L)
TCEP	-6.79 ± 12.95 %	-8.94 ± 8.03 %	-
Climbazole	4.64 ± 9.48 %	79.32 ± 1.49 %	250
Carbamazepine	-6.64 ± 4.37 %	88.24 ± 4.86 %	-
Fluconazole	-0.69 ± 2.51 %	25.46 ± 3.99 %	-
4-, 5-Methylbenzotriazole	1.7 ± 2.51 %	48.24 ± 7.9 %	5
Iopromide	-31.01 ± 23.06 %	34.31 ± 7.51 %	100
Caffeine	0.7 ± 2.58 %	86.08 ± 5.89 %	-
Phenytoin	-1.15 ± 4.61 %	23.62 ± 0.93 %	-
Benzotriazole	1.82 ± 0.77 %	21.92 ± 8.89 %	100
Primidone	6.5 ± 8 %	34.35 ± 6.35 %	-
Atenolol	28.8 ± 4.07 %	93.16 ± 2.52 %	10
Metoprolol	27.84 ± 3.11 %	96.04 ± 1.5 %	2.5



Sotalol	33.87 ± 5.51 %	98.6 ± 0.25 %	10
Tramadol	39.2 ± 3.94 %	96.51 ± 2.02 %	5
Venlafaxine	52.63 ± 6.08 %	99.25 ± 0.28 %	-
Sulfamethoxazole	36.59 ± 3.24 %	93.94 ± 1.87 %	-
Diclofenac	1.82 ± 2.57 %	98.56 ± 0.1 %	-
Trimethoprim	35.56 ± 6.5 %	98.7 ± 0.01 %	-
Citalopram	41.49 ± 7.18 %	96.9 ± 0.56 %	-
Amisulpride	79.82 ± 3.61 %	95.18 ± 0.25 %	-
Gabapentin	-3.11 ± 2.13 %	19.03 ± 3.76 %	-
4-Formylaminoantipyrin	6.9 ± 1.2 %	96.06 ± 0.2 %	250

<sup>a</sup> LOQs as provided in the table were used to calculate removal wherever is an entry. The values deviate partially from the original method in Müller et al. (2017) due to some sensitivity issues with single compounds in the current analyses. LOQs are based on the lowest calibration concentration, where the peak height is minimum 10 times higher than the maximum deviation of the background noise in the detection window. The concentration of the LOQ was then used as TOrcs concentration for removal calculations as conservative estimation.

Table 36: Removal of TOrcs (TW, 0.6 mM PMS, n=3). The removal calculation is related to the feed concentration before the start of the experiment. Removal higher than 20 % via direct PMS reaction is highlighted in red.

Compound	Removal in feed bottle (direct PMS reaction, ca. 75 min)	Column effluent	LOQ <sup>a</sup> (ng/L)
TCEP	-3.12 ± 3.32 %	-1.32 ± 4.62 %	-
Climbazole	-4.15 ± 9.92 %	77.1 ± 1.49 %	250
Carbamazepine	-1.44 ± 0.43 %	94.89 ± 0.18 %	50
Fluconazole	-2.76 ± 2.49 %	83.9 ± 5.27 %	-
4-, and 5-Methylbenzotriazole	-0.23 ± 1.6 %	98.37 ± 1.57 %	5
Iopromide	1.12 ± 11.48 %	83.12 ± 2.53 %	100
Caffeine	0.27 ± 1.73 %	97.04 ± 0.89 %	-
Phenytoin	1.26 ± 1.63 %	83.08 ± 9.1 %	-
Benzotriazole	3.88 ± 2.45 %	86.67 ± 0.53 %	100
Primidone	1.53 ± 4.57 %	81.46 ± 9.7 %	-
Atenolol	30.19 ± 3.81 %	97.82 ± 0.65 %	10
Metoprolol	31.71 ± 4.36 %	98.95 ± 0.86 %	2.5
Sotalol	44.42 ± 7.26 %	98.6 ± 0.05 %	10
Tramadol	54.82 ± 9.36 %	98.87 ± 0.53 %	5
Venlafaxine	70.13 ± 10.18 %	99.01 ± 0.04 %	5
Sulfamethoxazole	62.69 ± 17.02 %	95.83 ± 0.38 %	25
Diclofenac	69.27 ± 14.82 %	95.51 ± 0.43 %	25
Trimethoprim	69.68 ± 13.91 %	98.56 ± 0.07 %	10
Citalopram	91.21 ± 11.98 %	89.18 ± 10.55 %	25
Amisulpride	91.25 ± 3.99 %	98.27 ± 0.26 %	-
Gabapentin	50.17 ± 35.24 %	80.72 ± 13.29 %	-
4-Formylaminoantipyrin	78.19 ± 6.18 %	87.92 ± 1.72 %	250

<sup>a</sup> LOQs as provided in the table were used to calculate removal wherever is an entry. The values deviate partially from the original method in Müller et al. (2017) due to some sensitivity issues with single compounds in the current analyses. LOQs are based on the lowest calibration concentration, where the peak height is minimum 10 times higher than the maximum deviation of the background noise in the detection window. The concentration of the LOQ was then used as TOrcs concentration for removal calculations as conservative estimation.

Table 37: PMS concentrations as measured in TW and WW experiments (n=3).

	Feed bottle start / PMS (mM)	CFC outflow / PMS (mM)	Feed bottle end / PMS (mM)
TW	0.59499 ± 0.00270	0.05729 ± 0.01342	0.59494 ± 0.00729
WW	0.54706 ± 0.00612	0.17981 <sup>a</sup> ± 0.03990	0.52793 <sup>a</sup> ± 0.010607

<sup>a</sup> In one of the three repetitions (WW), the samples for the outflow were withdrawn after 90 min instead of 60 min due to problems adjusting the flow rate of the pump.

Table 38: Representative pH values in the inflow and outflow for TOrCs oxidation experiments.

	pH inflow	pH outflow (steady-state)
TW + 0.6 mM PMS + TOrCs	7.93	7.56
WW + 0.6 mM PMS + TOrCs	7.67	8.23

### 10.5.8 Text S8: Statistical analysis of six TOrCs – correlation of second order rate constants and removal values

The six compounds primidone, benzotriazole, carbamazepine, caffeine, iopromide, and phenytoin were chosen for statistical analysis because they did not react directly with PMS and did not adsorb onto the column set-up, therefore all of their reactivity can be attributed to catalytic oxidation. Additionally, their reactivity with  $\cdot\text{OH}$  and  $\text{SO}_4^{\cdot-}$  is well documented (Table 39).

Table 39: Reported second order reaction rate constants of statistically evaluated compounds for reactions with sulfate and hydroxyl radicals.

Compound	$k_{\text{SO}_4^{\cdot-}}$ ( $\text{M}^{-1} \text{s}^{-1}$ )	$k_{\text{OH}}$ ( $\text{M}^{-1} \text{s}^{-1}$ )
Primidone	$0.53 \cdot 10^9$ <sup>e</sup>	$6.70 \cdot 10^9$ <sup>b</sup>
Benzotriazole	$0.87 \cdot 10^9$ <sup>e</sup>	$8.00 \cdot 10^9$ <sup>d</sup>
Carbamazepine	$1.50 \cdot 10^9$ <sup>e</sup>	$8.20 \cdot 10^9$ <sup>a</sup>
Caffeine	$2.39 \cdot 10^9$ <sup>e</sup>	$6.40 \cdot 10^9$ <sup>a</sup>
Iopromide	$0.36 \cdot 10^9$ <sup>e</sup>	$3.30 \cdot 10^9$ <sup>c</sup>
Phenytoin	$0.62 \cdot 10^9$ <sup>e</sup>	$6.28 \cdot 10^9$ <sup>f</sup>

<sup>a</sup> Wols and Hofman-Caris (2012), <sup>b</sup> Real et al. (2009), <sup>c</sup> Huber et al. (2003), <sup>d</sup> Vel Leitner and Roshani (2010), <sup>e</sup> Nihemaiti et al. (2018), <sup>f</sup> Yuan et al. (2009).

The normalized removal,  $\ln(c_0/c)$ , was calculated independently for all compounds for six experiments (three repetitions of TW and WW experiments). The following equation was postulated, describing the removal of each individual compound based on its second order reaction kinetics with  $\cdot\text{OH}$  and  $\text{SO}_4^{\cdot-}$

$$\ln\left(\frac{c_0}{c}\right) = k_{\text{SO}_4^{\cdot-}} \int [\text{SO}_4^{\cdot-}] dt + k_{\text{OH}} \int [\text{OH}] dt \quad \text{Eq. S9}$$

where  $k_{SO_4^-}$  and  $k_{OH}$  are second order reaction rate constants ( $M^{-1} s^{-1}$ ) of each compound, and  $\int[SO_4^-]dt$  and  $\int[OH]dt$  the exposure to sulfate and hydroxyl radicals ( $M \cdot s$ ). Eq. S9 was used to establish a set of equations with the two exposures as unknowns and a multivariate linear regression analysis was performed using Matlab 2019 ©.  $\ln(c_0/c)$  removal of each compound and the respective reported second order reaction rate constants (Table 39) was inserted to Eq. S9 and the regression analysis was performed separately for the six experiments, as exposures were (slightly) different in each TW experiment and deviated substantially with changed water matrix (WW). Then,  $\ln(c_0/c)$  was calculated for each data point based on the regression results and the quality of the fit was evaluated based on the (adjusted) squared correlation coefficient ( $R^2$ ) of experimental and calculated  $\ln$ -removal. A Kolmogorov-Smirnov test was performed for the residuals of all regressions ( $\alpha=0.05$ ) to check for normal distribution. Three scenarios were considered in this analysis: both radical species contributed to removal (1), only  $SO_4^-$  contributed to removal (2), and only  $\cdot OH$  contributed to removal (3). As can be seen in Figure 61a, integration of both radical types in the multivariate linear regression led to good agreement of the regression values with experimentally observed ones ( $R^2_{TW} = 0.75 \pm 0.08$ ,  $R^2_{WW} = 0.67 \pm 0.03$ , Table 40). A regression with only  $SO_4^-$  resulted in similar agreement ( $R^2_{TW} = 0.74 \pm 0.01$ ,  $R^2_{WW} = 0.70 \pm 0.02$ , Figure 61b), while the fit with  $\cdot OH$  clearly agreed much less than in the other scenarios ( $R^2_{TW} = 0.36 \pm 0.09$ ,  $R^2_{WW} = 0.08 \pm 0.005$ , Figure 61c).

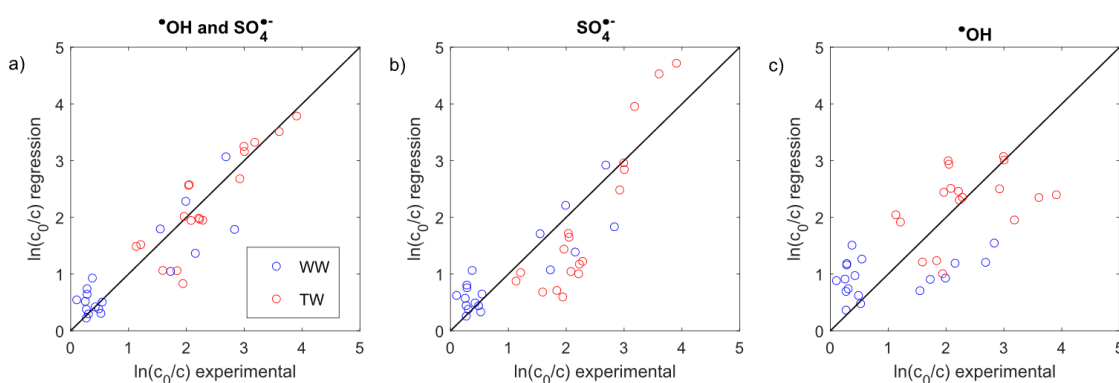


Figure 61: Correlation of experimentally observed removal of six TOxCs and the removal based on (multivariate) linear regression with their reported second order reaction rate constants.

The computed exposures are listed in Table 40. Interestingly, the results of (1) suggest that  $\cdot OH$  did not contribute to removal in WW as  $\int[OH]dt$  ( $M \cdot s$ ) is slightly negative ( $(-2.3 \pm 0.91) \cdot 10^{-11} M s$ ) and one order of magnitude smaller than for TW, while  $\int[SO_4^-]dt$  is similar in both water matrices. Such a domination of sulfate radicals in WW could be caused by different interactions of sulfate radicals with DOC, whose selective reactivity with electron-rich parts of DOC is known (Lei et al., 2022). For the scenario with  $SO_4^-$  only (2), an exposure reduction in WW due to scavenging is observed (Table 40), which

has been described previously and is more plausible than the result of the multivariate regression with both radical species for WW (Miklos et al., 2019; Nihemaiti et al., 2018). However, the differences between scenarios (1) and (2) for  $\int[SO_4^{\cdot-}]dt$  in WW are small.

From this analysis, it cannot be concluded whether or not  $\cdot OH$  contributed to the oxidation process, as substantial data scattering is observed in all regressions, which is also related to the fact, that the reproduction of second order reaction rate constants of  $\cdot OH$  or  $SO_4^{\cdot-}$  is challenging and can lead to different results. Additionally, only six compounds met criteria of this analysis. The inclusion of more compounds and removal over a wider range would provide more information. Furthermore, other reactive oxygen species such as singlet oxygen ( $^1O_2$ ) could in theory also be responsible for the removal of some compounds. Overall, the regression with  $k_{SO_4^{\cdot-}}$  and  $k_{OH}$  (1) and  $k_{SO_4^{\cdot-}}$  (2) led to the most convincing results and indicate that  $SO_4^{\cdot-}$  plays a major role in this process.

Table 40: Computed sulfate and hydroxyl radical exposures for TW and WW (n=3 each) for all investigated scenarios.

	$\int[SO_4^{\cdot-}]dt$ (M · s)	$\int[OH]dt$ (M · s)	R <sup>2</sup>
Both radical species			
TW	$(9.63 \pm 0.92) \cdot 10^{-10}$	$(1.93 \pm 0.45) \cdot 10^{-10}$	$0.75 \pm 0.08^a$
WW	$(1.06 \pm 0.29) \cdot 10^{-10}$	$(-2.3 \pm 0.91) \cdot 10^{-11}$	$0.67 \pm 0.03^a$
Only $SO_4^{\cdot-}$			
TW	$(1.84 \pm 0.17) \cdot 10^{-9}$	n.a.	$0.74 \pm 0.01$
WW	$(9.54 \pm 2.54) \cdot 10^{-10}$	n.a.	$0.70 \pm 0.02$
Only $\cdot OH$			
TW	n.a.	$(3.49 \pm 0.38) \cdot 10^{-10}$	$0.36 \pm 0.09$
WW	n.a.	$(1.48 \pm 0.39) \cdot 10^{-10}$	$0.08 \pm 0.005$

<sup>a</sup> Adjusted R<sup>2</sup>.

## 10.6 Ozonation of gabapentin in water—Investigating reaction kinetics and transformation mechanisms of a primary amine using isotopically labeled ozone (Article V)

The following appended chapter presents investigations that were partly preparatory work related to *research objective 2 (hypotheses 2.1 and 2.2): Evaluate the operation of ozone-releasing gas-liquid membrane contactors for ISCO applications with different contaminant types and porous media effects*

This chapter has been published with some editorial changes as follows:

*Bein, Emil; Sierra Olea, Millaray; Petersen, Sophie; Drewes, Jörg E.; Hübner, Uwe (2023): Ozonation of gabapentin in water—Investigating reaction kinetics and transformation mechanisms of a primary amine using isotopically labeled ozone. In: Environ. Sci. Technol. DOI: 10.1021/acs.est.2c06709.*

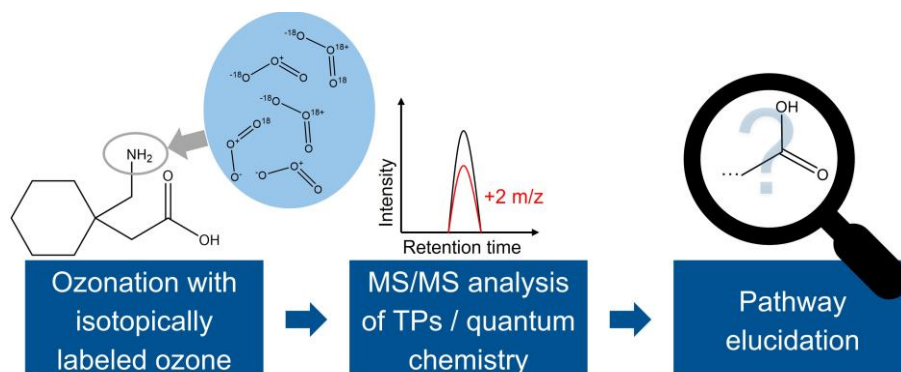
The Supporting Information for this article can be found at:

<https://pubs.acs.org/doi/abs/10.1021/acs.est.2c06709>

### 10.6.1 Abstract

Aliphatic amines are abundant micropollutants in wastewater treatment plant effluents. In order to mitigate such micropollutants, ozonation is one of the most commonly employed advanced treatment processes. Current research regarding ozone efficiency is heavily focusing on reaction mechanisms of different contaminant groups, including structures with amine moieties as reactive sites. This study analyzes pH-dependent reaction kinetics and pathways of gabapentin (GBP), an aliphatic primary amine with an additional carboxylic acid group. The transformation pathway was elucidated applying a novel approach using isotopically labeled ozone ( $^{18}\text{O}$ ) and quantum chemistry calculations. While the direct reaction of GBP with ozone is highly pH-dependent and slow at pH 7 ( $13.7 \text{ M}^{-1} \text{ s}^{-1}$ ), the rate constant of the deprotonated species ( $1.76 \cdot 10^5 \text{ M}^{-1} \text{ s}^{-1}$ ) is comparable to other amine compounds. Pathway analysis based on LC-MS/MS measurements revealed that ozonation of GBP leads to the formation of a carboxylic acid group and simultaneous nitrate formation, which was also observed in case of the aliphatic amino acid glycine. Nitrate was formed with a yield of approximately 100%. Experiments with  $^{18}\text{O}$ -labeled ozone demonstrated that the intermediate aldehyde does most likely not include any oxygen originating from ozone. Furthermore, quantum chemistry calculations did not provide an explanation for the C-N scission during GBP ozonation without ozone-involvement, although this reaction was slightly more favorable than for respective glycine and ethylamine reactions. Overall, this study contributes to a

deeper understanding of reaction mechanisms of aliphatic primary amines during wastewater ozonation.



**Keywords:** Ozone; wastewater; reaction kinetics; TOrCs; transformation products; aliphatic primary amines

## 10.6.2 Introduction

Ozonation is an effective treatment process for oxidizing various recalcitrant organic micropollutants commonly found in municipal wastewater effluents (Blackbeard et al., 2016; Hollender et al., 2009; Kovalova et al., 2013; Reungoat et al., 2010). The formation of transformation products (TPs) during wastewater ozonation is subject of ongoing research activities: Understanding toxicity and biodegradability before and after ozonation is crucial for future deployment of this technology as an advanced wastewater treatment (Muñoz et al., 2009; Stalter et al., 2010). Furthermore, data on reaction kinetics can be used to predict the removal of a large number of micropollutants in wastewater ozonation (Lee et al., 2013; Lee and von Gunten, 2016).

Reaction kinetics, transformation and biodegradability of aliphatic amines have gained increasing attention due to their wide abundance in wastewater (Hübner et al., 2015a; von Sonntag and von Gunten, 2012). Several studies have investigated the reaction of secondary or tertiary amines with ozone (Benner and Ternes, 2009a, 2009b; Knoop et al., 2018; Tekle-Röttering et al., 2016; Zimmermann et al., 2012; Zucker et al., 2018). However, incomplete information is available on the transformation of compounds containing primary amines as reactive site during wastewater ozonation. Lim et al. (2019) studied reaction kinetics and transformation of ethylamine, diethylamine and triethylamine as model compounds for aliphatic amines. Ozonation of ethylamine resulted in nitroethane as the most dominant transformation product and a reaction pathway was proposed that required 5.5 mole ozone per mole abated ethylamine. Analogously, increases of nitromethane concentrations have been observed in full scale multi-stage processes after ozonation, which may be related to the presence of

methylamine as precursor (McCurry et al., 2016; Shi et al., 2021). Nitrate formation and thus C-N scission was reported in several studies during ozonation of glycine and serine with scavenging of hydroxyl radicals, indicating a different pathway for amino acids in comparison to primary amines without carboxyl group nearby (Berger et al., 1999; de Vera et al., 2017; Le Lacheur and Glaze, 1996). In a systematic comparison, Essaïed et al. (Essaïed et al., 2021) recently measured nitrate formation during ozonation of a large variety of amine compounds to highlight the dependence of nitrate formation on structural differences. Hermes et al. (2020) screened for TPs of sitagliptin and identified a TP with a nitro group as the main product of ozonation. To the best of our knowledge, there are no other studies assessing wastewater ozonation of organic micropollutants that focus on a primary amine as location of ozone attack. Hence, there is a lack of experimental data verifying proposed pathways for ozonation of other aliphatic or aromatic primary amines. Such experimental data could help validate or improve predictive tools based on quantum chemistry, allowing an estimation of reaction kinetics and transformation pathways of ozone with compounds based on their structure (Lee et al., 2015b; Lee et al., 2017).

In this study, we investigate ozonation of the antiepileptic and analgesic drug gabapentin (GBP), one of the most abundant refractory micropollutants in wastewater treatment plant effluents and a representative of a primary amine (Bourgin et al., 2018; Kasprzyk-Hordern et al., 2009; Margot et al., 2013; Ra et al., 2020). Gulde et al. (2021) recently conducted a screening for TPs after pilot-scale ozonation of 51 micropollutants spiked to lake water. In their analysis, they were not able to identify any TPs originating from a direct reaction of ozone with GBP, but proposed a carbonyl formed from hydroxyl radical attack. Thus, little is known about the exact direct reaction mechanism of GBP with ozone in aqueous solution. In this study, we first determined pH-dependent second-order reaction rate constants of GBP with ozone. Secondly, a main TP by excluding hydroxyl radical reactions was identified. In a third step, we used ozone generated from a mixture of isotopically labeled ( $^{18}\text{O}_2$ ) and naturally abundant ( $^{16}\text{O}_2$ ) oxygen to further elucidate the transformation pathway according to a previously described concept by Sierra-Olea et al. (Sierra-Olea et al., 2023). By quantifying  $^{18}\text{O}/^{16}\text{O}$  ratios of TPs in comparison to the well characterized oxygen transfer reaction of venlafaxine (VLX) to venlafaxine N-oxide (NOV), ozone reaction pathways can be elucidated. The oxygen transfer required to form NOV must include oxygen from ozone (Zucker et al., 2018), thus making it a very suitable indicator of  $^{18}\text{O}$  concentrations in conducted experiments. Quantum chemistry calculations were performed to assess the thermodynamic potential of the proposed reactions compared to ozonation of ethylamine as primary amine without carboxyl group. Finally, we screened for the formed main TP in ozonated secondary effluent.

In summary, the aim of this study was, first, to enrich existing knowledge on ozonation of structurally different primary amines, and second, to demonstrate the potential of the used novel ozone-labelling technique for transformation pathway elucidation.

### 10.6.3 Materials and methods

#### 10.6.3.1 Chemicals and reagents

Micropollutants used in this study were of analytical quality. GBP (99.8% purity), venlafaxine (VLX, 99.98% purity), carbamazepine (CBZ, 98% purity), and primidone (PRI, 98% purity) were purchased from Sigma-Aldrich, GBP TP186 (1-Carboxycyclohexaneacetic acid, “Gabapentin related compound E”, 94% purity) and venlafaxine N-oxide (NOV, 98% purity) standards from Toronto Research Chemicals. Tertiary butanol (t-BuOH) was used at a purity of >99% (Carl Roth). Sodium thiosulfate pentahydrate, dihydrogen phosphate dihydrate, and disodium phosphate were obtained from Merck/Supelco in analytical grade. Phosphate buffer stock solution (0.5 M) at various pH was prepared by mixing sodium dihydrogen phosphate dihydrate and disodium phosphate in ultrapure water (UPW). The final pH was adjusted by adding either phosphoric acid or sodium hydroxide.

#### 10.6.3.2 Reaction kinetic experiments

Highly concentrated ozone stock solutions (1 – 1.2 mM) were produced in a cooled (4°C), stirred bubble glass container (2.5 L), where ozone was sparged continuously at ozone gas concentrations >200 g Nm<sup>-3</sup> and a gas flow rate of approximately 0.2-0.25 L min<sup>-1</sup>. Ozone was generated by a BMT 803 BT generator (BMT Messtechnik, Germany), supplied with pure oxygen (<sup>16</sup>O<sub>2</sub> ≥ 99.95%, Air Liquide). Stock solutions were taken via an integrated peristaltic pump and added to samples in stirred 1 L glass bottles or 20 mL amber vials.

Unless stated otherwise, UPW was used as solvent in all experiments. For low and neutral pH, second-order rate constants were determined by directly measuring ozone and GBP decomposition over time. Therefore, ozone stock solution was added to complete 500 mL batches to achieve initial ozone concentrations of approximately 0.2-0.25 mM. The batches completed with ozone stock solution contained 0.01 mM GBP, 10 mM phosphate buffer (pH 3, 6, 7 and 8), and 50 mM t-BuOH. Dissolved ozone concentrations were determined by the indigo method (19000 M<sup>-1</sup> cm<sup>-1</sup>) (Bader and Hoigné, 1981). Sample volumes from the ozone stock solution were taken with a pipette tip that was soaked in ozone stock solution. Samples from the batch reactor were taken by a dispenser after defined time intervals (1-20 min). Samples were directly mixed with indigo solution,



diluted to defined volumes and absorbance was measured at 610 nm by a DR6000 UV/VIS spectrophotometer (Hach, USA). Finally, a part of the dilution was mixed with internal standard and filtered through 0.22  $\mu\text{m}$  PVDF filters for GBP quantification. The slope of  $\ln([\text{GBP}]/[\text{GBP}_0])$  vs. ozone exposure equals the observed second-order reaction rate constants  $k_{\text{O}_3,\text{obs}}$ .

The higher rate constants at basic pH (10 and 11.5) were determined by a competition kinetics approach using CBZ as competitor ( $k_{\text{O}_3} = 3 \cdot 10^5 \text{ M}^{-1} \text{ s}^{-1}$  (Huber et al., 2003)) and dosing ozone at target stoichiometric ratios  $[\text{O}_3]:[\text{GBP}+\text{CBZ}]$  from 2:1 to 10:1 in 20 mL vials that were shaken immediately after mixing. The targeted initial concentration of GBP and CBZ was 2.5  $\mu\text{M}$  each. Detailed descriptions of applied methods to determine  $k_{\text{O}_3,\text{obs}}$  can be found in the Supplemental Information (SI), Text S1.

### 10.6.3.3 Identification and quantification of transformation products

Samples produced in reaction kinetic experiments at neutral pH were used for initial screening of TPs. Additionally, modified batch experiments were conducted to track TP formation over time, where we used 0.02 mM GBP, approximately 0.4 mM ozone, 5 mM phosphate buffer, and 50 mM t-BuOH in a 500 mL stirred batch. For each time step, separate samples were taken: first for measuring dissolved ozone and second for organic compounds (GBP, TP186) and nitrate. The latter samples were immediately quenched with  $\text{Na}_2\text{S}_2\text{O}_3$  solution (0.85 mM target). The final sample was taken without quenching after approximately 24 hours and prepared accordingly for subsequent analysis (Müller et al., 2017).

### 10.6.3.4 Experiments with $^{18}\text{O}$ labeling

A mixture of  $^{18}\text{O}_2$  and  $^{16}\text{O}_2$  was used to generate ozone with distinct  $^{18}\text{O}/^{16}\text{O}$  ratios in a modified ozonation system with a closed-loop configuration (Sierra-Olea et al., 2023). Briefly, for ozone generation  $\text{O}_2$  gas and  $^{18}\text{O}_2$  ( $\geq 97\%$ ) gas were used as input-gas for the ozone generator. The ozone gas was continuously bubbled into a 500 mL reactor filled with UPW (4 °C) and equipped with a gas-tight sampling port. The  $^{16}\text{O}_2/^{18}\text{O}_2$  ratio was controlled by pumping different amounts of  $^{18}\text{O}_2$  into the system that was pre-saturated with  $^{16}\text{O}_2$ . After the desired gas ratio (ca. 50%  $^{18}\text{O}_2$ ) was achieved, the system was closed, and ozone generation was initiated. The detailed protocol for producing  $^{18}\text{O}/^{16}\text{O}$  ozone stock solution is described in Sierra-Olea et al (Sierra-Olea et al., 2023). Samples were prepared with 1  $\mu\text{M}$  of GBP and 5  $\mu\text{M}$  of VLX in phosphate buffer (pH 7) with 50 mM t-BuOH as radical scavenger. 2  $\mu\text{M}$  PRI was added as ozone-resistant hydroxyl radical indicator (Real et al., 2009). Pre-defined volumes (0.83 – 3.33 mL) of heavy ozone stock solution (0.53 mM) were injected to different sample vials in randomized order (i.e., shuffled concentrations) to fill up to 20 mL final sample volumes. Samples were prepared

and analyzed after approximately 24 hours for GBP, VLX, NOV, PRI, TP186, and labeled transformation products NOV-18O (+2 m/z), and GBP TP186-18O (+2 and +4 m/z) in 0.01 dilutions (DF) for NOV and 0.1 dilutions for GBP TP186. The formation of NOV-18O compared to NOV-16O was directly used to calculate the share of  $^{18}\text{O}$  in the injected ozone solution.

For additional MS/MS scans and optimized MRM analyses to identify intermediates, samples containing 1  $\mu\text{M}$  GBP, 50 mM t-BuOH, and no phosphate buffer were conditioned with small volumes of concentrated NaOH (30%) to achieve an elevated pH (>10) and thus increase abundance of the ozone-reactive species before  $^{16}\text{O}$  or  $^{18}\text{O}/^{16}\text{O}$  ozone stock solution was added in variable amounts. Details on the procedure are provided in the SI, Text S4.

#### 10.6.3.5 *Quantum chemical calculations*

The computation of Gibbs free energy of reactions ( $\Delta G_r$ ) was performed using ORCA 4.2.0 (Neese, 2012, 2018). Geometries were first optimized with B3LYP/def2-TZVP (Weigend and Ahlrichs, 2005). Liquid phase electronic energies were computed at 298.15 K and 1 atm using M062X/6-31G\* with the SMD solvation model to take into account effects of water (Hehre et al., 1972; Marenich et al., 2009). High-resolution single point energies were obtained using DLPNO-CCSD(T) with the aug-cc-pVQZ basis set (Kendall et al., 1992). More details on the procedure for obtaining  $\Delta G_r$  can be found in the SI, Text S5.

#### 10.6.3.6 *Wastewater ozonation experiments*

Secondary effluent from the municipal WWTP Gut Marienhof, Munich, Germany (with a capacity of 1,000,000 PE), was used to observe GBP removal and a potential build-up of TPs. The previously described ozonation system was therefore modified for semi-batch experiments, where ozone is sparged into a 2.5 L sample of secondary effluent until a target dose is reached. Ozone residual is thereafter removed by sparging oxygen. The ozone gas concentration was approximately 30 g  $\text{Nm}^{-3}$  at a gas flow rate of 0.5 NL  $\text{min}^{-1}$ . The initial wastewater sample was analyzed for pH and  $\text{NO}_2^-$ , and for DOC after 0.45  $\mu\text{m}$  cellulose acetate filtration. GBP, TP186, and PRI were analyzed for all samples as described in section 10.6.3.7.

#### 10.6.3.7 *Analytical methods*

Masses of investigated organic compounds were detected by a SCIEX Triple Quad 6500 mass spectrometer (SCIEX, USA) coupled with a Knauer PLATINBLUE UHPLC (Knauer, Germany) and an XSelect HSS T3 (particle size 2.5  $\mu\text{m}$ ; 2.1 x 100 mm) column (Waters, USA) for compound separation. Quantitation was performed in scheduled MRM

mode (calibration standard concentrations 0.0025 – 10  $\mu\text{g L}^{-1}$ , two fragments) using isotope labeled standard (IS) correction for GBP and CBZ, and the calibration curve without IS correction for TP186 due to the lack of an available IS (SI, Table S4). More details on the basic principles of the LC-MS/MS method and sample preparation can be found in Müller et al. (2017) and SI, Text S2. For TP screening, MS<sup>1</sup> scans (50-350 m/z, 1,000 Da/s, see SI, Text S3) were performed in positive and negative mode on the same instrument. Additional enhanced product ion scans and MRM analyses were undertaken on a triple quadrupole linear ion trap MS (SCIEX QTrap 5500) coupled with an Agilent 1260 Infinity II HPLC (Agilent, USA) to detect intermediate TPs (SI, Text S4).

Tps containing <sup>18</sup>O in heavy ozone experiments were detected and quantified in MS/MS mode by applying the same MS settings (DP, CE, CXP) as for the respective <sup>16</sup>O compounds. The <sup>18</sup>O-labeled compounds were fragmented first to check for mass changes (+2 or +4 m/z) of compound fragments used for quantitation. The fragments used in MS/MS quantitation are summarized in Table S4. For quantitation of labeled TPs, the calibration of the respective <sup>16</sup>O TPs was used, including IS correction for NOV with VLX d6.

Nitrate was quantified using a 930 Compact IC Flex and a Metrosep A Supp 7 250/4.0 column for ion separation (Metrohm, Germany). The limit of quantification was defined as 50  $\mu\text{g/L}$ .

## 10.6.4 Results

### 10.6.4.1 Reaction kinetics

GBP has three species with only one being deprotonated at the primary amine moiety, thus a reaction with ozone is only expected for the species present in wastewater effluents at relevant concentrations at elevated pH well above 7 (Figure 62). This was also assumed for calculating species-specific rate constants and modeling the pH-dependent reaction over the entire range. Hence, reported experimental pK<sub>a</sub> values of 3.68/10.7 (Zour et al., 1992) indicate a very slow reaction in the acidic and neutral pH range, which is confirmed by results of this study for pH 3, 6 and 7 (Table 41). The observed k<sub>O<sub>3</sub>,obs</sub> of  $13.7 \pm 2 \text{ M}^{-1} \text{ s}^{-1}$  at pH 7 was more than one order of magnitude lower than  $220 \text{ M}^{-1} \text{ s}^{-1}$  estimated by Lee et al. (2014), using a quantitative structure-activity relationship (QSAR) approach. In contrast, Bourgin et al. (2018) determined k<sub>O<sub>3</sub>,obs</sub> of  $15 \text{ M}^{-1} \text{ s}^{-1}$  for GBP (pH 7), which is in close agreement with our results. The experimental values at neutral pH are very similar to the recently reported k<sub>O<sub>3</sub>,obs</sub> of 21 for ethylamine, which has a pK<sub>a</sub> of 10.6 for deprotonation of the amine moiety (Lim et al., 2019), and also for butylamine ( $8.8 \text{ M}^{-1} \text{ s}^{-1}$ ) reported for a pH of 6.7 (Pryor et al., 1984). The amino acid glycine has a pK<sub>a2</sub> of 9.78 and reacts substantially faster (ca.  $370 \text{ M}^{-1} \text{ s}^{-1}$ ) at pH 7 (Pryor et al., 1984).

Table 41: Observed second order reaction rate constants for gabapentin with ozone. The species-specific rate constant ( $k_{s3}$ ) was calculated by fitting rate constants and  $pK_{a2}$  (10.7).

pH	$k_{O_3,obs} / k_{s3} (M^{-1} s^{-1})$
3 (n=1)	No reaction observed
6 (n=1)	1.70
7 (n=3)	$13.7 \pm 2$
8 (n=1)	85.1
10 (n=2)	$2.7 \cdot 10^4 \pm 6 \cdot 10^3$
11.5 (n=1)	$1.50 \cdot 10^5$
Deprotonated species	$1.76 \cdot 10^5$

A species-specific rate constant for the fully deprotonated species ( $k_{s3} = 1.76 \cdot 10^5 M^{-1} s^{-1}$ ) was estimated using data points at pH 6, 7, 8, 10 and 11.5 (Figure 62). Data and model agree satisfyingly, however, values for pH 6 and 7 are slightly overestimated with this model fit ( $3.5 M^{-1} s^{-1}$  and  $35.1 M^{-1} s^{-1}$  for pH 6 and 7) and the fit deviates more substantially for pH 8 ( $351 M^{-1} s^{-1}$ ). This is related to the strong impact of the high values in basic pH on the model function (SI, Text S1). Deviations by a factor of 2-3 are reasonable and frequently observed in such experiments, the strong dependence of the fit on the higher  $pK_{a2}$  value may add some uncertainty as it was not confirmed experimentally in this study (von Sonntag and von Gunten, 2012).  $k_{s3}$  is higher than the value estimated by Lim et al. (2019) for ethylamine ( $9.3 \cdot 10^4 M^{-1} s^{-1}$ ) and  $1.3 \cdot 10^5 M^{-1} s^{-1}$  for glycine (Hoigné and Bader, 1983b), but very similar to the computed value  $1.8 \cdot 10^5 M^{-1} s^{-1}$  for GBP (Lee et al., 2014). Their comparably higher value of  $220 M^{-1} s^{-1}$  for neutral pH might be related to different fitting methods. The slow reaction of GBP with ozone indicates that removal during wastewater ozonation at neutral pH is mostly driven by radical-reactions, not direct ozonolysis (Lim et al., 2022). This is reflected in experimental findings in full-scale ozonation after biological treatment of wastewater, where 55% and 63% relative removal could be achieved at typical doses of 0.54 and 0.67 mg  $O_3$ /mg DOC (Bourgin et al., 2018), compared to ozone-resistant compounds like iopromide ( $k_{OH} = 3.3 \cdot 10^9 M^{-1} s^{-1}$  (Huber et al., 2003)) or primidone ( $k_{OH} = 6.7 \cdot 10^9 M^{-1} s^{-1}$  (Real et al., 2009)) that were removed by 53 and 70% at 0.67 mg  $O_3$  mgDOC $^{-1}$  in the same study.

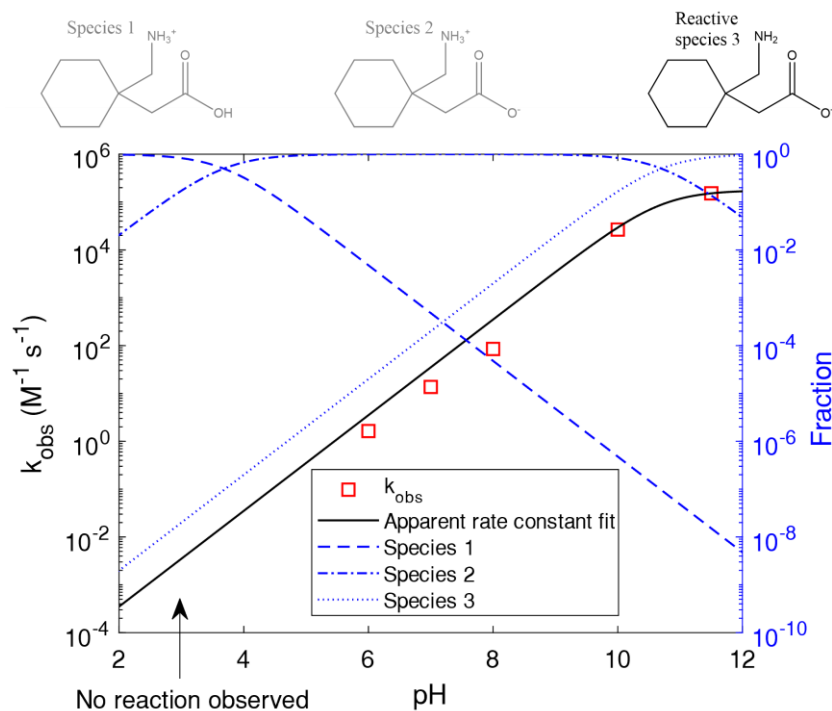


Figure 62: Combined plot of the model fit to determine the species-specific reaction rate constant of deprotonated reactive species 3 (black line), the dissociation of GBP (blue color, y-axis on the right), assuming  $\text{pK}_{\text{a}1} = 3.68$  and  $\text{pK}_{\text{a}2} = 10.7$ , and observed reaction rate constants at different pH values (red squares).

#### 10.6.4.2 Transformation product identification and quantification

In previous transformation product studies, oxidation of the amine moiety followed differing mechanisms for primary amines and amino acids (Berger et al., 1999; de Vera et al., 2017; Lim et al., 2019). Possible pathway alternatives are displayed for the transformation of GBP in Figure 63, leading to potential final products TP201 and TP186. All displayed pathways are initiated by two hydroxylation reactions (I and II), followed by a loss of H<sub>2</sub>O (III), which gives rise to a tautomerized oxime/nitroso-GBP intermediate. Ozone attack at the nitroso intermediate would directly result in a stable TP with a nitro moiety (reaction VI, TP201). This pathway has been described for the ozonation of ethylamine (Lim et al., 2019) and sitagliptin (Hermes et al., 2020). In contrast, TP186 (carboxy moiety) would be formed as result of de-hydration of the di-hydroxylated intermediate, which produces an oxime intermediate (reaction III), and then reacts further. For these subsequent steps exist different possibilities (reactions IVa and b). The oxime intermediate could be transformed to an aldehyde (TP170) either with water or with ozone in a Criegee-type reaction, as the oxime group is reportedly prone to ozone attack (Erickson et al., 1969). Erickson et al. (Erickson et al., 1969), however, conducted experiments in organic solvent (CH<sub>2</sub>Cl<sub>2</sub>), which was cooled to low temperatures (-78°C). Hence, there is a lack of knowledge on the ozonation of the oxime moiety under conditions relevant for water treatment. The removed nitrogen would be

quickly oxidized further to nitrate regardless, as observed for various amino acids (Berger et al., 1999; de Vera et al., 2017). The aldehyde (TP170) is subsequently oxidized to a carboxylic acid (TP186) with or without ozone involvement. Direct ozonation of aldehydes is energetically less likely but also mechanistically possible (Voukides et al., 2009). Typical second order reaction rate constants for aldehydes with ozone are  $1.5 \text{ M}^{-1} \text{ s}^{-1}$  (acetaldehyde) and  $2.5 \text{ M}^{-1} \text{ s}^{-1}$  (benzaldehyde) (Hoigné and Bader, 1983a). Another possibility that was recently discussed is the slow reaction of ozone with carbanion (i.e., negatively charged carbon), which could be present in a conjugate base of the comparably stable nitro TP201 (Lim et al., 2022). This proposed reaction would also lead to TP170 and, finally, to nitrate and TP186, however, experimental validation for such reaction mechanism with ozone is – to our knowledge – missing so far.

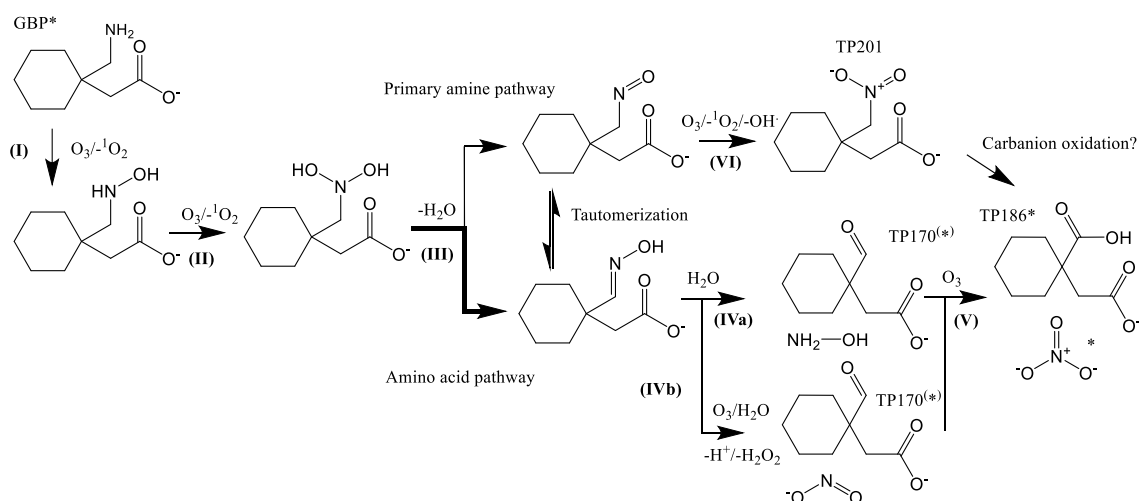


Figure 63: Investigated transformation pathways for the reaction of gabapentin with ozone, adapted from Lim et al. (Lim et al., 2019; Lim et al., 2022). All GBP-related compounds are displayed deprotonated. Compounds marked by an asterisk were detected and quantified, masses and fragmentation for suspected TP170 could be detected, but not confirmed by a standard.

In our initial screening, TP201 was not detected. Instead, one peak at approximately  $m/z$  185 was identified in  $\text{MS}^1$  scans (negative ESI) of ozonated samples and investigated in detail. Fragmentation resulted in two noteworthy fragments at  $m/z$  141 and 167, which corresponded to Mass Bank Record EQ331254 of 1-carboxycyclohexaneacetic acid (MassBank, 2015). Further testing using LC-MS/MS with a standard confirmed the identification of the proposed TP186 (retention time and fragmentation pattern). Subsequently, we quantified formation of TP186 and nitrate over time in order to investigate the extent of nitrogen detachment (Figure 64). The reacted GBP was stoichiometrically transformed to nitrate ( $110.8 \pm 8.4 \%$ ) after the reaction terminated, confirming that the reaction pathway must include C-N scission in any case.

Simultaneous to nitrate formation, TP186 was formed at a lower but still high yield of  $53.9 \pm 1.7 \%$ . However, due to the lacking internal standard, the exact yield might deviate considerably, and other products may be formed in smaller amounts that are not covered by the applied analytical approaches. A plausible fragmentation pattern of TP170 could be detected with enhanced product ion scans using a QTrap 5500 MS, and its formation without concentration increase over time was confirmed for neutral pH experiments using MRM analysis, suggesting it could be an intermediate in the reaction (Text S4, section 10.6.4.4). It is also noteworthy that 0.4 mM ozone got depleted almost completely after 25 min in presence of 0.02 mM GBP, which is a much higher consumption than implied by any of the proposed pathways. This could be caused by follow-up reactions of hydroxylamine with ozone, where high ozone consumptions at neutral pH were reported before (Yang et al., 2016).

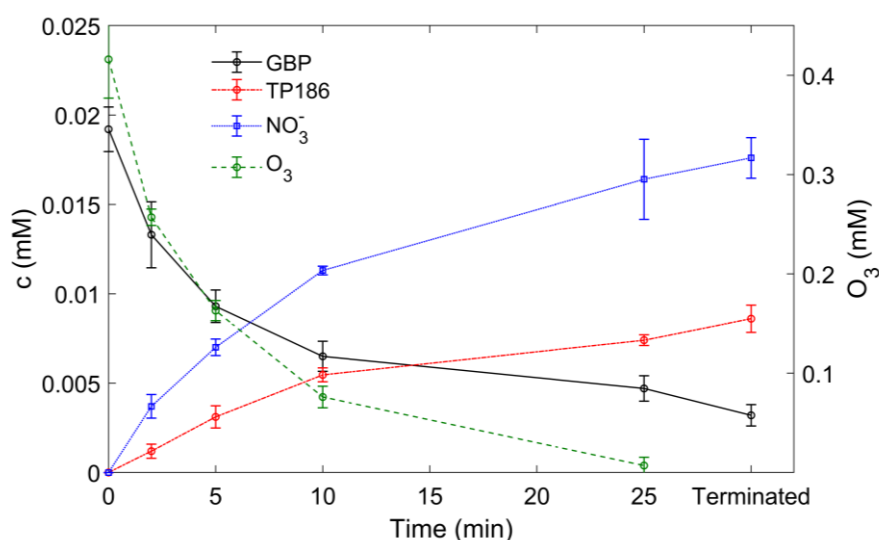


Figure 64: Formation of NO<sub>3</sub><sup>-</sup> and TP186 during ozonation of GBP (compound concentrations on the left y-axis, dissolved ozone concentration on the right y-axis, n=3).

#### 10.6.4.3 Oxidation experiments utilizing <sup>18</sup>O labeling

The transformation pathway, specifically the potential reaction of the oxime (reaction IV), was elucidated further by conducting experiments with isotopically labeled oxygen, where NOV was used to measure the <sup>18</sup>O:<sup>16</sup>O ratio. Due to the fast reaction of VLX with ozone, the amount of NOV peaked at low ozone dose and subsequently decreased due to secondary reactions ( $k_{O_3} = 310 \text{ M}^{-1} \text{ s}^{-1}$  (Zucker et al., 2018)) of NOV with ozone (Figure 65a). However, both NOV-18O and NOV-16O could be detected in all ozonated samples at stable ratios ( $48.5\% \pm 1.4\%$  NOV-18O), indicating equal contributions of both isotopes in the ozone stock solution (Figure 65b). GBP TP186 was formed similar as in <sup>16</sup>O experiments but at smaller amounts due to the competing reactions of VLX and GBP, where VLX reacts much faster ( $1.3 \cdot 10^3$  (Zucker et al., 2018) vs.  $13.7 \text{ M}^{-1} \text{ s}^{-1}$ ). PRI

concentrations did not change substantially (SI, Table S8), thus major reactions of hydroxyl radicals can be excluded that could, for example, lead to an attack on the GBP cyclohexane ring (Gulde et al., 2021). The labeled GBP TP186-18O ( $m/z$  187.1) was formed at a share of  $40.8\% \pm 1.4\%$ , which is lower than injected ozone indicated from NOV analysis. Interestingly, GBP TP186 containing two  $^{18}\text{O}$  atoms could not be detected in a significant amount, showing that one of the reactions leading to TP186 did not involve oxygen transfer from ozone. The  $^{18}\text{O}/^{16}\text{O}$  ratio did not fluctuate largely among the randomized samples (Figure 4b and Figure S12, SI). Additionally, Sierra-Olea et al. (Sierra-Olea et al., 2023) found a good correlation of  $^{18}\text{O}_2/^{16}\text{O}_2$  ratios determined by NOV formation with  $\text{O}_2/\text{N}_2$  ratios simulating the two oxygen isotopes in control experiments ( $R^2=0.96$ ). Thus, the observed phenomenon that there is a lower amount of GBP TP186-18O formed compared to NOV-18O seems to be systematic and related to reactions and not analytical issues. Nevertheless, the overall finding implies that one of the two oxygen attachments (reactions IV and V in Figure 2) originates from a direct ozone reaction.

We therefore tried to identify the structure of TP170 that is suspected to be an intermediate of the GBP/ $\text{O}_3$  reaction. Consequently, the presence of TP170-18O would indicate if the aldehyde is a result of direct ozonation of the oxime intermediate (Figure 63, reaction (IVb) or attack at the carbanion). To generate samples for aldehyde detection, 20 mL GBP solutions were ozonated at elevated pH (conditioned with NaOH) that contained 50 mM t-BuOH and were not buffered. At elevated pH, the reactive GBP species is present in excess and quickly consumes added ozone. Therefore, intermediates are supposedly available in higher concentrations. We detected a compound with  $m/z$  169 and one intense fragment of  $m/z$  125 in negative ESI, which agrees with the expected  $m/z$  of aldehyde TP170 (SI, Text S4). Direct injection and compound optimization was performed, and another fragment ( $m/z$  151) was identified that was not seen in any LC-MS/MS analysis of TP170. The compound's presence cannot be verified with the available analytical methods, but the fragmentation is plausible, as  $m/z$  125 and  $m/z$  151 represent losses of  $\text{CO}_2$  and  $\text{H}_2\text{O}$  also observed as main losses in the MS/MS spectrum for TP186, and TP170 differs from TP186 by one oxygen.

In a second step, we searched for an  $^{18}\text{O}$  aldehyde with  $m/z$  171 in negative ESI and a fragment of  $m/z$  127, as the fragment of the  $^{18}\text{O}$  compound should also be labeled according to the proposed fragmentation. However, such a compound ( $m/z$  171/127 and also 171/125) was not found at the same retention time as the present suspected TP170-16O (SI, Figures S5-S7). This implies that the oxygen source to form an aldehyde moiety in TP170 is not ozone and that the nitrogen removal from the oxime intermediate most likely proceeds via reaction (IVa). The alternative reaction, proposed by McCurry et al. (McCurry et al., 2016) and Lim et al. (Lim et al., 2022), where ozone attacks the carbanion, is less likely as major pathway for GBP, as this would also result in labeling



of the aldehyde. The results further indicate that the final oxidation of the aldehyde to the carboxylic compound (TP186) must involve an oxygen transfer reaction from ozone. In addition, we can exclude oxygen transfer from dissolved oxygen, as isotopically labeled dissolved oxygen is present in different amounts in the samples, while the ratio of  $^{18}\text{O}/^{16}\text{O}$  TPs is independent of the amount of stock solution added (SI, Figure S12). Generally, aldehydes and carboxylic acids both tend to accumulate in ozonated wastewater due to negligible reactivity with ozone (Liu et al., 2015). However, further oxidation for instance of a CBZ TP with aldehyde moiety by direct ozone attack was observed in the past (Hübner et al., 2014). This demonstrates that oxidation to a carboxylic acid can occur with ozone involvement. Overall, although gathered experimental data supports that the aldehyde TP170 in fact is oxidized to TP186 via ozone attack, final experimental evidence could not be generated with the used experimental and analytical tools.

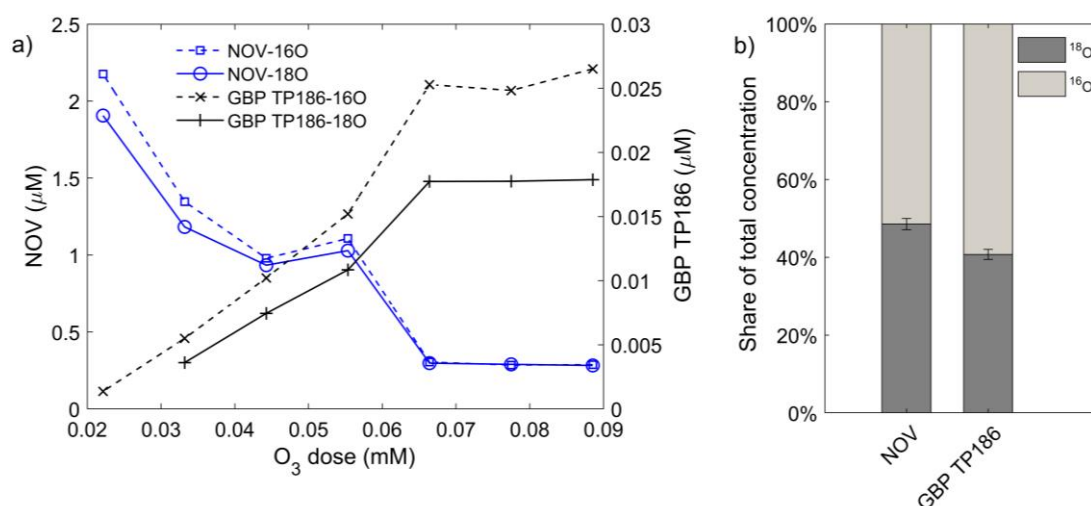


Figure 65: a) Formation of both, labeled and unlabeled NOV and GBP TP186 as function of ozone dose in  $^{18}\text{O}$  experiments. The concentration of GBP TP186- $^{18}\text{O}$  for the lowest ozone dose was below the LOQ. b) Average share of labeled and not labeled NOV and GBP TP186 of the respective total concentration (n=7 for NOV, n=6 for TP186).

#### 10.6.4.4 Nitrate formation mechanisms

Recent findings suggest that the nitrate yield in ozonation of primary amines negatively correlates with the  $\text{pK}_a$  of the amine moiety, which in turn is affected by neighboring functional groups (Essaïed et al., 2021). The highest nitrate yields were observed for amino acids with lower  $\text{pK}_a$  (<10) of the  $-\text{NH}_2$  group. Therefore, the observed complete mineralization of GBP to nitrate is surprising, as its amine  $\text{pK}_a$  of 10.7 is considerably higher and other functional groups than single carbon bonds are three carbon atoms away. The extent of nitrate formation and the strong presence of TP186 indicate that the reaction could – despite structural differences – follow a similar pathway as previously proposed for the ozonation of the amino acid glycine (C-N bond scission),

whereas ozonation of other primary amines (e.g., sitagliptin, ethylamine,  $\beta$ -alanine) predominantly leads to the formation of nitro-groups (Hermes et al., 2020; Lim et al., 2019).

Lim et al. (2019) proposed that the products of (III) in Figure 63 are a nitroso-oxime tautomeric pair, where the oxime tautomer drives the further oxidation in the case of amino acids and, conversely, the nitroso tautomer drives the further oxidation in the case of primary amines without carboxy group. The difference between ethylamine and GBP in reactions with ozone is therefore investigated further using quantum chemistry computations of Gibbs reaction energies for reactions (III), (IVa), (IVb) and (VI) in the hypothesized GBP pathway (Table 42). A part of the ethylamine pathway as proposed by Lim et al. (2019) was computed, which is analogous to reactions (III), (IVa and b) and (VI) (SI, Figure S11). Selected reactions were also computed for glycine to enable comparison to amino acids (Table 42).  $\Delta G_r$  is  $-21.1$  and  $-34.6$  kcal mol<sup>-1</sup> for the reaction of the amine intermediate with two hydroxyl groups to the nitroso and oxime intermediate in the GBP pathway, and  $-20.7$  and  $-39.5$  kcal mol<sup>-1</sup> for the same reactions in the ethylamine pathway. An energetic shift towards the oxime tautomer in case of GBP is therefore not visible, and  $\Delta G_r$  is similar for all three pathways. This is generally expected, as oximes are known to be more stable than the respective nitroso tautomer (Long et al., 2001). The previous study obtained a difference of  $15.8$  kcal mol<sup>-1</sup> for the nitroso-oxime tautomerism shown in Figure S11 (SI), which also includes solvation effects, and is similar to  $18.8$  kcal mol<sup>-1</sup> obtained in this study. A comparison of different tautomers is provided in the SI, Table S6. An energetic difference in the two pathways, however, becomes visible if we directly compare reaction (IVa) of GBP and ethylamine pathways.  $\Delta G_r$  for the reaction of the ethylamine oxime intermediate to acetaldehyde and hydroxylamine (NH<sub>2</sub>-OH) ( $+15.8$  kcal mol<sup>-1</sup>) and the analogous reaction in the GBP pathway are both endergonic ( $+7.1$  kcal mol<sup>-1</sup>, Table 42), with the latter one closer to the threshold of 0.  $\Delta G_r$  of the reaction of the GBP oxime intermediate with H<sub>2</sub>O and H<sup>+</sup>, leading to protonated hydroxylamine (<sup>+</sup>H<sub>3</sub>N-OH), is  $-8.2$  kcal mol<sup>-1</sup>, thus negative (SI, Text S5). <sup>+</sup>H<sub>3</sub>N-OH makes ca. 8% of hydroxylamine at neutral pH.  $\Delta G_r$  is positive for the analogous reaction of the ethylamine oxime intermediate to acetaldehyde ( $+0.4$  kcal mol<sup>-1</sup>, SI, Table S7), and also for the glycine oxime intermediate ( $+1.6$  kcal mol<sup>-1</sup>). Reaction (VI) is clearly exergonic in ethylamine and GBP pathways. The proposed Criegee-type alternative pathway (IVb) is also exergonic in both cases.  $\Delta G_r$  results indicate an energetic favorability of reaction (VI) and thus direct ozonation of GBP and ethylamine. However, the overwhelming presence of H<sub>2</sub>O as reaction partner compared to O<sub>3</sub> could make the contribution of (IVa) dominant in the GBP pathway. In addition, the labeled aldehyde TP170 (m/z 171) was not found which makes both, a Criegee-type mechanism but also a reaction with the carbanion more unlikely (section 10.6.4.2).

Absolute results of the quantum chemistry calculations should be interpreted with care, mainly because of the difficulties in correctly describing ozone as multireference system, and also singlet oxygen (here treated as ground state oxygen) with the employed computational approaches (Lim et al., 2019). However, similarities between GBP and glycine that could explain a common reaction pattern could not be confirmed by quantum chemistry in a direct comparison of individual reactions. We cannot exclude that carbanion oxidation is relevant for the ozonation of glycine and other amino acids, finally leading to nitrate.

Table 42: Results of quantum chemical calculations for GBP, ethylamine, and glycine, grouped by reactions of the discussed primary amine / amino acid pathways.

Reaction	Sum formula (generalized)	$\Delta G_r$ of different pathways (kcal mol <sup>-1</sup> )		
		GBP	Ethylamine	Glycine
(III)	$R-N-(OH)_2 \rightarrow R=N-OH + H_2O$	-21.1	-20.7	-20.9
(III)	$R-N-(OH)_2 \rightarrow R=N=O + H_2O$	-34.6	-39.5	-39.9
(IVa)	$R=N-OH + H_2O \rightarrow R=O + H_2N-OH$	+7.1	+15.8	+17.0
(IVb)	$R=N-OH + O_3 + H_2O \rightarrow R=O + NO_2^- + H^+ + H_2O_2$	-60.5	-51.9	n.a.
(VI)	$R-N=O + O_3 \rightarrow R-NO_2 + {}^1O_2^a$	-41.2	-43.7	n.a.

<sup>a</sup> Singlet oxygen here calculated as ground state oxygen, see Text S5 for further information.

#### 10.6.4.5 Relevance for the aquatic environment

Gulde et. al. (2021) screened for GBP TPs in lake water spiked with micropollutants and subsequently treated with ozone. However, they identified neither a TP with a nitro group, nor any other TP resulting from a direct ozone attack. We also checked for the presence of TP186 after the ozonation of secondary effluent (SI, Text S7) in semi-batch experiments. The specific ozone doses were ranging from 0.44 to 1.05 mgO<sub>3</sub> mgDOC<sup>-1</sup> (Table 43). The WWTP effluent sample had a DOC of 5.8 mg L<sup>-1</sup> and a pH of 7.1. Nitrite was below 0.015 mg N L<sup>-1</sup>. Applied ozone doses were determined by a recorded mass balance of ozone entering and leaving the semi-batch system after the system had been sparged with oxygen, as described in Müller et al. (2019). While GBP was removed from 48 up to 89% in these experiments, TP186 could not be found in any of these environmental samples (LOQ = 25 ng L<sup>-1</sup>). This is not surprising, as the direct reaction of GBP with ozone is very slow in these pH conditions. We estimated the ozone exposure with the specific ozone dose using an empirical equation in order to calculate the contribution of direct ozone reactions to GBP removal (SI, Text S8, Table S9). This results in a theoretical formation of up to 47 ng L<sup>-1</sup> of TP186 in the conducted wastewater ozonation experiments. As hydroxyl radical formation is not suppressed in this water matrix, it is likely that TP186 is formed, but also degraded at the same time by radical reactions, which cannot be estimated here due to the unknown reactivity of TP186 with

OH. The removal of ozone-resistant PRI is very similar to GBP, which also supports the assumption that only a small fraction of GBP was removed by direct ozone-reactions. It must be noted here that the ozone exposure calculation method is based on experimental data with high variability for different water samples, thus can only be seen as an estimation to assess the magnitude of TP186 formation and cannot replace an actual measurement of ozone exposures (Lee and von Gunten, 2016).

Although TP186 was not found in real ozonated wastewater, it may become more relevant in wastewater with higher pH. Furthermore, GBP is an interesting compound to study the aforementioned differences within the group of primary amines. Ozonation of any other compound with a similar set of functional groups (for example the drug pregabalin) can potentially result in similar TPs. A slightly different speciation of the ozone-reactive amine moiety can fundamentally enhance the reactivity with ozone at neutral pH and, therefore, TPs of such compounds could be found in the environment after ozonation, especially if ozone exposures are high. The  $^{18}\text{O}$ -labeling technique of ozone shows strong potential for future investigations to gain experimental data on carbanion and oxime oxidation and thus confirm transformation pathways of primary amines and amino acids and can also be used for many different moieties. Especially fast ozone reactions of larger organic molecules may be easier to analyze due to the better identification of unique fragmentation patterns.

Table 43: Removal of TOrCs in wastewater ozonation experiments.

O <sub>3</sub> dose (mg L <sup>-1</sup> )	Specific O <sub>3</sub> dose (mgO <sub>3</sub> mgDOC <sup>-1</sup> )	GBP (ng L <sup>-1</sup> )	Removal (GBP)	PRI (ng L <sup>-1</sup> )	Removal (PRI)	GBP (ng L <sup>-1</sup> )	TP186 (ng L <sup>-1</sup> )	Estimated formation of GBP TP186 (ng L <sup>-1</sup> )
0	0	659	0%	104	0%	<LOQ	0	
2.56	0.44	342	48%	45	57%	<LOQ	5	
2.80	0.48	314	52%	36	66%	<LOQ	7	
3.73	0.64	194	71%	28	73%	<LOQ	15	
6.09	1.05	80	88%	<LOQ	n.a.	<LOQ	47	

### 10.6.5 Supporting information

Description of the determination of second order reaction rate constants; analytical methods; transformation product identification descriptions and MS-spectra; quantum chemical calculations; data of labeled ozone experiments; description of the wastewater treatment plant; procedure for the calculation of ozone exposures in wastewater.

### **10.6.6 Acknowledgement**

This study was funded by the German Federal Ministry of Education and Research (BMBF) and the German Research Foundation (DFG), grant numbers 02WIL1523 and 428639365 (GZ: HU 2699/1-1). We would like to thank Dr. Oliver Knoop, Dr. Ignacio Sottorff, and Dr. Johann Müller for their advice, Danika Ahoor for her help on isotopically labeled ozone experiments, Christina Kordetzky for her help on wastewater ozonation experiments, and Myriam Reif and Wolfgang Schröder for analyzing DOC and nitrate. We would also like to thank the anonymous reviewers for their helpful comments.

**REFERENCES**

- Acero, J.L., von Gunten, U., 2001. Characterization of Oxidation processes: ozonation and the AOP  $O_3/H_2O_2$ . *J. Am. Water Works Assoc.* 93 (10), 90–100.
- Adamson, D.T., Anderson, R.H., Mahendra, S., Newell, C.J., 2015. Evidence of 1,4-dioxane attenuation at groundwater sites contaminated with chlorinated solvents and 1,4-dioxane. *Environ. Sci. Technol.* 49 (11), 6510–6518.
- Adamson, D.T., Mahendra, S., Walker, K.L., Rauch, S.R., Sengupta, S., Newell, C.J., 2014. A Multisite Survey To Identify the Scale of the 1,4-Dioxane Problem at Contaminated Groundwater Sites. *Environ. Sci. Technol. Lett.* 1 (5), 254–258.
- Agarwal, N., Semmens, M.J., Novak, P.J., Hozalski, R.M., 2005. Zone of influence of a gas permeable membrane system for delivery of gases to groundwater. *Water Resour. Res.* 41 (5), 1.
- Ahmed, T., Semmens, M.J., 1992. Use of sealed end hollow fibers for bubbleless membrane aeration: experimental studies. *J. Membr. Sci.* 69 (1-2), 1–10.
- Ahn, Y.-Y., Bae, H., Kim, H.-I., Kim, S.-H., Kim, J.-H., Lee, S.-G., Lee, J., 2019. Surface-loaded metal nanoparticles for peroxymonosulfate activation: Efficiency and mechanism reconnaissance. *Appl. Catal. B* 241, 561–569.
- Ahn, Y.-Y., Yun, E.-T., Seo, J.-W., Lee, C., Kim, S.H., Kim, J.-H., Lee, J., 2016. Activation of Peroxymonosulfate by Surface-Loaded Noble Metal Nanoparticles for Oxidative Degradation of Organic Compounds. *Environ. Sci. Technol.* 50 (18), 10187–10197.
- Alapi, T., Dombi, A., 2007. Comparative study of the UV and UV/VUV-induced photolysis of phenol in aqueous solution. *J. Photochem. Photobiol., A* 188 (2-3), 409–418.
- Amirache, L., Barka-Bouaifel, F., Borthakur, P., Das, M.R., Ahouari, H., Vezin, H., Barras, A., Ouddane, B., Szunerits, S., Boukherroub, R., 2021. Cobalt sulfide-reduced graphene oxide: An efficient catalyst for the degradation of rhodamine B and pentachlorophenol using peroxymonosulfate. *J. Environ. Chem. Eng.* 9 (5), 106018.
- Andaluri, G., Suri, R., 2017. Removal of 1,4-Dioxane and Volatile Organic Compounds from Groundwater Using Ozone-Based Advanced Oxidation Process. *Ozone: Sci. Eng.* 39 (6), 423–434.
- Anipsitakis, G.P., Dionysiou, D.D., 2004. Radical generation by the interaction of transition metals with common oxidants. *Environ. Sci. Technol.* 38 (13), 3705–3712.

- Atchariyawut, S., Phattaranawik, J., Leiknes, T., Jiraratananon, R., 2009. Application of ozonation membrane contacting system for dye wastewater treatment. *Sep. Purif. Technol.* 66 (1), 153–158.
- Baawain, M.S., Gamal El-Din, M., Smith, D.W., Mazzei, A., 2011. Hydrodynamic Characterization and Mass Transfer Analysis of an In-Line Multi-Jets Ozone Contactor. *Ozone Sci. Eng.* 33 (6), 449–462.
- Bader, H., Hoigné, J., 1981. Determination of ozone in water by the indigo method. *Water Res.* 15 (4), 449–456.
- Bahram, M., Bro, R., Stedmon, C., Afkhami, A., 2006. Handling of Rayleigh and Raman scatter for PARAFAC modeling of fluorescence data using interpolation. *J. Chemometrics* 20 (3-4), 99–105.
- Baker, R.W., 2012. *Membrane technology and applications*, 3rd ed. Wiley, Chichester.
- Bamperng, S., Suwannachart, T., Atchariyawut, S., Jiraratananon, R., 2010. Ozonation of dye wastewater by membrane contactor using PVDF and PTFE membranes. *Sep. Purif. Technol.* 72 (2), 186–193.
- Bazhenov, S.D., Bildyukevich, A.V., Volkov, A.V., 2018. Gas-Liquid Hollow Fiber Membrane Contactors for Different Applications. *Fibers* 6 (4), 76–117.
- Bein, E., Seiwert, B., Reemtsma, T., Drewes, J.E., Hübner, U., 2023a. Advanced oxidation processes for removal of monocyclic aromatic hydrocarbon from water: Effects of O<sub>3</sub>/H<sub>2</sub>O<sub>2</sub> and UV/H<sub>2</sub>O<sub>2</sub> treatment on product formation and biological post-treatment. *J. Hazard. Mater.* 188 (2-3), 131066.
- Bein, E., Sierra Olea, M., Petersen, S., Drewes, J.E., Hübner, U., 2023b. Ozonation of Gabapentin in Water—Investigating Reaction Kinetics and Transformation Mechanisms of a Primary Amine Using Isotopically Labeled Ozone. *Environ. Sci. Technol.* 57 (47), 18825–18833.
- Bein, E., Zucker, I., Drewes, J.E., Hübner, U., 2021. Ozone membrane contactors for water and wastewater treatment: A critical review on materials selection, mass transfer and process design. *Chem. Eng. J.* 413 (18), 127393.
- Benner, J., Salhi, E., Ternes, T., von Gunten, U., 2008. Ozonation of reverse osmosis concentrate: Kinetics and efficiency of beta blocker oxidation. *Water Res.* 42 (12), 3003–3012.
- Benner, J., Ternes, T.A., 2009a. Ozonation of metoprolol: elucidation of oxidation pathways and major oxidation products. *Environ. Sci. Technol.* 43 (14), 5472–5480.
- Benner, J., Ternes, T.A., 2009b. Ozonation of propranolol: formation of oxidation products. *Environ. Sci. Technol.* 43 (13), 5086–5093.

- Berdichevsky, Y., Khandurina, J., Guttman, A., Lo, Y.-H., 2004. UV/ozone modification of poly(dimethylsiloxane) microfluidic channels. *Sens. Actuators, B* 97 (2-3), 402–408.
- Berger, P., Karpel Vel Leitner, N., Doré, M., Legube, B., 1999. Ozone and hydroxyl radicals induced oxidation of glycine. *Water Res.* 33 (2), 433–441.
- Bergman, T.L., Incropera, F.P., DeWitt, D.P., Lavine, A.S., 2011. *Fundamentals of Heat and Mass Transfer*. Wiley, Hoboken, N.J.
- Berry, M., Taylor, C., King, W., Chew, Y., Wenk, J., 2017. Modelling of Ozone Mass-Transfer through Non-Porous Membranes for Water Treatment. *Water* 9 (7), 452–469.
- Biesinger, M.C., Payne, B.P., Grosvenor, A.P., Lau, L.W.M., Gerson, A.R., Smart, R.S.C., 2011. Resolving surface chemical states in XPS analysis of first row transition metals, oxides and hydroxides: Cr, Mn, Fe, Co and Ni. *Appl. Surf. Sci.* 257 (7), 2717–2730.
- Biń, A.K., Duczmal, B., Machniewski, P., 2001. Hydrodynamics and ozone mass transfer in a tall bubble column. *Chem. Eng. Sci.* 56 (21-22), 6233–6240.
- Blackbeard, J., Lloyd, J., Magyar, M., Mieog, J., Linden, K.G., Lester, Y., 2016. Demonstrating organic contaminant removal in an ozone-based water reuse process at full scale. *Environ. Sci.: Water Res. Technol.* 2 (1), 213–222.
- Borovik, A., Karanikola, V., Zucker, I., 2020. Platform selection of engineered nanomaterials for water decontamination applications. *Environ. Sci.: Nano* 7 (12), 3641–3654.
- Bourgin, M., Beck, B., Boehler, M., Borowska, E., Fleiner, J., Salhi, E., Teichler, R., von Gunten, U., Siegrist, H., McArdell, C.S., 2018. Evaluation of a full-scale wastewater treatment plant upgraded with ozonation and biological post-treatments: Abatement of micropollutants, formation of transformation products and oxidation by-products. *Water Res.* 129, 486–498.
- Broséus, R., Vincent, S., Aboulfadl, K., Daneshvar, A., Sauvé, S., Barbeau, B., Prévost, M., 2009. Ozone oxidation of pharmaceuticals, endocrine disruptors and pesticides during drinking water treatment. *Water Res.* 43 (18), 4707–4717.
- Buffle, M.-O., von Gunten, U., 2006. Phenols and Amine Induced HO • Generation During the Initial Phase of Natural Water Ozonation. *Environ. Sci. Technol.* 40 (9), 3057–3063.



- Bush, T.M., Hardwick, S., Wikol, M., 1998. Overcoming the barriers to cleaning with bubble-free ozonated de-ionized water, in: Goodman, J. (Ed.), IEEE SEMI Advanced Semiconductor Manufacturing Conference, pp. 226–229.
- Bustillo-Lecompte, C.F., Kakar, D., Mehrvar, M., 2018. Photochemical treatment of benzene, toluene, ethylbenzene, and xylenes (BTEX) in aqueous solutions using advanced oxidation processes: Towards a cleaner production in the petroleum refining and petrochemical industries. *J. Clean. Prod.* 186 (2), 609–617.
- Buxton, G.V., Greenstock, C.L., Helman, W.P., Ross, A.B., 1988. Critical Review of rate constants for reactions of hydrated electrons, hydrogen atoms and hydroxyl radicals ( $\cdot\text{OH}/\cdot\text{O}-$ ) in Aqueous Solution. *JPCRD* 17 (2), 513–886.
- Cao, B., Nagarajan, K., Loh, K.-C., 2009. Biodegradation of aromatic compounds: current status and opportunities for biomolecular approaches. *Appl. Microbiol. Biotechnol.* 85 (2), 207–228.
- Cashman, M., Ball, R., Lewis, T., Boving, T.B., 2022. Peroxone activated persulfate oxidation of 1,4-Dioxane under column scale conditions. *J. Contam. Hydrol.* 245, 103937.
- Cashman, M.A., Kirschenbaum, L., Holowachuk, J., Boving, T.B., 2019. Identification of hydroxyl and sulfate free radicals involved in the reaction of 1,4-dioxane with peroxone activated persulfate oxidant. *J. Hazard. Mater.* 380, 120875.
- Cassidy, D., Northup, A., Hampton, D., 2009. The effect of three chemical oxidants on subsequent biodegradation of 2,4-dinitrotoluene (DNT) in batch slurry reactors. *J. Chem. Technol. Biotechnol.* 84 (6), 820–826.
- Chaplin, B.P., Schnobrich, M.R., Widdowson, M.A., Semmens, M.J., Novak, P.J., 2009. Stimulating In Situ Hydrogenotrophic Denitrification with Membrane-Delivered Hydrogen under Passive and Pumped Groundwater Conditions. *J. Environ. Eng.* 135 (8), 666–676.
- Chapman, S.W., Byerley, B.T., Smyth, D.J.A., Mackay, D.M., 1997. A Pilot Test of Passive Oxygen Release for Enhancement of In Situ Bioremediation of BTEX-Contaminated Ground Water. *Ground Water Monit. Remediat.* 17 (2), 93–105.
- Charbonnet, J.A., Duan, Y., van Genuchten, C.M., Sedlak, D.L., 2018. Chemical Regeneration of Manganese Oxide-Coated Sand for Oxidation of Organic Stormwater Contaminants. *Environ. Sci. Technol.* 52 (18), 10728–10736.
- Chen, B.-R., Sun, W., Kitchaev, D.A., Mangum, J.S., Thampy, V., Garten, L.M., Ginley, D.S., Gorman, B.P., Stone, K.H., Ceder, G., Toney, M.F., Schelhas, L.T., 2018.

- Understanding crystallization pathways leading to manganese oxide polymorph formation. *Nat. Commun.* 9 (1), 2553.
- Chen, G., Zhang, X., Gao, Y., Zhu, G., Cheng, Q., Cheng, X., 2019. Novel magnetic MnO<sub>2</sub>/MnFe<sub>2</sub>O<sub>4</sub> nanocomposite as a heterogeneous catalyst for activation of peroxymonosulfate (PMS) toward oxidation of organic pollutants. *Sep. Purif. Technol.* 213, 456–464.
- Cho, Y.-C., Hsu, C.-C., Lin, Y.-P., 2022. Integration of in-situ chemical oxidation and permeable reactive barrier for the removal of chlorophenols by copper oxide activated peroxydisulfate. *J. Hazard. Mater.* 432, 128726.
- Chun, H., Yizhong, W., Hongxiao, T., 2000. Destruction of phenol aqueous solution by photocatalysis or direct photolysis. *Chemosphere* 41 (8), 1205–1209.
- Ciardelli, G., Capannelli, G., Bottino, A., 2001. Ozone treatment of textile wastewaters for reuse. *Water Sci. Technol.* 44 (5), 61–67.
- Ciardelli, G., Ciabatti, I., Ranieri, L., Capannelli, G., Bottino, A., 2003. Membrane contactors for textile wastewater ozonation. *Ann. N.Y. Acad. Sci.* 984, 29–38.
- Clayton, W.S., 1998. A Field and Laboratory Investigation of Air Fingering During Air Sparging. *Ground Water Monit. Remediat.* 18 (3), 134–145.
- Costello, M.J., Fane, A.G., Hogan, P.A., Schofield, R.W., 1993. The effect of shell side hydrodynamics on the performance of axial flow hollow fibre modules. *J. Membr. Sci.* 80 (1), 1–11.
- Côté, P., Bersillon, J.-L., Huyard, A., 1989. Bubble-free aeration using membranes: mass transfer analysis. *J. Membr. Sci.* 47 (1-2), 91–106.
- Criegee, R., 1975. Mechanismus der Ozonolyse. *Angew. Chem.* 87 (21), 765–771.
- Criquet, J., Leitner, N.K.V., 2009. Degradation of acetic acid with sulfate radical generated by persulfate ions photolysis. *Chemosphere* 77 (2), 194–200.
- Cui, H., Gu, X., Lu, S., Fu, X., Zhang, X., Fu, G.Y., Qiu, Z., Sui, Q., 2017. Degradation of ethylbenzene in aqueous solution by sodium percarbonate activated with EDDS–Fe(III) complex. *Chem. Eng. J.* 309, 80–88.
- Cui, J., Shao, S., Li, L., Zhang, P., Cui, J., Hu, C., Zhao, Y., 2022. Nanoconfinement-Regulated Peroxymonosulfate Activation via an Anomalously Efficient Mediated Electron-Transfer Pathway on Cobalt. *ACS ES&T Eng.* 2 (11), 2014–2022.
- Cussler, E.L., 2011. *Diffusion: Mass transfer in fluid systems*, 3rd ed. Cambridge University Press, Cambridge.

- Dawas, A., Yechezkel, Y., Bein, E., Hübner, U., Zucker, I., 2023. Passive Ozone Injection through Gas-Permeable Membranes for Advanced In Situ Groundwater Remediation. ACS ES&T Engineering.
- de Vera, G.A., Gernjak, W., Weinberg, H., Farré, M.J., Keller, J., von Gunten, U., 2017. Kinetics and mechanisms of nitrate and ammonium formation during ozonation of dissolved organic nitrogen. *Water Res.* 108, 451–461.
- DeCoursey, W.J., 1974. Absorption with chemical reaction: development of a new relation for the Danckwerts model. *Chem. Eng. Sci.* 29 (9), 1867–1872.
- Deng, J., Chen, Y.-J., Lu, Y.-A., Ma, X.-Y., Feng, S.-F., Gao, N., Li, J., 2017a. Synthesis of magnetic CoFe<sub>2</sub>O<sub>4</sub>/ordered mesoporous carbon nanocomposites and application in Fenton-like oxidation of rhodamine B. *Environ. Sci. Pollut. Res.* 24 (16), 14396–14408.
- Deng, J., Ge, Y., Tan, C., Wang, H., Li, Q., Zhou, S., Zhang, K., 2017b. Degradation of ciprofloxacin using  $\alpha$ -MnO<sub>2</sub> activated peroxymonosulfate process: Effect of water constituents, degradation intermediates and toxicity evaluation. *Chem. Eng. J.* 330 (1985), 1390–1400.
- Devi, R.R., Umlong, I.M., Das, B., Borah, K., Thakur, A.J., Raul, P.K., Banerjee, S., Singh, L., 2014. Removal of iron and arsenic (III) from drinking water using iron oxide-coated sand and limestone. *Appl Water Sci* 4 (2), 175–182.
- DeWeerd, K.A., Flanagan, W.P., Brennan, M.J., Principe, J.M., Spivack, J.L., 1998. Biodegradation of Trichloroethylene and Dichloromethane in Contaminated Soil and Groundwater. *Bioremediation J.* 2 (1), 29–42.
- Dingemans, M., Dewulf, J., van Hecke, W., van Langenhove, H., 2008. Determination of ozone solubility in polymeric materials. *Chem. Eng. J.* 138 (1-3), 172–178.
- Dutschke, M., Schnabel, T., Schütz, F., Springer, C., 2022. Degradation of chlorinated volatile organic compounds from contaminated ground water using a carrier-bound TiO<sub>2</sub>/UV/O<sub>3</sub>-system. *J. Environ. Manage.* 304, 114236.
- Edstrom, J.A., Semmens, M.J., Hozalski, R.M., Clapp, L.W., Novak, P.J., 2005. Stimulation of Dechlorination by Membrane-Delivered Hydrogen: Small Field Demonstration. *Environ. Eng. Sci.* 22 (3), 281–293.
- El-Din, M.G., Smith, D.W., 2003. Mass transfer analysis in ozone bubble columns. *J. Environ. Eng. Sci.* 2 (1), 63–76.
- Ellis, D.A., Mabury, S.A., Martin, J.W., Muir, D.C., 2001. Thermolysis of fluoropolymers as a potential source of halogenated organic acids in the environment. *Nature* 412 (6844), 321–324.

- El-Naas, M.H., Acio, J.A., El Telib, A.E., 2014. Aerobic biodegradation of BTEX: Progresses and Prospects. *J. Environ. Chem. Eng.* 2 (2), 1104–1122.
- Elovitz, M.S., von Gunten, U., 1999. Hydroxyl Radical/Ozone Ratios During Ozonation Processes. I. The  $R_{ct}$  Concept. *Ozone Sci. Eng.* 21 (3), 239–260.
- Erickson, R.E., Andrulis, P.J., Collins, J.C., Lungle, M.L., Mercer, G.D., 1969. Mechanism of ozonation reactions. IV. Carbon-nitrogen double bonds. *J. Org. Chem.* 34 (10), 2961–2966.
- Essaïed, K.-A., Brown, L.V., Gunten, U. von, 2021. Reactions of amines with ozone and chlorine: Two novel oxidative methods to evaluate the N-DBP formation potential from dissolved organic nitrogen. *Water Res.* 209, 117864.
- European Commission, 2022. Proposal for a DIRECTIVE OF THE EUROPEAN PARLIAMENT AND OF THE COUNCIL concerning urban wastewater treatment (recast) (accessed 21.03.2023). <https://eur-lex.europa.eu/legal-content/EN/TXT/?uri=CELEX:52022PC0541>.
- Fang, Y., Clapp, L.W., Hozalski, R.M., Novak, P.J., Semmens, M.J., 2004. Membrane gas transfer under conditions of creeping flow: modeling gas composition effects. *Water Res.* 38 (10), 2489–2498.
- Fang, Y., Hozalski, R.M., Clapp, L.W., Novak, P.J., Semmens, M.J., 2002. Passive dissolution of hydrogen gas into groundwater using hollow-fiber membranes. *Water Res.* 36 (14), 3533–3542.
- Farhadian, M., Vachelard, C., Duchez, D., Larroche, C., 2008. In situ bioremediation of monoaromatic pollutants in groundwater: a review. *Bioresour. Technol.* 99 (13), 5296–5308.
- Fernandes, A., Gałgól, M., Makoś, P., Khan, J.A., Boczkaj, G., 2019a. Integrated photocatalytic advanced oxidation system ( $TiO_2/UV/O_3/H_2O_2$ ) for degradation of volatile organic compounds. *Sep. Purif. Technol.* 224, 1–14.
- Fernandes, A., Makoś, P., Khan, J.A., Boczkaj, G., 2019b. Pilot scale degradation study of 16 selected volatile organic compounds by hydroxyl and sulfate radical based advanced oxidation processes. *J. Clean. Prod.* 208, 54–64.
- Frimer, A.A., 1979. The reaction of singlet oxygen with olefins: the question of mechanism. *Chem. Rev.* 79 (5), 359–387.
- Fu, Y.-J., Qui, H.-z., Liao, K.-S., Lue, S.J., Hu, C.-C., Lee, K.-R., Lai, J.-Y., 2010. Effect of UV-ozone treatment on poly(dimethylsiloxane) membranes: surface characterization and gas separation performance. *Langmuir* 26 (6), 4392–4399.

- Gabelman, A., Hwang, S.-T., 1999. Hollow fiber membrane contactors. *J. Membr. Sci.* 159 (1-2), 61–106.
- Gao, P., Tian, X., Nie, Y., Yang, C., Zhou, Z., Wang, Y., 2019. Promoted peroxymonosulfate activation into singlet oxygen over perovskite for ofloxacin degradation by controlling the oxygen defect concentration. *Chem. Eng. J.* 359, 828–839.
- Gardoni, D., Vailati, A., Canziani, R., 2012. Decay of Ozone in Water: A Review. *Ozone Sci. Eng.* 34 (4), 233–242.
- Garoma, T., Gurol, M.D., Osibodu, O., Thotakura, L., 2008. Treatment of groundwater contaminated with gasoline components by an ozone/UV process. *Chemosphere* 73 (5), 825–831.
- Gaston, L., Lapworth, D.J., Stuart, M., Arnscheidt, J., 2019. Prioritization Approaches for Substances of Emerging Concern in Groundwater: A Critical Review. *Environ. Sci. Technol.* 53 (11), 6107–6122.
- Gelman, F., Binstock, R., 2008. Natural attenuation of MTBE and BTEX compounds in a petroleum contaminated shallow coastal aquifer. *Environ Chem Lett* 6 (4), 259–262.
- George, C., Rassy, H.E., Chovelon, J.-M., 2001. Reactivity of selected volatile organic compounds (VOCs) toward the sulfate radical ( $\text{SO}_4^-$ ). *Int. J. Chem. Kinet.* 33 (9), 539–547.
- Ghanbari, F., Moradi, M., 2017. Application of peroxymonosulfate and its activation methods for degradation of environmental organic pollutants: Review. *Chem. Eng. J.* 310 (Part 2), 41–62.
- Gibson, T.L., Abdul, A.S., Chalmer, P.D., 1998. Enhancement of In Situ Bioremediation of BTEX-Contaminated Ground Water by Oxygen Diffusion from Silicone Tubing. *Groundwater Monitoring & Remediation* 18 (1), 93–104.
- Gómez-Pastora, J., Dominguez, S., Bringas, E., Rivero, M.J., Ortiz, I., Dionysiou, D.D., 2017. Review and perspectives on the use of magnetic nanophotocatalysts (MNPCs) in water treatment. *Chem. Eng. J.* 310, 407–427.
- Gonçalves, A.G., Órfão, J.J.M., Pereira, M.F.R., 2012. Catalytic ozonation of sulphamethoxazole in the presence of carbon materials: catalytic performance and reaction pathways. *J. Hazard. Mater.* 239-240, 167–174.
- Gottschalk, C., Beuscher, U., Hardwick, S., Kobayashi, M., Schweckendiek, J., Wikol, M., 1998. Production of High Concentrations of Bubble-Free Dissolved Ozone in Water. *SSP* 65-66, 59–62.

- Gottschalk, C., Libra, J.A., Saupe, A., 2010. Ozonation of water and waste water: A practical guide to understanding ozone and its applications, 2nd ed. Wiley-VCH, Weinheim.
- Graubner, V.-M., Jordan, R., Nuyken, O., Schnyder, B., Lippert, T., Kötz, R., Wokaun, A., 2004. Photochemical Modification of Cross-Linked Poly(dimethylsiloxane) by Irradiation at 172 nm. *Macromolecules* 37 (16), 5936–5943.
- Gross, S.A., Avens, H.J., Banducci, A.M., Sahmel, J., Panko, J.M., Tvermoes, B.E., 2013. Analysis of BTEX groundwater concentrations from surface spills associated with hydraulic fracturing operations. *J. Air Waste Manag. Assoc.* 63 (4), 424–432.
- Guan, C., Jiang, J., Pang, S., Chen, X., Webster, R.D., Lim, T.-T., 2020. Facile synthesis of pure g-C<sub>3</sub>N<sub>4</sub> materials for peroxymonosulfate activation to degrade bisphenol A: Effects of precursors and annealing ambience on catalytic oxidation. *Chem. Eng. J.* 387, 123726.
- Guha, A.K., Shanbhag, P.V., Sirkar, K.K., Vaccari, D.A., Trivedi, D.H., 1995. Multiphase ozonolysis of organics in wastewater by a novel membrane reactor. *AIChE J.* 41 (8), 1998–2012.
- Gulde, R., Clerc, B., Rutsch, M., Helbing, J., Salhi, E., McArdell, C.S., von Gunten, U., 2021. Oxidation of 51 micropollutants during drinking water ozonation: Formation of transformation products and their fate during biological post-filtration. *Water Res.* 58 (9), 117812.
- Gümüş, D., Akbal, F., 2017. A comparative study of ozonation, iron coated zeolite catalyzed ozonation and granular activated carbon catalyzed ozonation of humic acid. *Chemosphere* 174, 218–231.
- Guo, F., Wang, K., Lu, J., Chen, J., Dong, X., Xia, D., Zhang, A., Wang, Q., 2019. Activation of peroxymonosulfate by magnetic carbon supported Prussian blue nanocomposite for the degradation of organic contaminants with singlet oxygen and superoxide radicals. *Chemosphere* 218, 1071–1081.
- Guo, J., Cheng, L., Xu, M., 2009. Optimization design of shell-and-tube heat exchanger by entropy generation minimization and genetic algorithm. *Appl. Therm. Eng.* 29 (14-15), 2954–2960.
- Guo, Y., Zhan, J., Yu, G., Wang, Y., 2021a. Evaluation of the concentration and contribution of superoxide radical for micropollutant abatement during ozonation. *Water Res.* 194, 116927.

- Guo, Y., Zhang, Y., Yu, G., Wang, Y., 2021b. Revisiting the role of reactive oxygen species for pollutant abatement during catalytic ozonation: The probe approach versus the scavenger approach. *Appl. Catal. B* 280, 119418.
- Hammes, F., Salhi, E., Köster, O., Kaiser, H.-P., Egli, T., von Gunten, U., 2006. Mechanistic and kinetic evaluation of organic disinfection by-product and assimilable organic carbon (AOC) formation during the ozonation of drinking water. *Water Res.* 40 (12), 2275–2286.
- Hashino, M., Mori, Y., Fujii, Y., Motoyama, N., Kadokawa, N., Hoshikawa, H., Nishijima, W., Okada, M., 2000. Pilot plant evaluation of an ozone-microfiltration system for drinking water treatment. *Water Sci. Technol.* 41 (10-11), 17–23.
- Hatipoglu, A., Vione, D., Yalçın, Y., Minero, C., Çınar, Z., 2010. Photo-oxidative degradation of toluene in aqueous media by hydroxyl radicals. *Journal of Photochemistry and Photobiology A: Chemistry* 215 (1), 59–68.
- Haugen, K.S., Semmens, M.J., Novak, P.J., 2002. A novel in situ technology for the treatment of nitrate contaminated groundwater. *Water Res.* 36 (14), 3497–3506.
- He, Y., Wang, L., Chen, Z., Shen, B., Wei, J., Zeng, P., Wen, X., 2021. Catalytic ozonation for metoprolol and ibuprofen removal over different MnO<sub>2</sub> nanocrystals: Efficiency, transformation and mechanism. *Sci. Total Environ.* 785, 147328.
- Hehre, W.J., Ditchfield, R., Pople, J.A., 1972. Self—Consistent Molecular Orbital Methods. XII. Further Extensions of Gaussian—Type Basis Sets for Use in Molecular Orbital Studies of Organic Molecules. *J. Chem. Phys.* 56 (5), 2257–2261.
- Heng, S., Yeung, K.L., Djafer, M., Schrotter, J.-C., 2007. A novel membrane reactor for ozone water treatment. *J. Membr. Sci.* 289 (1-2), 67–75.
- Heng, S., Yeung, K.L., Julbe, A., Ayril, A., Schrotter, J.-C., 2008. Preparation of composite zeolite membrane separator/contactor for ozone water treatment. *Microporous Mesoporous Mater.* 115 (1-2), 137–146.
- Hermes, N., Jewell, K.S., Falås, P., Lutze, H.V., Wick, A., Ternes, T.A., 2020. Ozonation of Sitagliptin: Removal Kinetics and Elucidation of Oxidative Transformation Products. *Environ. Sci. Technol.* 54 (17), 10588–10598.
- Ho, H.L., Chan, W.K., Blondy, A., Yeung, K.L., Schrotter, J.-C., 2012. Experiment and modeling of advanced ozone membrane reactor for treatment of organic endocrine disrupting pollutants in water. *Catal. Today* 193 (1), 120–127.
- Hodges, B.C., Cates, E.L., Kim, J.-H., 2018. Challenges and prospects of advanced oxidation water treatment processes using catalytic nanomaterials. *Nat. Nanotechnol.* 13 (8), 642–650.

- Hoigné, J., Bader, H., 1983a. Rate constants of reactions of ozone with organic and inorganic compounds in water—I. *Water Res.* 17 (2), 173–183.
- Hoigné, J., Bader, H., 1983b. Rate constants of reactions of ozone with organic and inorganic compounds in water—II. *Water Res.* 17 (2), 185–194.
- Hoigné, J., Bader, H., Haag, W.R., Staehelin, J., 1985. Rate constants of reactions of ozone with organic and inorganic compounds in water—III. Inorganic compounds and radicals. *Water Res.* 19 (8), 993–1004.
- Hollender, J., Zimmermann, S.G., Koepke, S., Krauss, M., McArdell, C.S., Ort, C., Singer, H., von Gunten, U., Siegrist, H., 2009. Elimination of organic micropollutants in a municipal wastewater treatment plant upgraded with a full-scale post-ozonation followed by sand filtration. *Environ. Sci. Technol.* 43 (20), 7862–7869.
- Huang, C., Wang, Y., Gong, M., Wang, W., Mu, Y., Hu, Z.-H., 2020.  $\alpha$ -MnO<sub>2</sub>/Palygorskite composite as an effective catalyst for heterogeneous activation of peroxymonosulfate (PMS) for the degradation of Rhodamine B. *Sep. Purif. Technol.* 230 (1–3), 115877.
- Huang, D., Hu, C., Zeng, G., Cheng, M., Xu, P., Gong, X., Wang, R., Xue, W., 2017. Combination of Fenton processes and biotreatment for wastewater treatment and soil remediation. *Sci. Total Environ.* 574, 1599–1610.
- Huang, J., Dai, Y., Singewald, K., Liu, C.-C., Saxena, S., Zhang, H., 2019. Effects of MnO<sub>2</sub> of different structures on activation of peroxymonosulfate for bisphenol A degradation under acidic conditions. *Chem. Eng. J.* 370 (Part 1), 906–915.
- Huang, K.Z., Zhang, H., 2019. Direct Electron-Transfer-Based Peroxymonosulfate Activation by Iron-Doped Manganese Oxide ( $\delta$ -MnO<sub>2</sub>) and the Development of Galvanic Oxidation Processes (GOPs). *Environ. Sci. Technol.* 53 (21), 12610–12620.
- Huang, X., Li, X., Pan, B., Li, H., Zhang, Y., Xie, B., 2015. Self-enhanced ozonation of benzoic acid at acidic pHs. *Water Res.* 73, 9–16.
- Huber, M.M., Canonica, S., Park, G.-Y., von Gunten, U., 2003. Oxidation of pharmaceuticals during ozonation and advanced oxidation processes. *Environ. Sci. Technol.* 37 (5), 1016–1024.
- Huber, S.A., Balz, A., Abert, M., Pronk, W., 2011. Characterisation of aquatic humic and non-humic matter with size-exclusion chromatography--organic carbon detection--organic nitrogen detection (LC-OCD-OND). *Water Res.* 45 (2), 879–885.
- Hübner, U., Keller, S., Jekel, M., 2013. Evaluation of the prediction of trace organic compound removal during ozonation of secondary effluents using tracer substances and second order rate kinetics. *Water Res.* 47 (17), 6467–6474.



- Hübner, U., Mieke, U., Jekel, M., 2012. Optimized removal of dissolved organic carbon and trace organic contaminants during combined ozonation and artificial groundwater recharge. *Water Res.* 46 (18), 6059–6068.
- Hübner, U., Seiwert, B., Reemtsma, T., Jekel, M., 2014. Ozonation products of carbamazepine and their removal from secondary effluents by soil aquifer treatment - indications from column experiments. *Water Res.* 49, 34–43.
- Hübner, U., Spahr, S., Lutze, H., Wieland, A., Rüting, S., Gernjak, W., Wenk, J., 2022. Emerging advanced oxidation processes for water and wastewater treatment – guidance for systematic future research. <https://doi.org/10.31223/X5MH05>.
- Hübner, U., von Gunten, U., Jekel, M., 2015a. Evaluation of the persistence of transformation products from ozonation of trace organic compounds - a critical review. *Water Res.* 68, 150–170.
- Hübner, U., Zucker, I., Jekel, M., 2015b. Options and limitations of hydrogen peroxide addition to enhance radical formation during ozonation of secondary effluents. *J. Water Reuse Desalin.* 5 (1), 8–16.
- Huling, S., Pivetz, B., 2006. In-Situ Chemical Oxidation (accessed 6.07.2023). [https://archive.epa.gov/ada/web/pdf/insituchemicaloxidation\\_engineering\\_issue.pdf](https://archive.epa.gov/ada/web/pdf/insituchemicaloxidation_engineering_issue.pdf).
- Itzel, F., Baetz, N., Hohrenk, L.L., Gehrman, L., Antakyali, D., Schmidt, T.C., Tuerk, J., 2020. Evaluation of a biological post-treatment after full-scale ozonation at a municipal wastewater treatment plant. *Water Res.* 170, 115316.
- Janknecht, P., Picard, C., Larbot, A., Wilderer, P.A., 2004. Membrane Ozonation in Wastewater Treatment. *Acta Hydroch. Hydrob.* 32 (1), 33–39.
- Janknecht, P., Wilderer, P.A., Picard, C., Larbot, A., 2001. Ozone–water contacting by ceramic membranes. *Sep. Purif. Technol.* 25 (1-3), 341–346.
- Janknecht, P., Wilderer, P.A., Picard, C., Larbot, A., Sarrazin, J., 2000a. Bubble-free Ozone Contacting with Ceramic Membranes for Wet Oxidative Treatment. *Chem. Eng. Technol.* 23 (8), 674–677.
- Janknecht, P., Wilderer, P.A., Picard, C., Larbot, A., Sarrazin, J., 2000b. Investigations on Ozone Contacting by Ceramic Membranes. *Ozone Sci. Eng.* 22 (4), 379–392.
- Jansen, R.H.S., 2005. Ozonation of humic substances in a membrane contactor: Mass transfer, product characterization and biodegradability, Enschede.
- Jansen, R.H.S., Rijk, J.W. de, Zwijnenburg, A., Mulder, M.H.V., Wessling, M., 2005. Hollow fiber membrane contactors - A means to study the reaction kinetics of humic substance ozonation. *J. Membr. Sci.* 257 (1-2), 48–59.

- Jansen, R.H.S., Zwijnenburg, A., van der Meer, W.G.J., Wessling, M., 2006. Outside-in trimming of humic substances during ozonation in a membrane contactor. *Environ. Sci. Technol.* 40 (20), 6460–6465.
- Ji, F., Li, C., Liu, Y., Liu, P., 2014. Heterogeneous activation of peroxymonosulfate by Cu/ZSM5 for decolorization of Rhodamine B. *Sep. Purif. Technol.* 135, 1–6.
- Ji, Y., Wang, L., Jiang, M., Lu, J., Ferronato, C., Chovelon, J.-M., 2017. The role of nitrite in sulfate radical-based degradation of phenolic compounds: An unexpected nitration process relevant to groundwater remediation by in-situ chemical oxidation (ISCO). *Water Res.* 123, 249–257.
- Jung, H., Kim, J., Choi, H., 2004. Reaction Kinetics of Ozone in Variably Saturated Porous Media. *J. Environ. Eng.* 130 (4), 432–441.
- Kambhu, A., Comfort, S., Chokejaroenrat, C., Sakulthaew, C., 2012. Developing slow-release persulfate candles to treat BTEX contaminated groundwater. *Chemosphere* 89 (6), 656–664.
- Kämmler, J., Zoumpouli, G.A., Sellmann, J., Chew, Y.M.J., Wenk, J., Ernst, M., 2022. Decolorization and control of bromate formation in membrane ozonation of humic-rich groundwater. *Water Res.* 221, 118739.
- Kao, C.M., Huang, W.Y., Chang, L.J., Chen, T.Y., Chien, H.Y., Hou, F., 2006. Application of monitored natural attenuation to remediate a petroleum-hydrocarbon spill site. *Water Sci. Technol.* 53 (2), 321–328.
- Kaprara, E., Kostoglou, M., Koutsiantzi, C., Psaltou, S., Zouboulis, A.I., Mitrakas, M., 2020. Enhancement of ozonation efficiency employing dead-end hollow fiber membranes. *Environ. Sci.: Water Res. Technol.* 6 (9), 2619–2627.
- Karakurt-Fischer, S., Bein, E., Drewes, J.E., Hübner, U., 2020. Characterizing a novel in-situ oxygen delivery device for establishing controlled redox zonation within a high infiltration rate sequential biofilter. *Water Res.* 182, 116039.
- Kasprzyk-Hordern, B., Andrzejewski, P., Nawrocki, J., 2005. Catalytic Ozonation of Gasoline Compounds in Model and Natural Water in the Presence of Perfluorinated Alumina Bonded Phases. *Ozone Sci. Eng.* 27 (4), 301–310.
- Kasprzyk-Hordern, B., Dinsdale, R.M., Guwy, A.J., 2009. The removal of pharmaceuticals, personal care products, endocrine disruptors and illicit drugs during wastewater treatment and its impact on the quality of receiving waters. *Water Res.* 43 (2), 363–380.

- Katsoyiannis, I.A., Canonica, S., von Gunten, U., 2011. Efficiency and energy requirements for the transformation of organic micropollutants by ozone, O<sub>3</sub>/H<sub>2</sub>O<sub>2</sub> and UV/H<sub>2</sub>O<sub>2</sub>. *Water Res.* 45 (13), 3811–3822.
- Keen, O.S., Love, N.G., Linden, K.G., 2012. The role of effluent nitrate in trace organic chemical oxidation during UV disinfection. *Water Res.* 46 (16), 5224–5234.
- Kendall, R.A., Dunning, T.H., Harrison, R.J., 1992. Electron affinities of the first-row atoms revisited. Systematic basis sets and wave functions. *J. Chem. Phys.* 96 (9), 6796–6806.
- Khan, A., Wang, H., Liu, Y., Jawad, A., Ifthikar, J., Liao, Z., Wang, T., Chen, Z., 2018. Highly efficient  $\alpha$ -Mn<sub>2</sub>O<sub>3</sub>@ $\alpha$ -MnO<sub>2</sub>-500 nanocomposite for peroxymonosulfate activation: comprehensive investigation of manganese oxides. *J. Mater. Chem. A* 6 (4), 1590–1600.
- Kit Chan, W., Jouët, J., Heng, S., Lun Yeung, K., Schrotter, J.-C., 2012. Membrane contactor/separator for an advanced ozone membrane reactor for treatment of recalcitrant organic pollutants in water. *J. Solid State Chem.* 189, 96–100.
- Klaassen, R., Feron, P.H.M., Jansen, A.E., 2005. Membrane Contactors in Industrial Applications. *Chem. Eng. Res. Des.* 83 (3), 234–246.
- Knoop, O., Hohrenk, L.L., Lutze, H.V., Schmidt, T.C., 2018. Ozonation of Tamoxifen and Toremifene: Reaction Kinetics and Transformation Products. *Environ. Sci. Technol.* 52 (21), 12583–12591.
- Kohantorabi, M., Moussavi, G., Giannakis, S., 2021. A review of the innovations in metal- and carbon-based catalysts explored for heterogeneous peroxymonosulfate (PMS) activation, with focus on radical vs. non-radical degradation pathways of organic contaminants. *Chem. Eng. J.* 411 (49), 127957.
- Kohantorabi, M., Moussavi, G., Oulego, P., Giannakis, S., 2022. Heterogeneous catalytic ozonation and peroxone-mediated removal of Acetaminophen using natural and modified hematite-rich soil, as efficient and environmentally friendly catalysts. *Appl. Catal. B* 301 (5), 120786.
- Kovalova, L., Siegrist, H., von Gunten, U., Eugster, J., Hagenbuch, M., Wittmer, A., Moser, R., McArdell, C.S., 2013. Elimination of micropollutants during post-treatment of hospital wastewater with powdered activated carbon, ozone, and UV. *Environ. Sci. Technol.* 47 (14), 7899–7908.
- Krembs, F.J., Siegrist, R.L., Crimi, M.L., Furrer, R.F., Petri, B.G., 2010. ISCO for Groundwater Remediation: Analysis of Field Applications and Performance. *Ground Water Monit. Remediat.* 30 (4), 42–53.

- Kreulen, H., Smolders, C.A., Versteeg, G.F., van Swaaij, W.P.M., 1993a. Microporous hollow fibre membrane modules as gas-liquid contactors Part 2. Mass transfer with chemical reaction. *J. Membr. Sci.* 78 (3), 217–238.
- Kreulen, H., Smolders, C.A., Versteeg, G.F., van Swaaij, W.P.M., 1993b. Microporous hollow fibre membrane modules as gas-liquid contactors. Part 1. Physical mass transfer processes. *J. Membr. Sci.* 78 (3), 197–216.
- Kukuzaki, M., Fujimoto, K., Kai, S., Ohe, K., Oshima, T., Baba, Y., 2010. Ozone mass transfer in an ozone–water contacting process with Shirasu porous glass (SPG) membranes—A comparative study of hydrophilic and hydrophobic membranes. *Sep. Purif. Technol.* 72 (3), 347–356.
- Kumar, P., Hogendorn J.A., Feron, P.H.M., Versteeg, G.F., 2003. Approximate solution to predict the enhancement factor for the reactive absorption of a gas in a liquid flowing through a microporous membrane hollow fiber. *J. Membr. Sci.* 213 (1-2), 231–245.
- Kuo, C.H., 1982. Mass transfer in ozone absorption. An approximate analytical equation is derived for predicting the enhancement of mass transfer by decomposition and ozonation reactions. *Environ. Prog.* 1 (3), 189–195.
- Lamsal, R., Walsh, M.E., Gagnon, G.A., 2011. Comparison of advanced oxidation processes for the removal of natural organic matter. *Water Res.* 45 (10), 3263–3269.
- Langlais, B., Reckhow, D.A., Brink, D.R., 1991. *Ozone in Water Treatment*. Lewis Publishers, Boca Raton.
- Le Lacheur, R.M., Glaze, W.H., 1996. Reactions of Ozone and Hydroxyl Radicals with Serine. *Environ. Sci. Technol.* 30 (4), 1072–1080.
- Lee, J., von Gunten, U., Kim, J.-H., 2020. Persulfate-Based Advanced Oxidation: Critical Assessment of Opportunities and Roadblocks. *Environ. Sci. Technol.* 54 (6), 3064–3081.
- Lee, M., Blum, L.C., Schmid, E., Fenner, K., von Gunten, U., 2017. A computer-based prediction platform for the reaction of ozone with organic compounds in aqueous solution: kinetics and mechanisms. *Environ. Sci.: Process. Impacts* 19 (3), 465–476.
- Lee, M., Wu, Z., Li, K., 2015a. Advances in ceramic membranes for water treatment, in: Basile, A.B., Cassano, A., Rastogi, N.K. (Eds.), *Advances in membrane technologies for water treatment. Materials, processes and applications*. Woodhead publishing series in energy 75, Amsterdam, pp. 43–82.
- Lee, M., Zimmermann-Steffens, S.G., Arey, J.S., Fenner, K., von Gunten, U., 2015b. Development of Prediction Models for the Reactivity of Organic Compounds with

- Ozone in Aqueous Solution by Quantum Chemical Calculations: The Role of Delocalized and Localized Molecular Orbitals. *Environ. Sci. Technol.* 49 (16), 9925–9935.
- Lee, Y., Gerrity, D., Lee, M., Bogeat, A.E., Salhi, E., Gamage, S., Trenholm, R.A., Wert, E.C., Snyder, S.A., von Gunten, U., 2013. Prediction of micropollutant elimination during ozonation of municipal wastewater effluents: use of kinetic and water specific information. *Environ. Sci. Technol.* 47 (11), 5872–5881.
- Lee, Y., Kovalova, L., McArdell, C.S., von Gunten, U., 2014. Prediction of micropollutant elimination during ozonation of a hospital wastewater effluent. *Water Res.* 64, 134–148.
- Lee, Y., von Gunten, U., 2016. Advances in predicting organic contaminant abatement during ozonation of municipal wastewater effluent: reaction kinetics, transformation products, and changes of biological effects. *Environ. Sci.: Water Res. Technol.* 2 (3), 421–442.
- Lei, X., Lei, Y., Guan, J., Westerhoff, P., Yang, X., 2022. Kinetics and Transformations of Diverse Dissolved Organic Matter Fractions with Sulfate Radicals. *Environ. Sci. Technol.* 56 (7), 4457–4466.
- Leiknes, T., Phattaranawik, J., Boller, M., von Gunten, U., Pronk, W., 2005. Ozone transfer and design concepts for NOM decolourization in tubular membrane contactor. *Chem. Eng. J.* 111 (1), 53–61.
- Leitzke, A., von Sonntag, C., 2009. Ozonolysis of Unsaturated Acids in Aqueous Solution: Acrylic, Methacrylic, Maleic, Fumaric and Muconic Acids. *Ozone Sci. Eng.* 31 (4), 301–308.
- Li, H., Tian, J., Xiao, F., Huang, R., Gao, S., Cui, F., Wang, S., Duan, X., 2020. Structure-dependent catalysis of cuprous oxides in peroxymonosulfate activation via nonradical pathway with a high oxidation capacity. *J. Hazard. Mater.* 385, 121518.
- Li, K., Xu, L., Zhang, Y., Cao, A., Wang, Y., Huang, H., Wang, J., 2019a. A novel electro-catalytic membrane contactor for improving the efficiency of ozone on wastewater treatment. *Appl. Catal. B* 249, 316–321.
- Li, T., Ge, L., Peng, X., Wang, W., Zhang, W., 2021. Enhanced degradation of sulfamethoxazole by a novel Fenton-like system with significantly reduced consumption of H<sub>2</sub>O<sub>2</sub> activated by g-C<sub>3</sub>N<sub>4</sub>/MgO composite. *Water Res.* 190, 116777.
- Li, Y., Yeung, K.L., 2019. Polymeric catalytic membrane for ozone treatment of DEET in water. *Catal. Today* 331, 53–59.

- Li, Z., Liu, D., Zhao, Y., Li, S., Wei, X., Meng, F., Huang, W., Lei, Z., 2019b. Singlet oxygen dominated peroxymonosulfate activation by CuO-CeO<sub>2</sub> for organic pollutants degradation: Performance and mechanism. *Chemosphere* 233, 549–558.
- Liang, C., Huang, C.-F., Chen, Y.-J., 2008. Potential for activated persulfate degradation of BTEX contamination. *Water Res.* 42 (15), 4091–4100.
- Liang, Y., van Nostrand, J.D., Wang, J., Zhang, X., Zhou, J., Li, G., 2009. Microarray-based functional gene analysis of soil microbial communities during ozonation and biodegradation of crude oil. *Chemosphere* 75 (2), 193–199.
- Lim, H.-N., Choi, H., Hwang, T.-M., Kang, J.-W., 2002. Characterization of ozone decomposition in a soil slurry: kinetics and mechanism. *Water Res.* 36 (1), 219–229.
- Lim, S., McArdell, C.S., von Gunten, U., 2019. Reactions of aliphatic amines with ozone: Kinetics and mechanisms. *Water Res.* 157, 514–528.
- Lim, S., Shi, J.L., Gunten, U. von, McCurry, D.L., 2022. Ozonation of organic compounds in water and wastewater: A critical review. *Water Res.* 213, 118053.
- Lin, K.-Y.A., Chen, Y.-C., Lin, T.-Y., Yang, H., 2017a. Lanthanum cobaltite perovskite supported on zirconia as an efficient heterogeneous catalyst for activating Oxone in water. *J. Colloid Interface Sci.* 497, 325–332.
- Lin, K.-Y.A., Chen, Y.-C., Lin, Y.-F., 2017b. LaMO<sub>3</sub> perovskites (M=Co, Cu, Fe and Ni) as heterogeneous catalysts for activating peroxymonosulfate in water. *Chem. Eng. Sci.* 160, 96–105.
- Liu, C., Tang, X., Kim, J., Korshin, G.V., 2015. Formation of aldehydes and carboxylic acids in ozonated surface water and wastewater: a clear relationship with fluorescence changes. *Chemosphere* 125, 182–190.
- Lögager, T., Holcman, J., Sehested, K., Pedersen, T., 1992. Oxidation of ferrous ions by ozone in acidic solutions. *Inorg. Chem.* 31 (17), 3523–3529.
- Long, J.A., Harris, N.J., Lammertsma, K., 2001. Formaldehyde oxime  $\leftrightarrow$  nitrosomethane tautomerism. *J. Org. Chem.* 66 (20), 6762–6767.
- López, E., Schuhmacher, M., Domingo, J.L., 2008. Human health risks of petroleum-contaminated groundwater. *Environ. Sci. Pollut. Res.* 15 (3), 278–288.
- LUFA Speyer, 2023. Standardböden (accessed 13.02.2023). <https://www.lufaspeyer.de/index.php/dienstleistungen/standardboeden>.
- Luis, P., 2018. Membrane contactors, in: Luis, P. (Ed.), *Fundamental modeling of membrane systems. Membrane and process performance*. Elsevier, Amsterdam, pp. 153–208.

- Luo, J., Zhu, H.T., Fan, H.M., Liang, J.K., Shi, H.L., Rao, G.H., Li, J.B., Du, Z.M., Shen, Z.X., 2008. Synthesis of Single-Crystal Tetragonal  $\alpha$ -MnO<sub>2</sub> Nanotubes. *J. Phys. Chem. C* 112 (33), 12594–12598.
- Luo, Y., Guo, W., Ngo, H.H., Nghiem, L.D., Hai, F.I., Zhang, J., Liang, S., Wang, X.C., 2014. A review on the occurrence of micropollutants in the aquatic environment and their fate and removal during wastewater treatment. *Sci. Total Environ.* 473-474, 619–641.
- Lutze, H.V., Kerlin, N., Schmidt, T.C., 2015. Sulfate radical-based water treatment in presence of chloride: formation of chlorate, inter-conversion of sulfate radicals into hydroxyl radicals and influence of bicarbonate. *Water Res.* 72, 349–360.
- Ma, W., Wang, N., Fan, Y., Tong, T., Han, X., Du, Y., 2018. Non-radical-dominated catalytic degradation of bisphenol A by ZIF-67 derived nitrogen-doped carbon nanotubes frameworks in the presence of peroxymonosulfate. *Chem. Eng. J.* 336, 721–731.
- Mansourizadeh, A., Ismail, A.F., 2009. Hollow fiber gas-liquid membrane contactors for acid gas capture: a review. *J. Hazard. Mater.* 171 (1-3), 38–53.
- Marenich, A.V., Cramer, C.J., Truhlar, D.G., 2009. Universal solvation model based on solute electron density and on a continuum model of the solvent defined by the bulk dielectric constant and atomic surface tensions. *J. Phys. Chem. B* 113 (18), 6378–6396.
- Margot, J., Kienle, C., Magnet, A., Weil, M., Rossi, L., Alencastro, L.F. de, Abegglen, C., Thonney, D., Chèvre, N., Schärer, M., Barry, D.A., 2013. Treatment of micropollutants in municipal wastewater: ozone or powdered activated carbon? *Sci. Total Environ.* 461-462, 480–498.
- Marinescu, C., Ben Ali, M., Hamdi, A., Cherifi, Y., Barras, A., Coffinier, Y., Somacescu, S., Raditoiu, V., Szunerits, S., Boukherroub, R., 2018. Cobalt phthalocyanine-supported reduced graphene oxide: A highly efficient catalyst for heterogeneous activation of peroxymonosulfate for rhodamine B and pentachlorophenol degradation. *Chem. Eng. J.* 336, 465–475.
- MassBank, 2015. MassBank Record: EQ331254. <https://massbank.eu/MassBank/RecordDisplay?id=EQ331254&dsn=Eawag> (accessed 15.07.2022).
- Matienzo, L.J., Egitto, F.D., 2006. Transformation of poly(dimethylsiloxane) into thin surface films of SiO<sub>x</sub> by UV/ozone treatment. Part II: segregation and modification of doped polymer blends. *J. Mater. Sci.* 41 (19), 6374–6384.

- Matsumoto, A., Tsutsumi, K., Schumacher, K., Unger, K.K., 2002. Surface Functionalization and Stabilization of Mesoporous Silica Spheres by Silanization and Their Adsorption Characteristics. *Langmuir* 18 (10), 4014–4019.
- Mauter, M.S., Zucker, I., Perreault, F., Werber, J.R., Kim, J.-H., Elimelech, M., 2018. The role of nanotechnology in tackling global water challenges. *Nat. Sustain.* 1 (4), 166–175.
- McCurry, D.L., Quay, A.N., Mitch, W.A., 2016. Ozone Promotes Chloropicrin Formation by Oxidizing Amines to Nitro Compounds. *Environ. Sci. Technol.* 50 (3), 1209–1217.
- Merényi, G., Lind, J., Naumov, S., von Sonntag, C., 2010. The reaction of ozone with the hydroxide ion: mechanistic considerations based on thermokinetic and quantum chemical calculations and the role of HO<sup>-</sup> in superoxide dismutation. *Chem. Eur. J.* 16 (4), 1372–1377.
- Merga, G., Aravindakumar, C.T., Rao, B.S.M., Mohan, H., Mittal, J.P., 1994. Pulse radiolysis study of the reactions of SO<sup>-4</sup> with some substituted benzenes in aqueous solution. *J. Chem. Soc., Faraday Trans.* 90 (4), 597–604.
- Merle, T., Pronk, W., von Gunten, U., 2017. MEMBRO<sub>3</sub>X, a Novel Combination of a Membrane Contactor with Advanced Oxidation (O<sub>3</sub>/H<sub>2</sub>O<sub>2</sub>) for Simultaneous Micropollutant Abatement and Bromate Minimization. *Environ. Sci. Technol. Lett.* 4 (5), 180–185.
- Michael-Kordatou, I., Michael, C., Duan, X., He, X., Dionysiou, D.D., Mills, M.A., Fatta-Kassinos, D., 2015. Dissolved effluent organic matter: Characteristics and potential implications in wastewater treatment and reuse applications. *Water Res.* 77, 213–248.
- Miklos, D.B., Hartl, R., Michel, P., Linden, K.G., Drewes, J.E., Hübner, U., 2018a. UV/H<sub>2</sub>O<sub>2</sub> process stability and pilot-scale validation for trace organic chemical removal from wastewater treatment plant effluents. *Water Res.* 136, 169–179.
- Miklos, D.B., Remy, C., Jekel, M., Linden, K.G., Drewes, J.E., Hübner, U., 2018b. Evaluation of advanced oxidation processes for water and wastewater treatment - A critical review. *Water Res.* 139, 118–131.
- Miklos, D.B., Wang, W.-L., Linden, K.G., Drewes, J.E., Hübner, U., 2019. Comparison of UV-AOPs (UV/H<sub>2</sub>O<sub>2</sub>, UV/PDS and UV/Chlorine) for TOC removal from municipal wastewater effluent and optical surrogate model evaluation. *Chem. Eng. J.* 362, 537–547.
- Mohammadi, L., Rahdar, A., Bazrafshan, E., Dahmardeh, H., Thysiadou, A., Kyzas, G.Z., 2021. Benzene Removal from Aqueous Solutions by Heterogeneous Catalytic



- Ozonation Process with Magnesium Oxide Nanoparticles. *Ozone Sci. Eng.* 43 (2), 147–162.
- Mori, Y., Oota, T., Hashino, M., Takamura, M., Fujii, Y., 1998. Ozone-microfiltration system. *Desalination* 117 (1-3), 211–218.
- Mosadegh-Sedghi, S., Rodrigue, D., Brisson, J., Iliuta, M.C., 2014. Wetting phenomenon in membrane contactors – Causes and prevention. *J. Membr. Sci.* 452, 332–353.
- Müller, J., Drewes, J.E., Hübner, U., 2017. Sequential biofiltration - A novel approach for enhanced biological removal of trace organic chemicals from wastewater treatment plant effluent. *Water Res.* 127, 127–138.
- Müller, J., Drewes, J.E., Hübner, U., 2019. Investigating synergies in sequential biofiltration-based hybrid systems for the enhanced removal of trace organic chemicals from wastewater treatment plant effluents. *Environ. Sci.: Water Res. Technol.* 5 (8), 1423–1435.
- Muñoz, I., Rodríguez, A., Rosal, R., Fernández-Alba, A.R., 2009. Life Cycle Assessment of urban wastewater reuse with ozonation as tertiary treatment: a focus on toxicity-related impacts. *Sci. Total Environ.* 407 (4), 1245–1256.
- Mvula, E., von Sonntag, C., 2003. Ozonolysis of phenols in aqueous solution. *Org. Biomol. Chem.* 1 (10), 1749–1756.
- Nagakura, S., Kuboyama, A., 1954. Dipole Moments and Absorption Spectra of o-Benzoquinone and its Related Substances. *J. Am. Chem. Soc.* 76 (4), 1003–1005.
- Nagy, E., 2019. Membrane Contactors, in: Nagy, E. (Ed.), *Basic equations of mass transport through a membrane layer*, 2 ed., Amsterdam, pp. 337–345.
- Nam, K., Rodriguez, W., Kukor, J.J., 2001. Enhanced degradation of polycyclic aromatic hydrocarbons by biodegradation combined with a modified Fenton reaction. *Chemosphere* 45 (1), 11–20.
- Nawaz, F., Xie, Y., Cao, H., Xiao, J., Yueqiu, W., Zhang, X., Li, M., Duan, F., 2015. Catalytic ozonation of 4-nitrophenol over an mesoporous  $\alpha$ -MnO<sub>2</sub> with resistance to leaching. *Catal. Today* 258, 595–601.
- Neese, F., 2012. The ORCA program system. *Wiley Interdiscip. Rev. Comput. Mol. Sci.* 2 (1), 73–78.
- Neese, F., 2018. Software update: the ORCA program system, version 4.0. *WIREs Comput. Mol. Sci. (WIREs Computational Molecular Science)* 8 (1).
- Neta, P., Huie, R.E., Ross, A.B., 1988. Rate Constants for Reactions of Inorganic Radicals in Aqueous Solution. *JPCRD* 17 (3), 1027–1284.

- Ni, Y., Su, S., Kokot, S., 2006. Spectrofluorimetric studies on the binding of salicylic acid to bovine serum albumin using warfarin and ibuprofen as site markers with the aid of parallel factor analysis. *Anal. Chim. Acta* 580 (2), 206–215.
- Nihemaiti, M., Miklos, D.B., Hübner, U., Linden, K.G., Drewes, J.E., Croué, J.-P., 2018. Removal of trace organic chemicals in wastewater effluent by UV/H<sub>2</sub>O<sub>2</sub> and UV/PDS. *Water Res.* 145, 487–497.
- Nimmer, M.A., Wayner, B.D., Allen Morr, A., 2000. In-situ ozonation of contaminated groundwater. *Environ. Prog.* 19 (3), 183–196.
- Noda, S., Messaoudi, B., Kuzumoto, M., 2002. Generation of Highly Ozonized Water Using a Microporous Hollow Fiber Module. *Jpn. J. Appl. Phys.* 41, 1315.
- Nöthe, T., Fahlenkamp, H., von Sonntag, C., 2009. Ozonation of wastewater: rate of ozone consumption and hydroxyl radical yield. *Environ. Sci. Technol.* 43 (15), 5990–5995.
- Oh, W.-D., Dong, Z., Lim, T.-T., 2016. Generation of sulfate radical through heterogeneous catalysis for organic contaminants removal: Current development, challenges and prospects. *Appl. Catal. B* 194 (Part 2), 169–201.
- Oh, W.-D., Lim, T.-T., 2019. Design and application of heterogeneous catalysts as peroxydisulfate activator for organics removal: An overview. *Chem. Eng. J.* 358 (Part 1), 110–133.
- Oller, I., Malato, S., Sánchez-Pérez, J.A., 2011. Combination of Advanced Oxidation Processes and biological treatments for wastewater decontamination—A review. *Sci. Total Environ.* 409 (20), 4141–4166.
- Orgill, J.J., Abboud, M.C., Atiyeh, H.K., Devarapalli, M., Sun, X., Lewis, R.S., 2019. Measurement and prediction of mass transfer coefficients for syngas constituents in a hollow fiber reactor. *Bioresour. Technol.* 276, 1–7.
- Ortmeyer, F., Hansen, B., Banning, A., 2022. Groundwater nitrate problem and countermeasures in strongly affected EU countries—a comparison between Germany, Denmark and Ireland. *Grundwasser* 27 (24715092), 220.
- Pabby, A.K., Sastre, A.M., 2013. State-of-the-art review on hollow fibre contactor technology and membrane-based extraction processes. *J. Membr. Sci.* 430, 263–303.
- Pant, P., Pant, S., 2010. A review: advances in microbial remediation of trichloroethylene (TCE). *J. Environ. Sci. (China)* 22 (1), 116–126.
- Pariente, M., Martinez, F., Melero, J., Botas, J., Velegraki, T., Xekoukoulotakis, N., Mantzavinos, D., 2008. Heterogeneous photo-Fenton oxidation of benzoic acid in

- water: Effect of operating conditions, reaction by-products and coupling with biological treatment. *Appl. Catal. B* 85 (1-2), 24–32.
- Park, C.M., Heo, J., Wang, D., Su, C., Yoon, Y., 2018. Heterogeneous activation of persulfate by reduced graphene oxide-elemental silver/magnetite nanohybrids for the oxidative degradation of pharmaceuticals and endocrine disrupting compounds in water. *Appl. Catal. B* 225, 91–99.
- Park, H., Choi, W., 2005. Photocatalytic conversion of benzene to phenol using modified TiO<sub>2</sub> and polyoxometalates. *Catal. Today* 101 (3-4), 291–297.
- Patel, V.K., Savsani, V.J., Tawhid, M.A., 2019. *Thermal System Optimization*, Cham.
- Patterson, B.M., Franzmann, P.D., Davis, G.B., Elbers, J., Zappia, L.R., 2002. Using polymer mats to biodegrade atrazine in groundwater: laboratory column experiments. *J. Contam. Hydrol.* 54 (3), 195–213.
- Patterson, B.M., Grassi, M.E., Robertson, B.S., Davis, G.B., Smith, A.J., McKinley, A.J., 2004. Use of polymer mats in series for sequential reactive barrier remediation of ammonium-contaminated groundwater: field evaluation. *Environ. Sci. Technol.* 38 (24), 6846–6854.
- Peng, Q., Dai, Y., Liu, K., Luo, X., He, D., Tang, X., Huang, G., 2020. A novel carbon nanotube–magnesium oxide composite with excellent recyclability to efficiently activate peroxydisulfate for Rhodamine B degradation. *J. Mater. Sci.* 55 (25), 11267–11283.
- Peng, S., He, X., Pan, H., 2018. Spectroscopic study on transformations of dissolved organic matter in coal-to-liquids wastewater under integrated chemical oxidation and biological treatment process. *J. Environ. Sci. (China)* 70, 206–216.
- Pereira, V.J., Weinberg, H.S., Linden, K.G., Singer, P.C., 2007. UV degradation kinetics and modeling of pharmaceutical compounds in laboratory grade and surface water via direct and indirect photolysis at 254 nm. *Environ. Sci. Technol.* 41 (5), 1682–1688.
- Peters, C.A., Knightes, C.D., Brown, D.G., 1999. Long-Term Composition Dynamics of PAH-Containing NAPLs and Implications for Risk Assessment. *Environ. Sci. Technol.* 33 (24), 4499–4507.
- Phan, L.T., Schaar, H., Saracevic, E., Krampe, J., Kreuzinger, N., 2021. Effect of ozonation on the biodegradability of urban wastewater treatment plant effluent. *Sci. Total Environ.* 812, 152466.
- Phattaranawik, J., Leiknes, T., Pronk, W., 2005. Mass transfer studies in flat-sheet membrane contactor with ozonation. *J. Membr. Sci.* 247 (1-2), 153–167.

- Picard, C., Larbot, A., Guida-Pietrasanta, F., Boutevin, B., Ratsimihety, A., 2001. Grafting of ceramic membranes by fluorinated silanes: hydrophobic features. *Sep. Purif. Technol.* 25 (1-3), 65–69.
- Picard, C., Larbot, A., Tronel-Peyroz, E., Berjoan, R., 2004. Characterisation of hydrophilic ceramic membranes modified by fluoroalkylsilanes into hydrophobic membranes. *Solid State Sci.* 6 (6), 605–612.
- Pines, D.S., Min, K.-N., Ergas, S.J., Reckhow, D.A., 2005. Investigation of an Ozone Membrane Contactor System. *Ozone Sci. Eng.* 27 (3), 209–217.
- Podgorski, J., Berg, M., 2020. Global threat of arsenic in groundwater. *Science* 368 (6493), 845–850.
- Ponnusamy, G., Farzaneh, H., Tong, Y., Lawler, J., Liu, Z., Saththasivam, J., 2021. Enhanced catalytic ozonation of ibuprofen using a 3D structured catalyst with MnO<sub>2</sub> nanosheets on carbon microfibers. *Sci. Rep.* 11 (1), 6342.
- Power, J.F., Schepers, J.S., 1989. Nitrate contamination of groundwater in North America. *Agric. Ecosyst. Environ.* 26 (3-4), 165–187.
- Pryor, W.A., Giamalva, D.H., Church, D.F., 1984. Kinetics of ozonation. 2. Amino acids and model compounds in water and comparisons to rates in nonpolar solvents. *J. Am. Chem. Soc.* 106 (23), 7094–7100.
- Ra, J., Yoom, H., Son, H., Lee, Y., 2020. Occurrence and transformation of gabapentin in urban water quality engineering: Rapid formation of nitrile from amine during drinking water chlorination. *Water Res.* 184, 116123.
- Rabuni, M.F., Nik Sulaiman, N.M., Awanis Hashim, N., 2015. A systematic assessment method for the investigation of the PVDF membrane stability. *Desalination Water Treat.*, 1–12.
- Rahman, M.F., Peldszus, S., Anderson, W.B., 2014. Behaviour and fate of perfluoroalkyl and polyfluoroalkyl substances (PFASs) in drinking water treatment: a review. *Water Res.* 50, 318–340.
- Rakness, K.L., Hunter, G., Lew, J., Mundy, B., Wert, E.C., 2018. Design Considerations for Cost-Effective Ozone Mass Transfer in Sidestream Systems. *Ozone Sci. Eng.* 40 (3), 159–172.
- Ramseier, M.K., von Gunten, U., 2009. Mechanisms of Phenol Ozonation—Kinetics of Formation of Primary and Secondary Reaction Products. *Ozone Sci. Eng.* 31 (3), 201–215.
- Rangwala, H.A., 1996. Absorption of carbon dioxide into aqueous solutions using hollow fiber membrane contactors. *J. Membr. Sci.* 112 (2), 229–240.

- Rayaroth, M.P., Aravindakumar, C.T., Shah, N.S., Boczkaj, G., 2022. Advanced oxidation processes (AOPs) based wastewater treatment - unexpected nitration side reactions - a serious environmental issue: A review. *Chem. Eng. J.* 430 (3), 133002.
- Rayaroth, M.P., Marchel, M., Boczkaj, G., 2023. Advanced oxidation processes for the removal of mono and polycyclic aromatic hydrocarbons - A review. *Sci. Total Environ.* 857 (Pt 2), 159043.
- Rayaroth, M.P., Oh, D., Lee, C.-S., Kang, Y.-G., Chang, Y.-S., 2020. In situ chemical oxidation of contaminated groundwater using a sulfidized nanoscale zerovalent iron-persulfate system: Insights from a box-type study. *Chemosphere* 257, 127117.
- Real, F.J., Benitez, F.J., Acero, J.L., Sagasti, J.J.P., Casas, F., 2009. Kinetics of the Chemical Oxidation of the Pharmaceuticals Primidone, Ketoprofen, and Diatrizoate in Ultrapure and Natural Waters. *Ind. Eng. Chem. Res.* 48 (7), 3380–3388.
- Reddy, K.R., Kosgi, S., Zhou, J., 1995. A Review of In-Situ Air Sparging for the Remediation of VOC-Contaminated Saturated Soils and Groundwater. *Hazard. Waste Hazard. Mater.* 12 (2), 97–118.
- Reungoat, J., Macova, M., Escher, B.I., Carswell, S., Mueller, J.F., Keller, J., 2010. Removal of micropollutants and reduction of biological activity in a full scale reclamation plant using ozonation and activated carbon filtration. *Water Res.* 44 (2), 625–637.
- Richardson, S.D., Kimura, S.Y., 2020. Water Analysis: Emerging Contaminants and Current Issues. *Anal. Chem.* 92 (1), 473–505.
- Ritter, W.F., Scarborough, R.W., 1995. A review of bioremediation of contaminated soils and groundwater. *J. Environ. Sci. Health A* 30 (2), 333–357.
- Robinson, D.M., Go, Y.B., Mui, M., Gardner, G., Zhang, Z., Mastrogiovanni, D., Garfunkel, E., Li, J., Greenblatt, M., Dismukes, G.C., 2013. Photochemical water oxidation by crystalline polymorphs of manganese oxides: structural requirements for catalysis. *J. Am. Chem. Soc.* 135 (9), 3494–3501.
- Rosenfeldt, E.J., Linden, K.G., Canonica, S., von Gunten, U., 2006. Comparison of the efficiency of  $\cdot\text{OH}$  radical formation during ozonation and the advanced oxidation processes  $\text{O}_3/\text{H}_2\text{O}_2$  and  $\text{UV}/\text{H}_2\text{O}_2$ . *Water Res.* 40 (20), 3695–3704.
- Roustan, M., Wang, R.Y., Wolbert, D., 1996. Modeling Hydrodynamics And Mass Transfer Parameters In A Continuous Ozone Bubble Column. *Ozone Sci. Eng.* 18 (2), 99–115.
- Sabelfeld, M., Geißen, S.-U., 2019. Effect of helical structure on ozone mass transfer in a hollow fiber membrane contactor. *J. Membr. Sci.* 574, 222–234.

- Sander, R., 2015. Compilation of Henry's law constants (version 4.0) for water as solvent. *Atmos. Chem. Phys.* 15 (8), 4399–4981.
- Santos, F.R.A.d., Borges, C.P., Fonseca, F.V.d., 2015. Polymeric Materials for Membrane Contactor Devices Applied to Water Treatment by Ozonation. *Mater. Res.* 18 (5), 1015–1022.
- Saputra, E., Muhammad, S., Sun, H., Ang, H.M., Tadé, M.O., Wang, S., 2013. Different crystallographic one-dimensional MnO<sub>2</sub> nanomaterials and their superior performance in catalytic phenol degradation. *Environ. Sci. Technol.* 47 (11), 5882–5887.
- Schmitt, A., Mendret, J., Brosillon, S., 2022. Evaluation of an ozone diffusion process using a hollow fiber membrane contactor. *Chem. Eng. Res. Des.* 177, 291–303.
- Schmitt, A., Mendret, J., Roustan, M., Brosillon, S., 2020. Ozonation using hollow fiber contactor technology and its perspectives for micropollutants removal in water: A review. *Sci. Total Environ.* 729, 138664.
- Schneider, F., Ruhl, A.S., Hübner, U., Jekel, M., 2016. Removal of Residual Dissolved Ozone with Manganese Dioxide for Process Control with UV 254. *Ozone Sci. Eng.* 38 (2), 79–85.
- Schnobrich, M.R., Chaplin, B.P., Semmens, M.J., Novak, P.J., 2007. Stimulating hydrogenotrophic denitrification in simulated groundwater containing high dissolved oxygen and nitrate concentrations. *Water Res.* 41 (9), 1869–1876.
- Schollée, J.E., Bourgin, M., von Gunten, U., McArdell, C.S., Hollender, J., 2018. Non-target screening to trace ozonation transformation products in a wastewater treatment train including different post-treatments. *Water Res.* 142, 267–278.
- Schuler, R.H., Albarran, G., 2002. The rate constants for reaction of OH radicals with benzene and toluene. *Radiat. Phys. Chem.* 64 (3), 189–195.
- Schulz, C.R., Prendiville, P.W., 1993. Designing High Concentration Ozone Contactors for Drinking Water Treatment Plants. *Ozone Sci. Eng.* 15 (3), 245–266.
- Schwarz, A.E., Ligthart, T.N., Godoi Bizarro, D., Wild, P. de, Vreugdenhil, B., van Harmelen, T., 2021. Plastic recycling in a circular economy; determining environmental performance through an LCA matrix model approach. *Waste managem.* 121, 331–342.
- Schwarzenbach, R.P., Escher, B.I., Fenner, K., Hofstetter, T.B., Johnson, C.A., von Gunten, U., Wehrli, B., 2006. The challenge of micropollutants in aquatic systems. *Science* 313 (5790), 1072–1077.

- Sehested, K., Getoff, N., Schwoerer, F., Markovic, V.M., Nielsen, S.O., 1971. Pulse radiolysis of oxalic acid and oxalates. *J. Phys. Chem.* 75 (6), 749–755.
- Seiwert, B., Nihemaiti, M., Bauer, C., Muschket, M., Sauter, D., Gnirss, R., Reemtsma, T., 2021. Ozonation products from trace organic chemicals in municipal wastewater and from metformin: peering through the keyhole with supercritical fluid chromatography-mass spectrometry. *Water Res.* 196, 117024.
- Selbaş, R., Kızılkın, Ö., Reppich, M., 2006. A new design approach for shell-and-tube heat exchangers using genetic algorithms from economic point of view. *Chem. Eng. Process.* 45 (4), 268–275.
- Semmens, M.J., Qin, R., Zander, A., 1989. Using a Microporous Hollow-Fiber Membrane to Separate VOCs From Water. *J. Am. Water Works Assn.* 81 (4), 162–167.
- Sgroi, M., Anumol, T., Vagliasindi, F.G.A., Snyder, S.A., Roccaro, P., 2021. Comparison of the new Cl<sub>2</sub>/O<sub>3</sub>/UV process with different ozone- and UV-based AOPs for wastewater treatment at pilot scale: Removal of pharmaceuticals and changes in fluorescing organic matter. *Sci. Total Environ.* 765, 142720.
- Shahzad, A., Ali, J., Ifthikar, J., Aregay, G.G., Zhu, J., Chen, Z., Chen, Z., 2020. Non-radical PMS activation by the nanohybrid material with periodic confinement of reduced graphene oxide (rGO) and Cu hydroxides. *J. Hazard. Mater.* 392, 122316.
- Shanbhag, P.V., Guha, A.K., Sirkar, K.K., 1995. Single-phase membrane ozonation of hazardous organic compounds in aqueous streams. *J. Hazard. Mater.* 41 (1), 95–104.
- Shanbhag, P.V., Guha, A.K., Sirkar, K.K., 1998. Membrane-Based Ozonation of Organic Compounds. *Ind. Eng. Chem. Res.* 37 (11), 4388–4398.
- Shanbhag, P.V., Sirkar, K.K., 1998. Ozone and Oxygen permeation behavior of silicone capillary membranes employed in membrane ozonators. *J. Appl. Polym. Sci.* 69 (7), 1263–1273.
- Shang, N.C., Yu, Y.H., 2002. Toxicity and color formation during ozonation of mono-substituted aromatic compounds. *Environ. Technol.* 23 (1), 43–52.
- Sharma, B.M., Bečanová, J., Scherlinger, M., Sharma, A., Bharat, G.K., Whitehead, P.G., Klánová, J., Nizzetto, L., 2019. Health and ecological risk assessment of emerging contaminants (pharmaceuticals, personal care products, and artificial sweeteners) in surface and groundwater (drinking water) in the Ganges River Basin, India. *Sci. Total Environ.* 646, 1459–1467.

- Shaulsky, E., Karanikola, V., Straub, A.P., Deshmukh, A., Zucker, I., Elimelech, M., 2019. Asymmetric membranes for membrane distillation and thermo-osmotic energy conversion. *Desalination* 452, 141–148.
- Shen, S., Zhou, X., Zhao, Q., Jiang, W., Wang, J., He, L., Ma, Y., Yang, L., Chen, Z., 2022. Understanding the nonradical activation of peroxymonosulfate by different crystallographic MnO<sub>2</sub>: The pivotal role of Mn<sup>III</sup> content on the surface. *J. Hazard. Mater.* 439, 129613.
- Shi, J.L., Plata, S.L., Kleimans, M., Childress, A.E., McCurry, D.L., 2021. Formation and Fate of Nitromethane in Ozone-Based Water Reuse Processes. *Environ. Sci. Technol.* 55 (9), 6281–6289.
- Siegrist, R.L., Crimi, M., Simpkin, T.J., 2011. *In Situ Chemical Oxidation for Groundwater Remediation. SERDP/ESTCP Environmental Remediation Technology 3.* Springer Science+Business Media LLC, New York, NY.
- Sierra-Olea, M., Kölle, S., Bein, E., Reemtsma, T., Lechtenfeld, O.J., Hübner, U., 2023. Isotopically labeled ozone: A new approach to elucidate the formation of ozonation products. *Water Res.* 233, 119740.
- Sirkar, K.K., 1992. Other New Membrane Processes, in: Ho, W.S.W., Sirkar, K.K. (Eds.), *Membrane Handbook.* Springer, Boston, pp. 885–912.
- Stalter, D., Magdeburg, A., Weil, M., Knacker, T., Oehlmann, J., 2010. Toxication or detoxication? In vivo toxicity assessment of ozonation as advanced wastewater treatment with the rainbow trout. *Water Res.* 44 (2), 439–448.
- Steiner, M., Pronk, W., von Gunten, U., Boller, M., 2010. *Use of Membrane Contactors for the Diffusion of Ozone,* Dübendorf.
- Struse, A.M., Siegrist, R.L., Dawson, H.E., Urynowicz, M.A., 2002. Diffusive Transport of Permanganate during In Situ Oxidation. *J. Environ. Eng.* 128 (4), 327–334.
- Stuart, M., Lapworth, D., Crane, E., Hart, A., 2012. Review of risk from potential emerging contaminants in UK groundwater. *Sci. Total Environ.* 416, 1–21.
- Stylianou, S.K., Katsoyiannis, I.A., Ernst, M., Zouboulis, A.I., 2018a. Impact of O<sub>3</sub> or O<sub>3</sub>/H<sub>2</sub>O<sub>2</sub> treatment via a membrane contacting system on the composition and characteristics of the natural organic matter of surface waters. *Environ. Sci. Pollut. Res.* 25 (13), 12246–12255.
- Stylianou, S.K., Katsoyiannis, I.A., Mitrakas, M., Zouboulis, A.I., 2018b. Application of a ceramic membrane contacting process for ozone and peroxone treatment of micropollutant contaminated surface water. *J. Hazard. Mater.* 358, 129–135.



- Stylianou, S.K., Kostoglou, M., Zouboulis, A.I., 2016. Ozone Mass Transfer Studies in a Hydrophobized Ceramic Membrane Contactor: Experiments and Analysis. *Ind. Eng. Chem. Res.* 55 (28), 7587–7597.
- Stylianou, S.K., Sklari, S.D., Zamboulis, D., Zaspalis, V.T., Zouboulis, A.I., 2015a. Development of bubble-less ozonation and membrane filtration process for the treatment of contaminated water. *J. Membr. Sci.* 492, 40–47.
- Stylianou, S.K., Szymanska, K., Katsoyiannis, I.A., Zouboulis, A.I., 2015b. Novel Water Treatment Processes Based on Hybrid Membrane-Ozonation Systems: A Novel Ceramic Membrane Contactor for Bubbleless Ozonation of Emerging Micropollutants. *J. Chem.* 2015, 1–12.
- Sutton, N.B., Grotenhuis, J.T.C., Langenhoff, A.A.M., Rijnaarts, H.H.M., 2011. Efforts to improve coupled in situ chemical oxidation with bioremediation: a review of optimization strategies. *J. Soils Sediments* 11 (1), 129–140.
- Sutton, N.B., Kalisz, M., Krupanek, J., Marek, J., Grotenhuis, T., Smidt, H., Weert, J. de, Rijnaarts, H.H.M., van Gaans, P., Keijzer, T., 2014. Geochemical and microbiological characteristics during in situ chemical oxidation and in situ bioremediation at a diesel contaminated site. *Environ. Sci. Technol.* 48 (4), 2352–2360.
- Szczuka, A., Huang, N., MacDonald, J.A., Nayak, A., Zhang, Z., Mitch, W.A., 2020. N-Nitrosodimethylamine Formation during UV/Hydrogen Peroxide and UV/Chlorine Advanced Oxidation Process Treatment Following Reverse Osmosis for Potable Reuse. *Environ. Sci. Technol.* 54 (23), 15465–15475.
- Tekle-Röttering, A., Jewell, K.S., Reisz, E., Lutze, H.V., Ternes, T.A., Schmidt, W., Schmidt, T.C., 2016. Ozonation of piperidine, piperazine and morpholine: Kinetics, stoichiometry, product formation and mechanistic considerations. *Water Res.* 88, 960–971.
- Thanh, N.T.K., Maclean, N., Mahiddine, S., 2014. Mechanisms of nucleation and growth of nanoparticles in solution. *Chemical Reviews* 114 (15), 7610–7630.
- Thiruvengkatachari, R., Vigneswaran, S., Naidu, R., 2008. Permeable reactive barrier for groundwater remediation. *J. Ind. Eng. Chem.* 14 (2), 145–156.
- Tsitonaki, A., Petri, B.G., Crimi, M., Mosbæk, H., Siegrist, R.L., Bjerg, P.L., 2010. In Situ Chemical Oxidation of Contaminated Soil and Groundwater Using Persulfate: A Review. *Critical Reviews in Environmental Science and Technology* 40 (1), 55–91.
- Tu, C.-Y., Liu, Y.-L., Lee, K.-R., Lai, J.-Y., 2005. Surface grafting polymerization and modification on poly(tetrafluoroethylene) films by means of ozone treatment. *Polymer* 46 (18), 6976–6985.

- United States Environmental Protection Agency, 2023. Superfund Remedy Report: 17<sup>th</sup> Edition (accessed 5.07.2023). <https://www.epa.gov/system/files/documents/2023-01/100003149.pdf>.
- van Buren, J., Cuthbertson, A.A., Ocasio, D., Sedlak, D.L., 2021. Ubiquitous Production of Organosulfates During Treatment of Organic Contaminants with Sulfate Radicals. *Environ. Sci. Technol. Lett.* 8 (7), 574–580.
- van Swaaij, W.P.M., Versteeg, G.F., 1992. Mass transfer accompanied with complex reversible chemical reactions in gas—liquid systems: an overview. *Chem. Eng. Sci.* 47 (13-14), 3181–3195.
- Vatankhah, H., Szczuka, A., Mitch, W.A., Almaraz, N., Brannum, J., Bellona, C., 2019. Evaluation of Enhanced Ozone-Biologically Active Filtration Treatment for the Removal of 1,4-Dioxane and Disinfection Byproduct Precursors from Wastewater Effluent. *Environ. Sci. Technol.* 53 (5), 2720–2730.
- Vel Leitner, N.K., Roshani, B., 2010. Kinetic of benzotriazole oxidation by ozone and hydroxyl radical. *Water Res.* 44 (6), 2058–2066.
- von Gunten, U., 2003. Ozonation of drinking water: Part I. Oxidation kinetics and product formation. *Water Res.* 37 (7), 1443–1467.
- von Gunten, U., 2018. Oxidation Processes in Water Treatment: Are We on Track? *Environ. Sci. Technol.* 52 (9), 5062–5075.
- von Sonntag, C., von Gunten, U., 2012. Chemistry of ozone in water and wastewater treatment: From basic principles to applications. IWA Publishing, London.
- Voukides, A.C., Konrad, K.M., Johnson, R.P., 2009. Competing mechanistic channels in the oxidation of aldehydes by ozone. *J. Org. Chem.* 74 (5), 2108–2113.
- Wackett, L.P., 2021. Why Is the Biodegradation of Polyfluorinated Compounds So Rare? *mSphere* 6 (5), e0072121.
- Wacławek, S., Grübel, K., Černík, M., 2015. Simple spectrophotometric determination of monopersulfate. *Spectrochimica acta. Part A, Molecular and biomolecular spectroscopy* 149, 928–933.
- Wacławek, S., Lutze, H.V., Grübel, K., Padil, V.V.T., Černík, M., Dionysiou, D.D., 2017. Chemistry of persulfates in water and wastewater treatment: A review. *Chem. Eng. J.* 330 (69), 44–62.
- Wakida, F.T., Lerner, D.N., 2005. Non-agricultural sources of groundwater nitrate: a review and case study. *Water Res.* 39 (1), 3–16.

- Walzak, M.J., Flynn, S., Foerch, R., Hill, J.M., Karbasheski, E., Lin, A., Strobel, M., 1995. UV and ozone treatment of polypropylene and poly(ethylene terephthalate). *J. Adhes. Sci. Technol.* 9 (9), 1229–1248.
- Wang, B., Xiong, X., Shui, Y., Huang, Z., Tian, K., 2019. A systematic study of enhanced ozone mass transfer for ultrasonic-assisted PTFE hollow fiber membrane aeration process. *Chem. Eng. J.* 357, 678–688.
- Wang, G., Zhang, Y., Ge, L., Liu, Z., Zhu, X., Yang, S., Jin, P., Zeng, X., Zhang, X., 2022a. Monodispersed CuO nanoparticles supported on mineral substrates for groundwater remediation via a nonradical pathway. *J. Hazard. Mater.* 429, 128282.
- Wang, H., Liao, B., Hu, M., Ai, Y., Wen, L., Yang, S., Ye, Z., Qin, J., Liu, G., 2022b. Heterogeneous activation of peroxymonosulfate by natural chalcopyrite for efficient remediation of groundwater polluted by aged landfill leachate. *Appl. Catal. B* 300 (6), 120744.
- Wang, L., Lan, X., Peng, W., Wang, Z., 2021. Uncertainty and misinterpretation over identification, quantification and transformation of reactive species generated in catalytic oxidation processes: A review. *J. Hazard. Mater.* 408, 124436.
- Wang, R., Zhang, H.Y., Feron, P.H.M., Liang, D.T., 2005. Influence of membrane wetting on CO<sub>2</sub> capture in microporous hollow fiber membrane contactors. *Sep. Purif. Technol.* 46 (1-2), 33–40.
- Wang, Y., Sun, H., Ang, H.M., Tadé, M.O., Wang, S., 2015. 3D-hierarchically structured MnO<sub>2</sub> for catalytic oxidation of phenol solutions by activation of peroxymonosulfate: Structure dependence and mechanism. *Appl. Catal. B* 164, 159–167.
- Wang, Y., Yu, G., 2022. Challenges and pitfalls in the investigation of the catalytic ozonation mechanism: A critical review. *J. Hazard. Mater.* 436, 129157.
- Wang, Z., Lin, X., Huang, Y., Ma, L., 2022c. The role of hydroxylation on ·OH generation for enhanced ozonation of benzoic acids: Reactivity, ozonation efficiency and radical formation mechanism. *J. Hazard. Mater.* 431, 128620.
- Watts, M.J., Linden, K.G., 2009. Advanced oxidation kinetics of aqueous trialkyl phosphate flame retardants and plasticizers. *Environ. Sci. Technol.* 43 (8), 2937–2942.
- Watts, R.J., Teel, A.L., 2006. Treatment of Contaminated Soils and Groundwater Using ISCO. *Practice Periodical of Hazardous, Toxic, and Radioactive Waste Management* 10 (1), 2–9.

- Weigend, F., Ahlrichs, R., 2005. Balanced basis sets of split valence, triple zeta valence and quadruple zeta valence quality for H to Rn: Design and assessment of accuracy. *Physical chemistry chemical physics* : PCCP 7 (18), 3297–3305.
- Wenk, J., Aeschbacher, M., Salhi, E., Canonica, S., von Gunten, U., Sander, M., 2013. Chemical oxidation of dissolved organic matter by chlorine dioxide, chlorine, and ozone: effects on its optical and antioxidant properties. *Environ. Sci. Technol.* 47 (19), 11147–11156.
- Wenten, I.G., Julian, H., Panjaitan, N.T., 2012. Ozonation through ceramic membrane contactor for iodide oxidation during iodine recovery from brine water. *Desalination* 306, 29–34.
- Westerhoff, P., Aiken, G., Amy, G., Debroux, J., 1999. Relationships between the structure of natural organic matter and its reactivity towards molecular ozone and hydroxyl radicals. *Water Res.* 33 (10), 2265–2276.
- WHO, 2022. State of the world's drinking water: an urgent call to action to accelerate progress on ensuring safe drinking water for all (accessed 5.07.2023). <https://www.who.int/publications/i/item/9789240060807>.
- Wickramasinghe, S.R., Semmens, M.J., Cussler, E.L., 1992. Mass transfer in various hollow fiber geometries. *J. Membr. Sci.* 69 (3), 235–250.
- Wolfenden, B.S., Willson, R.L., 1982. Radical-cations as reference chromogens in kinetic studies of one-electron transfer reactions: pulse radiolysis studies of 2,2'-azinobis-(3-ethylbenzthiazoline-6-sulphonate). *J. Chem. Soc., Perkin Trans. 2* (7), 805–812.
- Wolicka, D., Suszek, A., Borkowski, A., Bielecka, A., 2009. Application of aerobic microorganisms in bioremediation in situ of soil contaminated by petroleum products. *Bioresour. Technol.* 100 (13), 3221–3227.
- Wols, B.A., Hofman, J.A.M.H., Uijtewaal, W.S.J., Rietveld, L.C., van Dijk, J.C., 2010. Evaluation of different disinfection calculation methods using CFD. *Environ. Model. Softw.* 25 (4), 573–582.
- Wols, B.A., Hofman-Caris, C.H.M., 2012. Review of photochemical reaction constants of organic micropollutants required for UV advanced oxidation processes in water. *Water Res.* 46 (9), 2815–2827.
- Wols, B.A., Hofman-Caris, C.H.M., Harmsen, D.J.H., Beerendonk, E.F., 2013. Degradation of 40 selected pharmaceuticals by UV/H<sub>2</sub>O<sub>2</sub>. *Water Res.* 47 (15), 5876–5888.
- Wolters, J., Usman, M., Mathiä, J., Dirichs, D., Bastian, D., Aumeier, B., Bolm, C., Linnemann, V., Wintgens, T., 2022. TACN-Mn catalyst use in an advanced oxidation

- process for efficient micropollutant abatement in wastewater: A transformation study of diclofenac and sulfamethoxazole. *J. Environ. Chem. Eng.* 10 (5), 108320.
- Wünsch, R., Mayer, C., Plattner, J., Eugster, F., Wülser, R., Gebhardt, J., Hübner, U., Canonica, S., Wintgens, T., von Gunten, U., 2021. Micropollutants as internal probe compounds to assess UV fluence and hydroxyl radical exposure in UV/H<sub>2</sub>O<sub>2</sub> treatment. *Water Res.* 195, 116940.
- Wünsch, R., Plattner, J., Cayon, D., Eugster, F., Gebhardt, J., Wülser, R., Gunten, U. von, Wintgens, T., 2019. Surface water treatment by UV/H<sub>2</sub>O<sub>2</sub> with subsequent soil aquifer treatment: impact on micropollutants, dissolved organic matter and biological activity. *Environ. Sci.: Water Res. Technol.* 5 (10), 1709–1722.
- Xiang, Y., Liu, H., Zhu, E., Yang, K., Yuan, D., Jiao, T., Zhang, Q., Tang, S., 2022. Application of inorganic materials as heterogeneous cocatalyst in Fenton/Fenton-like processes for wastewater treatment. *Sep. Purif. Technol.* 295 (3), 121293.
- Xiao, R., Bai, L., Liu, K., Shi, Y., Minakata, D., Huang, C.-H., Spinney, R., Seth, R., Dionysiou, D.D., Wei, Z., Sun, P., 2020. Elucidating sulfate radical-mediated disinfection profiles and mechanisms of *Escherichia coli* and *Enterococcus faecalis* in municipal wastewater. *Water Res.* 173, 115552.
- Xie, Z., Zhou, J., Wang, J., François-Xavier, C.P., Wintgens, T., 2019. Novel Fenton-like catalyst  $\gamma$ -Cu-Al<sub>2</sub>O<sub>3</sub>-Bi<sub>12</sub>O<sub>15</sub>Cl<sub>6</sub> with electron-poor Cu centre and electron-rich Bi centre for enhancement of phenolic compounds degradation and H<sub>2</sub>O<sub>2</sub> utilization: The synergistic effects of  $\sigma$ -Cu-ligand, dual-reaction centres and oxygen vacancies. *Appl. Catal. B* 253, 28–40.
- Xin, B.-P., Wu, C.-H., Wu, C.-H., Lin, C.-W., 2013. Bioaugmented remediation of high concentration BTEX-contaminated groundwater by permeable reactive barrier with immobilized bead. *J. Hazard. Mater.* 244-245, 765–772.
- Xu, B., Liu, S., Zhou, J.L., Zheng, C., Weifeng, J., Chen, B., Zhang, T., Qiu, W., 2021a. PFAS and their substitutes in groundwater: Occurrence, transformation and remediation. *J. Hazard. Mater.* 412, 125159.
- Xu, J., Zheng, X., Feng, Z., Lu, Z., Zhang, Z., Huang, W., Li, Y., Vuckovic, D., Li, Y., Dai, S., Chen, G., Wang, K., Wang, H., Chen, J.K., Mitch, W., Cui, Y., 2021b. Organic wastewater treatment by a single-atom catalyst and electrolytically produced H<sub>2</sub>O<sub>2</sub>. *Nat. Sustain.* 4, 233–241.
- Yan, Y., Wei, Z., Duan, X., Long, M., Spinney, R., Dionysiou, D.D., Xiao, R., Alvarez, P.J.J., 2023. Merits and Limitations of Radical vs. Nonradical Pathways in Persulfate-Based Advanced Oxidation Processes. *Environ. Sci. Technol.* 57 (33), 12153–12179.

- Yang, J., Li, J., Dong, W., Ma, J., Cao, J., Li, T., Li, J., Gu, J., Liu, P., 2016. Study on enhanced degradation of atrazine by ozonation in the presence of hydroxylamine. *J. Hazard. Mater.* 316, 110–121.
- Yang, M.-C., Cussler, E.L., 1986. Designing hollow-fiber contactors. *AIChE J.* 32 (11), 1910–1916.
- Yang, S., Wu, P., Liu, J., Chen, M., Ahmed, Z., Zhu, N., 2018a. Efficient removal of bisphenol A by superoxide radical and singlet oxygen generated from peroxymonosulfate activated with Fe0-montmorillonite. *Chem. Eng. J.* 350, 484–495.
- Yang, Y., Banerjee, G., Brudvig, G.W., Kim, J.-H., Pignatello, J.J., 2018b. Oxidation of Organic Compounds in Water by Unactivated Peroxymonosulfate. *Environ. Sci. Technol.* 52 (10), 5911–5919.
- Yang, Z., Qian, J., Shan, C., Li, H., Yin, Y., Pan, B., 2021. Toward Selective Oxidation of Contaminants in Aqueous Systems. *Environ. Sci. Technol.* 55 (21), 14494–14514.
- Yang, Z.-H., Verpoort, F., Dong, C.-D., Chen, C.-W., Chen, S., Kao, C.-M., 2020. Remediation of petroleum-hydrocarbon contaminated groundwater using optimized in situ chemical oxidation system: Batch and column studies. *Process Safety and Environmental Protection* 138 (Part B), 18–26.
- Ye, M., Schuler, R.H., 1989. Second-order combination reactions of phenoxy radicals. *J. Phys. Chem.* 93 (5), 1898–1902.
- Ye, T., Wei, Z., Spinney, R., Tang, C.-J., Luo, S., Xiao, R., Dionysiou, D.D., 2017. Chemical structure-based predictive model for the oxidation of trace organic contaminants by sulfate radical. *Water Res.* 116, 106–115.
- Yin, Z., Cagnetta, G., Huang, J., 2022. Mechanochemically sulfidated zero-valent iron as persulfate activation catalyst in permeable reactive barriers for groundwater remediation - A feasibility study. *Chemosphere* 311 (Pt 2), 137081.
- Ying, Z., Yechezkel, Y., Huo, M., Hübner, U., Zucker, I., 2021. Ozone Consumption by Soils: A Critical Factor in In Situ Ozonation Processes. *ACS ES&T Water (ACS ES&T Water)* 1 (11), 2403–2411.
- Yu, C., Li, G., Wei, L., Fan, Q., Shu, Q., Yu, J.C., 2014. Fabrication, characterization of  $\beta$ -MnO<sub>2</sub> microrod catalysts and their performance in rapid degradation of dyes of high concentration. *Catal. Today* 224 (17), 154–162.
- Yu, G., Wang, Y., Cao, H., Zhao, H., Xie, Y., 2020. Reactive Oxygen Species and Catalytic Active Sites in Heterogeneous Catalytic Ozonation for Water Purification. *Environ. Sci. Technol.* 54 (10), 5931–5946.

- Yu, M., Teel, A.L., Watts, R.J., 2016. Activation of Peroxymonosulfate by Subsurface Minerals. *J. Contam. Hydrol.* 191, 33–43.
- Yuan, F., Hu, C., Hu, X., Qu, J., Yang, M., 2009. Degradation of selected pharmaceuticals in aqueous solution with UV and UV/H<sub>2</sub>O<sub>2</sub>. *Water Res.* 43 (6), 1766–1774.
- Zhang, H., Jiang, M., Zhang, D., Xia, Q., 2009. Decomposition of 4-Nitrophenol by Ozonation in a Hollow Fiber Membrane Reactor. *Chem. Eng. Commun.* 197 (3), 377–386.
- Zhang, H., Wang, W., 2011. Oxidation of C.I. Acid Orange 7 with Ozone and Hydrogen Peroxide in a Hollow Fiber Membrane Reactor. *Chem. Eng. Commun.* 198 (12), 1530–1544.
- Zhang, Y., He, C., Sharma, V.K., Li, X.-z., Tian, S., Xiong, Y., 2011. A coupling process of membrane separation and heterogeneous Fenton-like catalytic oxidation for treatment of acid orange II-containing wastewater. *Sep. Purif. Technol.* 80 (1), 45–51.
- Zhang, Y., Li, K., Wang, J., Hou, D., Liu, H., 2017. Ozone mass transfer behaviors on physical and chemical absorption for hollow fiber membrane contactors. *Water Sci. Technol.* 76 (5-6), 1360–1369.
- Zhang, Y.-J., Huang, G.-X., Winter, L.R., Chen, J.-J., Tian, L., Mei, S.-C., Zhang, Z., Chen, F., Guo, Z.-Y., Ji, R., You, Y.-Z., Li, W.-W., Liu, X.-W., Yu, H.-Q., Elimelech, M., 2022. Simultaneous nanocatalytic surface activation of pollutants and oxidants for highly efficient water decontamination. *Nat. Commun.* 13 (1), 3005.
- Zhou, X., Ren, X., Chen, Y., Feng, H., Yu, J., Peng, K., Zhang, Y., Chen, W., Tang, J., Wang, J., Tang, L., 2023. Bacteria inactivation by sulfate radical: progress and non-negligible disinfection by-products. *Front. Environ. Sci. Eng.* 17 (3), 1000.
- Zhu, S., Li, X., Kang, J., Duan, X., Wang, S., 2019. Persulfate Activation on Crystallographic Manganese Oxides: Mechanism of Singlet Oxygen Evolution for Nonradical Selective Degradation of Aqueous Contaminants. *Environ. Sci. Technol.* 53 (1), 307–315.
- Zimmermann, S.G., Schmukat, A., Schulz, M., Benner, J., von Gunten, U., Ternes, T.A., 2012. Kinetic and mechanistic investigations of the oxidation of tramadol by ferrate and ozone. *Environ. Sci. Technol.* 46 (2), 876–884.
- Zoumpouli, G., Baker, R., Taylor, C., Chippendale, M., Smithers, C., Xian, S., Mattia, D., Chew, Y., Wenk, J., 2018. A Single Tube Contactor for Testing Membrane Ozonation. *Water* 10 (10), 1416–1430.
- Zour, E., Lodhi, S.A., Nesbitt, R.U., Silbering, S.B., Chaturvedi, P.R., 1992. Stability studies of gabapentin in aqueous solutions. *Pharm. Res.* 9 (5), 595–600.

- Zucker, I., Hashmi, S.M., Yang, J., He, Y., Pfefferle, L.D., Elimelech, M., 2019. Shape-Dependent Interactions of Manganese Oxide Nanomaterials with Lipid Bilayer Vesicles. *Langmuir* 35 (43), 13958–13966.
- Zucker, I., Mamane, H., Riani, A., Gozlan, I., Avisar, D., 2018. Formation and degradation of N-oxide venlafaxine during ozonation and biological post-treatment. *Sci. Total Environ.* 619-620, 578–586.